30 April 2010 | $10

Science

AAAS

Forget DNA purification

Choose Direct PCR

Take the direct route from sample to results

Finnzymes' Direct PCR approach saves you time and cost by allowing amplification of DNA directly from the source material. No DNA purification is needed. Direct PCR is suitable for various kinds of sample materials such as plant and animal tissues, blood, and FFPE tissue samples.

Direct PCR is based on Finnzymes' unique PCR enzymes, Phusion® High-Fidelity and Phire® Hot Start DNA Polymerases. These polymerases are exceptionally tolerant of many PCR inhibitors. To achieve the shortest possible protocols, combine the Direct PCR approach with Finnzymes' Piko® Thermal Cyclers and UTW® reaction vessels.

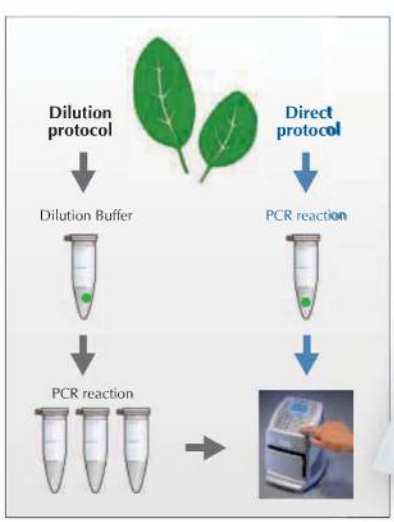

NEW!

Optimized kits available:

Phire® Plant Direct PCR Kit
for plant material

Phire® Animal Tissue Direct PCR Kit
for various animal tissues

Phusion® Blood Direct PCR Kit
for blood

See the latest results, application notes and product updates at www.finnzymes.com/directpcr

FINNZYMES
Part of Thermo Fisher Scientific

Call for Papers

Science Signaling

Science Signaling, from the publisher of ***Science***, AAAS, features top-notch, peer-reviewed, original research weekly. Submit your manuscripts in the following areas of cellular regulation:

- Biochemistry
- Bioinformatics
- Cell Biology
- Development
- Immunology
- Microbiology
- Molecular Biology
- Neuroscience
- Pharmacology
- Physiology and Medicine
- Systems Biology

Science Signaling is indexed in CrossRef and MEDLINE.

Submit your research at:
www.sciencesignaling.org/about/help/research.dtl

Subscribing to the weekly ***Science Signaling*** ensures that you and your lab have the latest cell signaling resources. For more information visit **www.ScienceSignaling.org**

Science Signaling
AAAS

GE Healthcare
Life Sciences

Biacore™ & MicroCal™

Confidence that comes with the right interactions.

Label-free analysis using Biacore and MicroCal systems provides comprehensive characterization of biomolecular interactions and biomolecule stability. The information-rich data enables key insights into the biological processes and molecular binding mechanisms crucial to your research. Equipped with the right information, you can make speedy, smart decisions with confidence.

Visit **www.gelifesciences.com/interactions**

Biacore systems

MicroCal DSC and iTC

imagination at work

GE05-10. First published April 2010.

EDITORIAL

NEWS OF THE WEEK

NEWS FOCUS

LETTERS

BOOKS *ET AL.*

POLICY FORUM

PERSPECTIVES

SCIENCE PRIZE ESSAY

CONTENTS continued >>

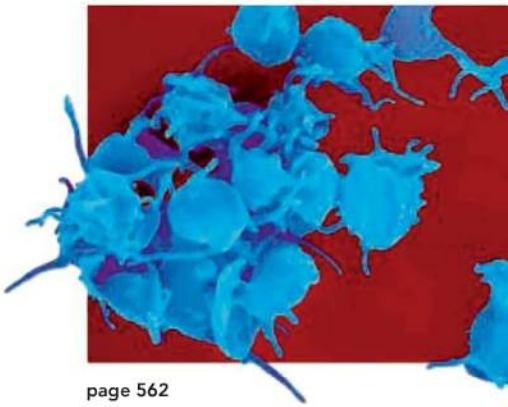

page 562

page 571

COVER

A late-stage *Xenopus tropicalis* (western clawed frog) tadpole, about 5 centimeters in length, with emerging hindlimbs. Through the skin of the head, the optic, trigeminal, and olfactory nerves, as well as the paired thymus and large blood vessels, are visible. A Report on page 633 describes the genome of this organism, which is an important model for vertebrate development.

Photo: Siwei Zhang, Jingjing Li, Enrique Amaya

DEPARTMENTS

Choose QIAGEN for detection

Detection platforms, assays, and analysis software by QIAGEN

Use QIAGEN® solutions from sample to result, and benefit from sensitive and reliable detection systems:

- **Quantitative, real-time PCR detection**
- **Automated analysis of DNA fragments and RNA**
- **Pyrosequencing® sequence-based DNA detection and quantification**
- **Optimized, ready-to-use assays and reagents**

Making improvements in life possible — www.qiagen.com

QIAGEN®

Sample & Assay Technologies

REVIEW

BREVIA

RESEARCH ARTICLE

REPORTS

CONTENTS continued >>

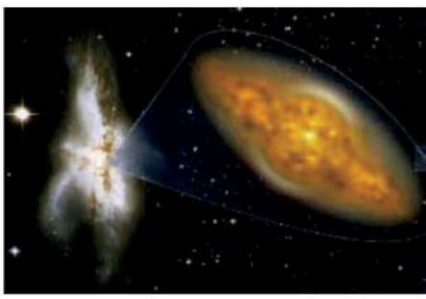

pages 576 & 600

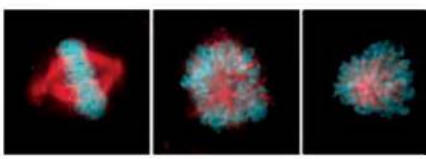

page 593

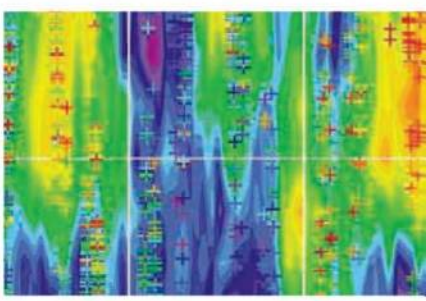

page 611

Submission deadline August 1

Your name here.

The GE & Science Prize for Young Life Scientists. Because brilliant ideas build better realities.

Imagine standing on the podium at the Grand Hotel in Stockholm, making your acceptance speech for the GE & Science Prize for Young Life Scientists. Imagine having your essay read by your peers around the world. Imagine discussing your work in a seminar with other prize winners and Nobel Laureates. Imagine what you could do with the $25,000 prize money. Now stop imagining. If you were awarded your Ph.D. in molecular biology in 2009, then submit your 1000-word essay by August 1, and you can make it reality.

Want to build a better reality? Go to www.gescienceprize.org

GE & Science Prize for Young Life Scientists

imagination at work

Science AAAS

* For the purpose of this prize, molecular biology is defined as "that part of biology which attempts to interpret biological events in terms of the physico-chemical properties of molecules in a cell".

(McGraw-Hill Dictionary of Scientific and Technical Terms, 4th Edition).

28-9402-06AB

SCIENCEONLINE

SCIENCEXPRESS
www.sciencexpress.org

Global Biodiversity: Indicators of Recent Declines
S. H. M. Butchart et al.

An analysis of 30 indicators shows that the Convention on Biological Diversity's 2010 reduction targets have not been met.
10.1126/science.1187512

Endosomal Chloride-Proton Exchange Rather Than Chloride Conductance Is Crucial for Renal Endocytosis
G. Novarino et al.
10.1126/science.1188070

Lysosomal Pathology and Osteopetrosis upon Loss of H^+-Driven Lysosomal Cl^- Accumulation
S. Weinert et al.

Chloride conductance and chloride-proton exchange on endolysosomal physiology are compared in two mouse models.
10.1126/science.1188072

Self-Assembled $M_{24}L_{48}$ Polyhedra and Their Sharp Structural Switch upon Subtle Ligand Variation
Q.-F. Sun et al.

A slight change in ligand geometry determines whether a 12- or 24-vertex polyhedron will form.
10.1126/science.1188605

Freshwater Outburst from Lake Superior as a Trigger for the Cold Event 9300 Years Ago
S.-Y. Yu et al.

The trigger for the dramatic North Atlantic cooling event 9300 years ago was an outburst flood from Lake Superior.
10.1126/science.1187860

SCIENCENOW
www.sciencenow.org
Highlights From Our Daily News Coverage

Chimps Grieve Over Dead Relatives

Two studies document an almost humanlike response to death.

Dark Matter Halos Look a Bit Like a Football

Clumps of the mysterious substance reveal surprisingly similar shapes.

Elephants Have an Alarm Call for Bees

Study suggests that pachyderms tailor vocal warnings to specific foes.

SCIENCESIGNALING
www.sciencesignaling.org
The Signal Transduction Knowledge Environment

RESEARCH ARTICLE: Ammonia Derived from Glutaminolysis Is a Diffusible Regulator of Autophagy
C. H. Eng et al.

A volatile metabolic by-product can promote cell survival through the induction of autophagy.

RESEARCH ARTICLE: SUMOylation of the Transcriptional Co-Repressor KAP1 Is Regulated by the Serine and Threonine Phosphatase PP1
X. Li et al.

Two isoforms of protein phosphatase 1 coordinate the recovery of cells from genotoxic stress.

RESEARCH ARTICLE: Evolution of CASK into a Mg^{2+}-Sensitive Kinase
K. Mukherjee et al.

The atypical kinase CASK evolved from a conventional Mg^{2+}-dependent kinase.

EDITORIAL GUIDE: Teaching Tools and Learning Opportunities
N. R. Gough
Science Signaling provides authoring experience for students and resources for educators.

JOURNAL CLUB: Costimulatory Role of CXCR4 with Pre-TCR and Its Crosstalk with PI3K in β-Selection of Thymocytes
J. A. Ahamed and P. Madhivadhani

Chemokine and pre-TCR signaling cooperate in β-selection of thymocytes and promote their subsequent proliferation.

JOURNAL CLUB: New Regulator for Energy Signaling Pathway in Plants Highlights Conservation Among Species
A. K. Meyer et al.

The kinase CIPK links plant pathways involved in oxygen-sensing and carbohydrate metabolism.

TEACHING RESOURCES: Animations of Canonical Signaling Pathways
J. D. Thatcher

Four pairs of animations provide tools for introducing core signaling pathways and a way for students to test their knowledge.

SCIENCECAREERS
www.sciencecareers.org/career_magazine
Free Career Resources for Scientists

Mind Matters: Back to Work After Baby, Part 2
I. S. Levine

New mothers can minimize stress and maximize productivity by adapting to their circumstances.

Navigating Historic Changes
N. Lubick

A sense of humor, hard work, and daring helped microbiologist Ingrid Grummt achieve success.

Science Careers Communities
Science *Careers Staff*

Connect with scientists from diverse backgrounds in MySciNet or with clinical and translational scientists in CTSciNet.

SCIENCETRANSLATIONAL MEDICINE
www.sciencetranslationalmedicine.org
Integrating Medicine and Science

COMMENTARY: Six Questions About Translational Due Diligence
E. Selinger

To maintain public support, the translational research enterprise must do more than provide results.

RESEARCH ARTICLE: Cystic Fibrosis Pigs Develop Lung Disease and Exhibit Defective Bacterial Eradication at Birth
D. A. Stoltz et al.

PERSPECTIVE: The Development of Lung Disease in Cystic Fibrosis Pigs
J. J. Wine

The lungs of piglets with CF fail to efficiently eliminate bacteria, suggesting that lung problems in CF patients may be secondary to impaired antibacterial defense.

RESEARCH ARTICLE: Wnt Proteins Promote Bone Regeneration
S. Minear et al.

A liposome-encased ligand for the Wnt signaling pathway can accelerate bone regeneration after injury.

SCIENCEPODCAST
www.sciencemag.org/multimedia/podcast
Free Weekly Show

Download the 30 April *Science* Podcast to hear about lab experiments of a dynamic social-ecological system, the return of Japan's Hayabusa asteroid mission, your letters to *Science*, and more.

SCIENCEINSIDER
news.sciencemag.org/scienceinsider
Science Policy News and Analysis

SCIENCE (ISSN 0036-8075) is published weekly on Friday, except the last week in December, by the American Association for the Advancement of Science, 1200 New York Avenue, NW, Washington, DC 20005. Periodicals Mail postage (publication No. 484460) paid at Washington, DC, and additional mailing offices. Domestic individual membership and subscription (51 issues): $146 ($74 allocated to subscription). Domestic institutional subscription (51 issues): $910; Foreign postage extra: Mexico, Caribbean (surface mail) $55; other countries (air assist delivery) $85. First class, airmail, student, and emeritus rates on request. Canadian rates with GST available upon request, GST #1254 88122. Publications Mail Agreement Number 1069624. **Printed in the U.S.A.**

Change of address: Allow 4 weeks, giving old and new addresses and 8-digit account number. **Postmaster:** Send change of address to AAAS, P.O. Box 96178, Washington, DC 20090–6178. **Single-copy sales:** $10.00 current issue, $15.00 back issue prepaid includes surface postage; bulk rates on request. The identification code for *Science* is 0036-8075. *Science* is indexed in the *Reader's Guide to Periodical Literature* and in several specialized indexes.

AAAS
ADVANCING SCIENCE, SERVING SOCIETY

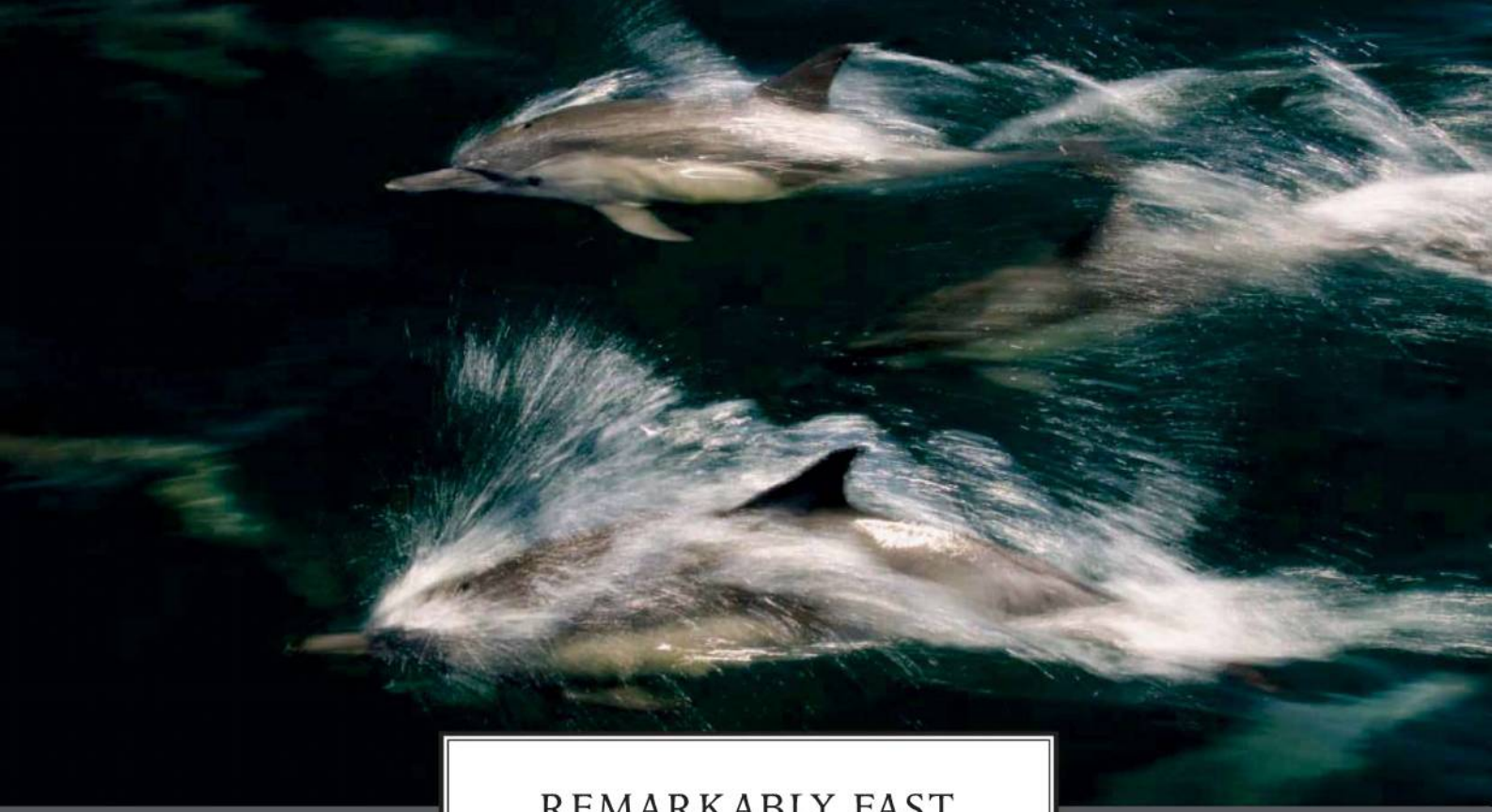

REMARKABLY FAST

Phusion® High-Fidelity DNA Polymerase

With Phusion® High-Fidelity DNA Polymerase, there is no need to compromise any aspect of your PCR performance. A superior choice for cloning, this recombinant polymerase has an error rate 50-fold lower than *Taq* DNA Polymerase, combining extreme precision with unparalleled speed and robustness.

Not all PCR polymerases are created equal

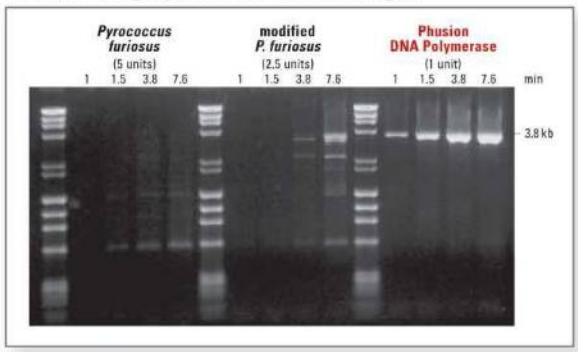

Amplification of a 3.8 kb fragment from the human beta globin gene clearly illustrates the extreme speed and robustness offered by using Phusion DNA Polymerase. Reactions were performed according to the suppliers' recommendations using varying extension times (shown above gel).

Phusion is a registered trademark of Finnzymes Oy.

Advantages:

- Extreme fidelity
- High yield
- High speed
- Specificity
- Robustness

Go to **www.neb.com/phusion** to find out how Phusion High-Fidelity DNA Polymerase can improve your PCR performance.

Produced by

FINNZYMES
TOOLS FOR MOLECULAR BIOLOGY

Distributed by

NEW ENGLAND BioLabs® Inc.
enabling technologies in the life sciences

CLONING & MAPPING	**DNA AMPLIFICATION & PCR**	RNA ANALYSIS	PROTEIN EXPRESSION & ANALYSIS	GENE EXPRESSION & CELLULAR ANALYSIS

www.neb.com

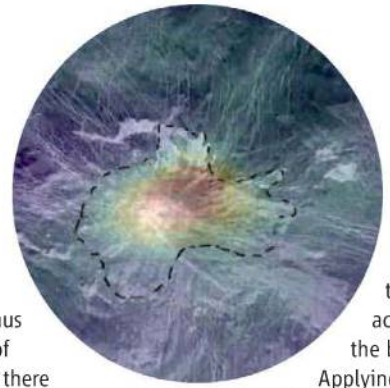

Hotspots on Venus

The surface of Venus shows clear signs of volcanism, but are there active volcanoes on Venus today? The answer to this question will bear on our understanding of the planet's climate evolution and interior dynamics. Using surface thermal emissivity data returned by the Venus Express spacecraft, **Smrekar *et al.*** (p. 605, published online 8 April) looked at three hotspots on Venus. These places were identified by analogy with terrestrial hotspots like Hawaii, which are believed to overlie mantle plumes and to be the most likely sites for current volcanic activity. Lava flows at the three hotspots have anomalously high thermal emissions when compared with their surroundings. Low emissivity is generally interpreted as the result of surface alteration by the corrosive atmosphere of Venus. High emissivity implies that not much alteration took place and thus that the hotspots must represent recently active volcanoes younger than 2.5 million years.

Grassland Emergence

The evolution of the C_4 photosynthetic pathway from the ancestral C_3 pathway in grasses led to the establishment of grasslands in warm climates during the Late Miocene (8 to 3 million years ago). This was a major event in plant evolutionary history, and their high rates of foliage production sustained high levels of herbivore consumption. The past decade has seen significant advances in understanding C_4 grassland ecosystem ecology, and now a wealth of data on the geological history of these ecosystems has accumulated and the phylogeny of grasses is much better known. **Edwards *et al.*** (p. 587) review this multidisciplinary research area and attempt to synthesize emerging knowledge about the evolution of grass species within the context of plant and ecosystem ecology.

Division Machinery Tagged

An international consortium of labs has been testing the feasibility of large-scale screening for insights into the function of mammalian proteins by expressing a tagged version of proteins from bacterial artificial chromosomes harbored in mammalian cells. Depending on the tag used, **Hutchins *et al.*** (p. 593, published online 1 April) were able to monitor localization of tagged proteins by microscopy or to isolate interacting proteins and subsequently identify the binding partners by mass spectrometry. Applying the technology to proteins implicated in control of cell division revealed about 100 protein machines required for mitosis.

Dusty Quasars

Quasars are energetic sources thought to be fueled by matter accreting onto black holes a billion times more massive than the Sun. Some quasars are difficult to detect because of surrounding clouds of gas and dust, so much so that this population of objects has remained elusive. Based on a compilation of x-ray, optical, and mid-infrared data, **Treister *et al.*** (p. 660, published online 25 March; see the Perspective by **Primack**) show that the evolution of quasars across cosmic time occurs during mergers of gas-rich galaxies, with an obscured phase preceding an unobscured state by about 100 million years. Other objects have been detected in diverse wavebands, including ultraluminous infrared galaxies, which are known to be the product of similar gas-rich mergers of massive galaxies.

Approaching Lactate Inorganically

Conversion of biomass to value-added chemical compounds currently relies in large part on fermentation. For full-scale displacement of petroleum as the chemical industry's primary feedstock, alternative conversion technologies will be necessary. **Holm *et al.*** (p. 602) have found that Lewis acidic zeolite derivatives suspended in methanol can catalyze the selective conversion of glucose, fructose, and sucrose sugars to methyl lactate, a versatile synthetic intermediate for commercial products. The catalysts were easily separated from product mixtures and proved robust over six reaction and regeneration cycles.

Riding the Monsoon

Most air transport from the troposphere to the stratosphere occurs in the tropics, but additional

Continued on page 545

Pink for Me, Green for You >>

Aphids come in different colors, a critical issue when fate is a question of pigmentation: Red aphids tend to be consumed by ladybugs and green ones by parasitic wasps. Aphid color is determined by carotenoids, the same group of chemicals that make flamingos pink. But unlike flamingos, which have to eat colored food to stay pink, aphids make their own pigment. Carotenoids are vital to animals, not only because of their decorative possibilities but also for their oxidation-protective qualities as visual pigments and immune-system modulators. On sifting through an aphid genome, **Moran and Jarvik** (p. 624; see the Perspective by **Fukatsu**) discovered that the machinery for producing carotenoids has been acquired by an ancestral aphid in a lateral transfer event from a fungus. Although a spontaneous yellow mutant aphid was found that still possesses the sequence for biosynthesis of the red carotenoid pigment torulene, the sequence was discovered to have a single point mutation that puts a stop to turning red.

CREDITS (TOP TO BOTTOM): SMREKAR *ET AL.*; CHARLES HEDGECOCK R.B.P.

www.454.com

GS Junior Sequencing System

The Next Big Thing in Sequencing *is small.*

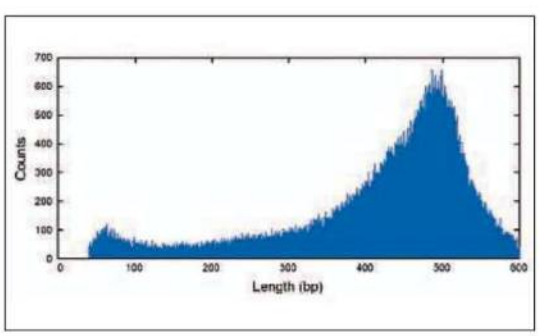

Figure 1: Example Read Length Distribution of 100,000 reads from *E. coli* K-12 (genome size approximately 4.5 Mb), from a single GS Junior System run.

Bring the power, performance, speed, and long reads of the GS FLX Titanium chemistry to your benchtop with the newest addition to the Roche genome sequencing portfolio – the **GS Junior Sequencing System**.

- **Make the most of your sequencing projects with our 400- to 500-base-pair read lengths (Figure 1).**
- **Benefit from established technology that has enabled hundreds of peer-reviewed publications.**
- **Accelerate your next discovery using the system's comprehensive suite of dedicated data analysis software.**

For complete information on the GS Junior System and all of the Roche sequencing solutions, visit ***www.454.com*** or contact your local Roche representative today.

For life science research only.
Not for use in diagnostic procedures.

454 SEQUENCING

Roche Diagnostics Corporation
Roche Applied Science
Indianapolis, Indiana

Roche

Continued from page 543

transport may occur in areas of strong upward convection. **Randel *et al.*** (p. 611, published online 25 March) report satellite measurements of atmospheric hydrogen cyanide over the region where the Asian summer monsoon occurs, which indicate that air is transported from the surface to deep within the stratosphere. This mechanism represents a pathway for pollutants to enter the global stratosphere, where they might affect ozone chemistry, aerosol characteristics, and radiative properties.

Learning to Work Together

In group endeavors, there is often a tension between working for the greater good of the group as a whole versus working for one's own benefit. Sometimes these paths coincide and sometimes they do not; furthermore, the choices made by other group members can influence the calculation of which path to take. A pair of studies now approaches this challenge from experimental and theoretical points of view. In a forest or fishery, harvesting of wood or food needs to take into account the renewable character of the resource, as well as spatial heterogeneity. **Janssen *et al.*** (p. 613; see the Perspective by **Putterman**) show that communication among the group members is key, both to establishing a maintainable rate of harvesting, as well as enforcement via punishment of noncompliers. **Boyd *et al.*** (p. 617; see the Perspective by **Putterman**) develop a model showing that punishment, which is a costly activity, is most effectively levied when implemented with the approval of group members; that is, coordinated punishment works to the benefit of the whole, whereas individual actions do not.

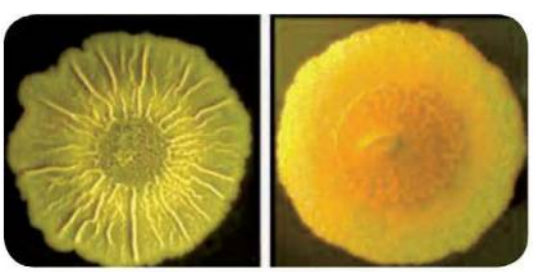

CREDIT: KOLODKIN-GAL *ET AL.*

Biofilm Today, Gone Tomorrow

Most bacteria can form complex, matrix-containing multicellular communities known as biofilms, which protect residents from environmental stresses such as antibiotic exposure. However, as biofilms age, nutrients become limiting and waste products accumulate, and biofim disassembly is triggered. Now **Kolodkin-Gal *et al.*** (p. 627) have found that D-amino acids found in conditioned medium from mature biofilms of *Bacillus subtilis* prevent biofilm formation and trigger existing biofilm disassembly.

Light Structures

Absorption of light by photosynthetic reaction centers causes structural changes and triggers a series of electron transfer reactions, resulting in a transmembrane potential difference that can be used to drive the subsequent chemistry. The initial electron transfer generates a charge-separated state that must be stabilized to prevent dissipation of energy through recombination. **Wöhri *et al.*** (p. 630) have used time-resolved Laue diffraction crystallography to observe light-induced conformational changes that occur within milliseconds of photooxidation of the dimer of bacteriochlorophyll molecules, known as the "special pair," in the photosynthetic reaction center of *Blastochloris viridis*. Stabilization appears to occur because of the deprotonation of a conserved tyrosine residue that moves closer to the special pair.

Frog Genome

The African clawed frog *Xenopus tropicalis* is the first amphibian to have its genome sequenced. **Hellsten *et al.*** (p. 633, see the cover) present an analysis of a draft assembly of the genome. The genome of the frog, which is an important model system for developmental biology, encodes over 20,000 protein-coding genes, of which more than 1700 genes have identified human disease associations. Detailed comparison of the content of protein-coding genes with other tetrapods—human and chicken—reveals extensive shared synteny, occasionally spanning entire chromosomes.

EMSL

Opportunity: Data integration in biology & interfacial science

Enhance the scope and impact of your research by using advanced instrumentation at EMSL

EMSL is making novel capabilities available for high-throughput data generation and integration in biology and interfacial science.

EMSL is soliciting concept papers on using these capabilities to address important problems in biology and interfacial science.

Visit EMSL's web site to learn more and to submit a short concept paper.
www.emsl.pnl.gov/access/research_call/

Access to capabilities and EMSL staff is free for open research.

CALL FOR CONCEPT PAPERS

R. A. Mashelkar is a CSIR Bhatnagar Fellow at the National Chemical Laboratory, Pune 411 008, India. E-mail: ram@ncl.res.in

Irreverence and Indian Science

NOBEL LAUREATE RICHARD FEYNMAN BELIEVED THAT CREATIVE PURSUIT IN SCIENCE REQUIRES irreverence. Sadly, this spirit is missing from Indian science today. As other nations pursue more innovative approaches to solving problems, India must free itself from a traditional attitude that condemns irreverence, so that it too can address local and global challenges and nurture future leaders in science. But how can the spirit of adventurism come to Indian science?

The situation has deep roots in Indian culture and tradition. The ancient Sanskrit saying "baba vakyam pramanam" means "the words of the elders are the ultimate truth," thus condemning the type of irreverence inspired by the persistent questioning that is necessary for science. The Indian educational system, which is textbook-centered rather than student-centered, discourages inquisitive attitudes at an early age. Rigid unimaginative curricula and examinations based on single correct answers further cement intolerance for creativity. And the bureaucracy inherited from the time of British rule overrides meritocracy.

Every January, the Indian Science Congress is addressed by the current prime minister of India. In 2001, Prime Minister Vajpayee said, "For Indian science to flourish, the administration and government officials should serve as facilitators of science and not as masters of scientists." In 2010, Prime Minister Singh lamented, "It is unfortunately true that red tape, political interference and lack of proper recognition of good work have all contributed to a regression in Indian science." Alas, during the interim years, little had changed.

One might assume that innovative funding mechanisms would spur an adventurous spirit in Indian science. As director of the National Chemical Laboratory and director general of the Council of Scientific and Industrial Research, I launched a Kite Flying Fund and a New Idea Fund to support audacious ideas. Finding enough fundable ideas became a challenge in both cases. But Indian science has had its great rebels. In his book *The Scientist as Rebel*, Freeman Dyson writes, "For the great Indian physicists of this century, Raman, Bose, and Saha, science was a double rebellion, first against English domination and second against the fatalistic ethic of Hinduism." Thus, the challenge now is to create a nurturing environment for creative irreverence within India.

The good news is that the environment is starting to change. India is experiencing a massive expansion in its higher educational system. Thirty new universities are being created. Additionally, five new Indian Institutes of Science Education and Research have just opened. These institutes are fostering a new culture of innovation through interactive learning methods, borderless course curricula, and new evaluation systems, in which even students participate in evaluating other students. Foreign companies have established 760 R&D centers that employ about 160,000 researchers, many of whom are Indian returnees from abroad who bring with them different innovation and work perspectives, while at the same time reversing the brain drain. The recent launch of Tata Nano, the world's least expensive automobile, is considered to be a rare game-changer as a product of India. The spirit of adventurism embodied in Nano is being promoted across the Tata Group of diverse companies through an annual innovation competition, with a special award called Daring to Try, which recognizes those who pursue ambitious ideas that fail. Hopefully, this spirit will rub off onto other enterprises and institutions.

India must seize this emerging transformative opportunity by working hard to produce new organizational values and creating a tolerance for risk-taking and failure, while introducing funding mechanisms to support disruptive ideas. If India can thereby build the spirit of irreverence that Feynman endorsed, then surely Indian science will create many Ramans of the 21st century.

– R. A. Mashelkar

10.1126/science.1191057

ECONOMICS

The Invisible College of Ideas

It is no longer uncommon to see multi-authored original research papers, and in many instances, these studies represent the fruits of collaborations between multiple laboratories, especially in the biomedical sciences. How important are the lead researchers in these social and scientific networks?

Answering this question empirically appears at first glance to be intractable, but Azoulay *et al.* have compiled a data set that enables them to take advantage of natural events—when still-active superstar researchers are subtracted from collaborations via death. Of the roughly 230,000 U.S. medical school faculty members, 10,000 were classified as elite according to seven objective professional criteria; during the last two decades of the 20th century, 112 of these scientists died suddenly. The effect on the productivity of the surviving faculty-level collaborators in these superstar-coauthor dyads was unambiguous and persistent: They suffered decrements of almost 10% in publications and funding. The authors' analyses of these consequences favor a causal explanation in which the critical factor in these downward trends was being deprived of the intellectual input from these superstars, as opposed to a loss of collective experimental expertise or of privileged channels of communication to funding panels and journal editors. — GJC

Q. J. Econ. **125**, 549 (2010).

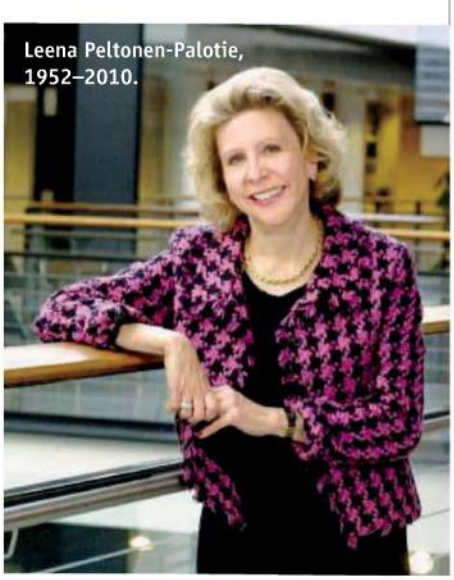

Leena Peltonen-Palotie, 1952–2010.

PALEONTOLOGY

A Wet Route South

For tens of millions of years, North and South America were mutually isolated and evolved their own flora and fauna. Plate motions gradually consolidated a series of volcanic islands and crustal fragments into a land bridge, the Isthmus of Panama, that finally closed approximately 3.5 million years ago. This closure changed ocean circulation, separated Pacific and Atlantic marine species, and accelerated the exchange of land animals between the formerly isolated continents. Documenting the earlier migrations, before final closure, can enhance understanding of the paleogeography of the region and biotic impacts of the invasions. Campbell *et al.* resolved the paleomagnetic record of Amazonian sediments containing some of the earliest North American fauna. This record implies that the sediments were deposited about 9 million years ago, consistent with some earlier notions. Thus, some early gomphotheres (similar to elephants), peccaries, and tapirs managed to make it to South America long before the final closure, presumably by swimming between distant islands. — BH

J. South Am. Earth Sci. **29**, 619 (2010).

CHEMISTRY

A Better Sort of Beads

Combinatorial libraries are widely used to find new active compounds—for example, in drug discovery. Traditionally, the library compounds are attached to a solid support, but this approach has several drawbacks. An alternative is the use of beads that are uniquely encoded, such that an active compound can easily be identified with optical methods. Meldal and Christensen have now developed a bead-encoding approach, termed MPM (microparticle matrix) encoding, that allows very large numbers of beads to be encoded rapidly and reliably, with automated screening and detection of active compounds. In a test scenario involving 3000 beads, the technique enabled identification of avidin ligands from a focused compound library.

Rasmussen *et al.* combined this methodology with virtual screening (in which the compound library itself is designed through computational screening of chemical building blocks) to identify small molecules for use in protein purification. They showed that the ligands thus discovered could efficiently isolate the targeted protein from a complex fermentation mixture. — JFU

Angew. Chem. Int. Ed. **49**, 10.1002/anie.200906563; 10.1002/anie.200906602 (2010).

IMMUNOLOGY

Intestinal Goings-On

Allelic variants in the human interleukin-23 (IL-23) receptor are associated with susceptibility to several inflammatory diseases, such as psoriasis and inflammatory bowel disease. In mice, both T cell–dependent and T cell–independent "innate" models of colitis are driven by IL-23–mediated inflammation. In T cell–dependent models, IL-23–dependent inflammation is primarily the result of pro-inflammatory cytokine production by $CD4^+$ T helper type 17 (T_H17) cells.

The mechanistic basis for IL-23–driven innate colitis has not been determined.

Buonocore *et al.* show that, in a manner similar to that of T cell–dependent colitis, innate colitis is also driven by T_H17-associated pro-inflammatory cytokines. Rather than being produced by T cells, however, these cytokines are produced by a population of IL-23–responsive colonic lamina propria cells. These cells are similar in phenotype to lymphoid tissue inducer–like cells, which have previously been shown to produce T_H17-associated cytokines. Depletion of these cells led to abrogation of colitis, and the authors were able to confirm their results in another mouse model of innate colitis. These results suggest that the T_H17 gene expression profile is an important driver of intestinal inflammation in both the innate and adaptive immune systems. — KLM

Nature 10.1038/nature08949 (2010).

CELL BIOLOGY

The More the Merrier

Many biological processes are compartmentalized within the cell by restricting the localization of proteins and other molecules. The spatial organization of these compartments, often bounded by internal membranes, can facilitate the delicate control of complex processes—for instance, the transcription of DNA into RNA,

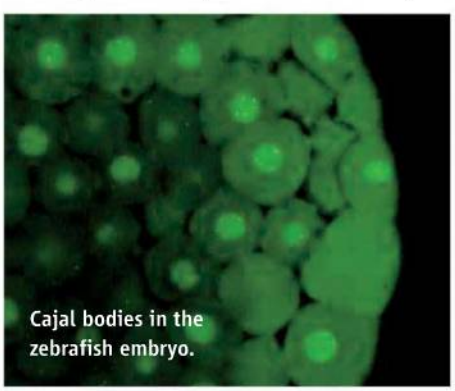

Cajal bodies in the zebrafish embryo.

CREDIT: MAGDALENA STRZELECKA

which occurs within the nucleus of eukaryotic cells. However, many non–membrane-bound intracellular compartments have known molecular compositions yet largely unknown functions. Studies attempting to identify their function by mutating or removing protein components to disrupt the compartment physically have been hard to interpret because of the apparent lack of phenotypic changes. This has led to speculation that this kind of compartmentalization may serve to increase the efficiency of an otherwise ongoing process, which may only become rate-limiting under rare physiological conditions. Strzelecka *et al.* have uncovered just such a critical role for coilin, which is a conserved component of Cajal bodies, during embryogenesis in zebrafish. Cajal bodies are 0.5- to 1-μm structures first described by Ramón y Cajal in 1903. They are found in the nuclei of plant and animal cells, most noticeably in those cells engaging intensely in transcription, and are composed of proteins and RNAs, such as the small nuclear ribonucleoprotein (snRNP) complexes that are important for pre-mRNA splicing. The snRNPs are complicated assemblies that undergo a multistep maturation process, which, it has been proposed, takes place in Cajal bodies. The authors depleted coilin in zebrafish embryos, which caused a disruption of Cajal bodies and the dispersal of snRNPs, before leading subsequently to cell death. These coilin morphants exhibited defective snRNP biogenesis and pre-mRNA splicing, which could be rescued by adding purified mature human snRNPs, revealing a role for coilin in snRNP biogenesis in the zebrafish embryo. The authors suggest that the formation of Cajal bodies concentrates snRNP components and promotes their faithful interaction, which is critical during early embryogenesis when transcriptional activity, and thus the need for snRNPs, is particularly high. These principles may be generally applicable to other non–membrane-bound subcellular compartments with currently unknown functions. — HP

Nat. Struct. Mol. Biol. **17**, 403 (2010).

CHEMISTRY

Location, Location, Location

Reductively coupling aldehydes with alkynes is a versatile means of preparing allylic alcohols. However, it has proven challenging to reliably select which of the two triply bonded carbon centers in the alkyne attacks the carbonyl. Modestly differing substituents at the two sites tend to induce a mixture of products, whereas substituents that favor one product have largely precluded access to the other by this route. Malik *et al.* show that careful ligand selection for a nickel catalyst can override such substrate preferences (or lack of preference) and thereby afford tunable control over the reaction's regiochemistry. They specifically screened a ligand set comprising three N-heterocyclic carbene scaffolds functionalized with a variety of bulky groups, and a fourth, less hindered cyclopropenyl derivative. The resulting catalysts permit selection of either alkynyl reaction site across a series of substitution patterns, with ratios in both directions ranging from 81:19 to >98:2. Yields for the room-temperature procedure ranged from 71 to 99%. — JSY

J. Am. Chem. Soc. **132**, 10.1021/ja102262v (2010).

www.sciencemag.org

Science

1200 New York Avenue, NW
Washington, DC 20005
Editorial: 202-326-6550, FAX 202-289-7562
News: 202-326-6581, FAX 202-371-9227
Bateman House, 82-88 Hills Road
Cambridge, UK CB2 1LQ
+44 (0) 1223 326500, FAX +44 (0) 1223 326501

Subscription Services For change of address, missing issues, new orders and renewals, and payment questions: 866-434-AAAS (2227) or 202-326-6417, FAX 202-842-1065. Mailing addresses: AAAS, P.O. Box 96178, Washington, DC 20090-6178 or AAAS Member Services, 1200 New York Avenue, NW, Washington, DC 20005

Institutional Site Licenses please call 202-326-6755 for any questions or information

Reprints: Author Inquiries 800-635-7181
Commercial Inquiries 803-359-4578

Permissions 202-326-7074, FAX 202-682-0816

Member Benefits AAAS/Barnes&Noble.com bookstore www.aaas.org/bn; AAAS Online Store www.apisource.com/aaas/ code MKB6; AAAS Travels: Betchart Expeditions 800-252-4910; Apple Store www.apple.com/eppstore/aaas; Bank of America MasterCard 1-800-833-6262 priority code FAA3YU; Cold Spring Harbor Laboratory Press Publications www.cshlpress.com/affiliates/aaas.htm; GEICO Auto Insurance www.geico.com/landingpage/go51.htm?logo=17624; Hertz 800-654-2200 CDP#343457; Office Depot https://bsd.officedepot.com/portalLogin.do; Seabury & Smith Life Insurance 800-424-9883; Subaru VIP Program 202-326-6417; VIP Moving Services www.vipmayflower.com/domestic/index.html; Other Benefits: AAAS Member Services 202-326-6417 or www.aaasmember.org.

science_editors@aaas.org	(for general editorial queries)
science_letters@aaas.org	(for queries about letters)
science_reviews@aaas.org	(for returning manuscript reviews)
science_bookrevs@aaas.org	(for book review queries)

Published by the American Association for the Advancement of Science (AAAS), *Science* serves its readers as a forum for the presentation and discussion of important issues related to the advancement of science, including the presentation of minority or conflicting points of view, rather than by publishing only material on which a consensus has been reached. Accordingly, all articles published in *Science*—including editorials, news and comment, and book reviews—are signed and reflect the individual views of the authors and not official points of view adopted by AAAS or the institutions with which the authors are affiliated.

AAAS was founded in 1848 and incorporated in 1874. Its mission is to advance science, engineering, and innovation throughout the world for the benefit of all people. The goals of the association are to: enhance communication among scientists, engineers, and the public; promote and defend the integrity of science and its use; strengthen support for the science and technology enterprise; provide a voice for science on societal issues; promote the responsible use of science in public policy; strengthen and diversify the science and technology workforce; foster education in science and technology for everyone; increase public engagement with science and technology; and advance international cooperation in science.

Information for Authors
See pages 352 and 353 of the 15 January 2010 issue or access www.sciencemag.org/about/authors

EDITOR-IN-CHIEF **Bruce Alberts**
EXECUTIVE EDITOR **Monica M. Bradford** NEWS EDITOR **Colin Norman**
MANAGING EDITOR, RESEARCH JOURNALS **Katrina L. Kelner**
DEPUTY EDITORS **R. Brooks Hanson, Barbara R. Jasny, Andrew M. Sugden**

Editorial senior editors/commentary Lisa D. Chong, Brad Wible; **senior editors** Gilbert J. Chin, Pamela J. Hines, Paula A. Kiberstis (Boston), Marc S. Lavine (Toronto), Beverly A. Purnell, L. Bryan Ray, Guy Riddihough, H. Jesse Smith, Phillip D. Szuromi (Tennessee), Valda Vinson, Jake S. Yeston; **associate editors** Kristen L. Mueller, Jelena Stajic, Nicholas S. Wigginton, Laura M. Zahn; **research associate** Alexis Wynne Mogul; **book review editor** Sherman J. Suter; **associate letters editor** Jennifer Sills; **editorial manager** Cara Tate; **senior copy editors** Jeffrey E. Cook, Cynthia Howe, Harry Jach, Lauren Kmec, Barbara P. Ordway, Trista Wagoner; **copy editor** Chris Filiatreau; **editorial coordinators** Carolyn Kyle, Beverly Shields; **publications assistants** Ramatoulaye Diop, Joi S. Granger, Emily Guise, Jeffrey Hearn, Michael Hicks, Lisa Johnson, Scott Miller, Jerry Richardson, Jennifer A. Seibert, Brian White, Anita Wynn; **editorial assistants** Emily C. Horton, Patricia M. Moore, Miriam Weinberg; **executive assistants** Alison Crawford; **administrative support** Maryrose Madrid; **editorial fellow** Melissa R. McCartney

Editorial director, web and new media Stewart Wills; **senior web editor** Tara S. Marathe; **web editor** Robert Frederick; **web development manager** Martyn Green; **web developer** Andrew Whitesell

News deputy news editors Robert Coontz, Eliot Marshall, Jeffrey Mervis, Leslie Roberts; **contributing editors** Elizabeth Culotta, Polly Shulman; **news writers** Yudhijit Bhattacharjee, Adrian Cho, Jennifer Couzin, David Grimm, Constance Holden, Jocelyn Kaiser, Richard A. Kerr, Eli Kintisch, Greg Miller, Elizabeth Pennisi, Robert F. Service (Pacific NW), Erik Stokstad, Jue Wang; **intern** Lauren Schenkman; **contributing correspondents** Jon Cohen (San Diego, CA), Daniel Ferber, Ann Gibbons, Sam Kean, Robert Koenig, Andrew Lawler, Mitch Leslie, Charles C. Mann, Virginia Morell, Gary Taubes; **copy editors** Linda B. Felaco, Melvin Gatling, Melissa Raimondi; **administrative support** Scherraine Mack; **bureaus** San Diego, CA: 760-942-3252, FAX 760-942-4979; Pacific Northwest: 503-963-1940

Production director James Landry; **senior manager** Wendy K. Shank; **assistant manager** Rebecca Doshi; **senior specialists** Steve Forrester, Chris Redwood, Anthony Rosen; **Preflight director** David M. Tompkins; **manager** Marcus Spiegler; **specialist** Jason Hillman

Art director Yael Kats; **associate art director** Laura Creveling; **senior illustrators** Chris Bickel, Katharine Sutliff; **illustrator** Yana Greenman; **senior art associates** Holly Bishop, Preston Huey, Nayomi Kevitiyagala; **art associates** Kay Engman, Matthew Twombly; **photo editor** Leslie Blizard

***Science* International**

Europe (science@science-int.co.uk) **editorial: international managing editor** Andrew M. Sugden; **senior editor/commentary** Julia Fahrenkamp-Uppenbrink; **senior editors** Caroline Ash, Stella M. Hurtley, Ian S. Osborne, Peter Stern; **associate editor** Maria Cruz; **locum editor** Helen Pickersgill; **editorial support** Deborah Dennison, Rachel Roberts, Alice Whaley; **administrative support** John Cannell, Janet Clements, Louise Hartwell; **news: europe news editor** John Travis; **deputy news editor** Daniel Clery; **contributing correspondents** Michael Balter (Paris), John Bohannon (Vienna), Martin Enserink (Amsterdam and Paris), Gretchen Vogel (Berlin); **intern** Tim Wogan

Latin America contributing correspondent Antonio Regalado

Asia Japan Office: Asca Corporation, Tomoko Furusawa, Rustic Bldg. 7F, 77 Tenjin-cho, Shinjuku-ku, Tokyo 162-0808, Japan; +81 3 6802 4616, FAX +81 3 6802 4615, inquiry@sciencemag.jp; **asia news editor** Richard Stone (Beijing: rstone@aaas.org); **contributing correspondents** Dennis Normile [Japan: +81 (0) 3 3391 0630, FAX +81 (0) 3 5936 3531; dnormile@gol.com]; Hao Xin [China: +86 (0) 10 6307 4439 or 6307 3676, FAX +86 (0) 10 6307 4358; cindyhao@gmail.com]; Pallava Bagla [South Asia: +91 (0) 11 2271 2896; pbagla@vsnl.com]

EXECUTIVE PUBLISHER **Alan I. Leshner**
PUBLISHER **Beth Rosner**

Fulfillment Systems and Operations (membership@aaas.org); **director** Waylon Butler; **customer service supervisor** Pat Butler; **specialists** Latoya Casteel, LaVonda Crawford, Vicki Linton, April Marshall; **data entry supervisor** Cynthia Johnson; **specialists** Shirlene Hall, Tarrika Hill, William Jones

Business Operations and Administration director Deborah Rivera-Wienhold; **business systems and financial analysis director** Randy Yi; **manager, business analysis** Eric Knott; **manager, business operations** Jessica Tierney; **financial analysts** Priti Pamnani, Celeste Troxler; **rights and permissions: administrator** Emilie David; **associate** Elizabeth Sandler; **marketing director** Ian King; **marketing managers** Allison Pritchard, Alison Chandler, Julianne Wielga; **marketing associates** Aimee Aponte, Mary Ellen Crowley, Wendy Wise; **senior marketing executive** Jennifer Reeves; **director, site licensing** Tom Ryan; **director, corporate relations** Eileen Bernadette Moran; **publisher relations, eresources specialist** Kiki Forsythe; **senior publisher relations specialist** Catherine Holland; **publisher relations, east coast** Phillip Smith; **publisher relations, west coast** Philip Tsolakidis; **fulfillment supervisor** Iquo Edim; **fulfillment coordinator** Carrie MacDonald; **marketing manager** Christina Schlecht; **electronic media: manager** Lizabeth Harman; **project manager** Trista Snyder; **assistant manager** Lisa Stanford; **senior production specialists** Ryan Atkins, Christopher Coleman, **computer specialist** Walter Jones; **production specialists** Nichele Johnston, Kimberly Oster; **director, web and new media** Will Collins

advertising director, worldwide ad sales Bill Moran
commercial editor Sean Sanders: 202-326-6430
project director, outreach Brianna Blaser

Product (science_advertising@aaas.org); **midwest** Rick Bongiovanni: 330-405-7080, FAX 330-405-7081; **east coast/e. canada** Laurie Faraday: 508-747-9395, FAX 617-507-8189; **west coast/w. canada** Lynne Stickrod: 415-931-9782, FAX 415-520-6940; **uk/europe/asia** Roger Goncalves: TEL/FAX +41 43 243 1358; **japan** ASCA Corporation, Nanako Ide +81 (0) 3 6802 4616, FAX +81 (0) 3 6802 4615; ads@sciencemag.jp; **senior traffic associate** Deiandra Simms

worldwide associate director of *Science* Careers Tracy Holmes: +44 (0) 1223 326525, FAX +44 (0) 1223 326532

Classified (advertise@sciencecareers.org); **u.s.: midwest/east coast** Tina Burks: 202-326-6577; **west/south central** Nicholas Hintibidze: 202-326-6533; **sales coordinators** Rohan Edmonson, Shirley Young; **europe/row sales:** Susanne Kharraz, Dan Pennington, Alex Palmer; **sales assistant** Lisa Patterson; **japan** ASCA Corporation, Jie Chin +81 (0) 3 6802 4616, FAX +81 (0) 3 6802 4615; careerads@sciencemag.jp; **advertising support manager** Karen Foote: 202-326-6740; **advertising production operations manager** Deborah Tompkins; **senior production specialist/graphic designer** Amy Hardcastle; **senior production specialist** Robert Buck; **senior traffic associate** Christine Hall

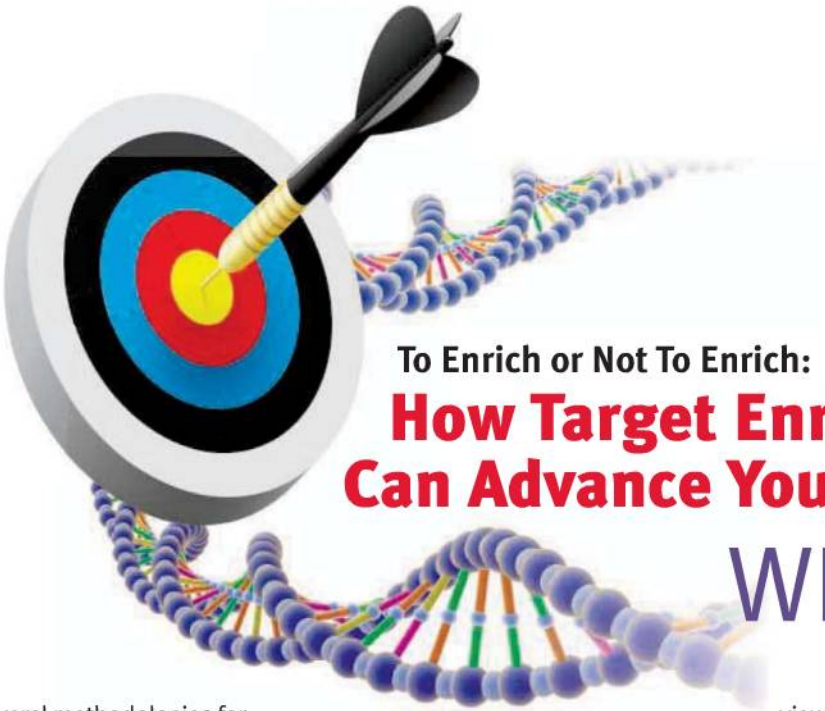

To Enrich or Not To Enrich:

How Target Enrichment Can Advance Your Research

WEBINAR

Several methodologies for performing DNA target enrichment prior to next generation sequencing have been developed and utilized in a growing number of experimental studies. As the price of next gen sequencing continues to fall, the debate around whether to perform some type of selection is ongoing.

A number of variables must be considered to make the best decision, including the number of samples, the amount of DNA available, the sequencing platform used, budget, reproducibility requirements, and the availability of automation. To clarify some of these issues, you are invited to view a discussion of the strategies for DNA target enrichment with our panel of distinguished thought leaders in a video webinar presented online and live at the AAAS headquarters in Washington, D.C.

During the webinar, the presenters:

- provide a general introduction to the target enrichment methods they use
- discuss how these technologies can be applied to the next gen sequencing workflow
- share data from studies that have benefited from their approaches

---

Recorded live on
Monday, April 19, 2010.
Now available on demand.

Watch our panel of experts
in this lively discussion.

www.sciencemag.org/webinar

Participating Experts:

Dr. Dale Hedges
Hussman Institute for Human Genomics
Miami, FL

Dr. Elaine Mardis
Washington University in St. Louis
St. Louis, MO

Dr. Jun S. Wei
National Institutes of Health
Bethesda, MD

Sponsored by:
Agilent Technologies

Science
AAAS

Brought to you by the *Science*/AAAS Business Office

EDITED BY LAUREN SCHENKMAN

FLIGHT PLAN

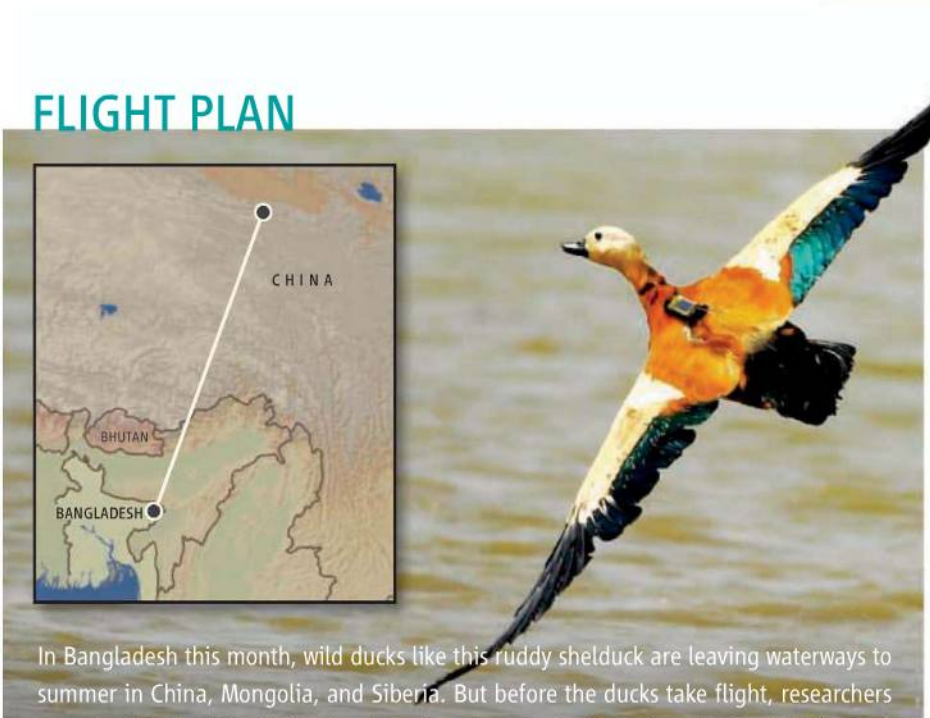

In Bangladesh this month, wild ducks like this ruddy shelduck are leaving waterways to summer in China, Mongolia, and Siberia. But before the ducks take flight, researchers organized by the Wildlife Trust and the Food and Agriculture Organization (FAO) of the United Nations are grabbing the ducks, swabbing their throats and rears to test for avian flu, and strapping satellite transmitters to their backs. The team will monitor the birds for a year, hoping to learn whether migrating birds spread the virus among countries with outbreaks, says molecular biologist and FAO team leader Mat Yamage.

CREDITS (TOP TO BOTTOM): SAMIUL MOHSANIN, WILDLIFE TRUST OF BANGLADESH; J. HEINTZ/UW, BBPIC, AND DEPARTMENT OF BACTERIOLOGY; ROCKY MOUNTAIN LABORATORIES, NIAID, NIH; THEMAGICISBAC.COM; (BOTTOM RIGHT) WEI FUWEN

Microbe Mascots

This month, Wisconsin became the first U.S. state to adopt an official microbe: *Lactococcus lactis*, the milk-curdling bacterium behind cheese. But researchers in other states are quick to suggest their own nominees.

For Hawaii, a state famous for species found nowhere else, microbiologist Stuart Donachie of the University of Hawaii, Manoa, suggests the ultrarare bacterium *Nesiotobacter exalbescens*, exclusive to a single lagoon on the uninhabited Laysan Atoll. Iowa might honor the nitrogen-fixing bacterium *Bradyrhizobium japonicum*, a soybean symbiont that "reduces nitrogen-fertilizer use yet allows the soybeans to grow tall and green and produce plenty of beans," says Joan Cunnick of Iowa State University in Ames.

Hog-farming North Carolina, on the other hand, "should impose the microbe non grata status" on food-poisoning bacterium *Salmonella typhimurium*, which colonizes livestock and contaminates meat, says José Bruno-Bárcena of North Carolina State University in Raleigh.

Wendy Schluchter of the University of New Orleans, Lakefront, harbors similar feelings toward sulfur-spouting *Acidithiobacillus ferrooxidans*, "a not-so-nice bacterium" that arrived in Chinese-made drywall used to rebuild Gulf Coast homes after Hurricane Katrina.

But microbes can have a bright side: Florida's tasty shrimp and eye-catching flamingos owe their stunning pinks to the carotenoid pigments in an alga at the bottom of the food chain, says Kathryn Jones of Florida State University in Tallahassee. *Dunaliella salina*, she says, "not only feeds Florida wildlife but makes it colorful and exciting."

Bruised Evidence

Forensic experts are routinely asked to tell the age of bruises from photographs of abuse and assault victims. Their opinions can put criminals behind bars, but a new study suggests that their expertise is not entirely beyond a reasonable doubt.

Peter Vanezis and his team of forensic medical scientists at Queen Mary, University of London, asked volunteers to bruise one of their upper arms with a suction pump. The team photographed the marks daily until they faded completely, amassing 132 photographs of 25 bruises that ranged from fresh to almost 9 days old.

Experts use color to estimate a bruise's age; bruises turn yellow as stale blood degrades. But when Vanezis's team asked 16 forensic medical examiners to date the bruises in the photographs, they were off by an average of 53 hours, the team reports in the April issue of the *Journal of Forensic and Legal Medicine*.

A photograph's lighting or exposure could alter bruise tone, explaining the errors, suggests Lawrence Kobilinsky, a forensic scientist at the John Jay College of Criminal Justice in New York City. But he stands by forensic bruise analysis: "My feeling is that as long as the report and testimony are given as a broad range of dates and is done conservatively, the judge and jury may trust the results."

Hope for Wild Pandas

China's government is moving to boost the country's smallest and most isolated population of giant pandas, after scientists warned that the animals could soon disappear.

Giant pandas are highly endangered, particularly in the Xiaoxiangling Mountains on the Tibetan plateau's eastern edge. When researchers led by ecologist Wei Fuwen of the Chinese Academy of Science's Institute of Zoology in Beijing screened DNA from 142 droppings collected from the area, they traced the scat to just 32 individuals.

Genetic analysis showed that the pandas' numbers had plummeted about 250 years ago, a time when Qing dynasty policies were encouraging farmers to settle the mountains. The booming human population's need for land and firewood whittled away the pandas' forest habitat by about 90% to two patches, split by a national highway, totaling 800 square km.

Unlike larger panda populations in other protected habitats, the Xiaoxiangling pandas don't have the numbers or the genetic diversity to survive long term without new blood, Wei's team argues in a paper published online this month in *Conservation Biology*. In response to preliminary results, the government moved one female panda to the area's Liziping reserve in April 2009.

"It's urgent to pay special attention to these kinds of isolated, small populations," says Wang Hao, a conservation biologist at Peking University, who was not involved in the work. But connecting and expanding the patches is also crucial, he says. Only then will "the increasing panda population have living space."

- **Manual dispensing**

- **Electronic dispensing**

- **Positive displacement tips**

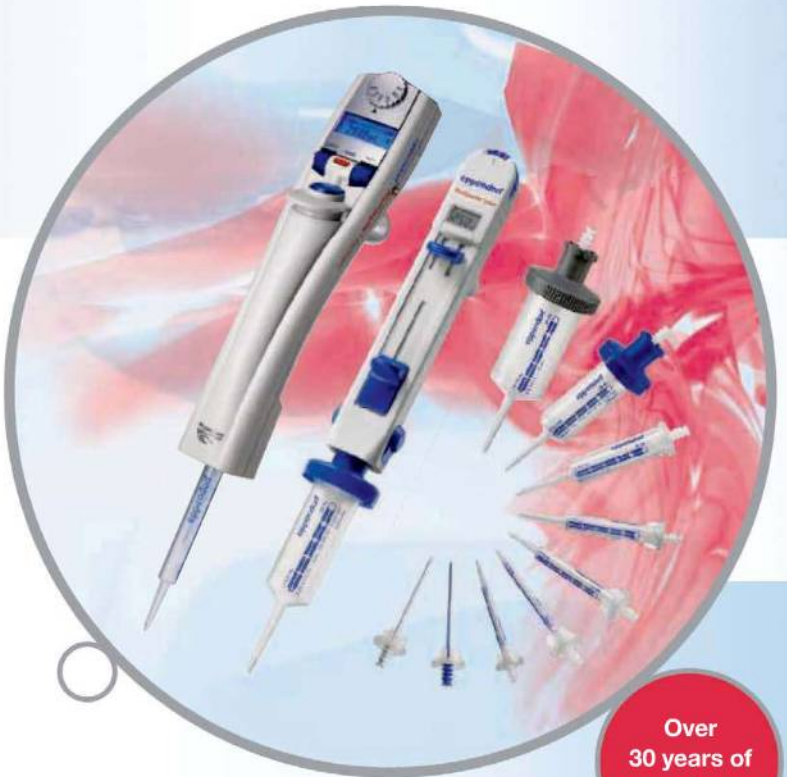

Over 30 years of experience

Performing for excellence

Serial dispensing at its best: Multipette®/Repeater®*

The Eppendorf Multipette/Repeater handheld dispensing system offers an outstanding range of benefits:

Together with Combitips plus®, both the electronic and manual hand dispenser, offers automatic tip recognition combined with an automatic volume calculation.
The positive displacement system ensures high-precision dispensing for all kinds of liquids including volatile and viscous solutions. 9 different sizes of tips offer a volume-range from 1 µL – 50 mL.

Easy volume setting

- Multipette/Repeater plus: 1 µL – 10 mL
- stream/Xstream: 1 µL – 50 mL

Up to 100 dispensing steps without stopping

- Multipette/Repeater plus:
  20 different adjustable volumes per tip
- stream/Xstream:
  1,000 different adjustable volumes per tip

For more information visit **www.eppendorf.com/mpplus**
or **www.eppendorf.com/mpxstream**

eppendorf
In touch with life

Your local distributor www.eppendorf.com/worldwide · **Application Support** E-mail: support@eppendorf.com
Eppendorf AG · Hamburg · Germany · Tel: +49 40 538 01-0 · Eppendorf North America, Inc. · USA · Tel: +1 800 645 3050 menu option 2

MARINE BIOLOGY

Deal to Legalize Whaling Would Sideline Science

The commercial killing of whales has been banned since 1986 by a body called the International Whaling Commission (IWC). At the time, commercial whaling had driven many whale populations nearly to extinction. But that ban was hobbled by several exceptions. Since then, a trio of whaling nations has killed more and more whales through the controversial loopholes, including research. "There isn't a real moratorium," says Monica Medina, the head of the U.S. delegation to IWC. And IWC itself has been riven by internal tensions between those who want to save whales and those who aim to hunt them.

Now, in a bid to tighten the organization's grip on its members' whaling and reduce the number of whales killed, IWC Chair Cristián Maquieira of Chile has proposed a controversial deal. In exchange for temporarily narrowing the loopholes, Japan, Norway, and Iceland would be allowed to commercially hunt whales for 10 years.

The draft proposal—and the catch limits that Maquieira unveiled in Washington, D.C., last week—have inflamed conservationists. They fear that legalizing any form of commercial whaling will open the door to other nations and ultimately lead to more, not fewer, whale deaths. "This is a bad deal for whales," says Patrick Ramage, global whale program manager for the International Fund for Animal Welfare in Yarmouth Port, Massachusetts. And several scientists on IWC's Scientific Committee charge that the proposed catch limits are not based on science—a stinging rebuke, since IWC's charter requires it to make its decisions using scientific findings.

The proposal is designed to give IWC more authority over whaling by restricting the loopholes for a decade, in particular the controversial research exemption (*Science*, 27 April 2007, p. 532). It should also significantly reduce the number of whales being killed, says Maquieira. Nearly 1700 whales were harpooned last year, up from 300 in 1990. Using the research exemption, Japan killed about half of those 1700 whales, taking more than 500 Antarctic minke whales alone in the Southern Ocean Sanctuary. The plan would limit Japan's minke kills to 400 annually for the first 5 years, and then to 200. It would also increase Japan's fin whale quota in the sanctuary to 10. (Last year, Japan killed one.)

Scientists say some of the proposed quotas were arrived at with little or no input from the scientific committee. In addition, the plan would permit Japan to commercially harpoon 120 common minkes annually in its coastal waters, from a population that many suspect is in trouble. Japan already kills more than 120 minkes there as by-catch, a term for accidental capture in fishing gear. "There's nothing in the proposal to limit the number of whales taken this way," points out Scott Baker, a conservation geneticist at Oregon State University in Newport and a U.S. delegate to the scientific committee. That means the number of whales caught from this population is likely to go up.

Other experts on IWC's Scientific Committee are not impressed, either. "The proposal is designed to look scientific," says Justin Cooke, a mathematical modeler in Freiburg, Germany, who represents the International Union for Conservation of Nature. "But when you look at it carefully, you realize it doesn't provide any place for the input of scientific advice."

For instance, although the draft mentions the committee's procedure for determining sustainable catch levels, it's ambiguous whether those methods will be used, says Cooke. Instead, annual catch limits will apparently be negotiated, then remain fixed for 10 years. It's uncertain if the quotas would be revised during that period, even if new scientific data warrant a change.

Maquieira counters that several key parts of the agreement, such as compelling whaling vessels to carry tracking devices and independent observers, come from the recommendations of IWC's Scientific Committee. The tracking data and observers' reports would show that whalers are abiding by their quotas, he says. The proposal also calls for the whaling nations to carry out market surveys of whale meat and establish a DNA registry to make sure only certain species are hunted. But it's not clear who would do this. "If it's the whaling country itself, then it won't work," Baker says. "It won't be the independent, transparent process it has to be to assure true compliance."

In another compromise, the proposal would create an enormous sanctuary for whales in the south Atlantic Ocean, running from the equator at Brazil to Tierra del Fuego and to West Africa, but would allow Japan to continue to hunt minke and fin whales in the existing Southern Ocean Sanctuary of Antarctica.

Negotiations on these and other issues are expected to continue right up to IWC's full meeting in late June in Agadir, Morocco. The proposal must then win the approval of three-quarters of the members, and ratification is far from certain. Although Japan, Norway, and Iceland have not commented publicly, Australia's Environment Minister, Peter Garrett, has called the plan unacceptable, and New Zealand has called it inflammatory. The United States is "carefully reviewing" the proposal, Medina says.

Already, conservation organizations are lobbying hard against the draft agreement and its catch limits. "They don't really reduce whaling but legitimize it," says Ramage. Even though the agreement would prohibit other member nations from beginning whaling, South Korea, perhaps sensing an opening, has already submitted a request to do just that.

–VIRGINIA MORELL

Slippery slope? Some experts fear a draft plan to eliminate research whaling will lead to more deaths, like those of this minke whale and her calf.

CREDIT: AUSTRALIAN CUSTOMS/SIPA/NEWSCOM

Plague risk in China 559

Antimatter probe delayed 561

SOCIAL SCIENCE

Survey to Reveal True Face of Chinese Society

For decades, social scientists looking for figures from China were hamstrung. The Chinese government collects copious data, but much is secret, and what isn't classified is often unreliable. The imperfect solution, more often than not, has been for researchers to go knocking on doors themselves.

This approach changed this month as scores of interviewers dispersed across China for the start of a study that aims to document everything from emotional stress to family planning (see table). They expect to reach 60,000 respondents in 25 provinces—making the survey the largest undertaking of its kind in the developing world. "This is just mammoth compared to other studies," says Robert Hauser, a demographer at the University of Wisconsin, Madison, who advised the survey's designers.

The Chinese Family Panel Studies, as the project is called, should provide abundant fodder for data-starved social scientists hoping to track how China's rapid development is shaping societal values, says Yu Xie, a sociologist at the University of Michigan, Ann Arbor, and Peking University who designed much of the new survey. Through this year's baseline survey and annual follow-up visits, he says, "we are going to be able to document some of the biggest changes in history."

The $8.8 million survey is broad as well as deep. Comparable U.S. efforts are often funded by government agencies seeking specific data, and as a result they home in on specific age groups or topics. The government-backed Chinese survey, by contrast, was crafted by scholars to fill myriad holes in social science data, meaning it will expand the body of information on China in one fell swoop. To achieve that range, interviewers are questioning every member of each household they visit.

The survey's architects hope that the extensive interviews will help build a vivid portrait of Chinese society. And a design modeled after similar studies in the West means demographers and sociologists will be able to use the results to compare across cultures, says Hauser: "It will really improve the quality of data worldwide."

Chinese family values

Not long ago, the Chinese government viewed most of the social sciences with suspicion. But by 2004, top leaders were bemoaning gaps in information as they sought to maintain social stability, sociologists say. With their university flush with research money, scholars from four Peking University departments convened to discuss the data dearth. They seized on the idea of a major panel survey and turned to Xie, who had experience with the University of Michigan's ongoing Panel Study of Income Dynamics, for help implementing it. What once might have been a prohibitively sensitive survey became a darling of China's most prestigious university.

After securing local backing for a new research center—Peking University's Institute of Social Science Survey (ISSS) in Beijing—the Chinese scholars sought input from abroad. In addition to the Michigan survey, they looked at the British Household Panel Survey, the Taiwanese Panel Study of Family Dynamics, and the German Socio-Economic Panel Study, says ISSS director and survey co–principal investigator Qiu Zeqi. Xie and colleagues borrowed elements from all these efforts, then adapted questions and methodology to the rapidly developing country.

China's effort has constraints. It steers clear of questions about the one-child policy, ethnicity, and politics. Minority regions like Tibet, Xinjiang, and Inner Mongolia are excluded, although Xie says this is mainly a logistical matter: Sending interviewers to query nomads on the Tibetan plateau, for instance, would be too costly.

Although some hot-button issues remain off limits, the project does address subjects such as quality of life, social service needs, and the rich-poor gap. In addition to using specialized survey software, a 380-strong army of interviewers has been trained to "observe how wealthy the family is, how they interact, how clean the house is," says Xie. The robust design allows researchers to analyze dynamics within families as well as make comparisons across neighborhoods, says demographer Robert Mare, president of the Population Association of America, who is not affiliated with the project. "Social scientists in the U.S. are very excited that this study will be carried out," he says.

In preparation for the project, the Chinese team in 2008 and 2009 conducted a pilot survey of more than 2300 households in Beijing, Shanghai, and Guangdong Province. Their findings, which are available upon request from ISSS, suggest that the economic reality in those major urban cen-

Going door to door. Chief survey designer Yu Xie queries a Gansu Province villager about his health and wealth.

A SLICE OF LIFE IN CHINA

Questionnaire	Examples of topics
Community	Water sources, employment stats, election participation, housing prices, medical facilities, family planning, income and expenditures
Household	Child care, family and friend networks, household economy, cost of living, family business ownership
Adult	Education, marital status, military experience, employment, transportation, *guanxi* (social networks), life satisfaction, confidence in the future, medical expenses, exercise, diet and nutrition
Adolescent	School enrollment, language use, parental supervision, allowance, leisure activities, dating
Interviewer Perceptions	Interviewee's behavior, household member relationships (e.g., estranged, authoritative, gender-equal), community conditions

CREDITS: (PHOTO AND TABLE) YU XIE/UNIVERSITY OF MICHIGAN

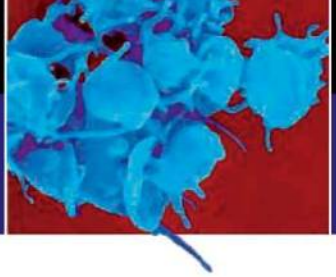

Multitasking platelets
562

Japan rescues asteroid mission
565

ters is a far cry from the picture frequently painted of China's boom.

Marketing executives often rhapsodize about the appetite for luxury goods among urban Chinese. But the pilot survey showed that even in developed areas like Beijing, Shanghai, and Guangdong, über-consumers are a small percentage of the population. In 2009, an average of 80% of residents' expenditures went toward basics such as food, housing, and transportation. These burdens were unequally distributed, moreover: Rural people spent considerably more on health care than did city dwellers. (Both Beijing and Shanghai are administrative areas with both rural and urban populations.) Only 45% of respondents said they were satisfied with their lives, with more Beijingers describing themselves as happier on the whole than did residents of other areas.

Expanding those inquiries nationwide will be far from easy. "One of the challenges is how to track people" for follow-up visits, says Qiu. Many rural Chinese lack home phones and change cell phone numbers frequently, and some 150 million to 180 million people migrate from the countryside to the cities for work. The solution, says Qiu, is to record contact information for three friends or relatives of each respondent. That safeguard proved invaluable during the pilot survey, when interviewers returning to study areas discovered that whole villages had been relocated to make way for construction projects. In the end, the team managed to track down about 80% of respondents.

That success rate bodes well for the Family Panel Studies, which aim to gather data from a representative sample that would cover 95% of the population. True advances may be years down the line, when data allow for comparisons over time. But scholars are already excited. "This survey will show us societal development from individuals' perspectives," says Ren Qiang, a sociologist at Peking University. That puts it far ahead of previous Chinese efforts, he says. "It's much, much better than what we had before."

–MARA HVISTENDAHL

Mara Hvistendahl is a writer based in Rotterdam, the Netherlands.

GENOMICS

Frog DNA Yields Clues to Vertebrate Genome Evolution

Add another group of animals to the growing menagerie of creatures whose genomes have been sequenced. On page 633 of this issue, Uffe Hellsten, a bioinformaticist at Lawrence Berkeley National Laboratory in California, and his colleagues describe the sequence of the Western clawed frog, *Xenopus tropicalis*, the first member of the amphibian branch of the tree of life to be so honored.

Amphibians branched off from other vertebrates about 350 million years ago, and the group has been evolving along a path separate from mammals, reptiles, and birds ever since. "For this reason, the frog genome sequence provides unique insights into genome dynamics over an extended period of evolution," says Ben Evans of McMaster University in Hamilton, Canada. "It fills in a crucial gap in our understanding of genome diversity and evolution of organisms," adds David Cannatella, an evolutionary biologist at the University of Texas, Austin.

The draft of the genome is in hundreds of pieces—not complete enough to be ordered chromosome by chromosome, but Hellsten and colleagues were able to match long stretches of contiguous sequence with equivalent sequences in the chicken and human genomes. A 150-million-base region in the center of human chromosome 1, for example, has a virtually identical counterpart in the frog and chicken genomes. "That implies that whole region has remained intact for 350 million years," says Hellsten, and it represents an ancient chromosome. Other matchups indicated that three stretches of DNA fused onto human chromosome 1 after breaking off from elsewhere in the genome. Another intact region in chicken and frog split up in the human genome and spread across six chromosomes. "There appears to have been more frequent chromosome fusion and fission in mammals than in birds and frogs," says Evans.

Floating to fame. An aquatic frog, the Western clawed frog, now has a sequenced genome.

The frog genome may offer new insights for not only evolutionary biologists but also biomedical scientists. It has 1700 genes that have been linked to human diseases such as type 2 diabetes, acute myeloid leukemia, alcoholism, sudden infant death syndrome, and congenital muscular dystrophy. These can be investigated using the frog to probe the basic mechanisms by which these genes work. "It opens a large number of doors for comparative and functional genomics," says Erica Bree Rosenblum, an evolutionary biologist at the University of Idaho, Moscow.

Researchers chose *X. tropicalis* to be the first amphibian sequenced because developmental biologists use it in their studies and it has a relatively small genome: 1.7 billion bases stretched across 10 chromosomes, about half the size of the human genome. Now, researchers are hungry for more. "One species of frog does not allow one to say very much about frogs," says Cannatella. Others point out that *Xenopus* is unusual among frogs, so "now they need to do a typical frog," says David Wake, an evolutionary biologist at the University of California, Berkeley. Cannatella would like to see the fire-bellied toad, *Bombina orientalis*, sequenced next.

Nonetheless, says Stephen O'Brien, a geneticist at the National Cancer Institute branch in Frederick, Maryland, this *Xenopus* genome "is an important beginning and a treat for comparative genomics."

–ELIZABETH PENNISI

CREDIT: DAVID CANNATELLA/UNIVERSITY OF TEXAS

ETHICS

DNA Returned to Tribe, Raising Questions About Consent

A tiny tribe of Native Americans who live beneath the cliffs of the Grand Canyon is shaking up genetics research, thanks to an unusual out-of-court agreement with Arizona State University (ASU). Tribe members charged that their DNA had been collected by university researchers without proper consent; after a 6-year legal battle, the university has now agreed—among other concessions—to return more than 100 DNA samples to the Havasupai and pay $700,000.

Although some tribe members had signed consent forms allowing blood samples collected 20 years ago to be studied broadly, they claimed in court that they had been told that the DNA would be used only for diabetes research. In fact, the data were used for a variety of studies. The outcome suggests that consent forms alone may not be enough to ensure that subjects understand how their samples may be used or to protect researchers.

Six-year battle. Havasupai tribe member Rex Tilousi speaks after Arizona State University agreed to return DNA research samples and pay a cash settlement.

The case may seem a footnote to popular medical studies that collect DNA and health information from thousands of people in the hunt for new disease genes. But to dismiss it as a story about Native American beliefs "would be unfortunate," says Hank Greely, a law professor at Stanford University in Palo Alto, California, who has followed the case closely. "The same sort of thing can happen to any of us."

DNA samples matched with health histories are a precious resource, Greely says. Researchers are driven to use them as broadly as they can—whether to help ailing patients or to win tenure and grants. Pressure also comes from funding agencies, which demand that such data be shared, including through a database housed at the U.S. National Institutes of Health (NIH) called dbGaP. NIH requires that researchers it funds for genome-wide association studies, which scan large stretches of the genome for disease DNA, deposit data in dbGaP. The agency is considering a similar requirement for all genomic data, says Laura Rodriguez, a genetics policy staffer at the National Human Genome Research Institute in Bethesda, Maryland, who helped design dbGaP.

The Havasupai case is unique in some ways. Tribe members alleged that the samples were used for schizophrenia and ancestry studies that were deeply offensive to them. (The lead researcher, Therese Markow, now at the University of California, San Diego, denies that any schizophrenia work was conducted.) Lawsuits filed by the Havasupai, seeking more than $50 million in damages, claimed that researchers took tribe members' blood without informed consent. Markow strongly denies that charge; those who gave blood samples, she said in an interview, signed broad consent forms, and "a huge explanation was given about the kinds of research that might be done."

Nonetheless, an uproar ensued. The Havasupai case has led other Indian tribes to refuse to participate in research. It also illustrates that "consent is not a form, it's a process," says Greely, who believes the tribe members didn't realize there might be any studies beyond diabetes, even years later. One alternative strategy for DNA research, described in a 2006 paper by a Canadian geneticist who works with aboriginal communities, is that individuals loan DNA for specific studies and retrieve their samples when the research is complete. "Research subjects need to have some ability to assert their property interests in their own biological samples," says Kimberly TallBear, who studies the role of science and technology in Native American governance at the University of California, Berkeley.

People who use dbGaP are well aware that they must be cautious about studies that go beyond the original intent for a particular set of genetic and health data. There are "multiple and specific checks of this exact issue, who's allowed to access the samples and for what purpose," says David Altshuler of the Broad Institute in Cambridge, Massachusetts, who serves on a dbGaP working group. In some cases, data are restricted to certain types of studies, such as those pertaining to health but not ancestry. All dbGaP data—and most genetics information in other data banks worldwide—are stripped of identifiers.

Most individuals who contribute their DNA, some studies have found, want science to benefit broadly and are not interested in being contacted for additional consent. But others may feel differently. Last year, a group from the state of Washington reported at the American Society of Human Genetics meeting that some volunteers had qualms about plans to put data from an Alzheimer's study in dbGaP. The local institutional review board had required that study leaders first ask subjects' permission, an unusual request. Of the 1340 surveyed, 88% consented, while 9.5% refused. The researchers were struck that even those who agreed were grateful to have been asked.

Consent forms may talk in general terms about future use of data without explicitly mentioning dbGaP or other databases—in part because these data banks didn't exist when many forms were drawn up. The generic approach seemed sufficient in the past: "There was this perception that if we go back and ask [participants], and they all say yes, did we really need to bother?" says S. Malia Fullerton, a bioethicist at the University of Washington, Seattle, who participated in the Alzheimer's work. "That's been driving a lot of thinking in the policy arena." But, she says, researchers may want to reconsider. Given that dbGaP now includes data from 188,000 individuals, if even a few percent don't want it there, "that's a lot of people," says Greely.

"Scientists had better be paying attention" to the Havasupai case, "and they better think how [their work] would look if publicized," says Ellen Wright Clayton, who directs the Center for Biomedical Ethics and Society at Vanderbilt University in Nashville, Tennessee. Losing the trust of research participants would decimate genetics studies, she and others note—and such trust wouldn't be easy to regain. **–JENNIFER COUZIN-FRANKEL**

CREDIT: ROSS D. FRANKLIN/AP PHOTO

Once bitten, twice shy. With care, researchers attempt to catch fleas at a marmot burrow in Qinghai.

CREDIT: COURTESY OF CHINESE CDC

CHINA

Race to Contain Plague in Quake Zone

BEIJING—Disease specialists have launched an emergency operation in western China to avert a possible outbreak of pneumonic plague in the wake of a magnitude-6.9 earthquake in Qinghai Province.

The 13 April quake, centered in Yushu County in southeastern Qinghai, killed 2220 people and left about 100,000 homeless. As relief crews race to shelter survivors and cremate victims, the Chinese Center for Disease Control and Prevention (CDC) this week dispatched to Qinghai a mobile biosafety level 3 (BSL-3) laboratory, capable of safely handling the most dangerous pathogens. The agency acquired the lab after the SARS epidemic in 2003; this is the first time it has been deployed. "We'll do whatever it takes to prevent an outbreak," says Xu Jianguo, director of CDC's National Institute for Communicable Disease Control and Prevention (NICDC) in Beijing.

Plague is endemic in 10 Chinese provinces; in Qinghai, it is spread by marmots, a burrowing rodent. In a typical year, western China reports a handful of plague cases, and most victims are marmot hunters. People bitten by fleas carrying *Yersinia pestis* can develop bubonic plague—the medieval Black Death—whereas those who inhale the bacterium can contract the pneumonic form. Both forms of the disease can be cured if antibiotics are given early, but pneumonic plague poses a greater threat because it spreads from person to person. The Yushu earthquake has created favorable conditions for pneumonic plague, says Nils Christian Stenseth, an ecologist at the University of Oslo who studies plague in China and Central Asia. He sees the potential for "a rather serious outbreak."

Like clockwork at about the end of April, marmots awaken from hibernation on the Qinghai-Tibetan Plateau. One scenario that Stenseth and others fear is that fleas will jump from infected marmots to rats and then to stray dogs and cats. An outbreak could spread quickly among survivors huddled in shelters.

A few dozen researchers from NICDC and the Qinghai Institute for Endemic Diseases Prevention and Control in Xining, Qinghai's capital, have fanned out in the quake-affected area. It hasn't been easy for plague watchers: Last week, one NICDC scientist came down with altitude sickness and had to return to Beijing. In Yushu, the quake damaged a plague-monitoring station; its staff remain unaccounted for as *Science* went to press.

Only about 40 plague cases have been reported in Yushu County in the past half-century, says NICDC senior plague specialist Yu Dongcheng. Of particular concern, he says, is the virulence of Qinghai's *Y. pestis* strain. "Inhaling even a single cell can cause disease," asserts Yu. In comparison, he says, it typically requires a few hundred cells of strains in neighboring Yunnan Province to cause disease. Thanks to the mobile BSL-3 lab—one trailer with a positive-air-pressure lab chamber, and a second carrying the generator and water—"we'll be able to do experiments that we can't normally do in the field," says Xu, such as isolating *Y. pestis* and running polymerase chain reaction tests.

Prevention is a tall order. Marmot hunting has been banned, but pelts are valuable: Fur coats fetch more than $1000. Increasing the temptation, marmots ill with plague are easy to catch, says Yu. To limit marmot-human contact, researchers will cordon off plague-infested marmot burrows. It will be impossible to maintain a vigil on all marmots and animals they might come into contact with. "But if there are any human cases, we'll know," Yu says. Only in September, when marmots hibernate for the winter, can researchers let down their guard. **–RICHARD STONE**

ScienceNOW

From *Science*'s Online Daily News Site

Chimps Grieve Over Dead Relatives
New studies of chimpanzees conclude that our closest evolutionary cousins share many humanlike responses to death, including mourning. The work is some of the first evidence of grieving in animals other than humans, and it suggests that chimps may be more emotionally affected by death than many researchers realized. http://bit.ly/chimpgrief

Dark Matter Halos Look a Bit Like a Football
Dark matter is distributed throughout the universe in giant, football-shaped clumps, according to new, indirect images of the mysterious substance that holds galaxies and galaxy clusters together. The work provides more evidence that dark matter, even on the largest scale, strongly affects the visible cosmos with its gravity, although it remains remarkably unaffected in return. http://bit.ly/darkmatter-footballs

Elephants Have an Alarm Call for Bees
East Africa's elephants face few threats in their savanna home, aside from humans and lions. But the behemoths are terrified of African bees, and with good reason. An angry swarm can sting elephants around their eyes and inside their trunks and pierce the skin of young calves. Now, a new study shows that the pachyderms utter a distinctive rumble in response to the sound of bees, the first time an alarm call has been identified in elephants. http://bit.ly/elephantalarm

Did Monster Eruptions Warm the World?
Talk about global warming. About 55 million years ago, the planet's temperature jumped by as much as 5°C and remained that way for about 170,000 years. Thousands of primitive marine species vanished. But the event also coincided with an unsurpassed era of plant diversity as well as the rise of mammals. Now, researchers think they've figured out what caused the hothouse: A series of massive undersea eruptions may have saturated the air with perhaps trillions of tons of methane—a much more potent greenhouse gas than carbon dioxide. http://bit.ly/monstereruptions

Read the full postings, comments, and more at **news.sciencemag.org/sciencenow.**

SCIENTIFIC FREEDOM

Iran Faculty Dismissals Seen as Result of New Policy

Iran's government has begun to remove academics who oppose the authoritarian regime of President Mahmoud Ahmedinijad, according to human-rights activists in the country. Activists say that the dismissal this month of two electrical engineering professors at the Iran University of Science and Technology in Tehran is consistent with a recent edict by the Iranian science minister to fire faculty members who do not share "the regime's direction."

Science was unable to ascertain the official reason for the 13 April firings of S. Ali-Asghar Beheshti Shirazi, an expert in telecommunications, and his colleague, Alireza Mohammad Shahri, who, among other things, studies the detection of landmines. But human-rights activists say the pair were among 56 faculty members at the university who signed a 10 January letter to the chancellor decrying disciplinary actions taken against students who had participated in political protests on campus. The letter also expressed unhappiness over the beatings of protesters by outsiders, noting that universities needed to be maintained as "a place for political growth and social growth for students."

Hadi Ghaemi, the New York City–based executive director of the International Campaign for Human Rights in Iran (ICHRI), says the 5 April ouster of Morteza Mardiha, a philosophy professor at Allameh Tabataba'i University, is another example of the government crackdown. Ghaemi points to a 4 March statement by Kamran Daneshjoo, Iran's minister of science, research, and technology, that faculty members who do not share "the regime's direction" and are not committed to the rule of the Supreme Leader would be fired. In addition to the firings, ICHRI claims that more than 50 prominent faculty members who are sympathetic to the reformist movement have been forced to retire over the past year.

No tolerance. Kamran Daneshjoo, Iran's science minister, says academics who oppose the regime will be fired.

In parallel, the Iranian government appears to have opened the door to hiring and promoting faculty members who openly endorse the regime. *Science* has obtained a recent directive from the science ministry to universities describing procedures for evaluating existing faculty members and applicants. One form, titled "scientific qualifications," lists academic criteria such as scientific publications and conference presentations. The other, titled "general qualifications," ticks off some 17 criteria, including belief in the system of the Islamic Republic, being active in a local mosque, and cooperating with the institutions representing the Supreme Leader. The memo includes a form addressed to the intelligence ministry, asking for a report on the applicant's political and social background.

This new evaluation process "opens up the system to political influence," says Farhad Ardalan, a physicist who retired last year from Sharif University and is now a researcher at the Institute for Research in Fundamental Sciences in Tehran. "They have lowered the minimum so much that pretty much anybody could be hired," he says. "It's the worst thing that has happened to Iranian universities in the past 30 years." Adds Ghaemi, "These policies will cause severe damage to the quality and reputation of Iranian academic institutions."

–YUDHIJIT BHATTACHARJEE

SCIENTIFIC COMMUNITY

Paul Nurse Chosen to Head Royal Society

Nobel Prize–winning biologist Paul Nurse is stepping down as president of Rockefeller University in New York City to become president of the Royal Society in London, the United Kingdom's science academy. Last week, the society's council nominated Nurse to succeed University of Cambridge astrophysicist Martin Rees, who ends his 5-year term in November. The society's 1327 fellows will vote in July.

The presidency of the 350-year-old Royal Society traditionally rotates between a biologist and a physical scientist. The council chose Nurse "with huge enthusiasm," says member Matthew Freeman, a cell biologist at the Medical Research Council Laboratory of Molecular Biology in Cambridge, U.K.

Home again. Nurse headed for London.

Nurse, 61, a British geneticist and cell biologist, shared the 2001 Nobel Prize in physiology or medicine with Leland Hartwell and Timothy Hunt for studies of cell cycle regulation. He came to Rockefeller in 2003 after serving as CEO of Cancer Research UK. Nurse will return to the United Kingdom at the end of this year but plans to maintain his 14-member yeast genetics and cell biology lab at Rockefeller. In a statement released by Rockefeller, Nurse said that his position as both leader and researcher at Rockefeller has been "ideal" and that "the decision to step down from the presidency is a very difficult one."

Nurse has an "astute political sense and ability to make a robust defense of the importance of fundamental research," Freeman says. In addition to his scientific and administrative skills, he says, Nurse has also been "very involved" in engaging with the public on scientific issues. University of Oxford theoretical ecologist Robert May, who preceded Rees, calls Nurse "a standout choice."

Although Nurse's predecessors continued to do science, they worked in theoretical areas. Nurse's decision to keep his U.S. biology lab may pose a greater challenge, May says. But "a well-organized person can do both."

–JOCELYN KAISER

CREDITS (TOP TO BOTTOM): RAHEB HOMAVANDI/REUTERS/LANDOV; ZACH VEILLEUX/THE ROCKEFELLER UNIVERSITY

SPACE PHYSICS

Redesign Postpones Launch of Long-Delayed Space Station Experiment

Driven and independent, Samuel C. C. Ting has campaigned for 16 years to send a massive particle detector to the International Space Station. But just as researchers are preparing the $1.5 billion, 7.5-ton Alpha Magnetic Spectrometer (AMS) for liftoff on the last flight of NASA's space shuttle, Ting, a Nobel Prize–winning physicist at the Massachusetts Institute of Technology in Cambridge, has decided to swap out a key piece of hardware. That change will delay the launch, which was scheduled for 29 July, by months. But Ting says the change will prolong AMS's lifetime by many years, and those who know him say the move is likely not as rash as it appears.

"I would never bet against Sam Ting," says Nicholas Samios, a physicist at Brookhaven National Laboratory in Upton, New York. "He's very aggressive," Samios says. But "he's a very careful guy, meticulous."

Proposed in 1994, AMS will search for antimatter lingering from the big bang, particles of dark matter, and other oddities by identifying every charged that passes through it. To distinguish electrons from positrons and iron nuclei from nickel, it measures how each particle's path bends in a magnetic field. The field was supposed to come from a 2350-kilogram superconducting coil that would generate a field about 17,000 times as strong as Earth's field. Now, Ting has decided to use a permanent magnet—akin to one on your refrigerator—that has a field one-fifth as strong and was used in a 1998 test run aboard the space shuttle. "The decision was fundamentally made by me," Ting says.

Part of the reason for the swap is because the superconducting coil generates more heat than expected. It must be chilled to nearly absolute zero with liquid helium, and the plan was to send along 2500 liters of liquid to keep AMS cold for 3 years. But recent tests at the European Space Agency's research and technology center in Noordwijk, Netherlands, suggest that AMS would boil off its helium in about 20 months, Ting says.

However, a bigger reason for the change is that revised plans for the space station give AMS a chance to run even longer than 3 years, Ting says. NASA had planned to "deorbit" the space station in 2015, but in February officials announced plans to keep it aloft until at least 2020. AMS could keep running all those extra years but only if scientists switch to the permanent magnet, which needs no coolant. Otherwise, "after 3 years we'd have a museum piece up there," Ting says.

The switch to the weaker magnet will slightly diminish AMS's ability to measure a particle's mass and to study really heavy ones. Still, "AMS is 100 times better than any other particle detector that's ever been put into space," says Jack Sandweiss, an AMS collaborator at Yale University.

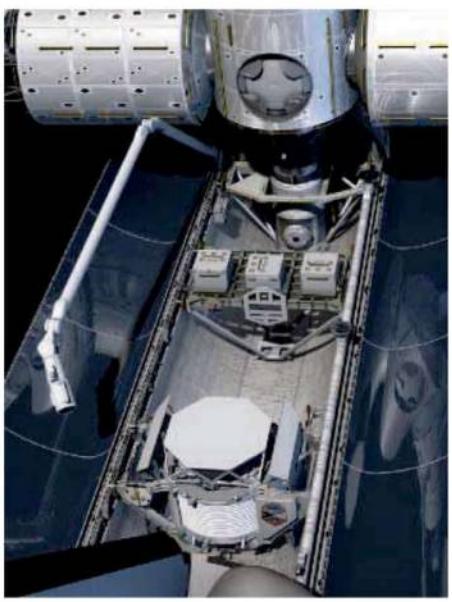

CREDIT: NASA

Someday. NASA's space shuttle will deliver the Alpha Magnetic Spectrometer (octagonal apparatus) to the International Space Station, as in this drawing.

The flash retrofit will be a challenge, but Trent Martin, AMS project manager at NASA's Johnson Space Center in Houston, Texas, thinks researchers can pull it off. "I spent the last 3 weeks in Europe looking at whether this is possible, and I'm comfortable that they can make the change," he says. No new launch date has been set.

Replacing its magnet is hardly the first change of plans for AMS. NASA had scheduled a launch for 2003 but postponed it after the space shuttle Columbia disintegrated upon reentry that February. In 2005, the agency scratched AMS from its to-do list, but 3 years later Congress mandated its launch. Ting's commitment has never wavered, colleagues say. "He's a guy who pushes," Samios says. "Any other mortal would have given up." But in making a last-minute design change, Ting may be pushing his luck.

–ADRIAN CHO

ScienceInsider

From the *Science* Policy Blog

NASA Administrator Charles Bolden told a Senate spending panel that **space science** could suffer if the U.S. Congress forces NASA to stick with the Constellation program. The Administration wants to terminate that rocket effort under President Barack Obama's new space policy, which calls for a 2011 budget request that would boost NASA science to $5 billion, an 11% increase over current levels. http://bit.ly/aU9RA6

A microbiologist who once worked with **suspected anthrax mailer Bruce Ivins says** his former colleague, who killed himself in 2008, wouldn't have had enough time to make all the spores contained in the 2001 letters. But another scientist who routinely makes anthrax stocks for research has disputed the testimony of Henry "Hank" Heine before a U.S. National Academies panel. http://bit.ly/d21aF2

A new report by the Institute of Medicine on Americans' **salt intake** suggests that the government gradually restrict the level of salt in food. It's also prompted speculation that the Food and Drug Administration plans to take action. http://bit.ly/dfRM2p

The **International Barcode of Life Project** got a $35 million boost from Canadian agencies. The 26-nation effort collects specimens, sequences their DNA, and builds an informatics platform using digital bar codes to store and share information for species identification and discovery. The new funds, part available now and part spread over 5 years, bring the government's commitment to the world's largest biodiversity genomics project to $80 million and includes $2.2 million to enable researchers in five developing countries—Argentina, Costa Rica, Kenya, Peru, and South Africa—to play key roles. http://bit.ly/bTbwBT

Mexico has established the Agencia Espacial Mexicana, its first **space agency**. It won't be sending astronauts into space or even building its own rockets but instead will develop space policy and stimulate aerospace investment. http://bit.ly/duNlfW

For the full postings and more, go to **news.sciencemag.org/scienceinsider.**

Coming unstuck. Platelets like these enmeshed in a blood clot perform numerous jobs in the body.

CREDIT: © DENNIS KUNKEL MICROSCOPY INC./VISUALS UNLIMITED/CORBIS

Beyond Clotting: The Powers of Platelets

Platelets are known for thwarting blood loss, but new research shows these simplified cells defend against microbes and perform other duties—and they're also drug targets in sepsis and other conditions

THIRTY YEARS AGO, RESEARCHERS WERE convinced that they had platelets pegged. Every milliliter of our blood, the thinking went, harbors hundreds of millions of these cell fragments for just one reason: to save us from bleeding to death. If we suffer a cut or other injury, platelets swarm into action, forming a plug that seals the wound.

But in recent years, platelets have displayed powers no one imagined they had. They are healers that pour out growth factors and other soothing molecules that help damaged tissue rebuild. They are soldiers that spark the protective response known as inflammation, alert immune cells, and even attack microbial interlopers. They are long-haul truckers that pick up and deliver chemicals such as serotonin, which helps the liver regenerate after injury (*Science*, 7 April 2006, p. 104). They are even engineers, shaping the vascular system in newborns. "Platelets are certainly not just the Band-Aids of the bloodstream," says hematologist Joseph Italiano of Harvard Medical School in Boston.

Additional platelet functions continue to come to light, and biologists have just described a novel way that the body might make these multitalented cells—a finding that could one day ease the demand for donated blood. The new view of platelets as more complex and capable "has really got momentum now," says hematologist Andrew Weyrich of the University of Utah in Salt Lake City.

Yet for all their benefits, platelets will be the death of most of us, through blood clots that cause strokes and heart attacks. Platelets also foster cancer, rheumatoid arthritis, and other diseases.

That means platelet-inhibiting medicines originally developed to stall blood clotting might have broader benefits, notes cardiologist Susan Smyth of the University of Kentucky in Lexington. Her lab, for instance, is investigating whether the anticlotting agent clopidogrel also helps against sepsis, an often-fatal condition in which bacterial infections run rampant in the bloodstream.

Platelet factory

It's easy to see why researchers underestimated platelets. Like the already simplified red blood cell, a platelet lacks a nucleus and all the myriad genes it normally contains. Yet platelets are even smaller—less than one-third the diameter of red blood cells—and some scientists maintain they don't even qualify as cells.

But researchers have learned that platelets share many features and abilities with conventional cells—even, at least according to a controversial new study, the capacity to reproduce. Biologists have long thought that platelets, rather than forming through mitosis as most cells do, arise by breaking off from hulking bone marrow cells called megakaryocytes. Three years ago, scientists for the first time observed how this separation occurs in the bone marrow of living mice (*Science*, 21 September 2007, p. 1767). Tendrils from a megakaryocyte bore into a vessel, and the force of flowing blood pulls off pieces that further fission and eventually become platelets.

But is that the only way platelets are born? The question is pressing because no lab has succeeded in growing clinical quantities of platelets—and they are desperately needed for medical traumas that involve lots of bleeding and for cancer patients whose platelet counts have plummeted because of chemotherapy. The supply for transfusions comes entirely from donated blood and can be stored for only about 5 days.

In a paper published in January in the journal *Blood*, Weyrich and colleagues reported that they had caught platelets isolated from fresh blood in the act of reproducing. Instead of going through a conventional mitotic cell division, a platelet sends out a strand with one or more beadlike bulges. These progeny—which sometimes break off but often remain tethered to their parent—harbor standard platelet proteins and latch onto clotting proteins as they would at the site of a cut. Previous studies had noted such platelet necklaces in blood samples, but most researchers assumed they derived from megakaryocytes, not from platelets themselves.

Weyrich says the findings show that platelets have the capacity for independent replication, though whether this process happens often enough naturally to lift a person's platelet count remains unclear. Italiano, whose lab is trying to cultivate platelets, concurs. "I think there's something here," he says. "But the question is to what extent does it occur in the bloodstream."

Unexpected chemistry

Platelets are chock-full of biologically influential molecules—not just ingredients for blood clotting but a wealth of growth factors, immune system messengers, enzymes, and other compounds. Researchers have identified more than 1100 kinds of proteins inside platelets or on their surface. The assumption had been that a platelet, given its lack of a nucleus, inherited these proteins from the megakaryocyte from which it had broken off.

Yet platelets "are just as metabolically active as nucleated cells," says immunologist John Semple of St. Michael's Hospital in Toronto, Canada. Indeed, platelets contain mitochondria, which provide cells with energy for chemical reactions and protein synthesis, and ribosomes, the structures cells use to make proteins from amino acids.

Hints that platelets could build their own proteins began accumulating in the 1960s, when biologists discovered that the cells absorb free amino acids. And in 1988, researchers confirmed that platelets store small amounts of messenger RNA molecules (mRNAs). Yet some scientists objected that any protein production using these mRNAs was unimportant.

In 1998, however, Weyrich and colleagues demonstrated that platelets fashion a particular protein, Bcl-3, in response to a specific stimulus, indicating that platelets carefully manage what they manufacture. Since then, Weyrich's group and other researchers have revealed that platelets make additional key proteins, such as the cytokine interleukin-1 , which induces inflammation, in response to chemical signals. Still, researchers need to pin down how much of its protein repertoire a platelet makes and how much it receives from its megakaryocyte mother.

Cardiologist Jane Freedman of Boston University Medical Center cautions against giving platelets too much credit. "I think that platelets do a lot more than people think they do, but they don't have a nucleus" and thus can't perform all the functions of a conventional cell. Nonetheless, a clear picture is emerging, Weyrich says: "A platelet is dynamic and independent."

Attack of the killer platelets

Their most visible profession is curbing blood loss, but platelets also "moonlight," as Italiano puts it, at an assortment of jobs. In the January issue of *Nature Medicine*, for example, Steffen Massberg of the German Heart Centre Munich and colleagues reported a new developmental role for the cells. In mice, the researchers discovered, platelets ensure that the ductus arteriosus, a shunt that allows blood to bypass the lungs during fetal development, closes once the animals are born. Platelets form a clot in the ductus arteriosus and spur cells in the lining to form a permanent seal. The same mechanism seems to work in humans. The scientists retrospectively studied premature infants and found that those with low platelet counts were more likely to have a ductus arteriosus that remained open. If this connection is confirmed, it might lead to a new way to treat infants and premature babies, who are particularly susceptible to the condition.

Platelets also appear to guard against microbial invasion. Six years ago, researchers discovered that, like pathogen-fighting macrophages and dendritic cells but unlike red blood cells, platelets sport Toll-like receptors (TLRs) that recognize molecular features of microbes. Semple and colleagues have found that when pathogens trip a platelet's TLRs, there's a surge in TNF-α, a compound that fuels inflammation, one of the body's most potent protections against infection.

Sometimes platelets play a more active role in defense, latching onto invaders. They usually turn their captives over to macrophages that can destroy the microbes. But recent work suggests that they can do the job themselves: By hooking onto the surface of a red blood cell, they can kill malaria parasites lurking inside—though how isn't clear (*Science*, 6 February 2009, p. 797).

Semple speculates that platelets are some of the most important pathogen detectors in the body. They are the second most numerous cells in the bloodstream, after red blood cells, and they circulate throughout the body and "pick up everything in the plasma," he says.

The immune talents of platelets are probably holdovers from an earlier era in animal evolution, when one cell type sufficed for microbial defense and hemostasis, or prevention of blood loss. Insects sport such multipurpose cells today, called hemocytes. "Platelets evolved to be hemostatic agents, but they kept their inflammatory functions," says Semple.

Gone septic

Platelets may help newborns and ward off microbes, but they also cause plenty of misery. More than half the people who died in the United States last year were killed by platelets. Most fatalities resulted when a blood clot orchestrated by the cells lodged in an artery and caused a heart attack or stroke. That's why aspirin, clopidogrel, and other antiplatelet agents have found widespread use in people with atherosclerosis or several other conditions.

Researchers have more recently found that another common killer owes a lot to platelets: sepsis, an inflammatory over-reaction to microbes in the blood that can devastate multiple organs. According to some estimates, sepsis kills more than 200,000 people in the United States every year.

Developing drugs to combat sepsis has proved difficult, but two recent studies suggest that targeting the effects of platelets could offer a novel strategy. In 2007, immunologist Paul Kubes of the University of Calgary in Canada and colleagues reported that during a bloodstream infection, platelets that have detected bacteria via their TLRs glom onto neutrophils, a type of bacteria-slaying white blood cell. In response, the immune cells release neutrophil extracellular traps (NETs), webs of DNA that ensnare some kinds of microbes. In a small blood vessel in the lungs or liver, several neutrophils could be clinging to the lining, spinning a curtain of sticky strands that detain bacteria trying

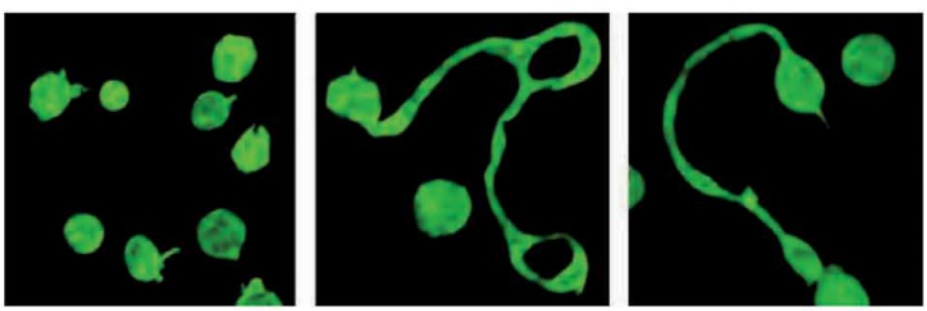

Parent and offspring? Platelet chains like these, in which the beadlike bulges contain standard platelet proteins, have convinced some researchers that the cells can reproduce.

CREDIT: H. SCHWERTZ *ET AL.*, *BLOOD* (JANUARY 2010)

to pass through. This defensive mechanism "may be a last gasp if you have to get rid of a systemic infection," says Kubes.

Yet NETs can "cause collateral damage," notes Kubes, by injuring the lining of blood vessels, which may harm the liver. When the team induced blood infections in rodents that lacked either platelets or neutrophils, the animals incurred less liver damage than did normal controls. Given this finding, Kubes speculates that drugs curbing platelet-triggered NET release could limit organ damage from sepsis.

Platelets gone wild are also at the heart of a sepsis complication called disseminated intravascular coagulation. This condition, which is responsible for up to half of sepsis deaths, involves bleeding and widespread clotting within blood vessels. In a 2008 study in *Nature Medicine*, molecular biologist Jamey Marth of the University of California, Santa Barbara, and colleagues solved a molecular mystery and revealed how the liver tries to combat this dangerous coagulation by removing platelets from circulation.

The researchers showed that some sepsis-causing bacteria release an enzyme called neuraminidase that prunes proteins on the surface of platelets. This modification might allow the bacteria to hook on and ride a platelet to a blood vessel injury, where they can infiltrate the surrounding tissue, Marth says. But the change also signals the body that a massive bacterial invasion is under way. And liver cells, using a protein called the Ashwell-Morell receptor, start grabbing and eliminating platelets sporting the altered proteins. The receptor is part of a last-ditch effort by the body to stop disseminated intravascular coagulation; no one had found a physiological function for this receptor despite 4 decades of study.

Marth and colleagues are hoping that administering drugs that emulate bacterial neuraminidase in the early stages of sepsis could jump-start platelet removal before disseminated intravascular coagulation sets in. They are now investigating that possibility in animals.

Platelet vs. joint

Platelets' Jekyll-and-Hyde nature may also be evident in rheumatoid arthritis (RA), an autoimmune attack on the lining of joints. Researchers have usually attributed the painful and sometimes crippling symptoms of RA to the actions of immune cells such as T cells and B cells. But platelets' facility for triggering inflammation recently inspired rheumatologist David Lee of Harvard Medical School and colleagues to check for an RA connection. The researchers induced a form of RA in mice and then injected some of the animals with an antibody that destroyed 95% of their platelets. The platelet-deficient animals suffered milder joint inflammation than did the other rodents (*Science*, 29 January, p. 580).

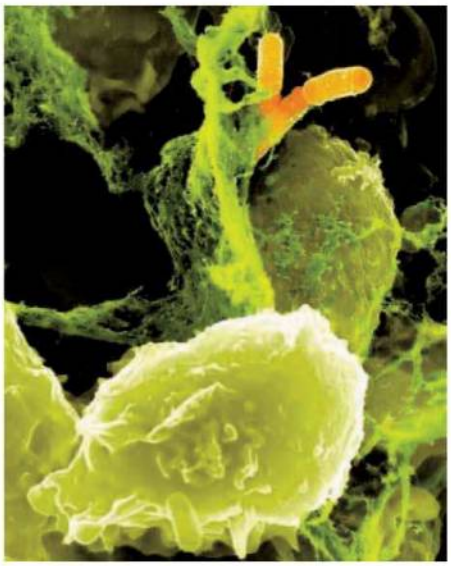

Done in by DNA. Bacteria (orange) caught in a mesh of DNA released by a neutrophil. Platelets that detect microbes can spur neutrophils to release these webs.

However, when the researchers examined fluid from the joints of people with RA, platelets were scarce. Instead, the team detected myriad microparticles, sometimes termed platelet dust. These tiny capsules, discharged by stimulated platelets, brimmed with the inflammatory molecule IL-1.

Lee and colleagues postulate a series of unfortunate events that begins when platelets passing through blood vessels of an already inflamed joint react to cartilage, releasing microparticles. In turn, the IL-1 in the particles prompts cells within the joint to emit molecules that promote further inflammation. Platelets don't instigate RA, they just worsen it, concludes Jerry Ware, a hematologist at the University of Arkansas for Medical Sciences in Little Rock who collaborated with Lee.

The trigger for microparticle release is the receptor glycoprotein VI on the platelet surface, and the researchers speculate that blocking this receptor could deter platelets from unloading their inflammatory cargo. "This is a pathway that has not been previously targeted" in connection with RA, says Lee.

Cancer's little helpers

Cancer, too, seems to get an unfortunate boost from platelets. For example, they might aid tumors by promoting angiogenesis, the formation of new blood vessels. The late Judah Folkman of Harvard Medical School, who championed the importance of angiogenesis for tumor growth, pursued that possibility for a decade. Last year, in a paper that carried Folkman's name as a co-author, some of his former colleagues revealed that cancer cells change the chemical lineup of platelets.

As part of its first-aid kit for injured tissue, a platelet carries molecules that spur or block angiogenesis, packaged into containers called granules. In mice with multiple tumors, platelet granules accumulated more angiogenesis-promoting molecules. "The tumor somehow subverts the platelet into making pro-angiogenic granules," says Italiano, who was one of the study co-authors. The team now hopes to identify the cancer signals that influence platelets.

Besides furnishing new blood vessels for a tumor, platelets might help maintain them, notes vascular biologist Denisa Wagner of Harvard Medical School. A tumor's blood supply is prone to leaks. That's because to immune cells "a tumor is kind of like a wound," she says. They swarm into the newly forming blood vessels and trigger inflammation that can cause the walls to rupture. Four years ago, Wagner, Folkman, and colleagues reported that platelets prevented this vessel deterioration. And in 2008, Wagner and colleagues offered evidence that platelets must release some kind of protective molecule: Platelets that had discharged their chemical contents lost their vessel-saving powers. The identity of the molecular sealant remains a mystery, however.

Cancers also recruit platelets to shield them from the immune system, according to research by tumor biologist Joseph Palumbo of the Cincinnati Children's Hospital Medical Center in Ohio and his colleague Jay Degen. Five years ago, they and their colleagues found that platelets protect tumors from attack by natural killer cells, one of the body's stalwart defenses against cancer. Although this protection wasn't necessary for the original growth to survive, it was essential for the tumor to spread, or metastasize. Palumbo suspects that platelets release a chemical or chemicals that disarm natural killer cells, but they remain unidentified.

Researchers are just starting to try to turn their new knowledge about platelets into medical treatments. And Weyrich says we should expect yet more platelet functions to turn up: "I continue to be surprised by these guys."

–MITCH LESLIE

CREDIT: MAX PLANCK INSTITUTE

PLANETARY SCIENCE

Spunky Hayabusa Heads Home With Possible Payload

A record-setting Japanese mission to an asteroid is due to land in June after overcoming a 7-year history of mishaps

SAGAMIHARA, JAPAN—In a voyage fast becoming the stuff of spacefaring legend, Japan's Hayabusa asteroid mission, once thought lost, is coming home. Launched in 2003, the spacecraft has endured one mishap after another in the course of traveling more than 4 billion kilometers to retrieve samples from the asteroid Itokawa. "Spacecraft aren't supposed to survive such a string of difficulties," says Erik Asphaug, a planetary scientist at the University of California, Santa Cruz.

If nothing else goes wrong, Hayabusa will be the first spacecraft to return to Earth after landing and lifting off a celestial body other than the moon. Last week in Tokyo, the Japan Aerospace Exploration Agency (JAXA) announced that Hayabusa's sample-return capsule, which may or may not hold material from the asteroid, is expected to land near Woomera, Australia, on 13 June. The craft itself will burn up in the atmosphere.

The mission has already achieved scientific stardom, however. The data transmitted back to Earth "changed the paradigm of how we think of small asteroids," says Paul Abell, a planetary scientist at the Planetary Science Institute in Tucson, Arizona. If the return capsule contains particles from Itokawa, they will be the first fragments retrieved from a planetary body since Apollo astronauts hauled back their last load of moon rocks nearly 40 years ago. "It will be a huge bonus," says Abell, who is a member of the Hayabusa science team assigned to NASA's Johnson Space Center in Houston, Texas.

Hayabusa's success is all the more stunning considering what it has endured since the spacecraft was launched on 9 May 2003. By the time it reached Itokawa in September 2005, its solar panels had been degraded by a solar flare, malfunctions had shut down one of its four ion engines that generate thrust by expelling ions drawn from a plasma, and two of its three gyroscopelike reaction wheels, used to control attitude, had failed.

Still, the mission soldiered on. To orient itself, Hayabusa relied on small thrusters originally intended to supplement the ion engines for rapid maneuvers. While the spacecraft maneuvered around the asteroid, a suite of instruments mapped Itokawa and determined its mineral and elemental composition, gravity, and density (*Science*, 2 June 2006, p. 1330).

Prodigal son. Hayabusa is expected to return in June—bearing dust from asteroid Itokawa, researchers hope.

Too far from Earth for real-time remote control, Hayabusa then autonomously navigated through a series of "practice" descents. During one, a microprobe intended to hop along the surface was lost after being released at the wrong altitude. Hayabusa then made two touchdowns, one lasting 30 minutes.

Online
sciencemag.org
Podcast interview with author Dennis Normile.

Shortly after the second liftoff, ground controllers had problems commanding the craft. On 8 December 2005, they lost contact altogether. "Honestly, we thought it was the end of the project," says Jun'ichiro Kawaguchi, Hayabusa project manager at JAXA's Institute of Space and Astronautical Science in Sagamihara, near Tokyo.

Resuming operations hinged on whether the spacecraft's solar panels were facing the sun when it stopped tumbling. But the first challenge was communications. Normally, heaters would keep the oscillators in the spacecraft's transmitter and receiver at a predetermined temperature and, thus, a known frequency. But the heaters switched off, as other systems did, at the time of the accident. The team finally picked up a signal in January 2006, and Kawaguchi says the scientist on duty "did not believe it" at first.

It took a couple of weeks to piece together a grim picture. Hayabusa's solar panels were just barely catching the sun's rays. Some of its batteries were shorted out. The hydrazine fuel used by the secondary propulsion system had bled off into space. The team surmised that a hydrazine "eruption" from a fuel line damaged during the second touchdown had knocked the craft into a tumble. Still, they concluded that they could point the ailing spacecraft on a route that would bring it to Earth by 2010, 3 years later than planned.

Regaining control over Hayabusa "was much more difficult than we had anticipated," Kawaguchi says. Finally, in April 2007, the spacecraft started its journey home. But troubles continued to pile up. A second ion engine failed, and a third lost its ability to generate the neutralizing electrons that must be emitted with the ions that provide thrust. The engine that idled early in the mission is now providing the necessary electrons. Setbacks aside, Kawaguchi says, the mission has shown that ion engines are effective for interplanetary travel and that autonomous navigation and control can land a spacecraft on distant bodies.

Hayabusa's sample-collection technique was never tested. During each touchdown, Hayabusa was supposed to fire projectiles into Itokawa and gather any surface material that rebounded into a collection horn. But it seems that none were fired. On the first touchdown, the craft entered a safe mode that precluded sampling; it is not clear what happened on the second touchdown. The team hopes that dust stirred up during the two touchdowns settled in the collector. "But we won't be surprised if that canister is empty," Kawaguchi says.

Asphaug says the team still deserves a hero's welcome if the sample-return shell lands in the Woomera desert. Its success lays the groundwork for more complex missions, one of which could soon be on the drawing board. U.S. President Barrack Obama earlier this month set a goal of having astronauts land on an asteroid by 2025, and the scientists who eventually tackle that challenge will be able to go to school on Hayabusa's harrowing adventure. **–DENNIS NORMILE**

CREDIT: ILLUSTRATION BY A. IKESHITA/MEF/ISAS

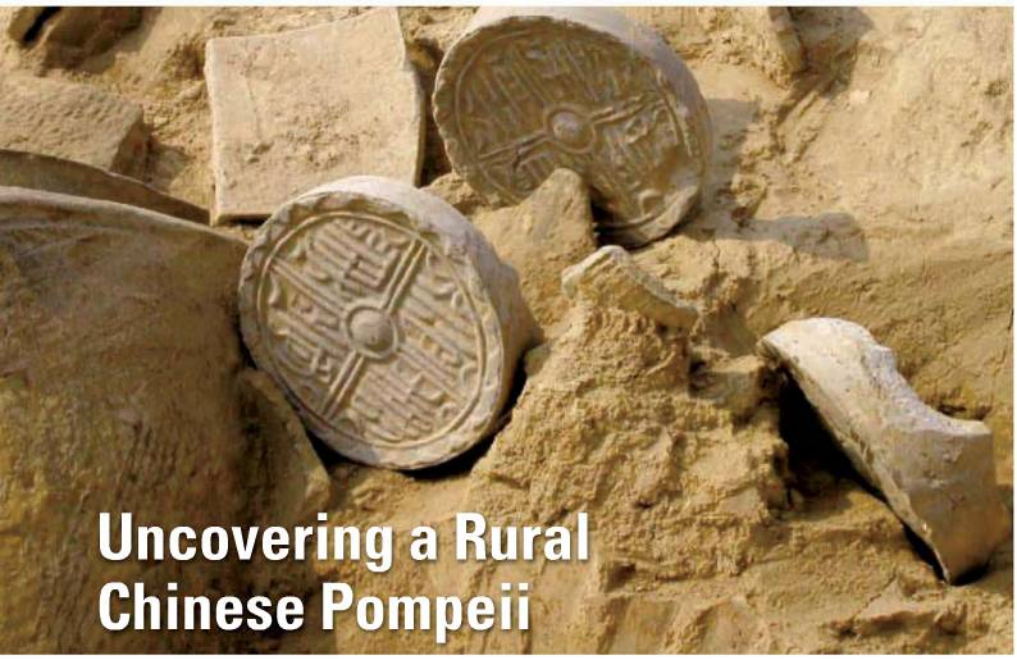

Uncovering a Rural Chinese Pompeii

When the flood came, villagers fled in terror before a wall of silt-laden water from the Yellow River, leaving behind their fields, plows, pottery, and tile-roofed homes. But what was a disaster for the ancient people of Sanyangzhuang is a miracle for modern archaeologists. Up to 70 centimeters of silt buried the settlement completely, protecting it from the depredations of time. Now excavators are peeling back the layers of dirt to reveal a unique 2000-year-old time capsule of Chinese rural life.

Although preserved texts record the official history of the Han dynasty at this time, Sanyangzhuang "offers us remarkable insight into daily life," says archaeologist Tristram Kidder of Washington University in St. Louis, Missouri, who is working at the site under the direction of his Chinese colleague Haiwang Liu of the Henan Provincial Institute of Cultural Relics and Archaeology in Zhengzhou. "It's a superb and unprecedented archive."

Raising the roof. A sudden flood buried tiles set aside to repair a Han house.

The village, northwest of Shanghai in central China, was hit with a sheet flood, a sudden burst of muddy liquid carrying more than 200 kilograms of sediment per cubic meter of water. There was little warning; workers reroofing one compound left behind their tools and tiles. Although touted as an "Asian Pompeii" by the Chinese media, Sanyangzhuang was not the pleasure destination of a wealthy elite like the ancient Roman city. Buried about 10 or 11 B.C.E.—just a few decades before Pompeii—the village was a prosperous but hardworking farming center at the end of the Western Han period.

Since Sanyangzhuang's initial discovery in 2003, archaeologists have begun to explore four large tile-roofed compounds with brick foundations, and they have found 10 more through coring 5 to 7 meters into the fine-grained sediment. Each compound examined so far is surrounded by rich fields of wheat worked by villagers, as well as fired-brick–lined wells, toilets, ponds, cart tracks, and the remains of trees that once shaded the settlement. Although the inhabitants appear to have

CREDITS (TOP TO BOTTOM): HENAN PROVINCIAL INSTITUTE OF CULTURAL RELICS AND ARCHAEOLOGY; KEVIN KRAJICK/EARTH INSTITUTE, COLUMBIA UNIVERSITY

The Long Reach Of the Monsoon

When the monsoons failed 6 centuries ago in Southeast Asia, they caused two terrible droughts that helped to bring down the Khmer civilization centered at Angkor Wat in today's Cambodia (*Science*, 20 February 2009, p. 999). Now researchers have evidence that later fluctuations in the monsoons can help explain dramatic social and political changes from India to China—and affect lives as far away as Mexico. New tree ring data detailing monsoon failures from 1250 C.E. to the present suggest that the droughts coincided with political upheaval, presumably by causing crop failure, says Brendan Buckley of Columbia University.

In his talk, Buckley first outlined the Angkor-related results, also summarized in a recent paper in the *Proceeding of the National Academy of Sciences*. Using tree rings for dating and the size of the tree's annual growth ring as a proxy for rainfall, the team showed that 2-decade droughts starting in the 1340s and 1400s, with severe flooding in between, hit not just the area around Angkor but a wider region of Southeast Asia as well.

Such megadroughts were not confined to medieval times, says Buckley, who is a co-author of another paper published last week in *Science* (p. 486) that uses tree rings to lay out the pattern of monsoon failures during the last millennium. During the past 5 years, a group led by Columbia's Edward Cook scoured a wide swath of Asia for long-lived trees. They gathered 300 tree cores from the Himalayas, Siberia, China, Japan, and into Southeast Asia. Monsoon rains affect all these regions and so presumably affected the trees' growth.

The team found many instances of monsoon failure that coincided with political upheaval. For example, a megadrought hit the region around Beijing prior to the demise of the Ming dynasty, a disaster which may have stoked the peasant revolt that upended the dynasty in 1644 C.E. Buckley said in his talk that the monsoon's long arm even extended to Mexico, affecting the El Niño cycle and contributing to a 16th century drought there; that drought coincided with Spanish-borne dis-

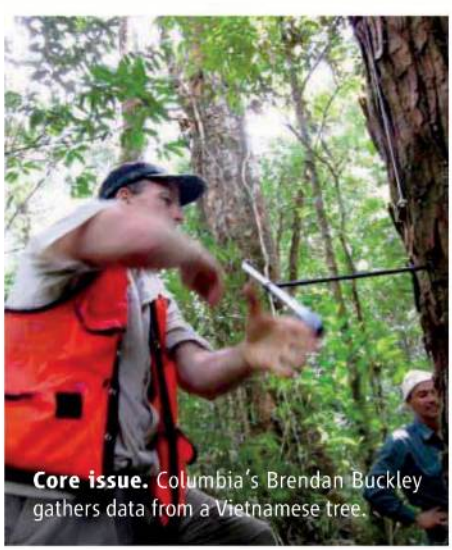

Core issue. Columbia's Brendan Buckley gathers data from a Vietnamese tree.

escaped, iron-tipped plows, hoof prints, and even the impressions of mulberry leaves—a sign of silk cultivation—were left behind. "This was a self-contained community as well as the start of the Silk Road," Kidder told colleagues in a talk here. Much of the data is yet to be analyzed, but Kidder said that the biggest surprise is the prosperous nature of what was a backwater rural area.

Henry Wright, an archaeologist at the University of Michigan, Ann Arbor, who has worked in China, said the digs promise to yield a detailed picture of China's hinterland at the height of the Han imperial state, which matched contemporary Rome in size and wealth. And he said that Kidder, who has dug in areas around the Mississippi River covered with similar silt, is providing Chinese archaeologists with new methods and tools for getting at the deeply buried material.

Kidder suspects there may be other buried villages, towns, fields, and roads, because the flood affected not just Sanyangzhuang but a vast area over 1800 square kilometers. Remains of a Han-era wall 5 kilometers away could mark the site of a still-buried walled town. "This was a massive and catastrophic event," he says, and it was noted in historical records of the time. Dikes in the area weren't repaired until 69 C.E., and the region did not recover until the 7th century C.E. Ironically, the disaster, like the violent end of Pompeii, may provide a wealth of information on the period. "A significant part of [this region] may be buried largely intact," he says. **–A.L.**

eases and may have been a factor in the dramatic reduction in native populations.

The team also pinpointed a megadrought that afflicted a wide area of southern Asia during the 1750s. This was a puzzling period when regimes from western India to Vietnam were roiled by revolts and wars that appear to have spread as far north as Siberia. Historian Victor Lieberman of the University of Michigan, Ann Arbor, has written extensively about the "strange parallels" of these 18th century upheavals. He welcomes what he calls "unprecedentedly reliable and detailed climatic data that have a strong bearing on political and economic reconstructions." The new climatic data "force me to rethink entirely my understanding of the 17th and 18th centuries," he says, by implicating climate as a potential common factor in the far-flung upheavals.

Buckley says he is far from done with milking tree rings for clues to past climate. He hopes to find trees old enough to extend the Asian record back to 900 C.E. **–A.L.**

CREDITS: WIKIPEDIA

Playing Politics Or Just a Game?

In ancient Mesoamerica, ball games weren't just for fun. The classic game, which involved a hard rubber ball and helmeted players on a rectangular field, had serious ritual and political goals—or at least that has been the conventional wisdom among archaeologists. But David Anderson of Tulane University in New Orleans, Louisiana, put a new twist on this story: He argued at the meeting that the ball courts found throughout Mesoamerica likely began as a communal game and only later were co-opted by elites who used them for their own ends.

Ball courts were widespread in the Mayan Classic period from about 250 C.E. to 900 C.E. They have been found primarily at complex sites with large social differences, a sign that they were associated with elites. Iconographic evidence suggests that such games were used as tools for settling factional disputes, negotiating power relations, and redistributing food and wealth, as summarized in a classic 1996 paper by Harvard University anthropologist John Gerard Fox.

Anderson analyzed a recent survey of northwest Yucatán by other archaeologists and found a different picture. The surveyors discovered nearly two dozen early ball courts from the Middle Preclassic period, which dates from 900 B.C.E. to 300 B.C.E. Only one was located at a place with obvious social distinctions—at Xtobo, once a thriving town that boasted nearly 400 structures, including pyramids and elite residences. But the other courts were all at modest villages. The smallest site, San Jeronimo I, consists of little more than the ball court itself. "Until recently, archaeology has focused primarily on the biggest sites, royal tombs, et cetera," says Anderson. Because the ball game was pervasive at these sites, "we came to think of it as an elite game," he says. "As we are now starting to look at the entire landscape, we are starting to find more and more signs of ball courts at smaller sites."

The data suggest that the ball game was brought to the Yucatán in the Early Preclassic, prior to about 900 B.C.E, "by the relatively egalitarian social groups of those times," says Anderson. Ceramic figurines from the Middle Preclassic depict ball players, but iconographic depictions of ball games in stone, which are common later, are relatively rare in the early periods. This, combined with the location of ball courts in small settlements, requires archaeologists to rethink their early origin and use, says Anderson. "The ball game was a communal tradition known to all and accessible to most," he says. "The earliest forms of the ball game in Mesoamerica represent a communal tradition of sport that was only later adopted by the sociopolitical elite to use for political ends."

Anderson's idea is intriguing, says Richard Diehl, a Mesoamerican anthropologist at the University of Alabama, Tuscaloosa. But he notes that there are hints that the game may have been played for ritual reasons, not just sport, even before Preclassic times. Rubber balls have been found in ritual caches dating back to 1400 B.C.E. at a Mexican site called El Manatí. This was during the time of the Olmec, the first in the region to develop a complex society. But evidence of ball courts in Olmec times remains questionable, Diehl and Anderson agree, and surprisingly few from any era have been excavated. To resolve Anderson's challenge, says Diehl, archaeologists need more digs. **–ANDREW LAWLER**

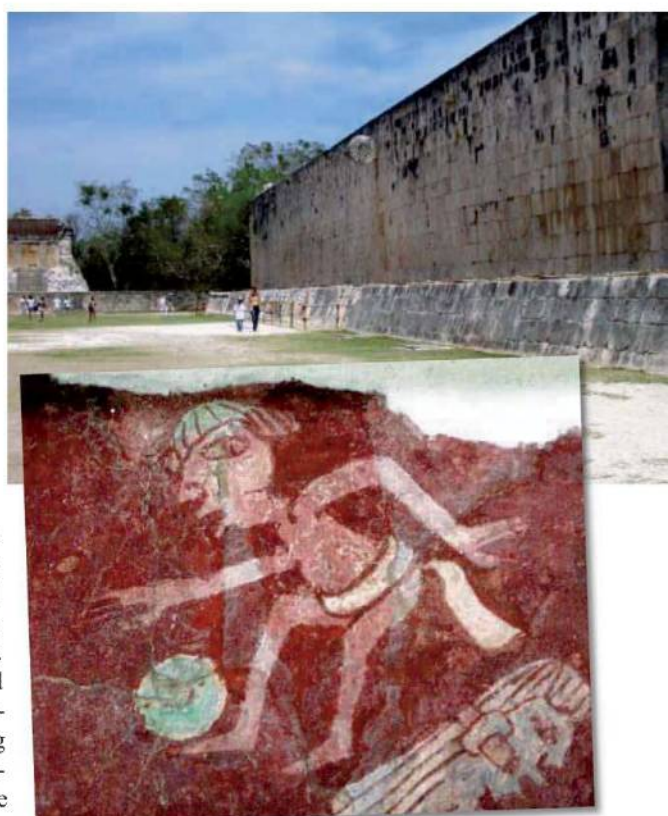

Play ball! The Chichen Itza ball court. The ritual Mayan game (*inset*) may have begun as a commoner's pastime.

LETTERS

edited by Jennifer Sills

Food Security: Farming Insects

G. VOGEL'S NEWS STORY "FOR MORE PROTEIN, FILET OF CRICKET" (12 FEBRUARY, SPECIAL section on Food Security, p. 811) draws attention to the potential role of insects in food security. Although insects such as mopane worms and termites are widely consumed by some societies, especially in Africa (*1*–*7*), globalization and creation of a food culture based largely on Western values has led to their marginalization (*1*, *5*, *6*). Unlike steak, such insects are easily accepted only where indigenous knowledge and willingness to consume them exists (*1*–*5*, *7*).

In addition to overcoming the cultural aversion to eating insects, it will be necessary to address ways to make them available throughout the year. Insects are seasonal, and there are technical difficulties in mass-rearing, processing, and storing them (*8*, *9*). Our experience (*8*, *9*) in Africa points to the need for greater public-private partnership in research and development. Governments could provide incentives to investors that come up with green business ideas on mass-production of edible insects. Currently, insects such as the mopane worm are treated as open-access resources, and their increasing commercialization is raising fears of extinction (*10*). Unsustainable wild harvesting could be reduced and conservation goals achieved with arrangements that encourage on-farm production of such insects.

GUDETA W. SILESHI[1]* AND MARC KENIS[2]

[1]Southern Africa Programme, World Agroforestry Centre ICRAF, Lilongwe, Malawi. [2]CABI Europe, Delémont, Switzerland.

*To whom correspondence should be addressed. E-mail: Sweldesemayat@cgiar.org

References

1. G. R. DeFoliart, *Annu. Rev. Entomol.* **44**, 21 (1999).
2. K. J. Mbata *et al.*, *J. Insect Conserv.* **6**, 115 (2002).
3. R. A. Hope *et al.*, *Dev. South. Afr.* **26**, 29 (2009).
4. S. M. Muntali, D. E. C. Mughogho, *Biodivers. Conserv.* **1**, 143 (1992).
5. P. Illgner, E. Nel, *Geog. J.* **166**, 336 (2000).
6. F. Malaisse, *Geo-Eco-Trop* **26**, 37 (2002).
7. G. W. Sileshi *et al.*, *Ecol. Soc.* **14**, 48 (2009).
8. K. Kloosterman, "Good grub in Africa," Emagazine.com (2006); www.emagazine.com/view/?3073&src.
9. M. Kenis *et al.*, "Towards conservation and sustainable utilization of edible caterpillars in the miombo" (CABI, 2006); www.northsouth.ethz.ch/news/past_events/past_events_zil/annualconference06/posterexhibition/Kenis.pdf.
10. W. Akpalu, *Environ. Dev. Econ.* **14**, 587 (2009).

CREDIT: KIRSTEN KASTNER

MRI Safety Not Scientifically Proven

WE APPRECIATE THE SIGNIFICANCE OF MAGnetic resonance imaging (MRI) for patients and research, but we are concerned by the tone of the News of the Week story "Fear of MRI scans trips up brain researchers" (L. Jiao, 19 February, p. 931), in which Arno Villringer (Max Planck Institute, Germany) says, "Millions of people have been examined with MRI so far; thus it seems now very unlikely that there would be a side effect." This statement cannot be advanced as a proof of MRI safety. Large patient groups have never been monitored longitudinally in a standardized FDA-approved study. A further argument for caution lies in the increasing evidence that MRI exposure can have biological effects (*1*, *2*).

The logical fallacy in this statement becomes apparent when we consider that this argument for MRI could also be applied to the risks of x-ray computed tomography (CT) exposure. In the case of x-rays, it may be factually correct to state that no study to date has shown that CT increases cancer risk, but it is incorrect to state that there are no cancer risks from the radiation exposure associated with CT. Absence of evidence is not proof of the absence of risk, and it is widely accepted that there are small but nonzero risks associated with CT (*3*).

Side effects of these procedures may take decades to detect. One example is the induction of severe side effects in a small fraction of the population years after administration of the MRI contrast agent gadolinium-DTPA (diethylenetriamine penta-acetic acid) (*4*). Now that this risk has been identified, benefit-risk ratio is known and thus manageable. In

Letters to the Editor

Letters (~300 words) discuss material published in *Science* in the previous 3 months or issues of general interest. They can be submitted through the Web (www.submit2science.org) or by regular mail (1200 New York Ave., NW, Washington, DC 20005, USA). Letters are not acknowledged upon receipt, nor are authors generally consulted before publication. Whether published in full or in part, letters are subject to editing for clarity and space.

How chimps use tools

579

SPORE prize essay

584

the case of caregivers volunteering their healthy children, however, the risk is unknown and there is little if any benefit to them; this practice should be questioned.

FRANK S. PRATO,[1]* ALEX W. THOMAS,[1] ALEXANDRE LEGROS,[1] JOHN A. ROBERTSON,[1] JULIEN MODOLO,[1] ROBERT Z. STODILKA,[1] JANICE M. DEMOOR,[1] WALTER HUDA[2]

[1]Imaging Program, Lawson Health Research Institute, London, ON N6A 4V2, Canada. [2]Department of Radiology and Radiological Science, Medical University of South Carolina, Charleston, SC 29425, USA.

*To whom correspondence should be addressed. E-mail: prato@lawsonimaging.ca

References

1. J. A. Robertson *et al.*, *J. R. Soc. Interface* **7**, 467 (2010).
2. M. Rohan *et al.*, *Am. J. Psychiatry* **161**, 93 (2004).
3. D. J. Brenner *et al.*, *Proc. Natl. Acad. Sci. U.S.A.* **100**, 13761 (2003).
4. S. E. Cowper, *Adv. Dermatol.* **23**, 131 (2007).

Fundamental Change in German Research Policy

UNTIL RECENTLY, AN ESSENTIAL INDICATOR in the evaluation of grant applicants by the Deutsche Forschungsgemeinschaft (DFG), Germany's leading research foundation, was the quantity and impact of the applicant's publications. This policy fit the increasing attention paid to Web of Science–listed publications, impact factors, and the h-index for competitive funding in science (*1*, *2*). The rationale is clear: On the basis of such variables, it is possible to compare performances and to provide a foundation for decisions. However, the process overlooks one fundamental point: the content of research.

The essence of the "Einsteins" of science history was surely not the quantity of their publications, but the quality of their research ideas. Ideas are hard to quantify—they are even harder to compare. But wise peer-referees can qualify them.

The DFG has recently taken an important step toward valuing content. The organization has changed its policy for evaluating research grants by restricting references in forthcoming applications to five of the authors' most important publications and limiting reports of finished projects to the two most important publications per year (*3*). This helps reviewers appreciate the quality and the innovativeness of research. Of course, not every paper can introduce a Theory of Relativity. But we must focus on quality rather than quantity if we are to advance the world's intellectual capital.

CLAUS-CHRISTIAN CARBON

Department of General Psychology and Methodology, University of Bamberg, Markusplatz 3, D-96047 Bamberg, Germany. E-mail: ccc@experimental-psychology.com

References

1. C. C. Carbon, *Curr. Sci.* **94**, 1234 (2008).
2. J. E. Hirsch, *Proc. Natl. Acad. Sci. U.S.A.* **102**, 16569 (2005).
3. DFG, Press release 7 (23 February 2010); www.dfg.de/en/service/press/press_releases/2010/pressemitteilung_nr_07/index.html.

Measuring Forest Changes

D. NEPSTAD *ET AL.* ("THE END OF DEFORESTATION in the Brazilian Amazon," Policy Forum, 4 December 2009, p. 1350) highlight promising efforts by Brazil to reduce Amazonian deforestation, in part by harnessing funds from international carbon payments—termed REDD (reducing emissions from deforestation and forest degradation). For a country to engage in REDD, reliable data on past and current changes in its forest carbon stocks are essential (*1*). Having established in 1989 a world-leading program to monitor its Amazonian deforestation using remotely sensed imagery, Brazil is in many ways uniquely poised for REDD (*2*).

Current efforts to promote REDD, including those with pilot funding from the World Bank, assume that each developing nation will develop its own estimates of changes in forest carbon stocks, as Brazil is doing. We believe that this approach is unrealistic and prone to conflicts of interest. First, even if standard monitoring tools are developed (*3*, *4*), the costs will be high if each country must independently develop the capacity to apply them. Second, when applying these tools, there will invariably be decisions—for example, about which remotely sensed images to use and how to interpret them—that offer opportunities to bias results. Such variability between nations has long plagued the U.N. Food and Agriculture Organization's efforts to estimate national changes in forest cover (*5*). Nations will have strong incentives to overestimate their past deforestation rates and underestimate their present rates in order to maximize their eligibility for REDD funds. This could create conflicts between those selling and buying forest-carbon credits that undermine REDD initiatives.

Rather than the current approach, we believe that an independent organization—such as the World Conservation Monitoring Centre of the United Nations Environment Programme—should be tasked and funded with determining historic and current rates of change in forest-carbon stocks, using cutting-edge approaches [e.g., (*4*)], in a consistent and unbiased manner across all developing nations. This will, we believe, be far more cost-effective and reliable than expecting each nation to develop its own estimates, even if these estimates are subject to third-party verification. Brazil's leading efforts to monitor its forests might provide useful lessons for scaling up to global monitoring.

WILLIAM F. LAURANCE[1]* AND OSCAR VENTER[2]

[1]School of Marine and Tropical Biology, James Cook University, Cairns, QLD 4870, Australia. [2]The Ecology Centre, University of Queensland, Brisbane, QLD 4072, Australia.

*To whom correspondence should be addressed. E-mail: bill.laurance@jcu.edu.au

References and Notes

1. W. F. Laurance, *Biotropica* **39**, 20 (2007). These data are essential for national-level carbon trading, which greatly reduces the likelihood of deforestation "leakage."
2. Brazilian National Institute for Space Research (INPE); www.obt.inpe.br.
3. H. Gibbs *et al.*, *Environ. Res. Lett.* **2**, 045023 (2007).
4. G. Asner, *Environ. Res. Lett.*, **4**, 034009 (2009).
5. P. Fearnside, *Clim. Change* **46**, 115 (2000).

CORRECTIONS AND CLARIFICATIONS

Reports: "Decorrelated neuronal firing in cortical microcircuits" by A. S. Ecker *et al.* (29 January, p. 584). In Fig. 1E, the labels (r_{sc} values and colored dots) were accidentally applied in reverse order. The correct labels (color *x*/color *y*/r_{sc}) should read for the first row from left to right: green/light blue/–0.01; dark blue/light blue/0.02; dark blue/green/–0.14; for the second row from left to right: red/light blue/–0.01; red/green/0.21; red/dark blue/0.04.

Reports: "Metagenome of a versatile chemolithoautotroph from expanding oceanic dead zones" by D. A. Walsh *et al.* (23 October 2009, p. 578). There are two changes to the names of sequences within tree 1 in Fig. 1A. The first two Eastern South Pacific clones are ESP60-K23I-54 (DQ810449), not ESP200-K23I-54, and ESP60-Khe2-29 (DQ810511), not K23II-30 (DQ810478).

Reports: "Parasite treatment affects maternal investment in sons," by T. E. Reed *et al.* (19 September 2008, p. 1681). The sample size of the experimental group receiving sham treatment in 2006 should read $n = 20$ nests, not 22 nests (see "Experimental methods" in the corrected Supporting Online Material). Therefore, the total sample size quoted in the main text should be $n = 81$ nests, not 83.

MEDICINE

The Impacts of Innovation

Richard S. Mathis

The stethoscope is now such an iconic symbol of physicians and medical practice that we have a hard time thinking of it as a technological advance. Yet it was just that, and as such it encountered the same issues that many medical advances face. Invented in 1816 by French physician René Laennec, the stethoscope reshaped medicine from a practice relying largely on patient narratives to one that also involved the use of an instrument. Such a change was not without controversy. The stethoscope's use required training, and those physicians who did not want to undergo the task of learning how to use it were skeptical of its value. Additionally, physicians worried that using such a tool would change the nature of their profession and cause them to be associated with the manual trades rather than with those requiring education and judgment. Such factors contributed to the nearly two decades that were required for the practice of auscultation by stethoscope to become fully accepted. Its final acceptance created another practice commonly associated with medicine—that of physicians not listening to subjective patient reports about illness but instead seeking objective information from technology.

In *Technological Medicine*, Stanley Joel Reiser explores the difficulties encountered by proposed technological advances as well as the practical and ethical conundrums these advances create once accepted. Reiser (a physician at George Washington University medical school) discusses such technologies as the x-ray, the artificial kidney, the artificial respirator, and the electronic medical patient record. He also examines innovations in the field of public health and indicates the contrasts (and conflicts) between those who treat individual patients and those who focus on populations.

Reiser is at his best when reviewing how a particular technology was developed, how it was advanced, and how it can be indicative of the general process of technological adoption. After discussing the stethoscope and the x-ray, for example, he points out the tendency of advocates of these technologies to attack existing approaches in favor of increasingly scientific and objective tools. Thus, advocates of the stethoscope pointed out the weakness of relying on the patient's story, and those of the x-ray criticized physicians who relied solely on the stethoscope and the senses. "It has become the norm in the battle for the succession of technologies in medicine," Reiser concludes, "to have winners and losers. Also a significant factor in this story is a vision held for centuries by doctors: of medicine becoming a science and thus eliminating subjective elements when they seem to be replaceable with objective ones."

Technological Medicine
The Changing World of Doctors and Patients
by Stanley Joel Reiser
Cambridge University Press, Cambridge, 2009. 245 pp. $30, £20. ISBN 9780521835695.

Other issues arose with more recent technological innovations, and it is interesting to see how these suggest features of the current landscape of reform. The artificial kidney offered an effective yet expensive treatment for those suffering from kidney disease. Access to this technology meant the difference between life and death. When, in the early 1960s, boards were established to choose who would receive the device, the ethical issues raised by rationing entered public discourse in a very real and emotionally charged manner. The artificial respirator, with its ability to keep patients in vegetative states alive for long periods of time, raised other difficult questions. Reiser goes into some detail regarding the Karen Ann Quinlan case, in which a young woman who became comatose in 1975 was placed on an artificial respirator. She was removed from the respirator a year later, after an intense legal battle that received national attention. The more recent Terri Schiavo case, which Reiser does not discuss, demonstrates the ethical, legal, and political issues that continue to confront us in this area.

Reiser could have improved his survey of the lessons of technological advance if he had gone through the development of devices in a sequential manner and used that approach to arrive at his conclusions. He instead leaves his principal topic in favor of forays into such areas as the growth of preventive medicine. Although certainly related to his theme, the discussions of such topics generally make the book less focused.

Despite this shortcoming of *Technological Medicine*, Reiser should be commended for his demonstration that technological advance throughout recent times has commonalities as well as unintended consequences. The funding of a Patient-Centered Outcomes Research Institute in the recently passed U.S. health care legislation suggests that his conclusions regarding technological advance may find an ear. Reiser calls for a better understanding of medicine that goes beyond technology for its own sake, stronger relationships between patients and medical professionals in widening the vision of medical technology, and informed social policy that is built on this new vision. The institute, with its proposed focus on the comparative clinical effectiveness of various new and established technologies, raises the possibility that a deeper understanding of technological innovations will find its way into thinking about health care. The history of medical advances is important to this thinking and can be instructive as we continue to confront the complexities of health care.

New way of seeing. The first x-ray of a human, Wilhelm Conrad Röntgen's 1895 image of his wife's hand.

CREDIT: IMAGES FROM THE HISTORY OF MEDICINE/COURTESY NATIONAL LIBRARY OF MEDICINE

The reviewer is at the Center for Medical Technology Policy, 401 East Pratt Street, Suite 631, Baltimore, MD 21202, USA. E-mail: richard.mathis@cmtpnet.org

10.1126/science.1188655

MEDICINE

The Costs of Innovation

Beryl Lieff Benderly

For more than 40 years, Daniel Callahan has specialized in asking hard, penetrating questions that science can't answer. In *Taming the Beloved Beast*, his 41st book, he asks one of potentially great interest to those involved in biomedical science: What is the proper role of technology in health care?

For many who spend their lives seeking new ways to understand and control illness and extend life, the question is probably a no-brainer. The near-infinity of pharmaceuticals, machines, and equipment used in patient care has saved countless lives, prevented untold suffering, and will, as innovation continues, do even better in the future. For most Americans, advancing health technology appears an unalloyed good, a view that we support with tens of billions of tax dollars each year.

But, Callahan notes, the engine of technological progress is also the chief driver of the soaring health care costs in the United States. These have priced tens of millions of Americans out of the health care market and will, if not controlled, bankrupt the health care system and perhaps the nation itself. He argues, "The idea that more research will reduce health care costs is a myth," simply unsupported by the evidence. Callahan sees the level of health that Americans generally enjoy as so good that "there is no longer a societal need for indefinite, endless improvement." Instead, he claims, we need to remove inequities and safeguard the nation's financial ability to continue providing care. Therefore, he concludes, the greater good requires imposing restraints on technological advance.

This idea violates a basic value of American medical science. However, as one of the nation's most trenchant bioethicists, Callahan (a member of the U.S. Institute of Medicine and cofounder and former longtime president of the Hastings Center) is not just an intellectual provocateur but a probing observer of American culture.

Health care in the United States is both highly technological and highly individualistic, letting everyone—or, at least, everyone who can pay out of their own or an insurance company's pocket—buy whatever treatments seem desirable, no matter how expensive or how unlikely to provide significant benefit. "It seems assumed," Callahan comments, "that any and all technology costs, as long as they can show some therapeutic benefit, ought to be considered acceptable and worth paying for."

Americans therefore use more—and more expensive—medical technology than any other country on Earth but, at least until the age of 80, have lower life expectancy and worse health outcomes than citizens of many countries that use and spend much less. At the same time that tens of millions of Americans lack health insurance, the United States has annually spent up to seven times as much per capita on cancer research as European Union countries, where everyone has health care. "The frightening thought that the innovation that has saved so many lives and reduced so much suffering could itself be playing a leading role in our health care discomfort," he notes, "is hard to accept, difficult to talk about openly, and politically controversial."

But he poses difficult questions anyway: He wonders "why the future lives that will be improved or saved from a steady stream of innovations are more important than the lives that could now be saved if prices were lower." He asks what would be the state of health of the population had innovation ceased a decade ago but everyone then and since received that moment's best treatment for all of their medical problems. He suspects Americans would not be worse off and that universal coverage for all would have improved our present situation. Some patients would have missed out on the newest treatments, but no one would have suffered or died—as thousands have—for lack of any treatment at all.

Callahan insists that the entire U.S. approach to medical technology needs to be rethought. For example, he believes we should reconsider the priority that the National Institutes of Health have long given to lethal diseases (such as cancer, heart disease, and stroke). He would reduce expenditures on higher technologies and expensive procedures while increasing financial support for more basic medical care and public health. The main focus of health care, he holds, should not be on preventing death no matter the patient's age. Rather, our goal should be to give as many people as possible a chance at "a full life," which he defines as reaching the late 70s or early 80s in reasonably functional condition. Approaching his 80th birthday as he finished this book, he has standing to make that argument.

Many readers may dismiss Callahan's brief for medical decisions based on population welfare rather than individually defined needs and his scheme for prioritizing access to expensive high-tech care according to age as objectionable, naïve, or unworkable in an American context. But no one who comes to *Taming the Beloved Beast* with an open mind can deny the intellectual and ethical power of the questions he poses. He probes issues central to resolving the enormous problems and inequities—not to mention the looming financial threats—that bedevil American medical care.

Taming the Beloved Beast
How Medical Technology Costs Are Destroying Our Health Care System
by Daniel Callahan
Princeton University Press, Princeton, NJ, 2009. 279 pp. $29.95, £20.95. ISBN 9780691142364.

The reviewer is a columnist for ScienceCareers.org.

BROWSINGS

Wellcome Image Awards 2009. Wellcome Collection, London. Through 1 June 2010. www.wellcomeimageawards.org
Bill McConkey's digital artwork *Mechanical Heart* is among the 19 striking and informative images currently on display at the Wellcome Collection's London gallery (and, with background information, on the Web). The other winning scanning electron and light micrographs, photographs, and illustrations include depictions of aspirin crystals, summer plankton, and sensory nerve fibers.

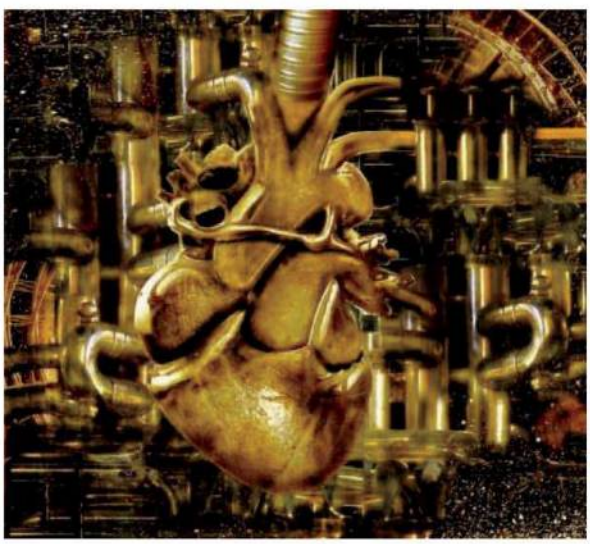

CREDIT: BILL MCCONKEY/WELLCOME IMAGES

10.1126/science.1188708

GLOBAL HEALTH

Fifty Years of U.S. Embargo: Cuba's Health Outcomes and Lessons

Despite sanctions' impacts on medicine and medical supplies, Cuban health outcomes are comparable to those of developed countries.

Paul K. Drain† and Michele Barry*

The U.S. trade embargo against Cuba, enacted after Fidel Castro's revolution overthrew the Batista regime, reaches 50 years in 2010. Its stated goal has been to bring democracy to the Cuban people (*1*), but a 2009 U.S. Senate report concluded "the unilateral embargo on Cuba has failed to achieve its stated purpose" (*2*). Domestic and international favor for the embargo is not strong (*3*). Many political and business leaders suggest changing U.S. policy toward Cuba, and President Obama eased travel and remittance restrictions of Cuban-Americans (*4*, *5*). In light of such changes in sentiment and policy, and also the impending overhaul of U.S. health care, we review health consequences and lessons from "one of the most complex and longstanding embargoes in modern history" (*2*).

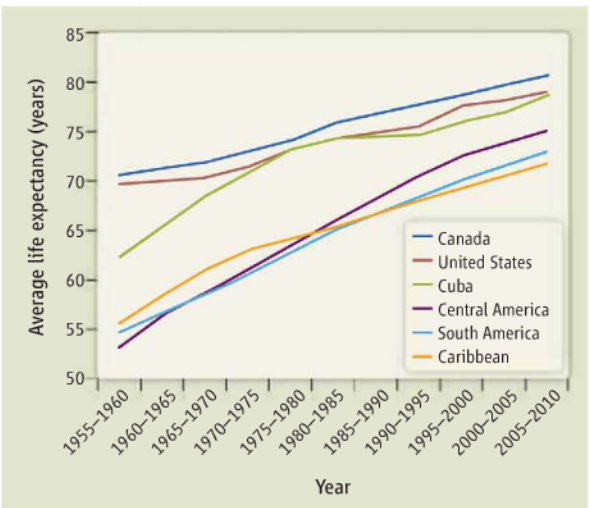

Life expectancy comparisons. Average life expectancy in Cuba and neighboring countries and regions. Data from (*11*). Cuba is included in the Caribbean region.

In the decades before 1960, U.S. economic support contributed to Cuba's achieving average life expectancies that, although they lagged behind North American neighbors United States and Canada, for example, still exceeded other Latin American regions (see the graph, right). In response to seizure of property owned by U.S. citizens, the United States restricted importation of Cuban sugar in 1960, followed in 1963 by prohibition of trade in food, medicines, and medical supplies (*6*). The embargo remained relatively unchanged and had little economic impact on Cuba during the Cold War era, mostly because of strong financial support from the Soviet Union (*7*, *8*) (fig. S1). By 1983, Cuba was producing >80% of its medication supply with raw chemical materials acquired from the Soviet Union and Europe, and there were scant reports of medication shortages (*9*, *10*). During the embargo's first 30 years, Cubans' average life expectancy increased 12.2 years, comparable to Caribbean and South American regions (see the graph) (*11*).

After the Collapse of the Soviet Union

When the Soviet Union collapsed in 1989, foreign aid faltered, and Cuba's economy and health suffered (*7*, *10*, *12*) (fig. S1). Adult caloric intake decreased 40%, the percentage of underweight newborns (<2500 g) increased 23%, anemia was common among pregnant women, and the number of surgeries performed decreased 30% (*8*, *12*). After a decade of steady declines, Cuba's total mortality rate increased 13% (*12*).

The U.S. "Torricelli Bill" of 1992 tightened the embargo (*13*); the number of foreign-based subsidiaries of U.S. companies granted licenses to sell medicines to Cuba declined dramatically (*14*). The 1996 U.S. "Helms-Burton Act" sought to further penalize foreign countries trading with Cuba (*15*). By the end of the 20th century, few international pharmaceutical companies supplied essential medicines or raw chemicals to Cuba (*10*, *14*).

Before Torricelli, Cuba imported U.S. $719 million worth of goods annually, 90% of which was food and medicines, from U.S. subsidiary companies (*12*). Between 1992 and 1995, only $0.3 million was approved for sale by U.S. subsidiaries (*12*). By 1996, the Cuban national formulary of 1300 medical products was reduced to <900 products (*12*, *16*). Medication shortages were associated with a 48% increase in tuberculosis deaths from 1992 to 1993; the number of tuberculosis cases in 1995 was threefold that in 1990 (*7*, *17*, *18*). An increase in diarrheal diseases in 1993 and 1994, and an outbreak of Guillain-Barré syndrome in 1994, attributed to *Campylobacter*-contaminated water, followed a shortage of chlorination chemicals (*12*). A national epidemic of optic and peripheral neuropathy, which started in 1991, was associated with malnutrition and food shortages (*19*–*22*). Although the United States in 2000 ended restrictions on selling food to Cuba (*2*, *23*, *24*), restrictions on medicines or medical supplies were not repealed. Cuban imports of medical products from the United States have not increased substantially since 2001 (*2*). Although establishing causality is difficult, U.S. trade sanctions altered the medication supply and likely had focal, serious consequences on Cubans' health (*17*, *19*, *25*).

Good Health Despite a Weak Economy

However, impacts of sanctions on Cuba's financial systems, medical supplies, and aggregate health measures appear to be attenuated by their successes in other aspects of health care. Despite the embargo, Cuba has produced better health outcomes than most Latin American countries, and they are comparable to those of most developed countries. Cuba has the highest average life expectancy (78.6 years) and density of physicians per capita (59 physicians per 10,000 people), and the lowest infant (5.0/1000 live births) and child (7.0/1000 live births) mortality rates among 33 Latin American and Caribbean countries (*11*, *26*).

In 2006, the Cuban government spent about $355 per capita on health, 7.1% of total Gross Domestic Product (GDP) (*11*, *26*). The annual cost of health care for an American was $6714, 15.3% of total U.S. GDP. Cuba also spent less on health than most European countries. But low health care costs alone may not fully explain Cuba's successes (*27*),

School of Medicine, Stanford University, Palo Alto, CA 94305, USA.

*Member of the Social Sciences Research Council Cuban Working Group of the American Council of Learned Societies.
†Author for correspondence. E-mail: pkdrain@stanford.edu

which may relate more to their emphasis on disease prevention and primary health care, which have been cultivated during the U.S. trade embargo.

Cuba has one of the most proactive primary health care systems in the world. By educating their population about disease prevention and health promotion, the Cubans rely less on medical supplies to maintain a healthy population. The converse is the United States, which relies heavily on medical supplies and technologies to maintain a healthy population, but at a very high cost.

The medical education and training system has emphasized primary care since 1960, when Cuba created the Rural Social Medical Service to encourage young physicians to work in rural areas (*28*). By 1974, all medical graduates were expected to spend up to 3 years practicing community medicine in a rural area (*9*). Currently, on completion of medical school, 97% of graduates enter a 3-year family medicine residency training, called "integrated general medicine" (*10*, *29*, *30*). After family medicine residency, about 65% of physicians will start practicing primary-care medicine, and the remainder will enter specialty training (*31*).

Cuba has also created a health care infrastructure to support primary-care medicine. In 1965, Cuba created a system of community-based polyclinics, which provide primary-care, specialty services, and laboratory and diagnostic testing to a catchment area of 25,000 to 30,000 people (*32*). Each of the country's 498 polyclinics tailors medical services and education to the epidemiologic profile of their local population (*30*). Cuba added another primary-care level in 1984 by establishing neighborhood-based family medicine clinics, called consultorios (*29*, *31*, *33*). A polyclinic serves as the organizational hub for 20 to 40 consultorios. Every Cuban is scheduled to visit, or be visited by, a consultorio physician at least yearly (*34*).

Cuba has some of the highest vaccination rates and percentage of births attended by skilled health workers in the world (*26*). Health care provided at the consultorios, polyclinics, and larger regional and national hospitals is free to patients, except for some subsidized medications (*7*, *10*, *29*). This emphasis on primary-care medicine, community health literacy, universal coverage, and accessibility of health services may be how Cuba achieves developed-world health outcomes with a developing-world budget.

Policy Lessons: Travel, Trade, Health Care

A majority of Americans, both Democrats and Republicans, favor improving relations with, or easing sanctions against, Cuba (*35*). Congress is considering a bill to eliminate travel restrictions (H.R. 874/S. 428), and bills that could lift the trade embargo and facilitate medical imports and travel to Cuba (H.R. 188, H.R. 1530, H.R 1531, and H.R. 2272). The Obama Administration seems willing to sign these bills into law (*4*). We encourage legislation that at least allows unrestricted travel to Cuba and eliminates medicine and medical supplies from the embargo. Better policy would eliminate the trade embargo.

In March 2010, Congress introduced a bill to strengthen health systems and to expand the supply of skilled health workers in developing countries (H.R. 4933). Cuba has been actively doing this since 1999, when they opened the Latin American School of Medicine to train over 10,000 medical students a year from around the world (*36*). Cuba also continues to deploy physicians to work in some of the world's poorest countries, a practice started in 1961.

On the U.S. domestic front, given recent momentum in support of health-care reform, there may be opportunities to learn from Cuba valuable lessons about developing a truly universal health care system that emphasizes primary care. Adopting some of Cuba's successful health-care policies may be the best first step toward normalizing relations. Congress could request an Institute of Medicine study of the successes of the Cuban health system and how to best embark on a new era of cooperation between U.S. and Cuban scientists.

References and Notes

1. U.S. Department of State, *U.S.-Cuba Relations*; www.state.gov/www/regions/wha/cuba/policy.html.
2. R. Lugar, *Changing Cuba Policy—in the United States National Interest: Staff Trip Report to the Committee on Foreign Relations, U.S. Senate* (Government Printing Office, Washington, DC, 2009); http://lugar.senate.gov/sfrc/pdf/Cuba.pdf.
3. The U.N. General Assembly has voted overwhelmingly against the embargo for the previous 17 years, and the Organization of American States has called the embargo on food and medicines a violation of international law (*37*, *38*). An April 2009 poll showed that the majority of Americans supported lifting the travel ban (64%) and reestablishing diplomatic relations (71%) with Cuba (*35*).
4. Office of the Press Secretary, The White House, "Fact Sheet: Reaching out to the Cuban People," released 13 April 2009; www.whitehouse.gov/the_press_office/Fact-Sheet-Reaching-out-to-the-Cuban-people.
5. S. J. Pastrana, M. T. Clegg, *Science* **322**, 345 (2008).
6. U.S. Department of the Treasury, Title 31: Money and Finance, Treasury; Chapt. V–Office of Foreign Assets Control, Part 515, Cuban Assets Control Regulation, Code of Federal Regulation, 2009; www.access.gpo.gov/nara/cfr/waisidx_07/31cfr515_07.html.
7. F. Rojas Ochoa, C. M. López Pardo, *Int. J. Health Serv.* **27**, 791 (1997).
8. K. Nayeri, C. M. López-Pardo, *Int. J. Health Serv.* **35**, 797 (2005).
9. R. N. Ubell, *N. Engl. J. Med.* **309**, 1468 (1983).
10. P. De Vos, *Int. J. Health Serv.* **35**, 189 (2005).
11. United Nations Population Division, *World Population Prospects: The 2008 Revision* (United Nations, Geneva, 2009); http://data.un.org.
12. R. Garfield, S. Santana, *Am. J. Public Health* **87**, 15 (1997).
13. Cuban Democracy Act, Title 22, U.S. Code, §6001 et seq.; http://treas.gov/offices/enforcement/ofac/legal/statutes/cda.pdf.
14. A. F. Kirkpatrick, *Lancet* **348**, 1489 (1996).
15. Cuban Liberty and Democracy Solidarity (Libertad) Act, Title 22, U.S. Code, Section 6032 et seq.; www.state.gov/www/regions/wha/cuba/democ_act_1992.html.
16. P. G. Bourne, *Denial of Food and Medicine: The Impact of the U.S. Embargo on Health and Nutrition in Cuba* (American Association for World Health, Washington, DC, 1997); http://archives.usaengage.org/archives/studies/cuba.html.
17. Ministry of Public Health, *Informe Annual, 1992* (Ministry of Public Health, Havana, Cuba, 1993).
18. A. Marrero, J. A. Caminero, R. Rodríguez, N. E. Billo, *Thorax* **55**, 39 (2000).
19. D. Kuntz, *Int. J. Health Serv.* **24**, 161 (1994).
20. G. C. Román, *Neurology* **44**, 1784 (1994).
21. The Cuba Neuropathy Field Investigation Team, *N. Engl. J. Med.* **333**, 1176 (1995).
22. G. C. Román, *Ann. Intern. Med.* **122**, 530 (1995).
23. Public Law 106-387–Appendix, Title IX–Trade Sanctions Reform and Export Enhancement Act, §901, 14 STAT, 1549A, pp. 67–73.
24. Cuba then began purchasing food directly from the United States, and by 2007, the United States had become Cuba's largest supplier of food (*39*).
25. American Public Health Association, *The Politics of Suffering: The Impact of the U.S. Embargo on the Health of the Cuban People* (American Public Health Association, Washington, DC, 1993).
26. World Health Organization (WHO), *Statistical Information System* (WHO, Geneva, Switzerland, 2006); www.who.int/whosis/en/.
27. After statistically adjusting Cuban physician salaries (about $216 to $324 per year) to approximate average U.S. primary care wages ($150,000 per year) (*8*), the cost of providing health care in Cuba increases more than threefold ($1248 per capita), which is comparable to many European countries.
28. F. R. Ochoa, *Revist. Cubana Med. Gen. Integr.* **19**, 56 (2003).
29. A. J. F. Cardelle, *Int. J. Health Serv.* **24**, 421 (1994).
30. G. Reed, *Bull. World Health Organ.* **86**, 327 (2008).
31. L. T. Dresang, L. Brebrick, D. Murray, A. Shallue, L. Sullivan-Vedder, *J. Am. Board Fam. Pract.* **18**, 297 (2005).
32. M. Márquez, *Lancet* **374**, 1574 (2009).
33. R. Y. Demers, S. Kemble, M. Orris, P. Orris, *Fam. Pract.* **10**, 164 (1993).
34. H. Veeken, *BMJ* **311**, 935 (1995).
35. C.N.N., C.N.N. Poll: Three-quarters favor relations with Cuba, 12 April 2009; http://edition.cnn.com/2009/POLITICS/04/10/poll.cuba/index.html#cnnSTCText.
36. F. Mullan, *N. Engl. J. Med.* **351**, 2680 (2004).
37. United Nations, General Assembly overwhelmingly calls for end to United States embargo of Cuba, United Nations General Assembly, GA/10649, 30 October 2007; www.un.org/News/Press/docs/2007/ga10649.doc.htm.
38. J. Walte, "U.S. urged to ease Cuban embargo," *USA Today*, 7 March 1995.
39. W. Weissert, "U.S. remains Cuba's top food source, exported $600M in agricultural products to island in 2007," Associated Press, 22 January 2008.

40. We thank J. Kassirer, G. Reed, J. Kates, at The Henry J. Kaiser Family Foundation, and S. Montaña, a Cuban physician, for reviewing drafts of the manuscript.

Supporting Online Material

www.sciencemag.org/cgi/content/full/328/5978/572/DC1

10.1126/science.1189680

EVOLUTION

A Fungal Past to Insect Color

Gene transfer from a fungus to an ancestral aphid is responsible for the insect's red and green coloration.

Takema Fukatsu

Many animals recognize and respond to the environment, foods, and enemies by making use of visual cues. Hence, animal body color is an ecologically important trait, often involved in prey-predator interactions through mimicry, aposematism (colors that warn), and crypsis (camouflage) (*1*). In the pea aphid *Acyrthosiphon pisum*, an insect that destroys plants by feeding on the sap, red and green color insects frequently coexist in natural populations (see the figure). Among its major natural enemies, lady beetles preferentially attack red aphids on green plants (*2*), whereas parasitoid wasps deposit eggs in green aphids more frequently (*3*). It has been hypothesized that these opposite predation and parasitism pressures maintain the color variation in natural aphid populations. This represents one of the classical views on the evolutionary ecology of animal color polymorphism (*1*). On page 624 of this issue, Moran and Jarvik (*4*) report an unexpected layer interwoven under this well-known evolutionary scenario: Genes transferred from a fungus to the aphid genome underlie the red and green coloration.

Moran and Jarvik analyzed pigments from red and green laboratory strains of *A. pisum* and identified marked differences in the composition of carotenoids, pigment molecules (including vitamin A) known for diverse metabolic and ecological functions (*5*). The authors determined that green aphids contain only yellow carotenoids (γ-, -, and α-carotenes), whereas red aphids possess red carotenoids (torulene and dehydro-γ,ψ-carotene) in addition to the yellow ones. Because animals are generally devoid of genes required for carotenoid biosynthesis (*5*), the carotenoids identified by Moran and Jarvik were expected to originate from either food or microbial associates of the aphid. However, carotenoids are lipid-soluble compounds and are unlikely to occur in substantial quantities in plant sap. The genome sequences of the obligate bacterial symbiont *Buchnera aphidicola* and the facultative symbionts *Hamiltonella defensa* and *Regiella insecticola* contained no carotenoid biosynthetic genes (*6*–*8*). Where, then, do the carotenoids come from?

The recently published draft genome sequence of *A. pisum* (*9*) provided a crucial clue to the origin of the aphid carotenoids. Searches against the aphid genome retrieved four copies of carotene desaturase genes and three copies of fused carotene cyclase–carotene synthase genes. Phylogenetic analysis revealed that, strikingly, all the aphid carotenoid synthetic genes clustered with fungal genes with high statistical confidence. Genomic features of these genes strongly suggested that they were transferred from a fungus to an aphid ancestor, and subsequently subjected to duplications in the aphid genome. Because these genes were also found in the green peach aphid *Myzus persicae*, the lateral transfer event must have occurred in the common ancestor of *A. pisum* and *M. persicae*.

Red or green? Color polymorphism in the pea aphid is determined by carotenoid genes that were transferred from a fungus to an ancestral insect. This highlights the potential impact of lateral gene transfer on animal ecology and adaptation.

Are the fungal carotenoid synthetic genes actually involved in the aphid color polymorphism? If so, which of the genes? When laboratory aphid strains were surveyed for the carotenoid synthetic genes, all the genes were detected in red aphid clones. However, one of the four carotenoid desaturases was consistently missing in green aphid clones because of a 30-kb deletion in the genomic region. The correlation between the absence of the carotenoid desaturase gene and the green aphid color was confirmed with a number of field-collected green and red aphids. The authors further examined a yellow-green aphid strain (5AY), which was derived from a red aphid strain (5A) as a spontaneous mutant. In the carotenoid desaturase gene of 5AY, a nucleotide substitution was identified, which resulted in an amino acid replacement at one of conserved catalytic residues in the enzyme. Again, loss of the red color was coincident with malfunction of the carotenoid desaturase gene, confirming the genotype-phenotype connection.

Although regarded as idiosyncratic in the past, lateral gene transfers from a bacterial symbiont to a host organism have now been shown to occur in diverse insects and other invertebrates (*10*–*13*). Some of the transferred genes have eroded and become pseudogenes; others have acquired regulated expression in specific host tissues, such as genes derived from *Wolbachia* bacteria that are expressed by the host mosquito in its salivary glands (*12*) and bacterial genes located on the aphid chromosome that are expressed in its bacteriocytes specifically (*13*). In these cases, however, their biological roles are yet unknown. The case of aphid carotenoid genes is remarkable in that the lateral gene transfer established a prominent external trait: body color. Thus, a laterally transferred gene can contribute to the ecological adaptation of host animals.

The finding of Moran and Jarvik may stir some debate of the widespread premise that animals are unable to synthesize carotenoids (*5*). Considering the vital necessity of vitamin A and other cofactors for animals, why haven't some animals occasionally acquired such metabolic properties through lateral gene transfer? Whether the aphid case is an exception or other cases are to be found, this question deserves future investigation. A molecular clock analysis estimated the common ancestor of *A. pisum* and *M. persicae* to be younger than 30 to 80 million years ago (*14*), providing a date estimate of the transfer event. Many aphids suffer fungal diseases and some harbor fungal endosymbionts (*15*). Such aphid-associated fungi could have been a candidate source of the transferred genes.

A survey of the draft aphid genome identified more than 10 genes of lateral transfer origin (*13*). However, the carotenoid synthetic genes were overlooked because the survey was designed to detect bacterial genes

National Institute of Advanced Industrial Science and Technology (AIST), Tsukuba 305-8566, Japan. E-mail: t-fukatsu@aist.go.jp

in the eukaryotic genome. In comparison with prokaryote-prokaryote and prokaryote-eukaryote lateral gene transfers, less attention has been paid to eukaryote-eukaryote lateral gene transfers (*16*). Although such transfer events might have been relatively rare, the recent explosive accumulation of eukaryotic genome information opens a new window to look into unexplored dynamic evolutionary processes.

References

1. G. D. Ruxton *et al.*, *Avoiding Attack: The Evolutionary Ecology of Crypsis, Warning Signals and Mimicry* (Oxford Univ. Press, Oxford, 2005).
2. J. E. Losey *et al.*, *Nature* **388**, 269 (1997).
3. R. Libbrecht *et al.*, *J. Insect Behav.* **20**, 25 (2007).
4. N. A. Moran, T. Jarvik, *Science* **328**, 624 (2010).
5. T. W. Goodwin, *Annu. Rev. Nutr.* **6**, 273 (1986).
6. S. Shigenobu *et al.*, *Nature* **407**, 81 (2000).
7. P. H. Degnan *et al.*, *Proc. Natl. Acad. Sci. U.S.A.* **106**, 9063 (2009).
8. P. H. Degnan *et al.*, *Environ. Microbiol.* (2009).
9. International Aphid Genomics Consortium, *PLoS Biol.* **8**, e1000313 (2010).
10. N. Kondo *et al.*, *Proc. Natl. Acad. Sci. U.S.A.* **99**, 14280 (2002).
11. J. C. Dunning Hotopp *et al.*, *Science* **317**, 1753 (2010); published online 30 August 2007 (10.1126/science.1142490).
12. M. Woolfit *et al.*, *Mol. Biol. Evol.* **26**, 367 (2009).
13. N. Nikoh *et al.*, *PLoS Genet.* **6**, e1000827 (2010).
14. N. A. Moran *et al.*, *Proc. R. Soc. London Ser. B.* **253**, 167 (1993).
15. T. Fukatsu *et al.*, *Zool. Sci.* **11**, 613 (1994).
16. J. O. Andersson, *Cell. Mol. Life Sci.* **62**, 1182 (2005).

10.1126/science.1190417

ECOLOGY

Matters of Scale

Recognition of the scale dependence of ecological processes helps explain the distribution and abundance of organisms.

Brian J. McGill

School of Natural Resources, University of Arizona, Tucson, AZ 85721, USA. E-mail: mcgillb@u.arizona.edu

In 1687, Newton reported that the same laws could describe Galileo's data on balls rolling down ramps and Brahe's data on planets moving around the Sun (*1*). This observation implied that a finite list of principles could explain our infinite universe. And it inspired a leap across scales: The rules at human scales are not unique. Newton's laws of motion are still the dominant explanatory tool across scales ranging from a few atoms to solar systems. However, over the past 25 years, ecologists have come to realize that, unlike physics, ecology is scale-dependent (*2*–*4*). In a recent paper, Gotelli, Graves, and Rahbek (*5*) highlight the importance of this scale dependence: They show that a process that occurs at small spatial scales, namely competition between individuals, plays an important role even at the large scale of an entire country.

The realization that ecology is scale dependent has recently helped to explain a multitude of seemingly conflicting data in ecology (*6*, *7*). Now consideration of scale is helping to address another key issue in ecology: the question of what controls the distribution and abundance of organisms. For example, why is the scissor-tailed flycatcher (*Tyrannus fortificatus*), one of North America's most striking birds, found mainly in Texas and Oklahoma? Four main factors limiting the distribution of species have been hypothesized. Climate explains why the polar bear lives in the Arctic and palm trees grow in the tropics (*8*, *9*). Random dispersal determines who can get somewhere first or in large numbers. Spe-

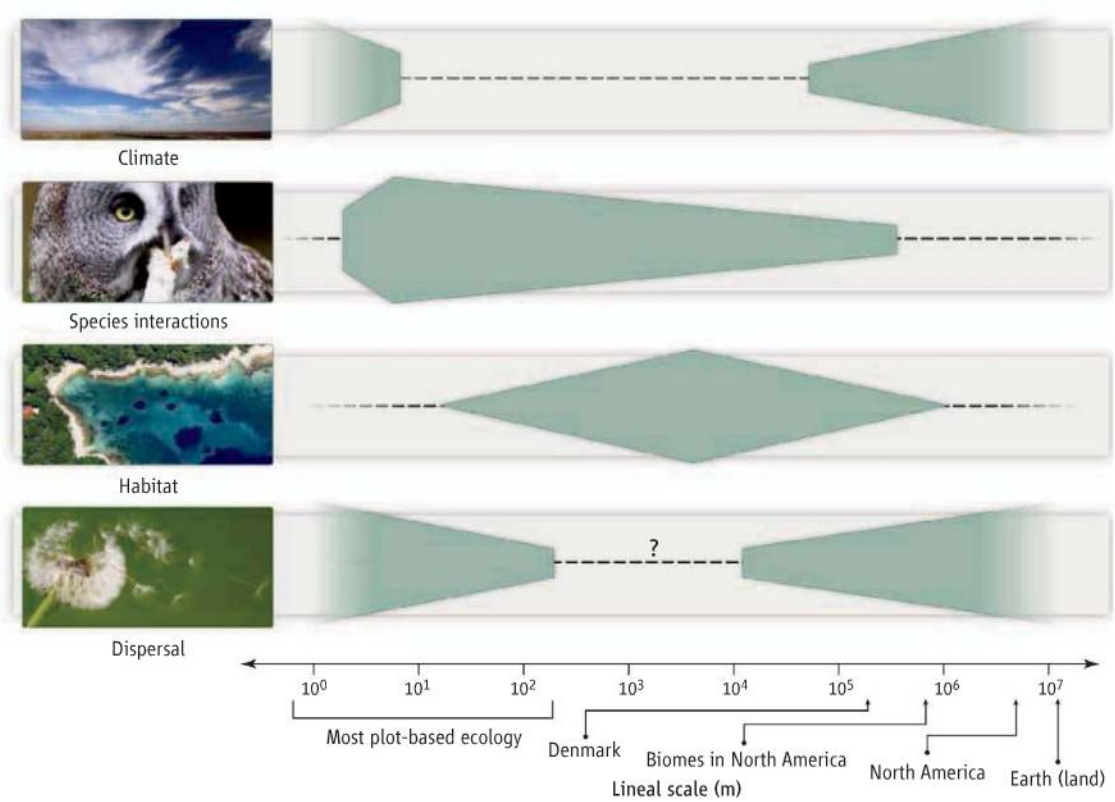

PHOTO CREDITS: JUPITERIMAGES

What controls the distribution of species? Four main processes (vertical axis) are believed to control the distribution of organisms; their relative importance changes with scale (horizontal axis). The thickness of the bar for a given factor at a given scale indicates how important that factor is at that scale. Ecologists began drawing such diagrams 25 years ago (*16*), but have only recently begun to perform empirical studies to test the suggested relationships. The question mark at intermediate scales of dispersal indicates that little data exist on this process at these scales. Climate is important for two scales, through two processes: microclimate (such as sun or shade) at small scales and biogeography at large scales. Most ecologists will disagree with some aspect of this figure, but it is the kind of complex, multifaceted, but testable hypothesis that ecology needs.

cies interactions (competition, predation, and disease) determine whether a species thrives or withers in a given environment (*10*–*12*). The final factor is habitat: Cottonwoods grow throughout the southwestern United States, but only along rivers. Which of these factors are most important?

It is becoming clear that the answer depends on scale. Competition is played out at small scales through interactions between individual organisms (birds in this case). It is difficult to imagine how the interaction between two birds can be influential at large scales, and indeed there is evidence that the role of competition drops off to close to zero at biome or nearly continental scales (*13*, *14*). But there is a big gap between small (up to hundreds of meters) and large (thousands of kilometers) scales. Where exactly does competition disappear?

Gotelli *et al*. assembled an impressive data set on the distribution of birds at the scale of a country (Denmark). Based on the evidence and thinking just mentioned, they expected that competition would no longer be influential at this scale, and that habitat (specifically, the varying types of vegetation) would be most important in controlling where bird species live. Surprisingly, they found that habitat appeared unimportant, but that competition was important in determining which bird species lived where.

The results help to put a band on the scales at which competition is important. Gotelli *et al*. show that at the scale of a few hundred kilometers on a side, competition is important, but we already know (*13*, *14*) that at the scale of a biome (roughly 1000 km by 500 km in the two cases studied), competition is not very important (see the figure). This is an astonishingly precise scale-dependent statement of when competition is important and unimportant.

Thus, Gotelli *et al*. provide an example of how ecology can proceed. Rather than debating which of the four forces is most important in general, ecologists need to ask which force (or forces) is most important at a given scale (see the figure).The first step toward identifying scale dependencies of this kind is to collect more data on what controls species distribution and other variables (such as richness, productivity, and abundance) across scales. However, this will lead to many distinct scale diagrams such as that in the figure, one for each variable to be explained. This raises several new challenges and questions.

What is the minimum number of scale diagrams that we need? Can we, for example, collapse the richness-area and richness-productivity diagrams into one? Given that scale is relative to organisms—forces acting at a scale of 1 m are unlikely to be the same for bacteria and elephants—how can we rescale depending on the organism? Another factor is time. It has been suggested that processes that dominate at large spatial scales usually occur over large temporal scales (*2*). Is this true? And can the importance of different processes (the thickness of the bars in the scale diagram) be measured quantitatively? Statistical techniques and nested sampling designs that tell us how much variation occurs in the variable of interest at each scale could help to address these questions (*15*). The answers will help to put ecology on a more quantitative footing.

References

1. I. Newton, *Philosophiæ Naturalis Principia Mathematica* (S. Pepys, London, 1687).
2. S. A. Levin, *Ecology* **73**, 1943 (1992).
3. J. A. Wiens, *Funct. Ecol.* **3**, 385 (1989).
4. D. C. Schneider, *Bioscience* **51**, 545 (2001).
5. N. J. Gotelli, G. Graves, C. Rahbek, *Proc. Natl. Acad. Sci. U.S.A.* **107**, 5030 (2010).
6. M. L. Rosenzweig, *Species Diversity in Space and Time* (Cambridge Univ. Press, Cambridge, 1995).
7. C. Rahbek, G. R. Graves, *Proc. Natl. Acad. Sci.* **98**, 4534 (2001).
8. G. Caughley, J. Short, G. C. Grigg, H. Nix, *J. Anim. Ecol.* **56**, 751 (1987).
9. T. Root, *J. Biogeogr.* **15**, 489 (1988).
10. R. H. MacArthur, *Geographical Ecology: Patterns in the Distribution of Species* (Princeton Univ. Press, Princeton, NJ, 1972).
11. G. E. Hutchinson, *Cold Spring Harb. Symp. Quant. Biol.* **22**, 415 (1957).
12. J. Silvertown, M. E. Dodd, D. J. G. Gowing, J. O. Mountford, *Nature* **400**, 61 (1999).
13. R. Russell, S. A. Wood, G. Allison, B. A. Menge, *Am. Nat.* **167**, E158 (2006).
14. J. A. Veech, *J. Biogeogr.* **33**, 2145 (2006).
15. B. J. McGill, *Am. Nat.* **172**, 88 (2008).
16. A. Shmida, S. Ellner, *Vegetatio* **58**, 29 (1984).

10.1126/science.1188528

ASTRONOMY

Hidden Growth of Supermassive Black Holes in Galaxy Mergers

Changes in the fraction of quasars hidden by gas and dust over cosmic time helps confirm models of the evolution and merger rates of galaxies.

Joel Primack

Black holes are found at the centers of massive galaxies. Although no light escapes from them, their presence can be revealed by the glow of surrounding gases compressed and heated by the driving force of the black hole's gravitation. This quasar emission ranges from low-energy radio waves to the highest-energy gamma-ray region of the electromagnetic spectrum. Quasar formation can be driven by galaxy mergers, which change the distribution of gas around the black hole. This process can also create stars that supernova and create interstellar dust that obscures our view of galactic centers in the visible to x-ray regions. On page 600 of this issue, Treister *et al*. (*1*) present an analysis of data from several space-based telescopes, showing that a greater fraction of quasars that formed in the early universe were obscured by dust, compared with its later stages. This is consistent with observational evidence on the evolution over cosmic time of gas-rich galaxies and a theoretical model for the rate at which they merge.

Like geologists and evolutionary biologists, astronomers reconstruct the past to understand the present. Landforms erode and only a tiny fraction of organisms fossilize, but all of the energy that was ever radiated by galaxies is still streaming through the universe and can be detected in some form. Some of this radiation is altered. For example, redshifting occurs because the wavelengths of photons stretch as the universe continues to expand, and some short-wavelength photons like x-rays and ultraviolet light are absorbed by dust and re-emitted at longer wavelengths. To figure out what happened in the cosmic past, we must see the entire electromagnetic spectrum, from the high-energy gamma rays to the long-wavelength radio waves. Fortunately, NASA's Great Observatories in space cover much of this wavelength range—x-rays (the Chandra X-ray Observatory), near ultraviolet to the near infrared (the refurbished

Physics Department, University of California Santa Cruz, Santa Cruz, CA 95064, USA. E-mail: joel@scipp.ucsc.edu

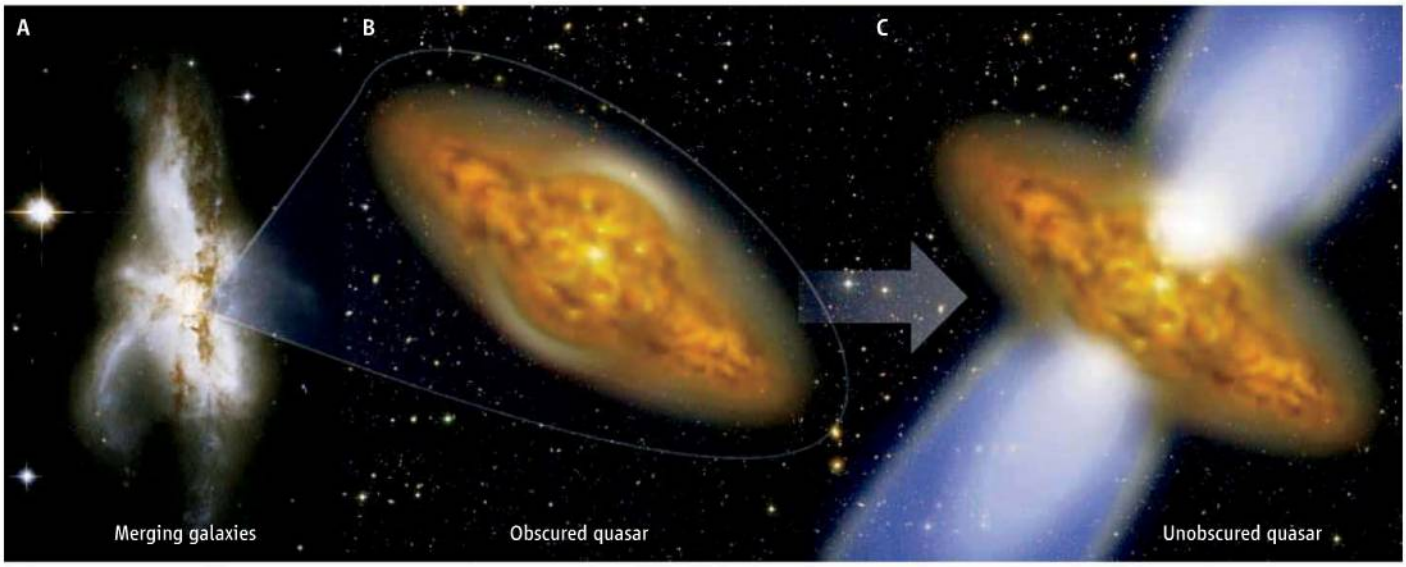

Varying degrees of transparency. (**A**) Galaxy mergers produce quasars (**B**) that are first hidden by gas and dust. (**C**) After about 100 million years, as the quasar radiation blows away the obscuring material, the quasars become visible. The quasar would still be obscured if viewed as seen here, but it would shine much more brightly than the entire galaxy if viewed from some perpendicular directions. The study by Treister *et al.* reveals how the formation of obscured versus visible quasars has changed since the early universe.

CREDITS: (A) GALAXY NGC6240 FROM THE HUBBLE HERITAGE/STSCI/AURA, ESA/HUBBLE COLLABORATION, AND A. EVANS/UNIVERSITY OF VIRGINIA, CHARLOTTESVILLE/NRAO/STONY BROOK UNIVERSITY; (B AND C) ARTIST'S VIEWS: KAREN TERAMURA/INSTITUTE FOR ASTRONOMY, UNIVERSITY OF HAWAII

Hubble Space Telescope), and infrared (the Spitzer Space Telescope).

What we hope to observe is the evolution of both black holes and their host galaxies, and to understand how both black holes and the stellar spheroids in which they are found can increase their masses by a factor of 100 or more during galaxy mergers. The mass of the black hole at the center of our Milky Way galaxy is relatively light, just 4 million times the mass of our Sun, and it resides at the very center of our galaxy's central mass of stars, the stellar spheroid (*2*), from which the spiral arms emanate. Black holes with masses up to billions of times greater than that of our Sun lurk at the centers of massive elliptical galaxies. In all cases, the mass of the black holes is about a thousandth the mass of their host stellar spheroids (*3*).

Black holes can exhaust the local neighborhood of material that feeds them. Some of the gas can be accelerated toward the black hole but may escape entry and shoot away from it at high speed. However, gas can be resupplied to the black hole when galaxies interact and merge (*4*). An example of a galaxy merger with a hidden quasar is shown in the figure, panel A. Computer simulations of such mergers of disk galaxies, which include their massive dark-matter halos, show that they produce elliptical galaxies, with the process sometimes accompanied by spectacular cosmic fireworks (*5*, *6*) (see movie s1).

Gravitational interaction between merging disk galaxies can drive gas into their central regions. The galaxy centers then merge, together with their black holes. The gas fuels gigantic bursts of star formation. Some of the stars produced are an order of magnitude more massive than the Sun. Their supernova explosions at the end of their lives produce great quantities of dust that obscure the galactic centers.

A small fraction of the central gas is accreted by the central black hole as an elliptical galaxy forms. The black hole's mass multiplies by a large factor, and the greater gravitational pull accelerates nearby matter, heating it and causing the radiation we see as a quasar. Late in cosmic time (the part of the universe near us), less than half of such accreting black holes are hidden by the surrounding gas and dust (as in the figure, panel B), whereas the other half shine as quasars in the visible spectrum and as x-rays (as in the figure, panel C). However, in the distant, early universe, the ratio of obscured to unobscured quasars was greater by about a factor of 10, according to observational evidence assembled by Treister *et al.* from the Spitzer, Hubble, and Chandra space telescopes.

These results agree with their modeling studies that use information on how the number of gas-rich galaxies and their merger rate evolved with cosmic time. The merger rate was determined by a large simulation (*7*) based on the Lambda–Cold Dark Matter (ΛCDM) model, the standard one used in modern cosmology (*8*). Most of the cosmic density is in two invisible ("dark") components, dark energy (lambda, about 72%) and cold dark matter (CDM, about 23%). Atomic matter is only about 5%, of which only about 0.5% of the total galactic mass is visible as stars, gas, or dust (*9*).

This agreement between observation and theory shows that the decrease in the fraction of obscured quasars in the nearby (late) universe is a consequence of the decreasing number of galaxies per unit volume as the universe expanded, the decreasing merger rate per galaxy, and the decreasing fraction of gas-rich galaxies as the gas turned into stars. Most of the growth of the mass of the supermassive black holes occurred in the quasar phase, much of it hidden by dust. However, the x-rays from this hidden black-hole accretion should be detectable by new focusing x-ray telescopes, including NASA's NuSTAR satellite (*10*), to be launched in 2011 and to be joined by the Japanese NeXT/Astro-H satellite (*11*) a few years later.

Part of the job of astronomers trying to discover how the universe formed is bookkeeping: counting galaxies of various types in various stages of evolution, both in observations and in increasingly powerful theoretical simulations. It is currently impossible to simulate all of the relevant physical processes, because even the most powerful supercomputers are not yet fast enough, and also because the physical phenomena are not yet understood sufficiently. The most productive approach for now is to simulate the formation of individual galaxies, including mergers, and then use these simulations and observations to guide larger bookkeeping efforts. The resulting semianalytic models attempt to follow the evolution of the entire galaxy population through cosmic time, including the formation of supermassive black holes (*12*, *13*). Fortunately, observations by satellite and ground-based observatories have determined

the cosmological parameters with great precision (*14*). The latest cosmological-scale simulations (*15*) are providing a basis for a new round of even more ambitious semianalytic models to be compared with new multiwavelength observations.

References and Notes

1. E. Treister *et al.*, Science **328**, 600 (2010); published online 25 March 2010 (10.1126/science 1184246).
2. F. Melia, *The Galactic Supermassive Black Hole* (Princeton Univ. Press, Princeton, NJ, 2007).
3. S. Tremaine *et al.*, *Astrophys. J.* **574**, 740 (2002).
4. A beautiful compilation of Hubble images of interacting galaxies is at http://hubblesite.org/newscenter/archive/releases/galaxy/interacting/2008/16/image/a
5. P. F. Hopkins, L. Hernquist, T. J. Cox, S. N. Dutta, B. Rothberg, *Astrophys. J.* **175**, (*Suppl.*), 390 (2008).
6. J. M. Lotz, P. Jonsson, T. J. Cox, J. Primack, *Mon. Not. R. Astron. Soc.* **391**, 1137 (2008).
7. V. Springel *et al.*, *Nature* **435**, 629 (2005).
8. J. R. Primack, N. E. Abrams, *The View from the Center of the Universe: Discovering Our Extraordinary Place in the Cosmos* (Riverhead, New York, 2006).
9. M. Fukugita, P. J. E. Peebles, *Astrophys. J.* **616**, 643 (2004).
10. www.nustar.caltech.edu
11. http://astro-h.isas.jaxa.jp/index.html.en
12. R. S. Somerville, P. F. Hopkins, T. J. Cox, B. E. Robertson, L. Hernquist, *Mon. Not. R. Astron. Soc.* **391**, 481 (2008).
13. N. Fanidakis *et al.*, http://de.arXiv.org/abs/0911.1128 (2009).
14. E. Komatsu *et al.*, http://arXiv.org/abs/1001.4538 (2010).
15. A. Klypin, S. Trujillo-Gomex, J. Primack, http://arXiv.org/abs/1002.3660 (2010).

Supporting Online Material

www.sciencemag.org/cgi/content/full/328/5978/576/DC1
Movie S1

10.1126/science.1189695

BEHAVIOR

Cooperation and Punishment

Punishment can support cooperative behavior in a group, but requires coordination.

Louis Putterman

In an era in which the "tragedy of the commons" has acquired new meaning on a global scale, social scientists are beginning to find hope in human nature. True, we are self-interested creatures capable of destroying the habitats that support us as we each focus on getting our share of the global commons before others beat us to it. Yet *Homo sapiens* could never have populated the planet and mastered complex technologies and organizational forms had nature not also made us sensitive to one another's regard. Both field studies and laboratory experiments depict humans as willing to cooperate when convinced that others are doing the same and that at least some will incur costs to sanction cheating. On page 613 in this issue, Janssen *et al.* (*1*) show that communication among members of a group is key to establishing cooperation and using punishment effectively, and on page 617, Boyd *et al.* (*2*) provide a model of how signaling (a stylized kind of communication) could have allowed punishment and cooperation to evolve.

For over a century, economists and social scientists have used the "*Homo economicus*" construct to depict humans as rational beings who act entirely in their own self-interest. Populating their models with *Homo economicus* gave economists the basis for predicting efficient outcomes in market interactions, but it also implied that mutually beneficial cooperation could not occur without binding contracts or outside enforcement. In the prisoners' dilemma game, each of two players has both a cooperative and a selfish option ("defection").

Achieving cooperation. Coordination is key to successful cooperation. A group in rural Burkino Faso is shown.

CREDIT: CURT CARNEMARK/THE WORLD BANK (1993)

While both would be better off with mutual cooperation than with mutual defection, the fact that the privately best option of each is to defect leads to the prediction of mutual defection, if the game is played once without binding agreements. Still, when real individuals are enlisted to play the game as experimental subjects, with real money at stake, substantial numbers try cooperation.

Related evidence that real individuals are not accurately depicted by the *Homo economicus* model came from experiments using the voluntary contribution mechanism, a variation on the prisoners' dilemma game, in which each individual can choose not only full cooperation or no cooperation, but also intermediate levels of cooperation in the form of contributing funds to a collectively advantageous group project. The first voluntary contribution mechanism experiments defied the *Homo economicus* prediction of universal "free-riding," finding instead that many players did contribute to the common good rather than defect by contributing nothing. But when the game was played repeatedly for a preannounced number of times, contributions fell off toward zero. However, a result frequently replicated in the last decade shows that when subjects are permitted to communicate before playing or are allowed to punish one another's actions, conditional cooperation trumps strict self-interest (and *Homo sapiens* triumphs over *Homo economicus*) (*3*).

In different ways, Janssen *et al.* and Boyd *et al.* address the same problem. Permitting costly punishment often leads to more sustained cooperation, and the willingness to incur a cost to punish is characteristic of *Homo sapiens*. But uncoordinated punish-

Department of Economics, Brown University, Providence, RI 02912, USA. E-mail: louis_putterman@brown.edu

ment is frequently counterproductive, and being punished for letting others do the punishing (free-riding on punishment) almost never occurs (*4*). This raises the question of why anyone incurs the cost of punishing.

The solutions that Janssen *et al*. and Boyd *et al*. propose share the common element that punishment solves the problem of cooperation efficiently only when it is coordinated. The study by Janssen *et al*. is a new-generation laboratory decision-making experiment using an interface that simulates the common pool resource problem, a cousin of the voluntary contribution mechanism, more realistically than past work. Like earlier experiments (*5*), it allows subjects either to communicate, to punish one another, or both. Both generations of experiments find that subjects engage in costly punishment, but that punishment enhances cooperation and efficiency (sustainable harvesting of the resource) only when combined with the coordinating advantages of communication. The new results are even stronger than the old, in that the opportunity to punish is found to be outright counterproductive when not combined with communication.

Boyd *et al*. were inspired in part by the mixed or negative experimental findings regarding uncoordinated punishment. They introduce coordination into a purely theoretical model of how the propensity to punish could have evolved. Their model recognizes that the anticipation of punishment for free-riding can make cooperative behavior individually beneficial, but being predisposed to letting others do the costly punishing would appear to give one's own genes an evolutionary advantage. One element of the solution discussed by Boyd and collaborators elsewhere is the idea that individual disadvantage can be outweighed evolutionarily by group advantage if the disadvantage is sufficiently small and there is sufficient separation of groups and/or barriers to mobility among groups. One possible solution (*6*) includes higher-order punishing of those who free-ride by not punishing other noncooperators. If punishing second-, third-, or still higher-order free-riding (where third-order free riding means failing to punish those who fail to punish noncooperators) were common enough, the argument is that first-order noncooperation would be so rare that true punishing types (those with a preference to punish, even if they are not punished for failing to do so) almost never incur the cost of punishing and thus suffer only a negligible individual fitness disadvantage. But retaliation for punishing is more common in the lab than is punishment for failing to punish, so the alternative solution of Boyd *et al*. appears preferable: Punishers avoid wasting resources by not punishing unless enough others will also do so, the key being the emission of credible preplay signals.

Achieving cooperation with informal methods of coordination is not a problem of primitive and small-scale societies only. Today's state and multilateral institutions function only because problems of free-riding are being solved on a day-to-day basis, in part through willingness to cooperate and inclination to punish defection. Whether humans can solve seemingly intractable problems such as those of climate change and nuclear weapons proliferation depends to a large extent on whether the human sociality that evolved in our small-group past is robust enough to overcome the ever-present temptations to free ride.

References

1. M. A. Janssen, R. Holahan, A. Lee, E. Ostrom, *Science* **328**, 613 (2010).
2. R. Boyd, H. Gintis, S. Bowles, *Science* **328**, 617 (2010).
3. S. Gächter, B. Herrmann, *Philos. Trans. R. Soc. B* **364**, 791 (2009).
4. M. Cinyabuguma, T. Page, L. Putterman, *Exp. Econ.* **9**, 265 (2006).
5. E. Ostrom, J. M. Walker, R. Gardner, *Am. Polit. Sci. Rev.* **86**, 404 (1992w).
6. J. Henrich, *J. Econ. Behav. Organ.* **53**, 3 (2004).

10.1126/science.1189969

EVOLUTION

Chimpanzee Technology

Chimpanzees are the only nonhuman animal species known to make and use a wide range of complex tools.

William C. McGrew

Almost 50 years ago, Jane Goodall watched an adult male chimpanzee in the Gombe Stream Reserve, Tanzania, make and use a blade of grass to "fish" termites from a mound for food (*1*). Her mentor, Louis Leakey, declared, "Now we must redefine 'tool,' redefine 'man,' or accept chimpanzees as humans!" (*2*). Today, we know that various vertebrates in nature have elementary technology, but chimpanzees across Africa continue to astonish us with their technical abilities. Recent findings have further blurred the boundaries between what we consider to be human versus nonhuman by showing that chimpanzees can use and combine tools in complex sequences and combinations.

Leverhulme Centre for Human Evolutionary Studies, University of Cambridge, Cambridge CB2 1QH, UK. E-mail: wcm21@cam.ac.uk

Since Goodall's discovery, scientific analyses of chimpanzee behavior have changed from natural history notes to descriptive, classifying ethnography, to theory-driven, hypothesis-testing ethnology (*3*, *4*). To systematic but serendipitous observation has been added experimentation, even with free-ranging apes (*5*, *6*). Eight populations of wild chimpanzees across Africa from Senegal to Tanzania are fully habituated (that is, they can be observed at close range from dawn to dusk). Scores more are not fully habituated, but leave behind artifacts that can be collected and analyzed.

Researchers use the term "tool kits" to describe the repertoire of tools used habitually by a group of chimpanzees (*7*, *8*). The tool kits of most chimpanzee populations consist of about 20 types of tools, which are used for various functions in daily life, including subsistence, sociality, sex, and self-maintenance. This tool-kit size is relatively constant, whether the apes live in rainforest or on savanna, with one regional exception: The tool kits of three Ugandan populations (Budongo, Kanyawara, and Ngogo), all well-habituated, are about half the usual size, for reasons as yet undetermined (*9*).

The uses to which tools are put vary across chimpanzee populations. At Goualougo, Republic of Congo, the most commonly used tools are for extractive foraging, whereas at Ngogo, they are for hygiene and courtship. However, some tools are used by all chimpanzee populations: They all make leaf sponges to obtain drinking water, show aimed throwing of missiles, and communicate by drumming on tree buttresses.

Chimpanzees also use tool sets, that is, they use two or more tools in an obligate sequence to achieve a single goal. In the most impressive example, a chimpanzee popula-

tion in Gabon uses a tool set of five objects—pounder, perforator, enlarger, collector, and swab—to obtain honey (*10*). Other tool sets are used to fish for termites or dip for army ants. All these tool sets must be used in the correct functional order to be successful. Some primatologists have argued that this necessity for sequential order is a sign of complex cognitive processes.

Another way of using tools is as a tool composite, that is, two or more objects are used simultaneously and complementarily to achieve a goal. Tool composites long used by humans include bow-and-arrow and mortar-and-pestle, but such composites are virtually unknown in other species. In chimpanzees, the main example is the use of stones or clubs as hammers to crack nuts on anvils of stone or wood (see the photo). This impressive technology provides access to embedded, high-calorie nut meat, with less expenditure of energy and less risk to the consumer's teeth. At Bossou, Guinea, chimpanzees have favorite combinations of hammer and anvil stones, which they use again and again (*11*).

Learning to use tools. Chimpanzee mother, juvenile, and infant at Bossou, Guinea. While the mother cracks oil palm nuts, the juvenile pays attention and the infant plays with nuts.

Less common are compound tools, in which two or more components are combined as a single working unit. Human examples are commonplace, including hafted spears (with shaft, point, and adhesive) and bead necklaces (with beads, string, and knot). Compound tools used by chimpanzees include the leaf sponge: Several fresh leaves are compressed into a single absorbent mass that allows water to be extracted from inaccessible tree holes (*12*). Another example is the wedge stone, which chimpanzees insert under a stone anvil to level its working surface, thus making it more efficient. Finally, to make their sleeping platforms (beds or nests), great apes daily interweave various branches, twigs, and leaves to make a frame, mattress, lining, and even a pillow (*13*).

How long have chimpanzees and their ancestors been making such complex tools? Chimpanzee tool use often modifies the raw materials (even stones), making them distinguishable from natural damage (*14*). Systematic excavation, radiometric dating, organic residues, wear patterns, actualistic experimentation (in which archaeologists seek to model past processes by recreating them in the present), and even museum studies have now been applied to the stone artifacts generated by ape tool users (*15*, *16*). The search is on for diagnostic wear patterns that allow the stone artifacts of the chimpanzee ancestors to be distinguished from those of early humans. Using apes as models may allow us to identify the precursors of the oldest known human tools by focusing on percussive technology, such as pounding tools, before the onset of Oldowan industries 2.6 million years ago.

Of the other living great apes, two taxa—bonobo and gorilla—show no habitual tool use in nature, which is puzzling given that laboratory studies show that their intelligence is comparable to that of chimpanzees. The fourth taxon—orangutan—shares many of the attributes of chimpanzees; for example, orangutan tool kits vary across populations. However, their largely arboreal lifestyle curtails their technical expression. (Most chimpanzees use tools while on the ground.) Among other animals, species such as the Galapagos woodpecker finch, California sea otter, and Egyptian vulture are specialists at a single kind of tool use. Of the birds, the impressive New Caledonian crow lags far behind the apes with regard to the types of elementary technology described above. New Caledonian crows make tools in the wild and in captivity, but only for extractive foraging. It is the only species of corvid habitually to make tools in nature. Of the other primates, the bearded capuchin monkeys top the tool use list: Their only well-established tool use is the use of hammer-and-anvil to crack nuts, but they also use stone tools to dig up roots at one site.

Among all animals, only chimpanzees appear to be able to use one type of raw material to make many kinds of tools (e.g., leaf as sponge, napkin, or fishing probe), or make one kind of tool from many raw materials (fishing probe from grass, bark, vine, and twig). Only chimpanzees have been shown to vary in their tool use at a multitude of levels, from individual, family, community, and population to subspecies. Chimpanzees also continue to yield new forms of tool use from continuing study (*17*, *18*): In the Nimba Mountains of Guinea, they "cleave" fibrous, basketball-sized fruits into manageable smaller pieces, using hammers and anvils (*19*); this is unlike nut-cracking, for example, which cracks open natural containers to get at the goal item inside.

With each passing day, the number of wild chimpanzees declines, with advancing deforestation and expansion of the bush-meat trade. Whole groups of chimpanzees already have been exterminated, and with them, their technological heritage, which probably will never be recovered. If we value the technology of our nearest living relations, in its own right or to help in understanding our ancestors, then we must not allow the apes to go extinct.

References

1. J. Goodall, *Nature* **201**, 1264 (1964).
2. D. Peterson, *Jane Goodall: The Woman Who Redefined Man* (Houghton-Mifflin, Boston, 2006), p. 212.
3. W. C. McGrew, *The Cultured Chimpanzee: Reflections on Cultural Primatology* (Cambridge Univ. Press, Cambridge, 2004).
4. T. Nishida *et al.*, *Primates* **50**, 23 (2009).
5. T. Matsuzawa, *Anim. Cogn.* **12**, (Suppl. 1), 1 (2009).
6. Wild is a subcategory of free-ranging. There are released chimpanzees on island sanctuaries who are studied experimentally, for example on Ngamba Island in Uganda: They are free-ranging but not wild.
7. A. Fowler, V. Sommer, *Int. J. Primatol.* **28**, 997 (2007).
8. C. M. Sanz, D. B. Morgan, *J. Hum. Evol.* **52**, 420 (2007).
9. D. P. Watts, *Int. J. Primatol.* **29**, 83 (2008).
10. C. Boesch *et al.*, *J. Hum. Evol.* **56**, 560 (2009).
11. S. Carvalho, D. Biro, W. C. McGrew, T. Matsuzawa, *Anim. Cogn.* **12** (suppl. 1), 103 (2009).
12. C. Sousa, D. Biro, T. Matsuzawa, *Anim. Cogn.* **12** (suppl. 1), 115 (2009).
13. F. A. Stewart, J. D. Pruetz, M. H. Hansell, *Am. J. Primatol.* **69**, 930 (2007).
14. J. Mercader *et al.*, *Proc. Natl. Acad. Sci. U.S.A.* **104**, 3043 (2007).
15. M. Haslam *et al.*, *Nature* **460**, 339 (2009).
16. S. Carvalho, E. Cunha, C. Sousa, T. Matsuzawa, *J. Hum. Evol.* **55**, 148 (2008).
17. R. A. Hernandez-Aguilar, J. Moore, T. R. Pickering, *Proc. Natl. Acad. Sci. U.S.A.* **104**, 19210 (2007).
18. J. D. Pruetz, P. Bertolani, *Curr. Biol.* **17**, 412 (2007).
19. K. Koops *et al.*, *Primates*, published online 8 December 2009; 10.1007/s10329-009-0178-6.

10.1126/science.1187921

CREDIT: E. NOGAMI, PRIMATE RESEARCH INSTITUTE/KYOTO UNIVERSITY

SYSTEMS BIOLOGY

Biological Systems Theory

The robustness of a biochemical network can be inferred mathematically from its architecture.

Jeremy Gunawardena

Mathematical models are fashionable in systems biology, but there is a world of difference between a model and a theorem. When researchers build models, they make assumptions about a specific experimental setting and have to choose values for rate constants and other parameters. A theorem, by contrast, can apply to a setting of arbitrary molecular complexity, such as a biochemical network with many components. In a recent study, Shinar and Feinberg (*1*) formulate a theorem that shows when such biochemical networks exhibit "absolute concentration robustness."

Robustness is a widely used concept in biology but notorious for being poorly defined. In the Shinar and Feinberg theorem, absolute concentration robustness means that the concentration of one of the network components remains exactly the same in any positive steady state of the network. This is true no matter how much of each of the other components is present. The robust concentration value depends only on the parameters of the network, not on amounts. Remarkably, Shinar and Feinberg discovered a condition that depends only on the structure of the biochemical reaction network, and not on parameter values, under which absolute concentration robustness occurs.

What makes this theorem of interest not just to mathematicians but also to biologists is that it distills and clarifies previous studies of bifunctional enzymes in the model bacterium *Escherichia coli* (*2*–*4*). The EnvZ-OmpR two-component osmoregulator (see the figure) and the glyoxylate bypass regulator (which allows two-carbon sugars like acetate to be used for biosynthetic purposes) both use bifunctional enzymes. In each case, the concentration of one of the key components in the biochemical network has been shown experimentally to have a high degree of robustness to changes in the amounts of the network components (*2*, *3*). With some plausible assumptions about the biochemistry, the theorem of Shinar and Feinberg explains why. Coincidentally, shortly after Shinar and Feinberg proposed their theorem, a new bifunctional metabolic enzyme (fructose 1,6-bisphosphate aldolase/phosphatase) was discovered among the archaea (*5*). Such enzymes occur in all walks of life. Thus, the theorem provides a starting point for understanding the advantages that bifunctionality might bring.

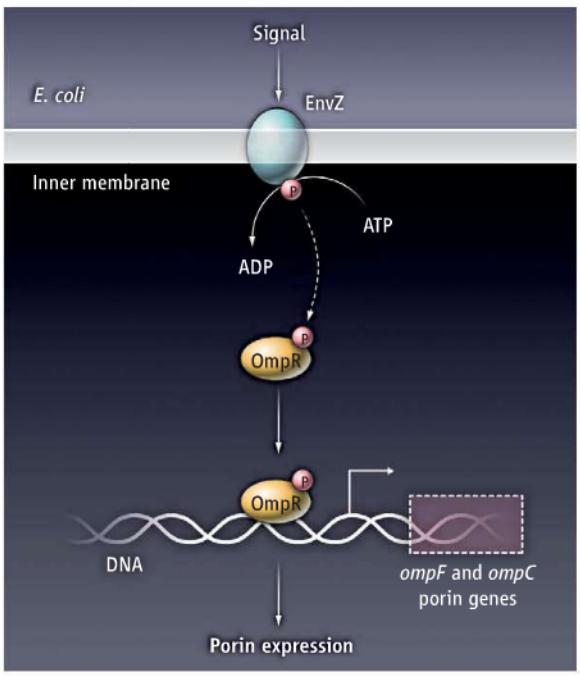

Biochemical network dynamics. A two-component regulatory system allows *E. coli* to respond to changes in environmental osmolarity. The histidine kinase EnvZ responds to a stimulus by transferring phosphate from ATP to a histidine residue. Phosphorylated EnvZ then transfers its phosphate to an aspartic acid on the response regulator, OmpR. The regulator then affects gene expression. Shinar and Feinberg's theorem can be applied to show that the concentration of phosphorylated OmpR is the same in any positive steady state (absolute concentration robustness), irrespective of the amounts of network components present.

Early embryologists were astounded by the robustness of development. Conrad Waddington conceived of the developmental process as a ball rolling down a landscape of branching valleys, with distinct differentiated states at the ends of valleys (*6*). This "epigenetic landscape" arises from the underlying network of gene and protein interactions, and its ridges and contours suggested how development could be robust to perturbations that pushed the ball off course without taking it across the ridges ("canalization"). This is a form of dynamical robustness; it is very far from a steady state.

Remarkably, Waddington's intuitive conception was formalized by the French mathematician René Thom, in what became known as "catastrophe theory" (*7*). This interdisciplinary marriage was one of the highlights of the 1960s explosion of interest in theoretical biology (*8*). Waddington is now an icon of evolutionary developmental biology, and the concepts he introduced are central to the field (*9*). As for catastrophe theory, it has had its fans as well as its detractors, but its biological roots are rarely remembered. Waddington and Thom did not know the molecular details, and their mathematics could not be guided by experiments and data. That is what distinguishes the systems biology of Shinar and Feinberg from the theoretical biology of the 1960s. Now that many of the molecular components are known, we can start to explain how robustness emerges from molecular mechanisms (*1*, *2*, *4*, *5*).

So far, the steady-state theorem of Shinar and Feinberg has been applied only to bifunctional enzymes. A robust variable is an example of an "invariant": a polynomial equation in the component concentrations that holds in any steady state (*10*). It is a particularly simple polynomial because it is linear and has only one variable. However, networks can have more complex invariants, as in the case of multisite protein phosphorylation (*10*). In this case, the invariant characterizes the network structure. If it is not satisfied at steady state, then additional reactions are present and the way in which the invariant breaks down can help to identify the new reactions. What is common to both absolute concentration robustness and invariants is that mass-action kinetics, which is the most systematic way to work out the rates of production and consumption of network components, always gives rise to polynomial rate equations from which invariants can be calculated. It becomes increasingly difficult to manipulate polynomials when there are several variables and higher degrees, as happens with mass-action biochemistry, but a branch of mathematics called computational algebraic geometry provides the tools for doing exactly that (*10*).

Department of Systems Biology, Harvard Medical School, Boston, MA 02115. E-mail: jeremy@hms.harvard.edu

Absolute concentration robustness and invariants are systems properties that arise from the coordinated behavior of all the components in the network. Such integrative analysis is still in its infancy. Does some evolutionary advantage accrue to the organism from absolute concentration robustness? This property can be verified experimentally for certain networks and we can speculate about why it is needed, yet the answer lies not in the network but in the environments in which the organism exists. *E. coli* is a gut microbe. Did absolute concentration robustness evolve in osmoregulation and in utilization of two-carbon sugars because of the intestinal physiology and ecology of the gut microbiota, or is it merely a spandrel in some molecular architecture that we cannot yet perceive (*11*)?

"Systems" thinking has always been present in biology, even if its importance has waxed and waned with changes in experimental capabilities. The disciplinary histories of embryology, ecology, genetics, physiology, immunology, and neuroscience, among others, suggest that mathematical tools become important when attention shifts from identifying the components to understanding their collective function. What is different today is that the molecular details are at the bottom of the biological hierarchy. Molecular biology was reductionism's finest hour. Now, there is nowhere left to go but up.

References

1. G. Shinar, M. Feinberg, *Science* **327**, 1389 (2010).
2. E. Batchelor, M. Goulian, *Proc. Natl. Acad. Sci. U.S.A.* **100**, 691 (2003).
3. D. C. LaPorte, P. E. Thorness, D. E. Koshland Jr., *J. Biol. Chem.* **260**, 10563 (1985).
4. G. Shinar *et al.*, *PLOS Comput. Biol.* **5**, e1000297 (2009).
5. R. F. Say, G. Fuchs, *Nature*, **464**, 1077 (2010).
6. C. H. Waddington, *The Strategy of the Genes: A Discussion of Some Aspects of Theoretical Biology* (Allen & Unwin, London, 1957).
7. R. Thom, *Structural Stability and Morphogenesis* (Benjamin, Reading, MA, 1975); English transl. of the 1972 French edition.
8. G. Mitchison, *Curr. Biol.* **14**, R97 (2004).
9. J. M. W. Slack, *Nat. Rev. Genet.* **3**, 889 (2002).
10. A. K. Manrai, J. Gunawardena, *Biophys. J.* **95**, 5533 (2008).
11. S. J. Gould, R. D. Lewontin, *Proc. R. Soc. Lond. B. Biol. Sci.* **205**, 581 (1979).

10.1126/science.1188974

APPLIED PHYSICS

The Road Ahead for Metamaterials

Metamaterials enable us to design our own "atoms" and thus create materials with new properties and functions.

Nikolay I. Zheludev

Metamaterials are artificial media structured on a size scale smaller than the wavelength of external stimuli. Whereas conventional materials derive their electromagnetic characteristics from the properties of atoms and molecules, metamaterials enable us to design our own "atoms" and thus access new functionalities, such as invisibility and imaging, with unlimited resolution.

The next stage of this technological revolution will be the development of active, controllable, and nonlinear metamaterials surpassing natural media as platforms for optical data processing and quantum information applications (*1*). Metamaterials are expected to have an impact across the entire range of technologies where electromagnetic radiation is used, and will provide a flexible platform for modeling and mimicking fundamental physical effects as diverse as superconductivity and cosmology and for templating electromagnetic landscapes to facilitate observations of phenomena that would otherwise be difficult to detect.

In terms of a Tree of Knowledge with roots embedded deep in the soil of microwave technology (see the figure), metamaterials became a big issue when the tree brought forth the "forbidden fruit" of negative-index media. Agressively contested when it frst appeared, the concept of negative index is now widely accepted and the focus of research has moved toward application. Other developments have been metamaterials with strong magnetic response and "magnetic mirror" functionality at optical frequencies, the discovery of structured surfaces exhibiting directional asymmetry in transmission, and metal structures invisible to electromagnetic radiation. Substantial effort has gone into the development of chiral "stereo" metamaterials for controlling the polarization state of light and achieving negative refraction. Metamaterials exhibiting properties suitable for use in delay lines and sensors have also been demonstrated across the entire spectral range, from microwaves to optics. Another active area of research has been in waveguide applications. The fascinating "transformation optics" idea of controlling the fabric of "electromagnetic space" (and thus light propagation) by filling it with metamaterial is being developed, requiring media with coordinate-dependent parameters, and offers cloaking and light-channeling solutions such as sophisticated lenses and "mirage" devices.

In developing active gain-assisted metamaterials, the main goal is the compensation of losses that dampen the coupled oscillations of electrons and light (known as plasmons) in the nanostructures. These losses render photonic negative-index media useless. One solution is to combine metamaterials with electrically and optically pumped gain media such as semiconductor quantum dots (*2*), semiconductor quantum wells, and organic dyes (*3*) embedded into the metal nanostructures. Electrically and optically pumped semiconductor gain media and emerging technology of carbon monolayers (graphene) could be expected to provide loss compensation from optical to terahertz spectral ranges. Alloys and band-structure engineering of metals also promise better plasmonic media.

Another grand goal is to develop a gain-assisted plasmon laser, or "lasing spaser" device (*4*): a flat laser with its emission fueled by plasmonic excitations in an array of coherently emitting metamolecules. In contrast to conventional lasers operating at wavelengths of suitable natural molecular transitions, the lasing spaser does not require an external resonator and its emission wavelength can be controlled by metamolecule design. Finally, the use of nanostructured high-permittivity materials offers the possibility of tailoring the electric and magnetic response in metamaterials consisting only of dielectric, thus removing the issue of losses at the source (*5*).

The development of nanoscale all-optical data processing circuits depends on the availability of fast and highly responsive nonlinear media that react to light by changing their refractive index and absorption. In all media where functionality depends on electronic or molecular anharmonicity, stronger responses come at the expense of longer reaction times, a constraint that is practically impossible to break. The plasmonic nonlinearity of metals constituting metamaterial nanostructures is extremely fast and could provide terahertz modulation, but requires high intensities to

Optoelectronics Research Centre and Centre for Nanostructured Photonic Metamaterials, University of Southampton, Southampton SO17 1BJ, UK. E-mail: niz@orc.soton.ac.uk

operate (*6*). Combining conventional nonlinear media with metamaterial nanostructures is a powerful way of engineering an enhanced response. Metamaterials can slow light, thereby increasing the interaction time with nonlinear medium embedded in it, or they can help by concentrating the local field and thus enhancing a nonlinear response. Prime contenders emerging for hybridization with metamaterials are semiconductors and semiconductor multiple–quantum well structures used as substrates for metallic framework, liquid crystals, conjugated polymers, carbon nanotubes (*7*), and fullerenes implanted into the fabric of the meta materials.

The ability to tune and switch the properties of materials, something very rarely offered by nature, can be achieved in metamaterials. Consider a metal metamaterial structure on a thin layer of dielectric, the properties of which can be controlled by external stimuli. A change in the refractive index in the layer will modify the plasmon resonances of the nanostructure. This will lead to a strong change in the resonant transmission and reflection of the hybrid (*8*). "Phase-change" materials are prime agents for switching: Chalcogenide glasses have been used in rewritable optical disk technology for several decades, providing fast and reproducible changes in optical properties in response to excitation. This functionality is underpinned by phase transitions between crystalline and amorphous states and may be engaged by optical or electrical stimulation; a nanoscale metamaterial electro-optical switch using chalcogenide glass has already been demonstrated (*9*). Similar properties are exhibited by transition metal oxides, in particular vanadium oxide (*10*, *11*). Switchable metamaterials based on arrays of micro- and nano-electromechanical devices are also being developed.

Conducting oxides and graphene are other favorites that promise to add electro-optical capability to metamaterials, in particular in the infrared and terahertz domains, by exploiting the spectral shift of electromagnetic response driven by applied voltage (*12*). The magnetic control of plasmons in layered structures of ferroelectric and noble metal can also be engaged to tune metamaterials (*13*). Sensor applications are another growth area in metamaterials research where planar structures with narrow resonances are well suited to detect low-concentration analytes; for instance, a single molecular layer of carbon can induce a multifold change in the transmission of a metamaterial (*14*).

Superconducting metamaterials (*15*) offer an incredibly fertile arena, as losses there are much lower than those of copper. Nonlinear and multistable behaviors could be observed in superconducting metamaterials, which may be extremely sensitive to external stimuli such as magnetic field, light, and current, promising highly reactive, switchable devices. Even more intriguing is the fact that the classical object of metamaterials research, the ubiquitous split ring metamolecule, has much in common with a fundamental unit of superconductivity, the Josephson junction ring. This invites one to think about exploiting quantum coherence in metamaterials: an array of superconducting Josephson phase qubits, each of which can be considered as macroscopic metamolecules with a multilevel quantum structure. By replacing the classical plasmonic resonators of today's metamaterials, Josephson qubits will allow for the engineering of truly quantum metamaterials, capable of demonstrating the entire palette of atomic spectroscopy phenomena.

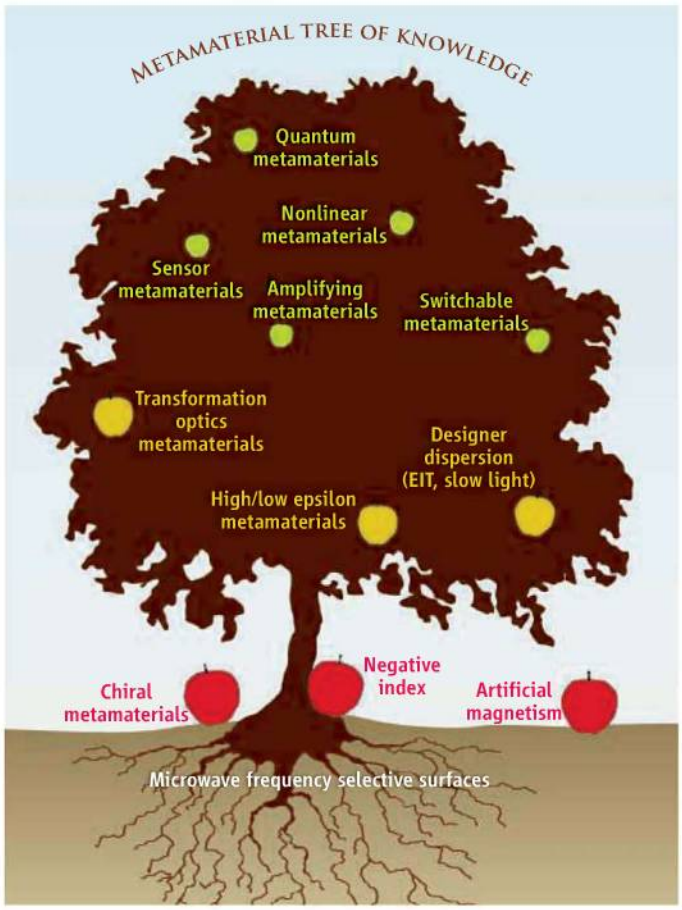

Fruit for the picking. The metamaterial Tree of Knowledge shows the progression and future of metamaterials research. The "forbidden fruit" of negative-index metamaterials is ripe: The concept is now widely accepted and research is now moving into the domain of application. Chiral metamaterials and those exhibiting artificial magnetism are also well researched. Studies on the control of electromagnetic response and its spatial distribution and dispersion are currently flourishing. Emerging directions of investigation are nonlinear, switchable, gain-assisted, sensor and quantum metamaterials.

Their functionality will be limited to the microwave and terahertz spectral domain, as higher frequencies destroy the superconducting phase.

No progress in metamaterials research will be possible without further developments in fabrication, however. New techniques will have to achieve perfection of nanostructures at close to the molecular level, and at low cost. We need to go beyond electron beam lithography, focused ion beam milling, and nano-imprint techniques. The new techniques will have to occupy a position between chemical processes controlled by self-organizing forces on the truly molecular level and the less accurate, top-down methods, which can build metamaterials to almost any blueprint.

References

1. Optical Society of America video podcast "Metamaterials: The Next Photonic Revolution" (www.osa-opn.org/Podcasts/Default.aspx).
2. E. Plum, V. A. Fedotov, P. Kuo, D. P. Tsai, N. I. Zheludev, *Opt. Express* **17**, 8548 (2009).
3. M. A. Noginov *et al.*, *Phys. Rev. Lett.* **101**, 226806 (2008).
4. N. I. Zheludev, S. L. Prosvirnin, N. Papasimakis, V. A. Fedotov, *Nat. Photon.* **2**, 351 (2008).
5. A. Ahmadi, H. Mosallaei, *Phys. Rev. B* **77**, 045104 (2008).
6. K. F. MacDonald, Z. L. Sámson, M. I. Stockman, N. I. Zheludev, *Nat. Photon.* **3**, 55 (2008).
7. A. E. Nikolaenko *et al.*, *Phys. Rev. Lett.* **104**, 153902 (2010).
8. W. J. Padilla *et al.*, *Phys. Rev. Lett.* **96**, 107401 (2006).
9. Z. L. Samson *et al.*, *Appl. Phys. Lett.* **96**, 143105 (2010).
10. M. J. Dicken *et al.*, *Opt. Express* **17**, 18330 (2009).
11. T. Driscoll *et al.*, *Science* **325**, 1518 (2009).
12. F. Wang *et al.*, *Science* **320**, 206 (2008).
13. V. V. Temnov *et al.*, *Nat. Photon.* **4**, 107 (2010).
14. N. Papasimakis *et al.*, *Opt. Express* **18**, 8353 (2010).
15. M. Ricci, N. Orloff, S. M. Anlage, *Appl. Phys. Lett.* **87**, 034102 (2005).

10.1126/science.1186756

SPORE* SERIES WINNER

The ChemCollective—Virtual Labs for Introductory Chemistry Courses

A collection of online activities emphasizes the design and interpretation of experiments.

David Yaron,† Michael Karabinos, Donovan Lange, James G. Greeno, Gaea Leinhardt

Chemistry concepts are abstract and can be difficult to attach to real-world experiences. For this reason, high-school and college chemistry courses focus on a concrete set of problem types that have become canonized in textbooks and standard exams. These problem types emphasize development of the core notational and computational tools of chemistry. Even though these tools may form the underlying procedural knowledge base from which the "real stuff" can be approached, when taught out of contexts that show their utility or that draw connections to core ideas of science, they can appear as a disconnected bag of tricks (*1*).

The ChemCollective (www.chemcollective.org) is a digital library of online activities for general chemistry instruction that engages students in more authentic problem-solving activities than those found in most textbooks. Our goal is to create activities that allow students to use their chemistry knowledge in ways that resemble the activities of practicing chemists. Our guiding hypothesis is that better conceptual understanding is obtained if algebraic computations are complemented with design and interpretation of experiments. This is achieved through the ChemCollective "Virtual Lab," which allows students to design and carry out their own experiments while experiencing representations of chemistry that go beyond what is possible in a physical laboratory. The goal is not to replace, or even to emulate, the physical laboratory, but to supplement textbook problem-solving by connecting abstract concepts to experiments and real-world applications. We believe that such authentic activities may improve learning and may better help to bring the essence of science into the introductory chemistry classroom.

In the virtual lab (see the figure, right), the panel on the left is a customizable stockroom of chemical reagents, which may include common reagents or fictional materials that have properties specified by the instructor. The middle work space provides an area for performing experiments. The right panel provides multiple representations of the contents of the selected solution, including the temperature and pH, and a list of chemical species with amounts shown as moles, grams, or molar concentrations. These quantities are the players in the computational procedures of the course, and so this panel provides an explicit link between the paper-and-pencil calculations of the traditional course and the chemical experiments the student performs on the workbench.

The virtual lab supports new forms of problem-solving. Consider how the concept of limiting reagents in a reaction is usually taught. A student's practice with this concept typically centers around learning a standard computational procedure for predicting the final amount of chemical reagents, given the initial amounts. Our "unknown reaction" virtual lab activity provides a different mode of practice. Students are given four unknown chemicals (A, B, C, and D) and asked to design and perform experiments to determine the reactions between them (i.e., $A + 2C \rightarrow 3B + D$). We found that roughly 50% of students in our course (363 of 647 students over a 4-year period) misinterpreted the results of their experiments in a way that revealed fundamental conceptual misunderstandings. When these students mixed A with C and found that A remained in the solution, they concluded that A is a product of the reaction, as opposed to leftover reactant, and wrote an equation such as $A + C \rightarrow B + D + A$, in which A is both a reactant and product.

This group of students has high proficiency in limiting-reagent calculations, as each was required to achieve a score greater than 85% on a mastery exam of stoichiometry before enrolling in the class. Therefore, this result indicates that it is possible to be proficient in the algebraic procedure while still missing core aspects of the underlying concept. The virtual lab provided immediate feedback that explained the conceptual aspects of this error and allowed the student to answer the question again.

Virtual lab activities also challenge students to move beyond problem-solving strategies that are effective for completing homework but may not support deeper conceptual learning. For instance, we gave students stock solutions of two reactants and asked them to design and carry out an experiment to measure the enthalpy of their reaction. In this case, the experimental design is fairly simple: Mix known amounts of stock solutions

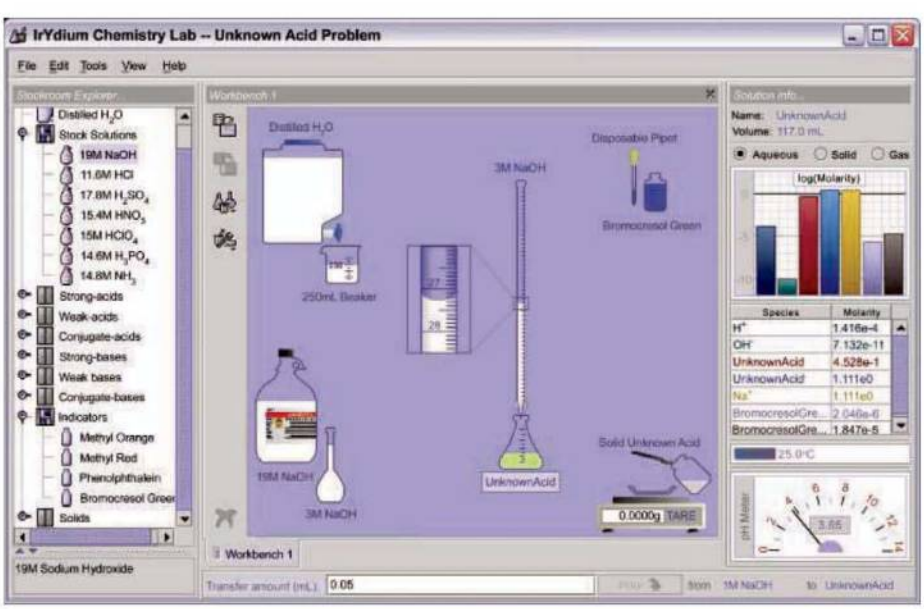

The ChemCollective virtual lab. A java applet that allows students to design and carry out their own experiments (www.chemcollective.org).

Department of Chemistry, Carnegie Mellon University, Pittsburgh, PA 15213–3890, USA.

*SPORE, *Science* Prize for Online Resources in Education; www.sciencemag.org/special/spore/.

†Author for correspondence. E-mail: yaron@cmu.edu

together and measure the temperature change of the resulting mixture. We were surprised to find that students struggled much more with the virtual lab problem than the textbook problems. Our student observations suggest that, as in physics, students solve the textbook problems through a means-ends analysis that provides a powerful, but potentially superficial, approach to such word problems (*2*). In means-ends analysis, the problem statement is first analyzed for given and unknown quantities, and algebraic relations are then sought that can link the givens to the unknowns. In contrast, a problem posed in the virtual lab cannot be approached by this strategy, because the student must decide what information to generate to achieve the desired goal.

Analysis of a full-semester lecture course (177 students) showed that homework using the virtual lab with real-world scenarios contributes significantly to learning (*3*). A structural equation model that predicts 48% of the total variance in students' overall course achievement showed that the virtual lab homework accounts for 24% of the total variance in course achievement. Virtual lab homework scores were not predicted by what the students knew before the course began (pretest scores), which suggests that even students with weaker backgrounds found opportunities to learn.

In an online course that we developed on stoichiometry, engagement with the virtual lab, as indicated by number of virtual lab manipulations, was the best predictor of posttest performance (as compared with overall time in the online environment, Scholastic Aptitude Test score, and gender), even though the final assessments were traditional stoichiometric calculations (*4*).

We chose to develop online homework to ease integration into undergraduate courses. Most instructors feel personal ownership of their lectures, and physical labs are difficult to modify because of practical and economic constraints. However, instructors often assign textbook problems as homework, making a collection of online homework that substitutes for part of these textbook assignments a viable strategy for shifting toward an improved instructional approach.

The virtual lab allows others to develop problem scenarios. Of the 117 virtual labs in the current collection, 56 were contributed by 11 different groups in the user community. Contributions include both instructional materials and translations to other languages, and they come from instructors at universities, community colleges, and high schools. A broad author base helps ensure that activities meet the needs of diverse classrooms, including laboratory courses where virtual activities have been used as prelaboratory assignments and to teach the relation between laboratory procedure and measurement precision (*5*). Because the software is freely distributed at our exhibit booth at conferences and via our Web site, usage is not fully monitored, but the virtual lab was run more than 100,000 times from our Web site last year and downloaded over 25,000 times.

We continue to add activities and topics, including a number of scenario-based learning activities that embed chemistry concepts in real-world contexts so as to highlight the utility of chemistry to bigger problems in everyday science or the broader scientific enterprise (*6*). One such activity is Mixed Reception, which allows students to use concepts covered early in a high-school course to solve a murder that occurs in a research group whose work focuses on synthesis of an antitoxin for spider bites.

The ChemCollective's growing collection of tutorials, which combine instruction on key concepts with practice activities, is being developed in collaboration with Carnegie Mellon's Open Learning Initiative. These tutorials focus on core concepts that are powerful for reasoning about chemistry but difficult to learn. For example, our analysis of the ways in which chemical equilibrium is usually taught revealed key components of the knowledge that were left implicit in traditional instruction. We have found that instruction that explicitly addresses these components more than doubled student performance on related problem types (*7*).

The virtual lab can record all student interactions for analysis. In collaboration with the Pittsburgh Science of Learning Center, we are working on ways to analyze these data to better understand how students learn and to identify ways to best support student problem-solving through immediate feedback generated while monitoring their actions (*8*).

The student experience in introductory chemistry courses is largely set by the activities they practice. The current canon of problem types evolved when student activities outside the physical laboratory were limited to paper and pencil. The availability of online interactivity, combined with recent advances in our understanding of how people learn, creates the opportunity to reconceptualize the set of activities in a way that better conveys the power and beauty of chemistry to the large student populations enrolled in our introductory courses (*9*).

ChemCollective members. From left to right: Michael Karabinos, James Greeno, David Yaron, and Gaea Leinhardt

David Yaron is an associate professor of chemistry at Carnegie Mellon. In 1998, he began development of the virtual lab with Donovan Lange, who was then an undergraduate student in computer science. Donovan has since moved to Microsoft, where he is a software design engineer. Michael Karabinos joined the project in 2000 and oversees curriculum development and community support for the ChemCollective. Also in 2000, Gaea Leinhardt, a professor of education at the University of Pittsburgh, began working on the design and implementation of studies on how students learn with the virtual lab and the other online resources in the ChemCollective. In 2006, the ChemCollective began collaborating with James Greeno on analysis of what makes certain chemistry concepts particularly challenging to learn and on instructional approaches that can help students reach better understandings. James is also a professor of education at the University of Pittsburgh.

References and Notes

1. M. Nakhleh, D. Bunce, T. Schwartz, *J. Coll. Sci. Teach.* **25**, 174 (1995).
2. J. Larkin, J. McDermott, D. P. Simon, H. A. Simon, *Science* **208**, 1335 (1980).
3. G. Leinhardt, J. Cuadros, D. Yaron, *J. Chem. Educ.* **84**, 1047 (2007).
4. K. Evans, D. Yaron, G. Leinhardt, *Chem. Educ. Res. Pract.* **9**, 208 (2008).
5. J. Nakonechny, C. Lomas, S. Nussbaum, *Proc. ED-Media* **2003**, 2475 (2003).
6. K. L. Evans, G. Leinhardt, M. Karabinos, D. Yaron, *J. Chem. Educ.* **83**, 655 (2006).
7. J. Davenport, D. Yaron, K. Koedinger, D. Klahr, in *Proceedings of the Thirtieth Annual Conference of the Cognitive Science Society*, V. Sloutsky, B. Love, and K. McRae, Eds., Washington, DC, 23 to 26 July 2008 (Cognitive Science Society, Austin, TX, 2008), pp. 1699–1704.
8. K. Koedinger, V. Aleven, *Educ. Psychol. Rev.* **19**, 239 (2007).
9. J. D. Bransford, A. L. Brown, R. R. Cocking, *How People Learn: Brain, Mind, Experience, and School, Expanded Edition* (National Academy Press, Washington, DC, 2000).
10. Supported by the National Science Foundation through the Course Curriculum and Laboratory Improvement (CCLI) and National Science Distributed Learning (NSDL) programs.

10.1126/science.1182435

SCIENCE POLICY

Uncertainty Should Be Powerful Motivator on Climate, Expert Says

With climate change science under political attack in the United States and little global consensus on how to move forward, an eminent climate policy expert urged that scientists and policy leaders embrace the persuasive power of uncertainty.

There is no doubt that humans are causing climate change and that existing technology can limit greenhouse gas emissions, Mohamed El-Ashry said at the 10th Annual Science & Technology in Society Conference cosponsored by AAAS. But science and policy leaders might gain more traction in the public debate over emissions by "highlighting the uncertainty of what might happen over the next 50 years, which is much scarier," he said.

Mohamed El-Ashry and Vicki Seyfert-Margolis

El-Ashry, a senior fellow at the United Nations Foundation, suggested that the challenging political climate requires science and policy leaders to refine their strategy—and bolster their credibility—both in the United States and around the world. New research must explore climate change impacts in developing nations, he said, and the United States must lead by example to build a new global consensus on climate.

The conference—"Innovating the Future: Critical Perspectives in Science & Technology"—brought several top policy leaders together with more than 125 graduate students in Washington, D.C. The event, held 9 to 11 April, was cosponsored by AAAS, the National Academies and the ST Global Consortium, comprised of six U.S. and European universities.

While El-Ashry and the other plenary speakers covered a range of topics, all shared a common theme: bringing the latest science and technology to bear on global challenges.

Vint Cerf, vice president and chief Internet evangelist for Google, cited Google's plans to show that ultra-high-speed broadband in U.S. cities can be done economically.

Vicki Seyfert-Margolis, senior advisor to the chief scientist at the U.S. Food and Drug Administration, said that her agency, which regulates one-quarter of the U.S. economy, will use science to increase public safety and drive innovation.

"We need more innovative and transparent processes for drug development and approval to encourage scientists and pharmaceutical companies to develop the next generation of life-saving drugs," she said. "We are beginning to address this with our new initiative in regulatory science."

John P. Holdren, director of the White House Office of Science and Technology Policy, stressed that President Barack Obama is committed to maintaining the U.S. competitive advantage through strong budget support for science and technology and related educational fields. But Holdren, a former AAAS president, rejected claims that "one country's gain is another's loss."

"There are many benefits to other countries increasing their science and technology investments," he said, "including more partners with whom our scientists can collaborate."

El-Ashry, born in Egypt, is the former chief executive officer and chairman of the Global Environment Facility, an independent financial organization which creates partnerships among international institutions, nongovernmental organizations, the private sector, and 181 member governments to address environmental issues. He has held high-ranking research, teaching, and administrative positions in organizations as diverse as Cairo University, the Tennessee Valley Authority, and the World Bank.

Echoing Holdren's remarks on international science, El-Ashry called for more regional modeling of climate change and better assessment of how healthy ecosystems support local and national economies.

Focusing on local effects—like harsher weather conditions or changes in the timing of snowmelt used in agriculture—could help governments recognize that climate change has an impact "not just over there in the Arctic," he said, "but on our farms and within our borders."

El-Ashry said that access to clean energy also could be critical, both for building political support in the United States and bringing developing nations into climate discussions.

—Benjamin Somers

PUBLIC ENGAGEMENT

AAAS Shares Spring Science at the White House

South Lawn scientists. Gabriel Caprio, 4, sorts seeds at the 2010 AAAS exhibit.

Hundreds of children and students found that the South Lawn of the White House was a great place to do research, as they studied seeds and the growth and development of lima beans at an AAAS–*Science* exhibit on the science of spring.

"We are very pleased to have been invited once again to showcase science at the White House Egg Roll," said AAAS CEO and *Science* Executive Publisher Alan I. Leshner. "Watching both children and their parents be fascinated by the 'science of spring' is a true delight for anyone interested in engaging the public with science."

The booth, developed by AAAS's Education and Human Resources staff, featured a seed dissection table and microscope stations to inspect pollen, petals, and sprouts. Children from all 50 states attended the annual White House event, which this year featured games, stories, and other activities focused on healthy eating and exercise.

—Molly McElroy and Benjamin Somers

CREDITS: (SEYFERT-MARGOLIS) IMMUNE TOLERANCE NETWORK; (EL-ASHRY) UNITED NATIONS FOUNDATION; (BOTTOM) B. SOMERS/AAAS

The Origins of C_4 Grasslands: Integrating Evolutionary and Ecosystem Science

Erika J. Edwards,[1]*† Colin P. Osborne,[2]*† Caroline A. E. Strömberg,[3]*† Stephen A. Smith,[4] C_4 Grasses Consortium‡

The evolution of grasses using C_4 photosynthesis and their sudden rise to ecological dominance 3 to 8 million years ago is among the most dramatic examples of biome assembly in the geological record. A growing body of work suggests that the patterns and drivers of C_4 grassland expansion were considerably more complex than originally assumed. Previous research has benefited substantially from dialog between geologists and ecologists, but current research must now integrate fully with phylogenetics. A synthesis of grass evolutionary biology with grassland ecosystem science will further our knowledge of the evolution of traits that promote dominance in grassland systems and will provide a new context in which to evaluate the relative importance of C_4 photosynthesis in transforming ecosystems across large regions of Earth.

Photosynthesis is the fundamental biological process that transforms solar energy into the chemical fuel for life by generating sugars from water and CO_2. The ancestral pathway (C_3 photosynthesis) evolved in a CO_2-rich atmosphere more than 2800 million years ago (Ma), but depletion of atmospheric CO_2 about 30 Ma has reduced the efficiency and rate of carbon uptake in many terrestrial plants, especially under high temperatures and water deficits (*1*). This limitation has been alleviated through the convergent evolution of C_4 photosynthesis in more than 45 independent flowering plant lineages (*1*). C_4 photosynthesis is a coordinated system of anatomical and physiological traits that concentrate CO_2 around the C_3 photosynthetic machinery, through the use of a solar-powered biochemical cycle. The emergence of ecosystems dominated by C_4 species has transformed the biosphere; although comprising only 3% of vascular plant species (*1*), they account for some 25% of terrestrial photosynthesis (*2*).

Sixty percent of C_4 species are grasses, dominating warm-climate grasslands and savannas (Fig. 1A), where their high rates of foliage production sustain Earth's highest levels of herbivore consumption (*3*). Stable carbon isotopic data ($\delta^{13}C$) collected over the past 20 years document a worldwide expansion of C_4 grasslands through the displacement of C_3 vegetation during the Late Miocene and Pliocene (3 to 8 Ma) (*4*). This was a dramatic event of biome evolution in Earth's history, outpacing the rise to dominance of flowering plants during the Cretaceous by one order of magnitude (*5*), but its drivers are still debated.

The last decade has seen much progress in our understanding of C_4 grass ecophysiology, C_4 grassland ecosystem ecology and geologic history, and the evolutionary history of the C_4 pathway within the grass lineage. However, these independent strands of research are not well integrated. Here, we outline a framework that explicitly links the evolutionary biology of grasses with the ecology and history of grasslands. We review the current state of knowledge in the field and argue that a shift in emphasis from photosynthetic pathway to broader assemblages of plant traits may be essential for understanding the rise of C_4 grasslands. This boils down to one question: Just how responsible is C_4 photosynthesis for the distribution of C_4 grasslands?

Crossing Environmental Thresholds

Today's C_4 grasses are mostly confined to low latitudes and altitudes, whereas C_3 species dominate at higher latitudes and elevations (Fig. 1A). These patterns correlate best with temperature, with several classic studies (*6*) showing the relationship on every continent. Explanations of these gradients have traditionally focused on fundamental physiological differences between C_3 and C_4 photosynthesis. At high temperatures and low atmospheric CO_2, the key C_3 photosynthetic enzyme rubisco fails to completely distinguish CO_2 and O_2. The process of O_2 uptake leads to photorespiration in C_3 plants, resulting in net losses of $\leq$40% of photosynthetic carbon in today's low-CO_2 atmosphere (*1*). C_4 photosynthesis suppresses photorespiration by concentrating CO_2 internally, but this comes with an energetic cost, which exceeds the photorespiratory costs of C_3 photosynthesis at

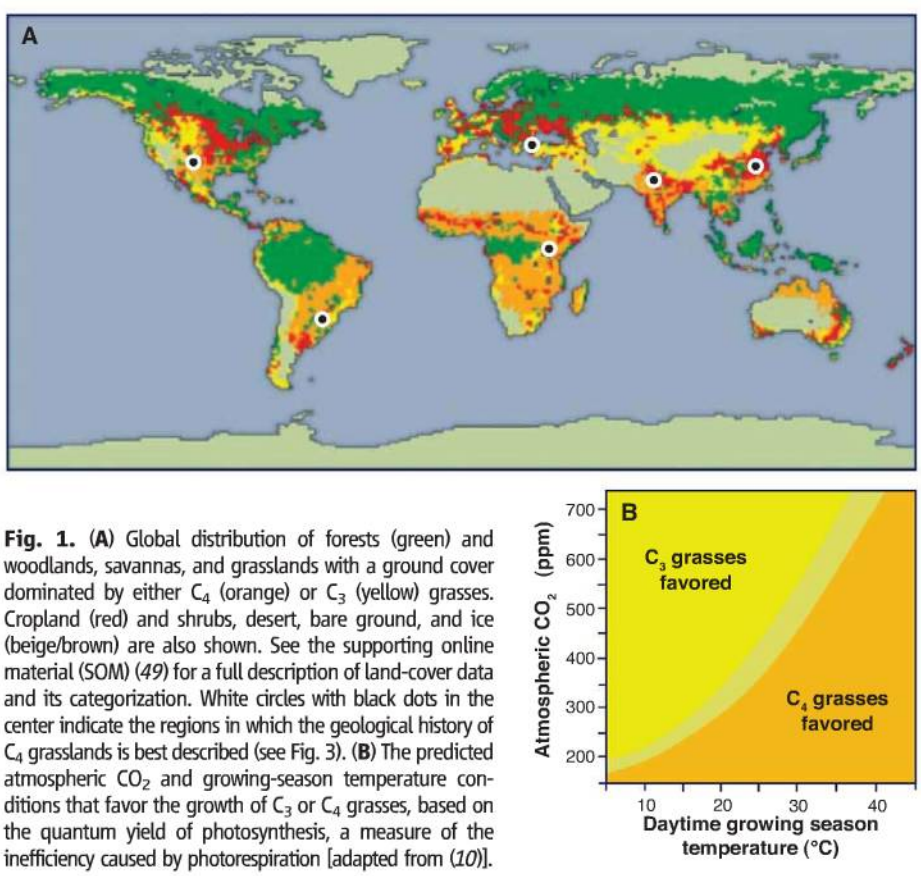

Fig. 1. (**A**) Global distribution of forests (green) and woodlands, savannas, and grasslands with a ground cover dominated by either C_4 (orange) or C_3 (yellow) grasses. Cropland (red) and shrubs, desert, bare ground, and ice (beige/brown) are also shown. See the supporting online material (SOM) (*49*) for a full description of land-cover data and its categorization. White circles with black dots in the center indicate the regions in which the geological history of C_4 grasslands is best described (see Fig. 3). (**B**) The predicted atmospheric CO_2 and growing-season temperature conditions that favor the growth of C_3 or C_4 grasses, based on the quantum yield of photosynthesis, a measure of the inefficiency caused by photorespiration [adapted from (*10*)].

[1]Department of Ecology and Evolutionary Biology, Brown University, Providence, RI 02912, USA. [2]Department of Animal and Plant Sciences, University of Sheffield, Sheffield S10 2TN, UK. [3]Department of Biology and Burke Museum, University of Washington, Seattle, WA 98195–1800, USA. [4]National Evolutionary Synthesis Center, Durham, NC 27705–4667, USA.

*These authors contributed equally to this work.
†To whom correspondence should be addressed. E-mail: erika_edwards@brown.edu (E.J.E.); c.p.osborne@sheffield.ac.uk (C.P.O.); caestrom@u.washington.edu (C.A.E.S.)
‡All authors with their affiliations appear at the end of this paper.

high CO_2 and low temperatures (*7*, *8*). All else being equal, C_4 grasses will therefore outperform C_3 grasses below a critical threshold in CO_2, the level of which depends on growing-season temperature (Fig. 1B) (*7*, *8*). By saturating rubisco with CO_2, the C_4 pathway also allows the enzyme to achieve maximum catalytic rates under high-light conditions (*9*); conversely, the overall C_4 advantage is often lost in shaded forest understories, where cool conditions improve the quantum efficiency in C_3 species (*7*).

This functional model forms the central basis for understanding the current distribution of C_4 grasses and grasslands (Fig. 1A) and the general absence of C_4 grasses from forest understory habitats (*10*). It explains glacial-interglacial cycles of C_4 grassland expansion and contraction (*10*) and underpins forecasts of future impacts of global change on Earth's C_3-C_4 balance (*11*). The extension of this model to the geological past generates the hypothesis that declining atmospheric CO_2 drove the displacement of C_3 plants by C_4 grasses (*4*, *8*, *10*). Because lower temperatures reduce the crucial CO_2 threshold for a C_4 photosynthetic advantage (Fig. 1B), C_4 grasslands should have appeared first in the tropics at 350 to 550 parts per million (ppm) CO_2 and then spread to higher latitudes as CO_2 declined further (*10*).

Reconstructing a Botanical Revolution

It is probable that tectonic events ultimately drove a major decline in CO_2 during the Early Oligocene (*12*, *13*), but the subsequent history of CO_2 is less certain. Most CO_2 proxy records and model calculations indicate CO_2 levels substantially lower than 550 ppm for the past 28 million years (My) (Fig. 2), thus also indicating an uncoupling of C_4 grassland expansion from atmospheric CO_2 during the Miocene (*12*). In contrast, two recent studies show CO_2 variation close to the C_4 crossover threshold during the Middle or Late Miocene (Fig. 2) (*14*, *15*). The assumptions, uncertainties, and imprecision inherent to each CO_2 proxy, as well as the range of uncertainty in the CO_2 crossover threshold itself, make these alternatives difficult to evaluate. Nevertheless, CO_2 does seem to have fallen below the upper bound of the threshold 20 My before the origin of C_4 grasslands, provoking a reappraisal of the ecological context and environmental drivers of C_4 grassland expansion.

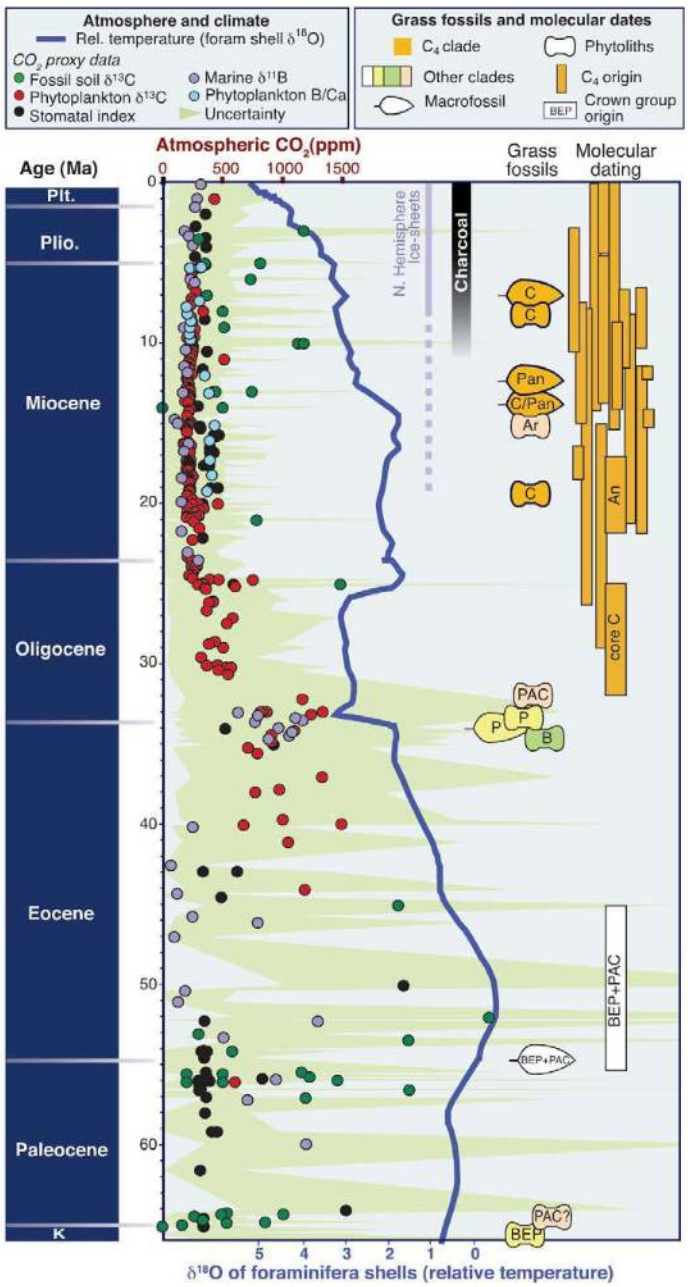

Fig. 2. Cenozoic record of CO_2 and temperature change, including evidence for Arctic glaciation, fossil and molecular dating evidence for grass evolution, and charcoal records. See the SOM (*49*) for data sources and methods. Plt., Pleistocene; Plio., Pliocene; K, Cretaceous; C, Chloridoideae; Pan, Panicoideae; Ar, Arundinoideae; An, Andropogoneae; B, Bambusoideae; P, Pooideae; BEP, Bambusoideae-Ehrhartoideae-Pooideae; PAC, PACMAD.

Recent phylogenetic reconstructions show that C_4 photosynthesis has evolved multiple times in grasses (*16*, *17*). Time-calibration of these phylogenies using fossilized grass pollen and inflorescences places the earliest probable origin in the Early Oligocene (~30 to 32 Ma) (Fig. 2) and suggests that subsequent origins arose in clusters (for example, in the Middle Miocene). This timing has led researchers to hypothesize that the Early Oligocene drop in CO_2 triggered evolution of the C_4 pathway (*16*, *17*). However, the proposal is challenged by the discovery of Late Cretaceous microscopic plant silica (phytoliths) diagnostic of grasses (Fig. 2), suggesting that this lineage may be much older than previously thought (*18*). A recalibration with these fossils would date the earliest C_4 grasses to the Middle Eocene (*17*), a time of warm equable climates and probably of high CO_2 (Fig. 2). Even more controversial are $\delta^{13}C$ records from leaf-wax molecules (*n*-alkanes) in marine sediments, indicating that C_4 photosynthesis existed in Cretaceous land plants (*19*), albeit not necessarily in grasses.

New paleontological evidence also reveals crucial information about the Miocene environments that preceded C_4 grasslands. Rather than being forested, as initially thought (*20*), it now appears that landscapes were relatively open. The evolution of ungulate grazers or mixed feeders (feeding on grasses and broad-leaved plants) and pollen data (*21*) supplemented by new, phytolith-based reconstructions of vegetation (*22*) document the emergence of savannas or woodlands with predominantly C_3 grasses in the Early-Middle Miocene (11 to 24 Ma), several million years before C_4 grasslands spread (Fig. 3). This vegetation shift is evident in all of the studied cases, although its timing and pace seem to have varied among regions (Fig. 3).

C_4 grasses occurred in the landscape soon after this transition. Phytoliths show that C_4 Chloridoideae species were represented in North American grassland communities 19 Ma (Fig. 2). Similarly, $\delta^{13}C$ records from fossil soils suggest that C_4 grasses contributed 20 to 40% of local vegetation in several regions for many million years before C_4 species completely dominated communities (Fig. 3) (*23*, *24*). Spatially detailed sedimentological and isotopic reconstructions of the paleolandscape (*25*, *26*) indicate substantial heterogeneity in vegetation structure, with tree-grass mosaics before and during the C_3-C_4 shift. C_4 grasses seemed to have first invaded drier parts of floodplains, whereas C_3 plants preferred moister habitats in topographic lows (*25*, *26*).

The explosive, broadly synchronous Late Miocene–to–Pliocene spread of C_4 grasses, originally diagnosed by the $\delta^{13}C$ of fossil soil carbonates (*20*), has since been abundantly documented by $\delta^{13}C$ records of ungulate teeth (*4*, *27*) and *n*-alkanes in soils and marine sediments (*24*, *28*) across many low- to mid-latitude regions (Fig. 3). However, with more C_4 proxy data available for each region, it has become clear that the $\delta^{13}C$

records of tooth enamel and soil carbonate record different aspects of C_4 expansion. Evaluating both proxies concurrently allows us to distinguish overall vegetation change, recorded by soil $\delta^{13}C$, from changes in herbivore food source, mirrored in tooth enamel $\delta^{13}C$. Specifically, data from North America, Siwaliks (Himalayan foreland in Pakistan), Argentina, and Kenya show that particular mammals started feeding largely on C_4 grasses ≥1 My before these grasses became abundant (>50%) in the ecosystem (Fig. 3) (*29*). The rapid adoption of C_4 grazing in these herbivores may mark the emergence of C_4 dietary specialists in faunal communities or else expansion of C_4 grasses at the expense of C_3 grasses, but not necessarily at the expense of C_3 woody vegetation.

In contrast, the overall C_3-C_4 transition in vegetation (inferred from soil carbonate $\delta^{13}C$) seems to have typically been much slower, with little evidence of the latitudinal gradient in C_4 grassland appearance expected from the crossover threshold model. It occurred ~3 My earlier in the Siwaliks and China, compared with temperate North America and tropical Kenya (Fig. 3). The Eastern Mediterranean, North America, and China were located at roughly equivalent paleolatitudes, yet only the latter two became C_4-dominated in the Late Miocene, and at slightly different times and rates. The Eastern Mediterranean remained dominated by C_3 plants throughout the Neogene, although the summer droughts that are now thought to exclude C_4 grasses from this region originated only 3 Ma (*30*).

The wealth of high-resolution data now available point to a complex Late Miocene–to–Pliocene ecological transition, where the roughly correlated C_3-C_4 shifts across continents differ in many details. The decoupling in time of the transition from forest to C_3 grassland and the later expansion of C_4 grasses indicate that different drivers were probably involved. Similarly, the lag between the origins of C_4 grasses and their subsequent rise to dominance suggest separate triggers. These observations necessitate a reassessment of the factors driving C_4 grassland origins and suggest that the problem is best framed as two related questions: (i) What drove the forest-to-grassland transition? (ii) Why did these grasslands later become C_4-dominated in warm-climate regions?

What Drove the Forest-to-Grassland Transition?

The abundance of woody vegetation (i.e., trees and shrubs) versus grasses in modern grasslands is maintained by two primary mechanisms. First, C_3 and C_4 grasses may tolerate soil factors or climatic extremes that limit the establishment or survival of woody plants. Second, grasslands are sustained by fires and herbivory, which limit the recruitment and growth of woody species (*31*). Improved understanding of these different drivers and their interactions has inspired novel hypotheses about the origins of C_4 grasslands and has revived some old ones. All invoke regional or local factors and focus on increased aridity and/or shifts in disturbance regime. Stable oxygen isotope ratios ($\delta^{18}O$), sedimentology, and floral records point to the development of seasonal climates with warm-season precipitation in South Asia (*20*, *32*). The onset of a dry season causing intensified fire cycles in this region is therefore favored as a driver of the forest-to-grassland transition and is supported by charcoal records indicating increased occurrence of fire on several continents (*29*, *33*). Based on $\delta^{18}O$ and leaf-wax hydrogen isotope ratios (δD), an overall increase in aridity (as opposed to seasonality) has been proposed for both South Asia and East Africa (*28*, *34*, *35*), with no explicit role for disturbance. In a third scenario using fossil-soil data from South Asia, East Africa, and North America, dry-adapted C_4 grasses evolved herbivore resistance and/or traits leading to fuel accumulation, allowing them to expand their ecological niche into more mesic habitats, at the expense of trees (*36*, *37*).

A major problem with these Late Miocene and Pliocene scenarios is that they rely on mechanisms that today maintain the grass-to-tree/shrub balance in C_4-dominated ecosystems, whereas the fossil record shows that the (much earlier) forest-to-grassland transition involved mainly C_3 grass species (Fig. 3). Whether similar processes drove the spread of C_3 grasslands is an important question that remains to be tackled (*22*). Nevertheless, modern ecology illustrates that the abundance of grass versus woody vegetation is controlled by complex sets of factors playing out over different spatial scales. At the regional scale, grasslands are sustained by climate/soil/disturbance interactions, mediated by the traits of the grass flora and herbivore fauna. Locally, topographic effects generate microhabitat variation that supports a mosaic of distinct grass communities with very different trait combinations (*38*, *39*). The general message is clear: Traits that are, at best, only indirectly related to C_4 photosynthesis currently play important roles in allowing grasses to dominate vast areas of natural grassland.

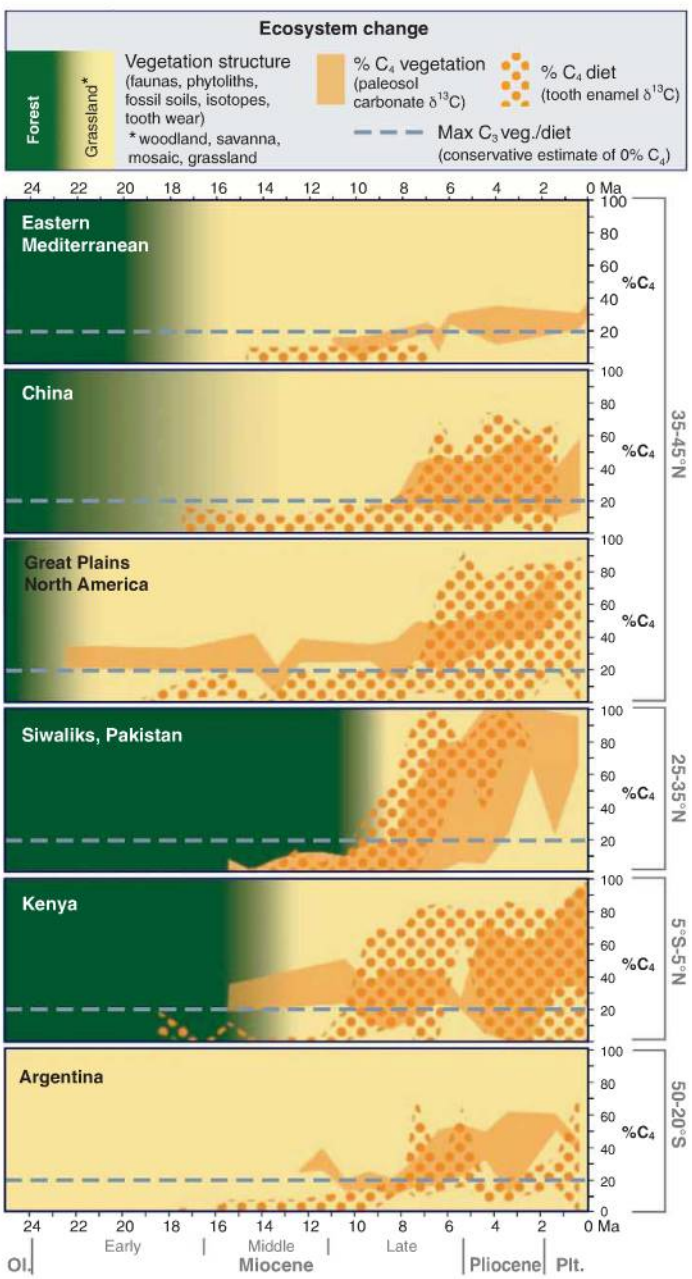

Fig. 3. Neogene record of changes in vegetation structure (from forest vegetation to an environment with substantial amount of grass cover), and of photosynthetic pathway (C_3 versus C_4), in vegetation and in diet of ungulates from various regions (*49*). Ol., Oligocene.

Why Did Grasslands Become C_4-Dominated?

Questions of this scale have historically fallen into the realm of ecosystem ecologists and plant physiologists and have rarely received attention from the field of evolutionary biology (*40*). Our understanding of grass phylogenetics and patterns of C_4 evolution in grasses has improved considerably over the past decade (*16*, *17*, *41*). Though obviously im-

portant for understanding C_4 origins, phylogeny should play an equally large role in evaluating ecological and physiological consequences of the pathway.

Most previous studies comparing C_3 and C_4 grasses have chosen taxa that span the deepest divergences within the grass lineage, comparing members of the Pooideae, a strictly C_3 lineage, with C_4 members of "PACMAD" (an acronym for Panicoideae, Aristidoideae, Chloridoideae, Micrairioideae, Arundinoideae, and Danthonioideae lineages), a large clade of C_3 and C_4 grasses containing ~18 independent origins of the C_4 pathway (Fig. 4). However, Pooideae and PACMAD last shared a common ancestor >50 Ma, allowing both lineages to evolve many differences that will confound any potential C_3-C_4 signal (*40*). Recent work indicates that PACMAD species tend to be warm-adapted whether or not they are C_4, suggesting that the evolution of cold tolerance in Pooideae may be as important as C_3-C_4 differences in establishing the ecological sorting of grass species along temperature gradients (*42*). Therefore, isolating the effects of C_4 photosynthesis on any aspect of grass biology (from biochemistry to ecology) requires comparisons between closely related C_3 and C_4 taxa within the PACMAD clade. For example, studies show that responses to climatic extremes of cold and drought are as important as differing photosynthetic performance in determining the ecological characteristics of C_3 and C_4 subspecies of the grass *Alloteropsis semialata* (*43*).

Similarly, grouping the multiple, independently derived C_4 lineages within PACMAD into a single C_4 functional type probably masks underlying variation in other traits that could be important at the community and/or ecosystem level. Key differences among C_4 plants have been acknowledged for many years because of the presence of C_4 photosynthetic subtypes distinguished by variation in anatomy, biochemistry, and physiology (*44*–*46*). The recurrent evolution of the C_4 pathway in grasses presents another opportunity for variation, as each origin arose within a unique internal (and probably external) environment. Researchers have already documented that independent C_4 lineages exhibit different growth responses to elevated CO_2 (*47*) and that previously recognized sorting of subtypes along climate gradients is better explained by the sorting of different C_4 lineages (*48*).

The above studies indicate that seemingly self-evident relationships between C_4 photosynthesis and physiological properties or ecological tolerances become decidedly less certain when viewed within a phylogenetic context. Phylogenies emphasize the rich organismal diversity that is contained within the C_4 grass functional type and also provide the perfect framework for evaluating how different grassland systems have been assembled from these independent lineages. The major challenge in this area is to understand how the C_4 pathway has been functionally integrated into each of these diverse organismal backgrounds, and in turn, how the resulting ecological characteristics of these lineages influence such large-scale processes as biome development and ecosystem function.

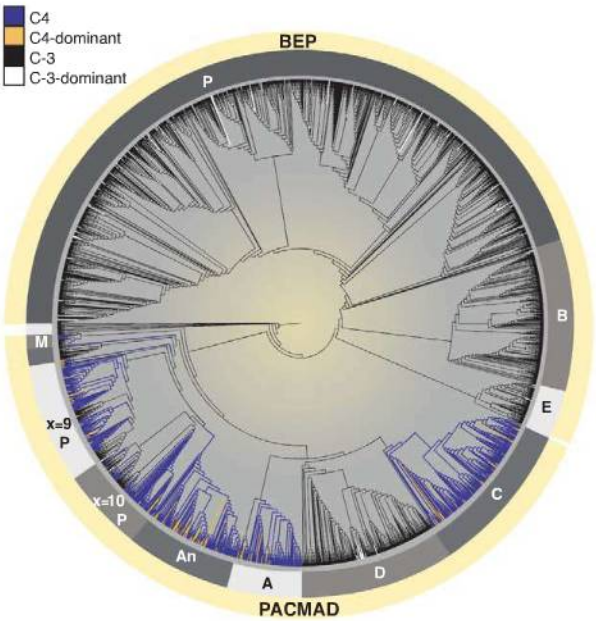

Fig. 4. The evolution of photosynthetic pathway and grassland dominants in Poaceae (the grass family). A 2684-taxon tree of Poaceae and outgroups, constructed from molecular-sequence data (*49*). Evolutionary patterns of photosynthetic-pathway variation and grassland dominance (*49*) are indicated by branch colors. The origins of both C_4 photosynthesis and dominance were more clustered on the phylogeny than expected by chance ($P < 0.05$), which was inferred by comparing the total of number of changes in each trait to a null distribution generated by re-shuffling tip values across the phylogeny 1000 times. This clustering indicates that some lineages are more prone than others to evolving dominant grassland species, and focusing comparative studies in these regions of the phylogenetic tree may uncover traits that played a key role in the origins of grassland ecosystems. Letters indicate major clades. E, Ehrhartoideae; M, Micrairioideae; A, Aristidoideae; D, Danthonioideae; x = 10P, Paniceae (base chromosome number x = 10); x = 9P, Paniceae (base chromosome number x = 9).

Most Grass Species Do Not Dominate Grasslands

The complexity of many ecosystems makes it difficult to understand how individual species influence ecosystem function. However, just a handful of species make up the majority of the standing biomass in most grasslands, and species richness is largely contributed by taxa occurring in very low densities. Furthermore, a minority of grasses (~600 out of ~11,000 species) is documented as being ecologically dominant in grasslands (*49*). These dominant species are phylogenetically clustered, suggesting that certain clades of grasses are more prone than others to evolve traits that promote ecological dominance (Fig. 4). The pattern implies that important characteristics other than the C_4 pathway enable these particular species to become abundant in grasslands. If we assume that paleograsslands had a similar diversity structure as their modern analogs, then understanding the Miocene expansion of C_4-dominated ecosystems hinges on the question of "How did particular grassland dominants (as opposed to C_4 grasses in general) come to occupy such a large fraction of the land surface?" A phylogenetic approach can immediately help to organize new research questions about the evolution of grassland dominants. Below, we highlight key examples of how knowledge from other fields can be integrated within this framework.

How do environmental niche preferences differ between dominant and nondominant grasses? A fundamental question is whether the Late Miocene–to–Pliocene spread of grasslands resulted from the evolution of new environmental niche tolerances in a handful of C_4 grasses, or whether climatological changes promoted the geographical expansion of particular niches already inhabited by those grasses. The truth is likely to be some combination of both scenarios. We currently have little quantitative information on how environmental niches are distributed within the PACMAD clade. By reconstructing the evolution of environmental niche space across the grass phylogeny (*42*), we will be able to address when and how key changes occurred. Is the environmental niche relatively conserved across certain clades of PACMAD, or is it evolutionarily labile? Have dominants from different lineages converged on similar niche space when living in the same biogeographical region? Do dominant species always exhibit broader ecological ranges than their nondominant sister taxa?

How do grass species dominate grasslands? Understanding the timing and phylogenetic distribution of C_4 origins in grasses is obviously fundamental to understanding the rise of C_4 grasslands. The same is true for other traits that promote species' dominance, highlighted in the rich ecological literature on competitive interactions in grasslands (*50*). Multiple comparisons of dominant and subdominant sister taxa will help to identify traits associated with shifts to dominance, and broader surveys of how those traits are distributed across PACMAD will improve our understanding of their evolutionary history. In fire-driven grasslands of African monsoonal climate regions, for instance, dominant grasses typically have well-protected buds and storage reserves, and they resprout quickly after defoliation (*31*). Other traits act to induce fire: High wet-season growth rates and slow rates of leaf decomposition result in large fuel accumulation (*31*). When and where

in grasses did these traits evolve, and in what order? Dating the appearance of such important ecological traits, in addition to shifts in photosynthetic pathway, may bridge the time gap between the origins of C_4 grasses and the origins of C_4 grasslands.

What role does C_4 photosynthesis play in the evolution of dominance? Clearly, the C_4 pathway must fundamentally influence the ability of PACMAD grasses to establish dominance, as evidenced by the dearth of C_3 PACMAD species with high abundances in grasslands (16 of 145 species sampled for Fig. 4). However, C_4 photosynthesis will also probably confer different advantages in different circumstances. For instance, in the fire-adapted example above, the C_4 pathway would facilitate biomass accumulation by supporting high photosynthetic rates and nitrogen-use efficiencies, especially in the high-light environment after a fire (*37*, *46*). In contrast, the North American short-grass prairies are water-limited and far less productive than tropical savannas; in this case, the higher water-use efficiency afforded by C_4 metabolism might provide the competitive edge (*37*). These two ecosystem types are dominated by different C_4 PACMAD lineages. In African Andropogoneae, C_4 works within an organismal context of a large, fire-adapted plant that quickly accumulates biomass between fires. In North American Chloridoideae, C_4 operates within a short-statured, drought-resistant plant. C_4 photosynthesis is a well-integrated component of each of these strategies, resulting in two grassland systems that are dominated by C_4 grasses, but for very different reasons.

Establishing these patterns of trait assembly for modern grasses could permit specific ecological inferences to be made about C_3/C_4 lineages that are recognized in the fossil record using phytoliths and other plant fossils. Such inferences will allow detailed reconstruction of the grass communities present in the Miocene and, by inference, the type of environment that may have promoted C_4 grass expansion in different regions (*37*).

Research Priorities

The current acceleration of computing power and molecular-sequence accumulation makes a completely sampled grass phylogeny a realistic near-term goal, which will greatly facilitate a lineage-centered focus on the C_4 grassland problem. Linking the grass phylogeny to databases detailing climatic, ecological, morphological, and physiological information for individual grass taxa is already possible, permitting the application of tools developed for ecological bioinformatics and spatial ecology. Similarly, reconstructions of turnover in paleocommunities are becoming much more refined, using phytolith data to track major grass lineages through time. This growing body of paleobotanical evidence also promises the ongoing improvement in dating of key events in grass evolutionary history. To keep pace with these developments, comparative biological investigations of grass species are urgently required to understand trait evolution in grassland dominants. A stronger synthesis between evolutionary processes, plant function, and ecosystem composition will provide new opportunities for sharpening our hypotheses about the factors that drove the Late Miocene–to–Pliocene emergence of C_4 grassland biomes.

References and Notes

1. R. F. Sage, *New Phytol.* **161**, 341 (2004).
2. C. J. Still, J. A. Berry, G. J. Collatz, R. S. DeFries, *Global Biogeochem. Cycles* **17**, 1006 (2003).
3. S. A. Heckathorn, S. J. McNaughton, J. S. Coleman, in *C_4 Plant Biology*, R. F. Sage, R. K. Monson, Eds. (Academic Press, San Diego, 1999), pp. 285–312.
4. T. E. Cerling *et al.*, *Nature* **389**, 153 (1997).
5. R. Lupia, S. Lidgard, P. R. Crane, *Paleobiology* **25**, 305 (1999).
6. J. A. Teeri, L. G. Stowe, *Oecologia* **23**, 1 (1976).
7. J. R. Ehleringer, *Oecologia* **31**, 255 (1978).
8. J. R. Ehleringer, R. F. Sage, L. B. Flanagan, R. W. Pearcy, *Trends Ecol. Evol.* **6**, 95 (1991).
9. S. P. Long, in *C_4 Plant Biology*, R. F. Sage, R. K. Monson, Eds. (Academic Press, San Diego, 1999), pp. 215–249.
10. J. R. Ehleringer, T. E. Cerling, B. R. Helliker, *Oecologia* **112**, 285 (1997).
11. S. Sitch *et al.*, *Glob. Change Biol.* **14**, 2015 (2008).
12. M. Pagani, J. C. Zachos, K. H. Freeman, B. J. Tipple, S. Bohaty, *Science* **309**, 600 (2005); published online 16 June 2005 (10.1126/science.1110063).
13. Z. Liu *et al.*, *Science* **323**, 1187 (2009).
14. W. M. Kürschner, Z. Kvacek, D. L. Dilcher, *Proc. Natl. Acad. Sci. U.S.A.* **105**, 449 (2008).
15. A. K. Tripati, C. D. Roberts, R. A. Eagle, *Science* **326**, 1394 (2009); published online 8 October 2009 (10.1126/science.1178296).
16. P. A. Christin *et al.*, *Curr. Biol.* **18**, 37 (2008).
17. A. Vicentini, J. C. Barber, S. S. Aliscioni, L. M. Giussani, E. A. Kellogg, *Glob. Change Biol.* **14**, 2963 (2008).
18. V. Prasad, C. A. E. Strömberg, H. Alimohammadian, A. Sahni, *Science* **310**, 1177 (2005).
19. M. M. M. Kuypers, R. D. Pancost, J. S. S. Damsté, *Nature* **399**, 342 (1999).
20. J. Quade, T. E. Cerling, J. R. Bowman, *Nature* **342**, 163 (1989).
21. B. F. Jacobs, J. D. Kingston, L. L. Jacobs, *Ann. Mo. Bot. Gard.* **86**, 590 (1999).
22. C. A. E. Strömberg, *Proc. Natl. Acad. Sci. U.S.A.* **102**, 11980 (2005).
23. D. L. Fox, P. L. Koch, *Geology* **31**, 809 (2003).
24. B. J. Tipple, M. Pagani, *Annu. Rev. Earth Planet. Sci.* **35**, 435 (2007).
25. A. K. Behrensmeyer *et al.*, *Geol. Soc. Am. Bull.* **119**, 1486 (2007).
26. N. E. Levin, J. Quade, S. W. Simpson, S. Semaw, M. Rogers, *Earth Planet. Sci. Lett.* **219**, 93 (2004).
27. B. H. Passey *et al.*, *Earth Planet. Sci. Lett.* **277**, 443 (2009).
28. Y. Huang, S. C. Clemens, W. Liu, Y. Wang, W. L. Prell, *Geology* **35**, 531 (2007).
29. J. E. Keeley, P. W. Rundel, *Int. J. Plant Sci.* **164**, S55 (2003).
30. J. P. Suc, *Nature* **307**, 429 (1984).
31. W. J. Bond, *Annu. Rev. Ecol. Syst.* **39**, 641 (2008).
32. A. Zhisheng, J. E. Kutzbach, W. L. Prell, S. C. Porter, *Nature* **411**, 62 (2001).
33. C. P. Osborne, D. J. Beerling, *Philos. Trans. R. Soc. London Ser. B* **361**, 173 (2006).
34. D. Dettman *et al.*, *Geology* **29**, 31 (2001).
35. P. Sepulchre *et al.*, *Science* **313**, 1419 (2006).
36. G. J. Retallack, *J. Geol.* **109**, 407 (2001).
37. C. P. Osborne, *J. Ecol.* **96**, 35 (2008).
38. R. T. Coupland, Ed., *Natural Grasslands: Introduction and Western Hemisphere (Ecosystems of the World)*, vol. 8A (Elsevier, Amsterdam, 1992).
39. R. T. Coupland, Ed., *Natural Grasslands: Eastern Hemisphere and Résumé (Ecosystems of the World)*, vol. 8B (Elsevier, Amsterdam, 1993).
40. E. J. Edwards, C. J. Still, M. J. Donoghue, *Trends Ecol. Evol.* **22**, 243 (2007).
41. Grass Phylogeny Working Group, *Ann. Mo. Bot. Gard.* **88**, 373 (2001).
42. E. J. Edwards, S. A. Smith, *Proc. Natl. Acad. Sci. U.S.A.* **107**, 2532 (2010).
43. D. G. Ibrahim, M. E. Gilbert, B. S. Ripley, C. P. Osborne, *Plant Cell Environ.* **31**, 1038 (2008).
44. M. Gutierrez, V. E. Gracen, G. E. Edwards, *Planta* **119**, 279 (1974).
45. A. B. Cousins, M. R. Badger, S. von Caemmerer, *J. Exp. Bot.* **59**, 1695 (2008).
46. O. Ghannoum *et al.*, *Plant Physiol.* **137**, 638 (2005).
47. E. A. Kellogg, E. J. Farnsworth, E. T. Russo, F. Bazzaz, *Ann. Bot. (London)* **84**, 279 (1999).
48. D. R. Taub, *Am. J. Bot.* **87**, 1211 (2000).
49. Materials and methods are available as supporting material on *Science* Online.
50. J. M. Craine, *Resource Strategies of Wild Plants* (Princeton Univ. Press, Princeton, NJ, 2009).

51. We thank the NSF National Evolutionary Synthesis Center (NESCent) for funding the catalysis meeting "Toward a new synthesis of the evolutionary history and ecology of C_4 grasses," which inspired this paper. We thank B. Passey (Johns Hopkins Univ.) for many stimulating discussions; D. Beerling and M. Donoghue for their critical comments on the manuscript; and V. Visser, M. Lomas, and I. Woodward for their help with Fig. 1. Funding was provided by The Royal Society (University Research Fellowship to C.P.O.).

C_4 Grasses Consortium

Erika J. Edwards,[1] Colin P. Osborne,[2] Caroline A. E. Strömberg,[3] Stephen A. Smith,[4] William J. Bond,[5] Pascal-Antoine Christin,[6] Asaph B. Cousins,[7] Melvin R. Duvall,[8] David L. Fox,[9] Robert P. Freckleton,[2] Oula Ghannoum,[10] James Hartwell,[11] Yongsong Huang,[12] Christine M. Janis,[1] Jon E. Keeley,[13,14] Elizabeth A. Kellogg,[15] Alan K. Knapp,[16] Andrew D. B. Leakey,[17] David M. Nelson,[18] Jeffery M. Saarela,[19] Rowan F. Sage,[20] Osvaldo E. Sala,[1] Nicolas Salamin,[6,21] Christopher J. Still,[22] Brett Tipple[23]

[1]Department of Ecology and Evolutionary Biology, Brown University, Providence, RI 02912, USA. [2]Department of Animal and Plant Sciences, University of Sheffield, Sheffield S10 2TN, UK. [3]Department of Biology and Burke Museum, University of Washington, Seattle, WA 98195–1800, USA. [4]National Evolutionary Synthesis Center, Durham, NC 27705–4667, USA. [5]Department of Botany, University of Cape Town, Cape Town, South Africa. [6]Department of Ecology and Evolution, University of Lausanne, CH-1015 Lausanne, Switzerland. [7]School of Biological Sciences, Washington State University, Pullman, WA 99164, USA. [8]Department of Biological Sciences, Northern Illinois University, DeKalb, IL 60115, USA. [9]Department of Geology and Geophysics, University of Minnesota, Minneapolis, MN 55455, USA. [10]Department of Plants, Soil and Environment, University of Western Sydney, South Penrith Distribution Centre, New South Wales 1797, Australia. [11]School of Biological Sciences, University of Liverpool, Liverpool L69 7ZB, UK. [12]Department of Geological Sciences, Brown University, Providence, RI 02912, USA. [13]U.S. Geological Survey, Western Ecological Research Center, Sequoia-Kings Canyon Field Station, Three Rivers, CA 93271, USA. [14]Department of Ecology and Evolutionary Biology, University of California, Los Angeles, CA 90095, USA. [15]Department of Biology, University of Missouri, St. Louis, MO 63121, USA. [16]Department of Biology, Colorado State University, Fort Collins, CO 80523, USA. [17]Institute for Genomic Biology, Department of Plant Biology, University of Illinois at Urbana-Champaign, Urbana, IL 61801, USA. [18]University of Maryland, Center for Environmental Science Appalachian Laboratory, Frostburg, MD 21532, USA. [19]Canadian Museum of Nature, Research Division, Ottawa, Ontario K1P 6P4, Canada. [20]Department of Ecology and Evolutionary Biology, University of Toronto, Toronto, Ontario M5S 3B2, Canada. [21]The Swiss Institute of Bioinformatics, Quartier Sorge, 1015 Lausanne, Switzerland. [22]Department of Geography and Institute for Computational Earth System Science, University of California, Santa Barbara, CA 93106, USA. [23]Department of Biology, University of Utah, Salt Lake City, UT 84112, USA.

Supporting Online Material

www.sciencemag.org/cgi/content/full/328/5978/587/DC1
Materials and Methods
SOM Text
Table S1
References

10.1126/science.1177216

Mutations in *DCC* Cause Congenital Mirror Movements

Myriam Srour,[1*] Jean-Baptiste Rivière,[1*] Jessica M. T. Pham,[2] Marie-Pierre Dubé,[1,3] Simon Girard,[1] Steves Morin,[2] Patrick A. Dion,[1] Géraldine Asselin,[3] Daniel Rochefort,[1] Pascale Hince,[1] Sabrina Diab,[1] Naser Sharafaddinzadeh,[4] Sylvain Chouinard,[1] Hugo Théoret,[5] Frédéric Charron,[2] Guy A. Rouleau[1]†

Mirror movements (MM) are contralateral involuntary movements that mirror voluntary ones. MM are occasionally found in young children, but persistence beyond age 10 is unusual except in certain disorders of nervous system crossing such as Klippel-Feil and Kallmann syndrome. The study of individuals with MM can provide important insights into the mechanisms of contralateral innervation.

We recently described a large four-generation French Canadian (FC) family with isolated congenital MM (CMM) (*1*). Pedigree analysis suggested autosomal dominant inheritance with incomplete penetrance. We conducted a genome-wide linkage analysis and identified a single significant locus on chromosome 18q21.2. Haplotype analysis indicated that all affected individuals share a common risk haplotype (figs. S1 and S2). The region spans 2.5 Mb and contains three known genes, including *DCC* (deleted in colorectal carcinoma).

Sequencing of the 29 coding exons of *DCC* revealed a guanine to adenine substitution at the first intronic nucleotide after exon 6, in the splice donor consensus sequence of the exon (c.1140+1G>A, Fig. 1A left). The mutation segregated with the risk haplotype and was not found in 760 unrelated Caucasian controls, including 512 FC. Copy number variation analysis in 315 FC controls did not reveal any structural variants encompassing *DCC* exons.

To assess the effect of this mutation on splicing, we extracted RNA from immortalized lymphoblast cells derived from four mutation carriers and one noncarrier relative and performed reverse transcription polymerase chain reaction (RT-PCR). Amplification of the cDNA between exons 4 and 7 and subsequent gel electrophoresis identified a 408–base pair (bp) fragment corresponding to the predicted amplicon size found in all individuals and a 253-bp fragment found only in affected individuals (Fig. 1B). Sequence analysis confirmed that the 253-bp fragment corresponds to an aberrant transcript lacking exon 6. Abnormal skipping of exon 6 leads to a frameshift mutation from amino acid 329 and the introduction of a stop codon 15 amino acids further down the new reading frame (p.V329GfsX15). This mutation is predicted to result in a truncated DCC protein lacking most of its functional domains. This mutant DCC does not bind netrin (Fig. 1, C and D, and fig. S3).

To confirm the role of *DCC* in CMM, we sequenced *DCC* in a previously described Iranian family with CMM (*2*). We found a guanine insertion in exon 3 (Fig. 1A right) segregating with the disorder (fig. S4) that results in a frameshift also predicted to result in a truncated DCC protein [c.571dupG; p.V191GfsX35 (Fig. 1D)]. This mutation was absent in 538 unrelated control individuals.

DCC is a receptor for netrin-1, a diffusible extracellular protein that helps guide axons of the developing nervous system across the body's midline (*3*). The fourth and fifth fibronectin type III repeats in DCC are responsible for its binding to netrin-1 (*4*). Mice with homozygous null *DCC* mutations have severe defects of commissural development in the brain and spinal cord, with absent corpus callosum and decreased number and misrouting of commissural axons (*5*). "Kanga" mice have deletions of *DCC* exon 29 and exhibit mirror-type movements that result in a distinctive hopping gait (*6*). The latter mutant also shows defects in the crossing of corticospinal tracts and persistence of ipsilateral corticospinal tracts in hindbrain and spinal cord. This is consistent with human neurophysiological studies in which unilateral stimulation of the motor cortex in patients with MM evokes, in contrast to normal participants, a bilateral response (*7*) (fig. S5), indicating a misdirected ipsilateral corticospinal connection.

We propose that the *DCC* mutations in individuals with CMM cause a reduction in gene dosage and less robust midline guidance, which may lead to a partial failure of axonal fiber crossing and development of an abnormal ipsilateral connection. Our genetic findings confirm that *DCC* has a central role in the development of human nervous system lateralization.

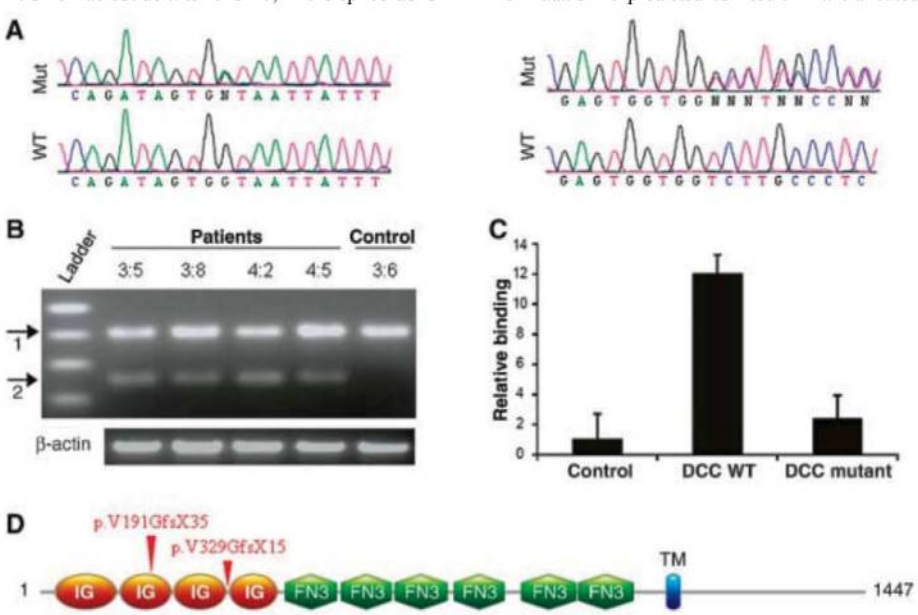

Fig. 1. *DCC* mutations in individuals with CMM. (**A**) *DCC* sequence data showing c.1140+1G>A mutation in the FC family (left) and c.571dupG mutation in the Iranian family (right). The traces show the mutant (Mut) and wild-type (WT) sequences. (**B**) Electrophoresis of RT-PCR products derived from FC patient mRNA. Shown are the normal 408-bp fragment (arrow 1) and the aberrant 253-bp (arrow 2) fragment. β-actin was coamplified as an internal control. (**C**) Mutant DCC from the FC family does not bind netrin. COS7 cells were transfected with a control plasmid, a plasmid expressing wild-type (WT) DCC (IB07), or a plasmid expressing mutant DCC (HZ29). (**D**) Schematic of the DCC protein, showing the four extracellular immunoglobulin-like C2-type domains (IG), the six extracellular fibronectin type 3 domains (FN3), and the transmembrane domain (TM). Arrowheads above the protein show the positions of the frameshift mutations.

References

1. M. Srour *et al.*, *Neurology* **73**, 729 (2009).
2. N. Sharafaddinzadeh, R. Bavarsad, M. Yousefkhah, A. M. Aleali, *Neurol. India* **56**, 482 (2008).
3. K. Keino-Masu *et al.*, *Cell* **87**, 175 (1996).
4. B. V. Geisbrecht, K. A. Dowd, R. W. Barfield, P. A. Longo, D. J. Leahy, *J. Biol. Chem.* **278**, 32561 (2003).
5. A. Fazeli *et al.*, *Nature* **386**, 796 (1997).
6. J. H. Finger *et al.*, *J. Neurosci.* **22**, 10346 (2002).
7. S. F. Farmer, D. A. Ingram, J. A. Stephens, *J. Physiol.* **428**, 467 (1990).

Supporting Online Material

www.sciencemag.org/cgi/content/full/328/5978/592/DC1
Materials and Methods
Figs. S1 to S5
Table S1
References

28 December 2009; accepted 6 April 2010
10.1126/science.1186463

[1]Center of Excellence in Neuromics, Université de Montréal, Montréal, QC H2L 2W5, Canada. [2]Molecular Biology of Neural Development, Institute de Recherches Cliniques de Montréal, Montréal, QC H2W 1R7, Canada. [3]Montréal Heart Institute, Montréal, QC H1T 1C8, Canada. [4]Department of Neurology, Jundishapour University of Medical Sciences, Ahwaz, Iran. [5]Psychology, Université de Montréal, Montréal, QC H2V 2S9, Canada.

*These authors contributed equally to this work.
†To whom correspondence should be addressed. E-mail: guy.rouleau@umontreal.ca

Systematic Analysis of Human Protein Complexes Identifies Chromosome Segregation Proteins

James R. A. Hutchins,[1]* Yusuke Toyoda,[2]* Björn Hegemann,[1]*† Ina Poser,[2]* Jean-Karim Hériché,[3,4] Martina M. Sykora,[1] Martina Augsburg,[2] Otto Hudecz,[1] Bettina A. Buschhorn,[1] Jutta Bulkescher,[4] Christian Conrad,[4] David Comartin,[5,6] Alexander Schleiffer,[1] Mihail Sarov,[2] Andrei Pozniakovsky,[2] Mikolaj Michal Slabicki,[2] Siegfried Schloissnig,[2,7] Ines Steinmacher,[1] Marit Leuschner,[2] Andrea Ssykor,[2] Steffen Lawo,[5,6] Laurence Pelletier,[5,6] Holger Stark,[8] Kim Nasmyth,[1]‡ Jan Ellenberg,[4] Richard Durbin,[3] Frank Buchholz,[2] Karl Mechtler,[1] Anthony A. Hyman,[2]§ Jan-Michael Peters[1]§

Chromosome segregation and cell division are essential, highly ordered processes that depend on numerous protein complexes. Results from recent RNA interference screens indicate that the identity and composition of these protein complexes is incompletely understood. Using gene tagging on bacterial artificial chromosomes, protein localization, and tandem-affinity purification–mass spectrometry, the MitoCheck consortium has analyzed about 100 human protein complexes, many of which had not or had only incompletely been characterized. This work has led to the discovery of previously unknown, evolutionarily conserved subunits of the anaphase-promoting complex and the γ-tubulin ring complex—large complexes that are essential for spindle assembly and chromosome segregation. The approaches we describe here are generally applicable to high-throughput follow-up analyses of phenotypic screens in mammalian cells.

Phenotypic screens using random mutagenesis, systematic gene deletion, or RNA interference (RNAi) are powerful techniques for cataloguing gene function. To interpret the resulting genotype-phenotype relationships, detailed molecular analyses are required, among which protein localization and identification of protein interactions are particularly informative. In yeast, the modification of most genes at their endogenous loci with tag-coding sequences has been valuable for systems-wide analyses of protein function (*1*–*4*). In mammalian cells, however, large-scale localization and interaction studies of proteins expressed under control of their own regulatory sequences have so far lagged behind phenotypic analysis. The MitoCheck consortium (www.mitocheck.org) has therefore used recombineering techniques (*5*) to develop a fast and reliable procedure for the introduction of genes tagged in bacterial artificial chromosomes (BACs) into human tissue culture cells. This technique allows the stable expression of genes under their own promoters at near-physiological levels (*6*). We have combined this "BAC TransgeneOmics" technology with large-scale protein localization and interaction experiments to characterize about 100 mitotic protein complexes (Fig. 1A). By using this combined approach, we discovered previously unknown subunits of the γ-tubulin ring complex (γ-TuRC) and the anaphase-promoting complex (APC/C), complexes that are essential for spindle assembly and chromosome segregation, respectively (*7*, *8*).

Generation of a library of HeLa cell pools stably expressing green fluorescent protein (GFP)–tagged BACs. We chose to characterize proteins required for mitosis because this process is essential for eukaryotic life, is of relevance for tumor biology, and is known to depend on numerous protein complexes. Many of these had been characterized before, providing prior knowledge that we could use to control our approaches and to draw hypotheses for unknown genes. RNAi screens performed in *C. elegans*, *Drosophila*, and mammalian cells as well as proteomic studies have furthermore identified numerous uncharacterized proteins required for mitosis (*9*–*17*). In addition, the MitoCheck consortium carried out a genome-wide RNAi screen by means of time-lapse imaging of chromosome segregation in live cells that provided detailed phenotypic information for the majority of human proteins (*16*).

From these screens and the literature, we selected 696 proteins (table S1) for C-terminal tagging with a combined localization affinity-purification (LAP) tag (*18*), using high-throughput BAC recombineering in *Escherichia coli* (*6*). In most cases, we tagged mouse genes and expressed them in human cells because this allows functional testing of the tagged proteins through RNAi-mediated depletion of their endogenous counterparts (*19*). N-terminal tags were introduced if C-terminal tagging failed or in some cases to validate data obtained with the C-terminal tag. We were able to tag and stably express 591 (89%) of the selected proteins in HeLa cells (fig. S1). For each gene, we obtained at least one non-clonal pool of stably expressing cells, resulting in a library of 657 pools. Using antibodies to the GFP moiety of the LAP tag, we could detect the tagged proteins in 559 pools (85%), corresponding to 504 unique proteins (77%), by means of immunofluorescence microscopy (IFM) (table S1 and fig. S1C).

Localization of mitotic proteins. First, we analyzed all cell pools in which a GFP signal could be detected for the intracellular localization of tagged proteins in interphase, metaphase, and telophase, using fixed cells stained with antibodies to GFP and α-tubulin, and 4′,6-diamidino-2-phenylindole (DAPI) to visualize DNA (Fig. 1B). In mitotic cells, we observed specific association with centrosomes, spindles, kinetochores, chromosomes, cleavage furrows, midbodies, or cortical structures for 180 proteins, of which 25 had not been characterized in mitosis and 54 not at all (fig. S1C). For 14 proteins, we confirmed our fixed-cell data by means of time-lapse imaging of living cells (Fig. 1C and fig. S2).

To identify proteins with potential roles in spindle assembly, we localized in more detail 102 proteins that showed mitotic centrosome or spindle association. Of these, 23 had not been characterized in mitosis and 9 not at all. Immunofluorescence images were classified into 87 staining patterns at five different mitotic stages, resulting in specific localization trajectories (Fig. 1B and fig. S3). The frequency distribution of different patterns was scored manually, and the 102 proteins were clustered into 10 groups according to these scores (Fig. 2). Localization analysis with this resolution allowed separation even of complexes with very similar localization, such as the kinetochore complex MIS12 and the mitotic checkpoint complex (MCC), into separate localization trajectories (see fig. S3). In all cases, subunits of known complexes were recovered in the same clusters [chromosomal passenger complex (CPC), centralspindlin, MIS12, Aurora

[1]Research Institute of Molecular Pathology (IMP), Dr. Bohr-Gasse 7, A-1030 Vienna, Austria. [2]Max Planck Institute (MPI) for Molecular Cell Biology and Genetics, Pfotenhauerstrasse 108, D-01307 Dresden, Germany. [3]Wellcome Trust Sanger Institute, Wellcome Trust Genome Campus, Hinxton, Cambridge CB10 1HH, UK. [4]Cell Biology and Biophysics Unit, European Molecular Biology Laboratory, Meyerhofstrasse 1, D-69117 Heidelberg, Germany. [5]Samuel Lunenfeld Research Institute, Mount Sinai Hospital, 600 University Avenue, Toronto, Ontario M5G 1X5, Canada. [6]Department of Molecular Genetics, University of Toronto, Toronto, Ontario M5S 1A8, Canada. [7]German Cancer Research Center, Im Neuenheimer Feld 280, 69120 Heidelberg, Germany. [8]Max Planck Institute for Biophysical Chemistry, Am Fassberg 11, D-37077 Göttingen, Germany.

*These authors contributed equally to this work.
†Present address: Institute of Biochemistry, Eidgenössische Technische Hochschule Zürich, Schafmattstrasse 18, CH-8093 Zürich, Switzerland.
‡Present address: Department of Biochemistry, University of Oxford, South Parks Road, Oxford OX1 3QU, UK.
§To whom correspondence should be addressed. E-mail: hyman@mpi-cbg.de (A.A.H.); peters@imp.univie.ac.at (J.-M.P.)

A-targeting protein for Xklp2 (TPX2), and γ-TuRC], although prior knowledge about the existence of these complexes had not been used to "train" the cluster algorithm. This suggests that clustering of localization trajectories can be used to formulate hypotheses about functions and physical interactions of uncharacterized proteins. For example, centrosomal protein of 120 kD (CEP120) clustered with proteins required for centriole duplication, suggesting that CEP120 may have a role in this process. RNAi experiments indicated that this is indeed the case (fig. S4).

Identification of mitotic protein complexes. To characterize mitotic protein complexes, we isolated LAP-tagged proteins from cells arrested in mitosis using tandem-affinity purification (TAP) (fig. S5) (*6*). Samples were analyzed with SDS–polyacrylamide gel electrophoresis (SDS-PAGE) followed by silver staining and with in-solution trypsinization and tandem mass spectrometry (MS). Initially, proteins were selected on the basis of localization identified by means of GFP imaging or on reported mitotic functions. Once interaction partners had been identified, interaction mapping was performed iteratively by producing new LAP-tagged cell pools to validate a subset of the interactions through reciprocal analyses. In total, cell pools containing 254 different tagged genes were analyzed. In 239 cases (94%), the "bait" proteins could be identified. These interacted with a total of 936 "prey" proteins that were present in specific samples, corresponding to 2011 distinct pair-wise interactions (*20*). Other proteins, which were found in more than 4.5% of all samples or in "mock" purifications, were excluded from further analyses because these proteins might represent contaminants (tables S2 and S3). For a complete pre-

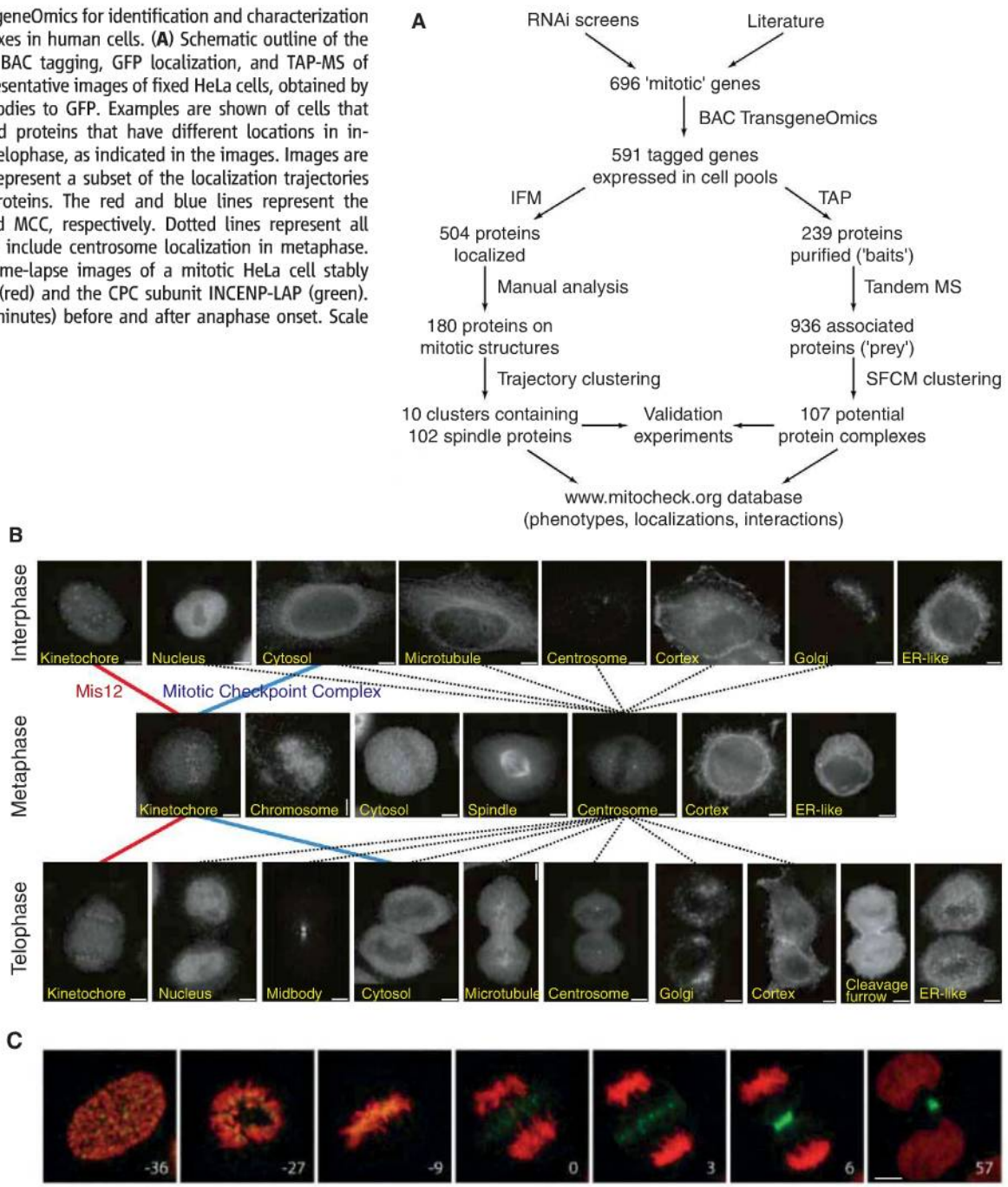

Fig. 1. Use of BAC TransgeneOmics for identification and characterization of mitotic protein complexes in human cells. (**A**) Schematic outline of the workflow established for BAC tagging, GFP localization, and TAP-MS of mitotic proteins. (**B**) Representative images of fixed HeLa cells, obtained by means of IFM with antibodies to GFP. Examples are shown of cells that stably express LAP-tagged proteins that have different locations in interphase, metaphase, or telophase, as indicated in the images. Images are connected by lines that represent a subset of the localization trajectories observed for different proteins. The red and blue lines represent the trajectories of MIS12 and MCC, respectively. Dotted lines represent all observed trajectories that include centrosome localization in metaphase. Scale bar, 10 μm. (**C**) Time-lapse images of a mitotic HeLa cell stably expressing H2B-mCherry (red) and the CPC subunit INCENP-LAP (green). Numbers indicate time (minutes) before and after anaphase onset. Scale bar, 10 μm.

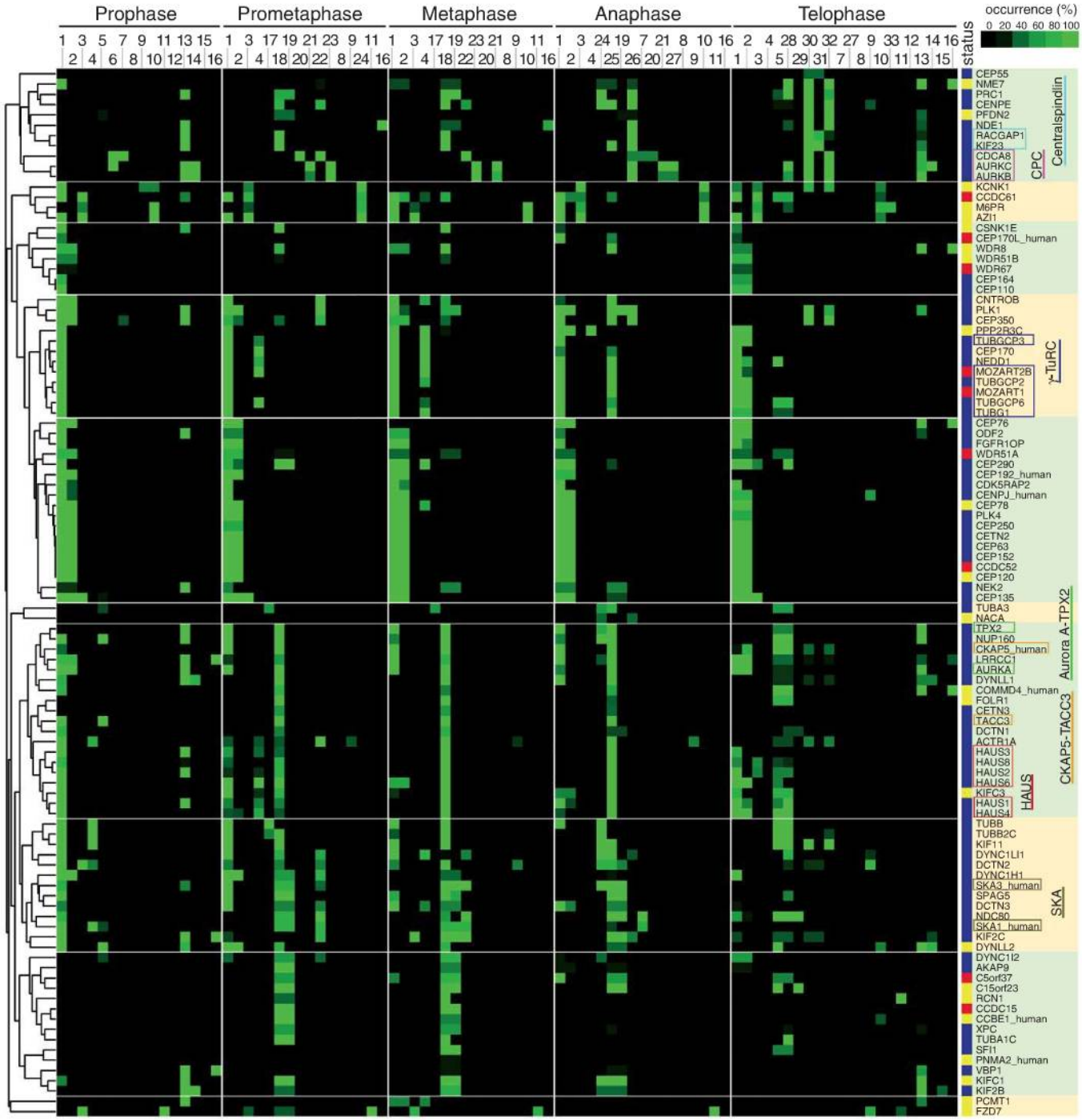

Fig. 2. Heat map showing hierarchical clustering of the localization trajectories of 102 spindle and centrosome proteins. IFM images of fixed HeLa cells expressing LAP-tagged proteins (listed on the *y* axis) in five mitotic phases were classified into 33 staining patterns (mouse ortholog proteins were imaged unless suffixed as "_human"). The frequency with which each staining pattern was observed for each protein in each phase is represented by a square, with color ranging from black (0% occurrence) to bright green (100% occurrence). The number codes for the staining patterns are as follows: 1, centrosome (PCM-like); 2, centrosome (fine dots); 3, dots near centrosome; 4, centrosome and partial microtubule (MT); 5, microtubule; 6, chromosome; 7, kinetochore; 8, cortex (whole); 9, cortex (partial); 10, dots in cytoplasm; 11, ER-like meshwork; 12, nuclear envelope; 13, nucleus; 14, dots in nucleus; 15, nucleolus; 16, whole cell; 17, spindle MT (whole); 18, spindle MT (K-fiber); 19, spindle matrix-like; 20, chromosome (axis); 21, chromosome (periphery); 22, kinetochore (sisters); 23, kinetochore (inner); 24, microtubule (whole); 25, microtubule (K-fiber); 26, spindle midzone; 27, cleavage furrow; 28, microtubule next to midbody; 29, microtubule (unclear); 30, midbody; 31, midbody ring; 32, midbody next to ring; and 33, Golgi-like. The "status" column shows the characterization status of each gene, as defined by literature searching in PubMed, according to the following color scheme: blue, reported to be involved in mitosis; yellow, some function reported but not in the context of mitosis; and red, functionally uncharacterized. The dendrogram on the left indicates the relative similarities of the trajectories of individual proteins to the entire trajectory pattern. The clustered heat map was divided into 10 subclusters on the basis of a visual inspection of clustered localization patterns (subclusters indicated by alternating green and yellow shading). The names of subunits of previously identified complexes are boxed in different colors (Centralspindlin, light blue; CPC, magenta; γ-TuRC, dark blue; Aurora A-TPX2, bright green; chTOG-TACC3, orange; Augmin/HAUS, red; SKA, olive-green).

sentation of all data, see www.mitocheck.org. Additional information on tagged BACs can be found at http://hymanlab.mpi-cbg.de/BACE.

We analyzed baits from 11 previously described reference complexes which, according to the literature, contain 74 subunits (fig. S6A). Our experiments identified 70 of these, indicating a low false-negative detection rate (fig. S6B). In 175 cases, our experiments revealed interactions between two proteins, both of which had been tagged and used as baits. Of these interactions, 94 (54%) could be detected with both baits. This frequency of reciprocal interactions is higher than in previous studies performed in yeast [15% in (*3*); 8% in (*4*)]. These results suggest that the number of false-positive interactions in our data set is relatively low. However, we cannot exclude that some false-positive interactions were detected.

To identify previously unknown complexes, we analyzed the data set of all interactions for the presence of proteins that are densely connected with each other (fig. S7) using a clustering algorithm that we call spectral fuzzy C-means (SFCM). We identified 35 singletons (cases in which only the bait had been found), 107 clusters that contain between two and 20 proteins, and 13 clusters with more than 20 components (Fig. 3, figs. S7 and S8, and table S4). The 13 large clusters contain sets of loosely connected proteins, which presumably had been grouped together because the density of the interaction network was not high enough to separate these proteins into smaller, more meaningful clusters. However, among the 107 small clusters 11 matched the reference complexes with an average precision of 59% (the fraction of cluster members that belong to the same reference complex) and an average recall of 89% (the fraction of the reference complex subunits assigned to the same cluster). These values indicate that many of the small clusters represent bona fide protein complexes or groups of closely related complexes (for example, different isoforms of cohesin complexes clustered together) (table S4). As an example, Fig. 3 shows a graphical representation of 10 of the 107 small clusters and how they compare with reference complexes described in the literature. The entire interaction network can be seen in the supporting visualization S1 file.

Identification and characterization of mitotic protein complexes by combined interaction and localization studies. To test whether co-purifying proteins interact in vivo, we analyzed in how many cases similar localization patterns had been obtained for interacting proteins. We manually annotated a subset of 728 interactions and found that 49% of all pairwise interacting bait and prey proteins had similar localizations. This frequency was even higher (79%) when only reciprocally confirmed interactions were considered (fig. S9). For example, we observed that CEP120 both co-localized and physically interacted with coiled coil domain–containing 52 (CCDC52), suggesting that these proteins form a complex

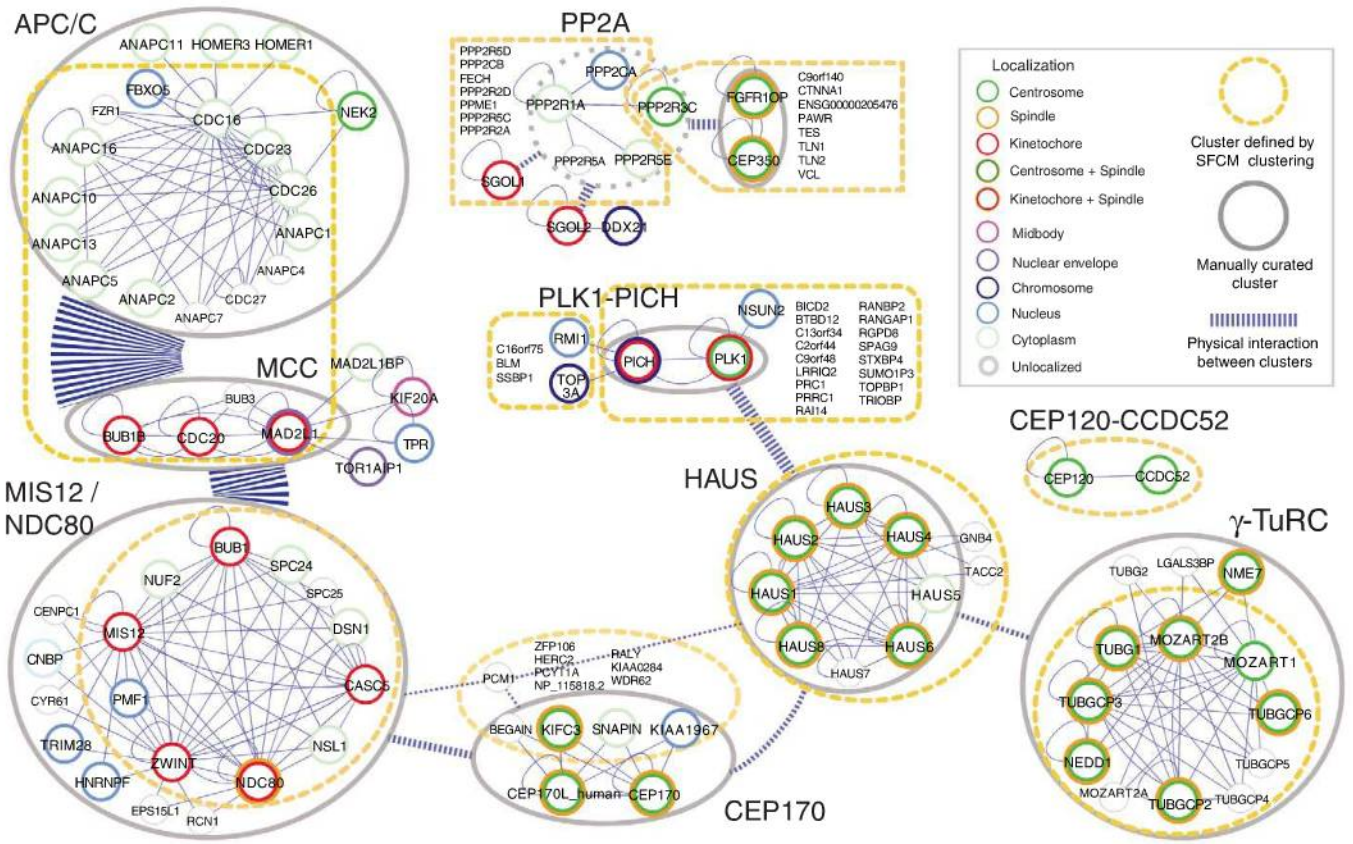

Fig. 3. Combined interaction and localization map for a selection of 10 out of 107 small clusters (cluster size, 2 to 20 proteins). Protein interaction data obtained by means of TAP-MS were analyzed with SFCM clustering. The resulting clusters (enclosed by orange dashed lines) were manually annotated according to literature knowledge (for composition of reference complexes as described in the literature, see fig. S6) (*29*). The resulting curated clusters are shown as gray ellipses: Complexes containing reciprocal interactions are enclosed by solid gray lines, whereas those without reciprocal interactions are denoted by dashed gray lines. Inter- and intra-cluster interactions are represented by dashed and solid blue lines, respectively, with the number of interactions corresponding to the thickness of these lines. Localization as determined by use of GFP imaging is shown in the color codes as indicated. Cluster and protein complexes can have interactions with several other clusters/complexes. For example, MCC co-purified and therefore co-clustered both with APC/C and with the MIS12/NDC80 cluster. The former association reflects binding of MCC to APC/C in prometaphase cells (*30*), from which these proteins were purified, whereas MCC association with MIS12/NDC80 may reflect recruitment of MCC components to unattached kinetochores in prometaphase (*31*). For an expanded "master map," integrating localization and interaction data for more proteins, see fig. S8.

(Figs. 2 and 3). Similarly, we observed that eight proteins, which had not been characterized when we performed our experiments, interacted reciprocally with each other and were all located on mitotic spindles (fig. S10). These proteins are subunits of the Augmin/HAUS complex, which has recently been shown to be essential for spindle function (*21*–*23*). Combining localization and interaction data can also identify unknown interactions between well-characterized proteins and complexes, as is illustrated by our finding that Polo-like kinase 1-interacting checkpoint helicase [PICH, also known as excision repair cross-complementing rodent repair deficiency, complementation group 6-like (ERCC6L)] interacts and co-localizes on chromosome bridges with subunits of the RTR complex [RecQ helicase (BLM)-topoisomerase III (TOP3A)–RecQ mediated genome instability 1 (RMI1) complex] (fig. S11) (*24*).

Identification of C10orf104 as a subunit of the APC/C. We further characterized chromosome 10 open reading frame 104 (C10orf104) because this 11.7-kD protein co-purified with seven different APC/C subunits (fig. S12A), but not with any other bait, and thus co-clustered with the APC/C in our SFCM analysis (Fig. 3). The APC/C is a 1.5-MD ubiquitin ligase complex that is essential for chromosome segregation and mitotic exit (*8*). Because APC/C has been characterized in detail, it was surprising that a previously uncharacterized protein co-purified with APC/C subunits. However, when C10orf104 also was used as bait several APC/C subunits were detected (fig. S12A), and antibodies raised against C10orf104 immunoprecipitated the entire APC/C and its associated cyclin B ubiquitylation activity (Fig. 4, A and B). Immunoblot experiments showed that C10orf104 is present throughout the cell cycle (fig. S12, B and C), and density gradient centrifugation experiments indicated that most of C10orf104 is associated with the APC/C (Fig. 4C). These observations indicate that C10orf104 is a constitutive subunit of the APC/C and not a substrate or a transiently associating regulatory protein. Electron microscopic analysis of APC/C labeled with antibodies to C10orf104 suggested that C10orf104 is located at the top of APC/C's "arc lamp" domain, in the vicinity of the subunit CDC27 (Fig. 4D and fig. S12, D to F). The amino acid sequence of C10orf104 is highly conserved among vertebrates (95% identical between human and zebrafish), suggesting that despite its small size, this protein performs an important function within the APC/C. Related sequences also exist in invertebrates (fig. S12G), although we could not yet identify homologous sequences in yeast. These observations indicate that C10orf104 is an evolutionarily conserved APC/C subunit, which we propose to call APC16 (gene symbol ANAPC16). We suspect that APC16 has previously escaped detection in protein gels or through MS because of its small size.

Identification of proteins interacting with the γ-TuRC. We also characterized chromosome 13 open reading frame 37 (C13orf37) and two closely related proteins, called family with sequence similarity 128 member A and member B (FAM128A and FAM128B), because these proteins co-purified with three different subunits of the γ-TuRC. This complex is located at centrosomes and mediates the formation of bipolar spindles in mitosis (*7*). When C13orf37 and FAM128B were used as baits, all six known γ-TuRC subunits were identified (Fig. 3 and Fig. 5, A and B). Sucrose density gradient centrifugation experiments confirmed that C13orf37 and FAM128B are associated with the γ-TuRC component tubulin gamma 1 (TUBG1) (fig S13A). Similar to γ-TuRC subunits, C13orf37 and FAM128B were located on centrosomes throughout the cell cycle and to a lesser extent on mitotic spindles (Fig. 2, Fig. 5, C and D, and fig. S13B). Proteins homologous to C13orf37 and FAM128A/B are predicted to exist in many eukaryotes, including in the case of C13orf37 the fission yeast *Schizosaccharomyces pombe* (fig. S13, C and D). However, the corresponding genomic sequences have not been annotated as genes in all organisms, possibly because C13orf37 and FAM128A/B are small proteins of 8.5 and 16.2 kD, respectively. C13orf37 and FAM128A/B may thus be evolutionarily conserved γ-TuRC subunits that previously may not have been detected because of their small size. However, unlike the known subunits of γ-TuRC [tubulin, gamma complex–

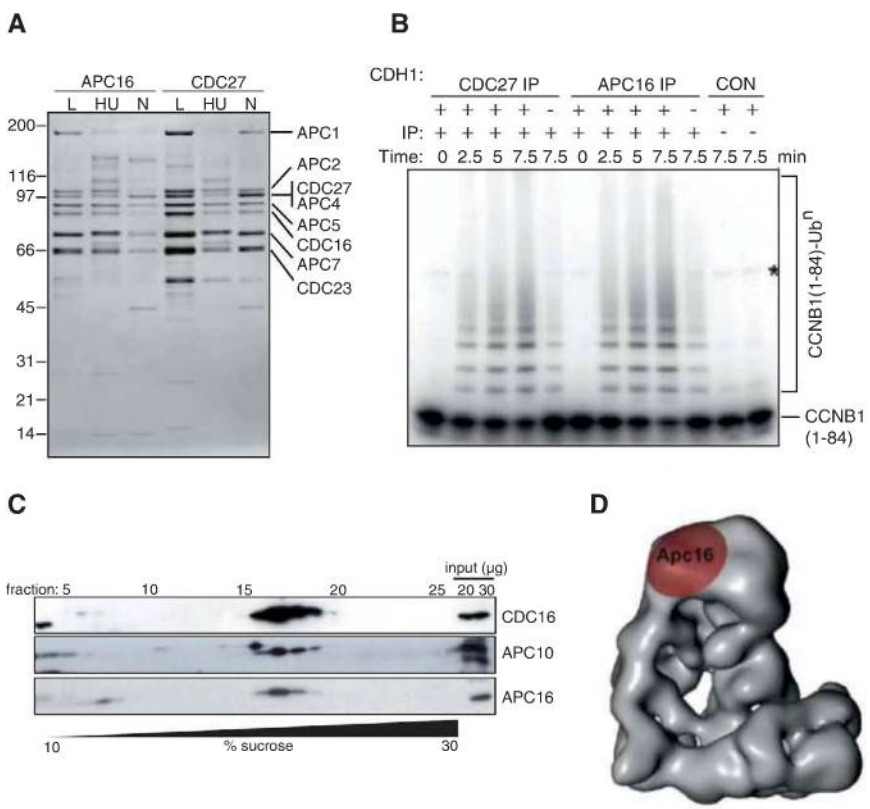

Fig. 4. Characterization of APC16, a previously unknown subunit of the APC/C. (**A**) Silver-stained SDS-PAGE gel showing proteins immunoprecipitated by using antibodies to APC16 or CDC27 from extracts of HeLa cells, cultured under logarithmic growth conditions (L), or arrested in S phase by means of treatment for 18 hours with hydroxyurea (HU) or arrested in prometaphase by treatment for 18 hours with nocodazole (N). Numbers on the left indicate the molecular masses of reference proteins. (**B**) Phosphorimage showing the ubiquitylation of Cyclin B1 (CCNB1), catalyzed by CDC27 and APC16 immunoprecipitates. [^{125}I]-labeled human CCNB1 fragment (amino acids 1 to 84) was incubated with CDC27 or APC16 immunoprecipitates from logarithmically growing HeLa cells, plus E1 and E2 enzymes, ubiquitin, and adenosine 5′-triphosphate (ATP), with or without the recombinant co-activator protein CDH1, for the times indicated and then analyzed with SDS-PAGE and phosphorimaging. CON indicates empty protein-A beads (left) and a condensin antibody immunoprecipitate (right). The asterisk marks a contaminating band present in the CCNB1 sample. (**C**) Immunoblots showing the co-sedimentation of APC16 with core APC/C subunits CDC16 and APC10, after density gradient centrifugation. An extract of logarithmically growing HeLa cells was subjected to centrifugation through a 10 to 30% sucrose density gradient. Twenty-eight fractions were collected and analyzed with SDS-PAGE and immunoblotting with the antibodies indicated. (**D**) Three-dimensional model of the human APC/C obtained with electron microscopy (*30*) showing the location of APC16, as determined by means of antibody labeling.

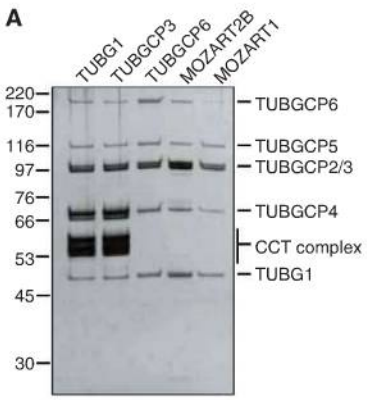

B

Protein	Other name	Mass (kDa)	LAP-tagged bait				
			TUBG1	TUBGCP3	TUBGCP6	MOZART1	MOZART2B
TUBG1	γ-Tubulin	51.2	33.7%	85.6%	10.9%	11.8%	18.0%
TUBGCP2	GCP-2	102.5	28.8%	56.9%	23.2%	26.8%	51.7%
TUBGCP3	GCP-3	103.6	25.8%	55.4%	20.7%	21.6%	34.1%
TUBGCP4	GCP-4	76.1	15.2%	31.1%	9.5%	12.3%	30.5%
TUBGCP5	GCP-5	118.3	17.5%	20.8%	15.2%	18.1%	30.9%
TUBGCP6	GCP-6	200.5	12.0%	7.0%	18.1%	7.6%	16.1%
MOZART1	C13orf37	8.5	32.9%	52.4%	32.9%	34.6%	32.9%
MOZART2A	FAM128A	16.2	10.1% *	-	10.1% *	24.1%	24.1%
MOZART2B	FAM128B	16.2	-	51.9%	-	-	22.0%

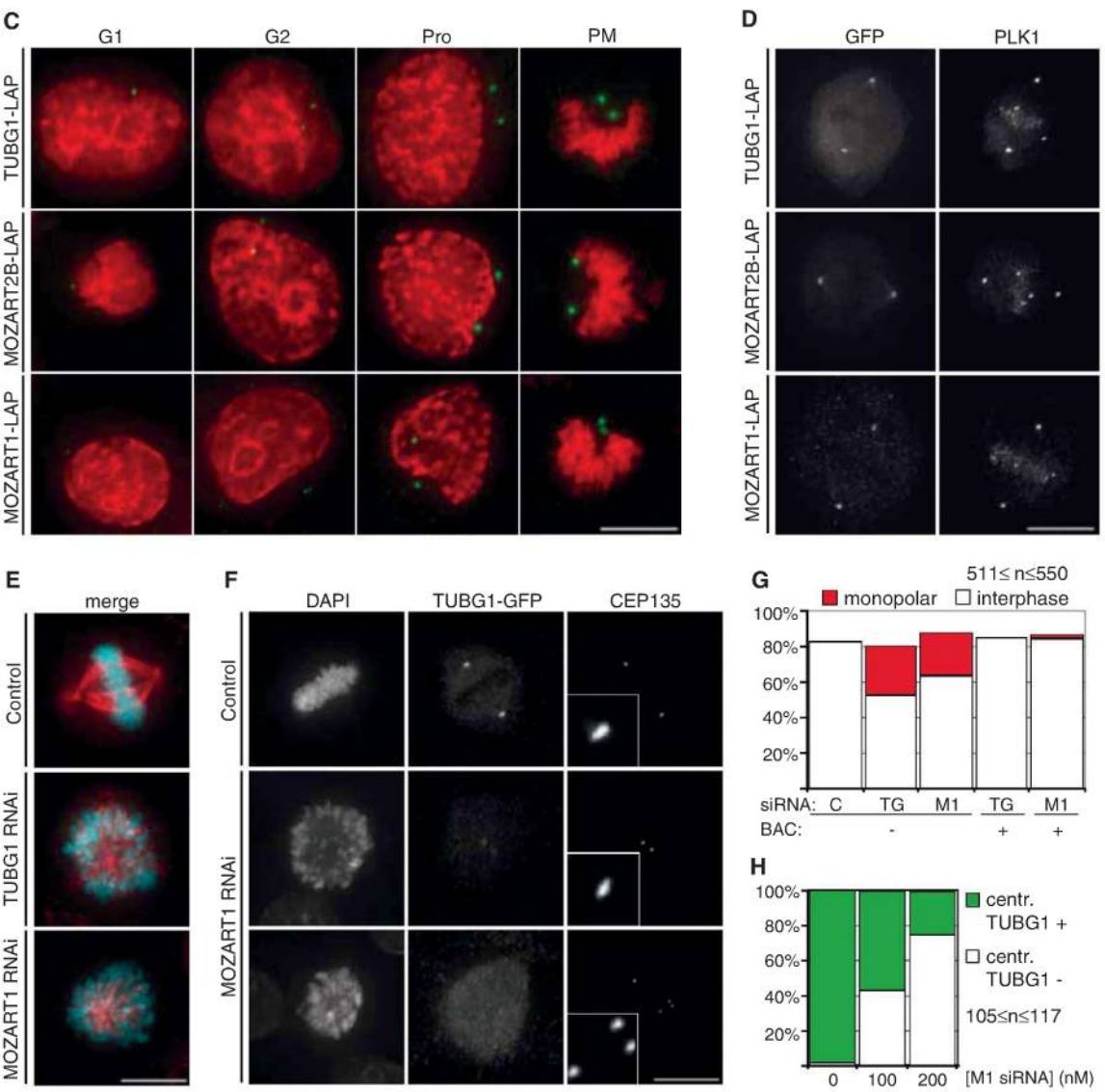

Fig. 5. Characterization of the γ-TuRC interacting proteins MOZART1 and MOZART2B. (**A**) Silver-stained SDS-PAGE gel of LAP-purified TUBG1, TUBGCP3, TUBGCP6, MOZART2B, and MOZART1. Numbers on the left indicate the molecular masses of reference proteins. Proteins annotated according to expected electrophoretic mobility are listed on the right. CCT, chaperonin-containing T-complex. (**B**) MS results obtained from the samples in (A), showing identification of γ-TuRC subunits plus MOZART1, MOZART2A, and MOZART2B. Entries highlighted in orange are bait proteins, yellow indicates proteins whose interaction with the bait has previously been reported, and a white background indicates that the interaction was previously unknown. Asterisks indicate proteins identified by a single peptide. (**C**) IFM images showing centrosomal localization of TUBG1, MOZART2B, and MOZART1 through the cell cycle [G_1 phase, G_2 phase, prophase (Pro), or prometaphase (PM)]. HeLa cells expressing the indicated proteins were fixed and stained with antibodies to GFP (green) and with DAPI (red). (**D**) IFM images showing localization of TUBG1, MOZART2B, and MOZART1 to centrosomes and the mitotic spindle in metaphase in fixed LAP cells stained with antibodies to GFP and PLK1. All images in this figure are maximum-intensity projections of DeltaVision stacks. Scale bar, 10 μm. (**E**) IFM images of HeLa cells treated for 72 hours with 100 nM siRNA specific to either TUBG1 or MOZART1. Cells were fixed and stained with DAPI (blue) and TUBA1A antibodies (red). Scale bar, 10 μm. (**F**) IFM images of TUBG1-LAP HeLa cells treated for 72 hours with 100 nM siRNA against TUBG1 so as to deplete the endogenous TUBG1 and, simultaneously, transfected either with luciferase siRNA (control siRNA) or MOZART1 siRNA. Cells were fixed and stained with DAPI, GFP antibodies (to visualize TUBG1-LAP), and CEP135 (to stain centrioles). Two distinct phenotypes were observed: CEP135 foci in close proximity to each other that colocalize with faint TUBG1-GFP foci (middle row) and CEP135 foci dispersed randomly dispersed throughout the cell with no detectable TUBG1-GFP foci (bottom row). Insets in the third column are magnified fivefold to show one centrosome. Scale bar, 10 μm. (**G**) Histogram showing quantification of the experiment described in (E). In addition, cells containing the mouse TUBG1-LAP or the mouse MOZART1-LAP (BAC +) were treated with 100 nM siRNA specific for TUBG1 or MOZART1, respectively, and fixed and stained as in (E). C, control; TG, TUBG1 siRNA; M1, MOZART1 siRNA. (**H**) Histogram showing quantification of the experiment described in (F). The number of cells with GFP-positive (TUBG1 +) or -negative (TUBG1 –) centrosomes was counted. The GFP-negative cells are a combination of both MOZART1-depletion phenotypes shown in (F).

associated proteins (TUBGCP2 to -6)], C13orf37 and FAM128A/B do not contain the conserved "Spc97_Spc98" GCP domain (*25*). The TUBGCP nomenclature can therefore not be applied to C13orf37, FAM128A, or FAM128B. Instead, we propose to call these proteins mitotic-spindle organizing proteins associated with a ring of γ-tubulin (MOZART1, MOZART2A and MOZART2B, respectively).

MOZART1, an evolutionarily conserved protein essential for γ-TuRC function. To test whether the MOZARTs are important for γ-TuRC function, we performed RNAi experiments in HeLa cells. Transfection of MOZART2A/B small interfering RNA (siRNA) did not result in detectable mitotic phenotypes, but we cannot exclude that this was due to incomplete depletion of these proteins. In contrast, depletion of either MOZART1 or TUBG1 led to the accumulation of prometaphase cells with monopolar spindles and closely spaced centrosome pairs (Fig. 5, E to G). These phenotypes were fully reverted through stable integration of the corresponding LAP-tagged mouse genes on BACs (Fig. 5G), ruling out off-target RNAi effects and showing that the LAP-tagged proteins used for localization and interaction mapping are functional.

Monopolar spindle phenotypes have been observed after depletion of γ-TuRC, but also after inactivation of PLK1 (*26*) or Aurora A kinase (*27*). We therefore tested whether MOZART1 depletion could interfere with spindle assembly directly by preventing γ-tubulin recruitment to centrosomes, or indirectly by decreasing PLK1 or Aurora A activity. In IFM experiments, MOZART1-depleted cells were stained equally well as control cells with antibodies specific for phospho-epitopes generated by PLK1 or Aurora A (fig S13, E and F), suggesting that MOZART1 is not required for the activation of these kinases. However, depletion of MOZART1 did strongly reduce TUBG1-LAP–staining at centrosomes in 70% of the cells (Fig. 5, F and H). These observations indicate that MOZART1 is required for γ-TuRC recruitment to centrosomes. Because orthologs of MOZART1 exist in lower eukaryotes, including fission yeast, it is possible that this function has been highly conserved during evolution.

A human functional-genomics database. The data obtained in this study have enabled us to identify previously unknown protein complexes (CEP120-CCDC52 and Augmin/HAUS), new subunits of well-studied protein complexes such as the APC/C (APC16) and γ-TuRC (the MOZARTs), and unknown interactions between known proteins and complexes (PICH-RTR). However, the majority of our data has not yet been used for follow-up experiments. We suspect that such experiments will lead to additional important discoveries about the functions of human protein complexes in mitosis (*28*). This notion is supported by the observation that most of the protein interactions detected in our experiments have not been previously reported. For example, for 60 of the 107 small SFCM clusters none of the interactions have been reported in seven major public-interaction databases (fig. S7A). Many of these clusters may therefore represent uncharacterized protein complexes. To enable the exploitation of these data by the scientific community, we have generated a human genome-wide database (www.mitocheck.org) that contains all data generated by the MitoCheck consortium (fig. S14). These include information on tagged BACs, immunofluorescence images obtained through GFP localization, silver-stained SDS-PAGE gels of all protein samples obtained through TAP, and all protein interaction lists obtained through in-solution trypsinization-tandem MS. In addition, this database contains movies from the MitoCheck RNAi screen, in which mitosis has been analyzed by means of live imaging of cells in which all human proteins have been targeted by siRNAs (*16*). The database also provides information about gene synonyms used in the literature, orthologs in other species, and protein interactions reported in public databases. This collection of localization, interaction, and phenotypic data will be a useful resource for understanding the functions of human proteins.

Conclusion. The widespread application of RNAi for phenotypic screens has not been accompanied by the development of approaches to rapidly study protein function. This means that it is difficult to characterize the results of such screens. Similar problems apply to the results of human genetic and genomic studies, which often identify many uncharacterized proteins potentially associated with disease. The combined use of BAC tagging, protein localization, and interaction mapping techniques that we describe here for mitotic proteins helps to overcome this limitation by allowing systems-scale approaches to studying protein function. These systematic nongenetic approaches represent a valuable counterpart to RNAi screens, in which limited penetrance and off-target effects can result in ambiguity in the identification of gene function. Rather than relying on phenotypic screens, hypotheses can be generated and tested from analysis of the protein complexes and localization of uncharacterized proteins.

References and Notes

1. S. Ghaemmaghami *et al.*, *Nature* **425**, 737 (2003).
2. W. K. Huh *et al.*, *Nature* **425**, 686 (2003).
3. A. C. Gavin *et al.*, *Nature* **440**, 631 (2006).
4. N. J. Krogan *et al.*, *Nature* **440**, 637 (2006).
5. Y. Zhang, F. Buchholz, J. P. Muyrers, A. F. Stewart, *Nat. Genet.* **20**, 123 (1998).
6. I. Poser *et al.*, *Nat. Methods* **5**, 409 (2008).
7. U. Patel, T. Stearns, *Curr. Biol.* **12**, R408 (2002).
8. J. M. Peters, *Nat. Rev. Mol. Cell Biol.* **7**, 644 (2006).
9. P. Gönczy *et al.*, *Nature* **408**, 331 (2000).
10. J. S. Andersen *et al.*, *Nature* **426**, 570 (2003).
11. R. S. Kamath *et al.*, *Nature* **421**, 231 (2003).
12. B. Sönnichsen *et al.*, *Nature* **434**, 462 (2005).
13. G. Goshima *et al.*, *Science* **316**, 417 (2007).
14. R. Kittler *et al.*, *Nat. Cell Biol.* **9**, 1401 (2007).
15. M. P. Somma *et al.*, *PLoS Genet.* **4**, e1000126 (2008).
16. B. Neumann *et al.*, *Nature* **464**, 721 (2010).
17. M. Theis *et al.*, *EMBO J.* **28**, 1453 (2009).
18. I. M. Cheeseman, A. Desai, *Sci. STKE* **2005**, pl1 (2005).
19. R. Kittler *et al.*, *Proc. Natl. Acad. Sci. U.S.A.* **102**, 2396 (2005).
20. The protein interactions from this publication have been submitted to the International Molecular Exchange (IMEx) Consortium (http://imex.sf.net) through IntAct (www.ebi.ac.uk/intact), and assigned the identifier IM-11719.
21. G. Goshima, M. Mayer, N. Zhang, N. Stuurman, R. D. Vale, *J. Cell Biol.* **181**, 421 (2008).
22. S. Lawo *et al.*, *Curr. Biol.* **19**, 816 (2009).
23. R. Uehara *et al.*, *Proc. Natl. Acad. Sci. U.S.A.* **106**, 6998 (2009).
24. H. W. Mankouri, I. D. Hickson, *Trends Biochem. Sci.* **32**, 538 (2007).
25. R. D. Finn *et al.*, *Nucleic Acids Res.* **38** (Database issue), D211 (2010).
26. P. Lénárt *et al.*, *Curr. Biol.* **17**, 304 (2007).
27. E. Hannak, M. Kirkham, A. A. Hyman, K. Oegema, *J. Cell Biol.* **155**, 1109 (2001).
28. R. Kittler, L. Pelletier, F. Buchholz, *Cell Cycle* **7**, 2123 (2008).
29. Materials and methods are available as supporting material on *Science* Online.
30. F. Herzog *et al.*, *Science* **323**, 1477 (2009).
31. A. Musacchio, E. D. Salmon, *Nat. Rev. Mol. Cell Biol.* **8**, 379 (2007).

32. We are grateful to the following colleagues for their excellent assistance: E. Kreidl, M. Mazanek, M. Madalinski, G. Mitulović, M. Novatchkova, C. Stingl, Y. Sun (IMP and Institute of Molecular Biotechnology of the Austrian Academy of Sciences, Vienna); A. Bird, K. Kozak, D. Krastev, Z. Maliga, D. Richter, M. Theis, M. Toyoda (MPI, Dresden); P. Dube (MPI, Göttingen); and N. Kraut (Boehringer Ingelheim, Vienna). This work was funded in the most part by the European Commission via the Sixth Framework Programme Integrated Project MitoCheck (LSHG-CT-2004-503464). Work in the laboratories of J.-M.P. and K.M. received support from Boehringer Ingelheim, the Vienna Spots of Excellence Programme, the Austrian Science Fund Special Research Programme "Chromosome Dynamics," and the Genome Research in Austria Programme. Work in the laboratories of A.A.H. and F.B. received support from the Max Planck Society and from Bundesministerium für Bildung und Forschung grants NGFN-2 SMP-RNAi (01GR0402) and NGFN-Plus (01GS0859). Work in the laboratory of L.P. was supported by operating grants from the Natural Science and Engineering Research Council of Canada (RGPIN-355644-2008), the National Cancer Institute of Canada (019562), and the Human Frontier Science Program (CDA0044/200). L.P. holds a Canada Research Chair in Centrosome Biogenesis and Function. Y.T. was supported by a Postdoctoral Fellowship for Research Abroad from the Japan Society for the Promotion of Science.

Supporting Online Material

www.sciencemag.org/cgi/content/full/science.1181348/DC1
Materials and Methods
Figs. S1 to S14
Tables S1 to S4
References
Supporting Visualization S1

31 August 2009; accepted 22 March 2010
Published online 1 April 2010;
10.1126/science.1181348
Include this information when citing this paper.

Major Galaxy Mergers and the Growth of Supermassive Black Holes in Quasars

Ezequiel Treister,[1*] Priyamvada Natarajan,[2,3,4*] David B. Sanders,[1] C. Megan Urry,[2,3,4] Kevin Schawinski,[3,4] Jeyhan Kartaltepe[1,5]

Despite observed strong correlations between central supermassive black holes (SMBHs) and star formation in galactic nuclei, uncertainties exist in our understanding of their coupling. We present observations of the ratio of heavily obscured to unobscured quasars as a function of cosmic epoch up to $z \cong 3$ and show that a simple physical model describing mergers of massive, gas-rich galaxies matches these observations. In the context of this model, every obscured and unobscured quasar represents two distinct phases that result from a massive galaxy merger event. Much of the mass growth of the SMBH occurs during the heavily obscured phase. These observations provide additional evidence for a causal link between gas-rich galaxy mergers, accretion onto the nuclear SMBH, and coeval star formation.

While unobscured quasars (*1*) have been known for a long time (*2*) and their statistical properties are well studied (*3*), the numbers of the heavily obscured quasar population and its variation with cosmic epoch are still strongly debated. This population has been uncovered with multiwavelength selection techniques that simultaneously exploit x-ray (*4*), optical (*5*), and mid-infrared (mid-IR) (*6*) wavelengths. As a result of the efficiency of these techniques, the sample sizes of obscured quasars are growing substantially. The existence of a large number of heavily obscured quasars at $z \sim 2$ was predicted by early active galactic nuclei (AGN) population synthesis models that successfully explain the generation of the x-ray background (*7*). However, their space density cannot be constrained by these calculations (*8*). What population these obscured sources evolve into or proceed from is poorly understood at present.

The link between ultraluminous infrared galaxies (ULIRGs) and quasars was first suggested by Sanders *et al.* (*9*). There is substantial observational evidence that ULIRGs, at least locally, are the product of the gas-rich merger of two massive [$M \gtrsim 10^{11}\ M_{\odot}$ (solar mass)] galaxies (*10*). The merger process is believed to switch on accretion onto the central black hole as it provides efficient transport of gas to the nucleus (*11*). The gas funneled to the center is expected to fuel the supermassive black hole and induce star formation. The origin of the infrared luminosity of these sources, whether they are powered primarily by star-formation processes (*12*) or the AGN (*9*) activity, is still debated. Here, we present recent measurements of the space density of heavily obscured quasars as a function of redshift and estimate the duration of the obscured stage by comparing models with observations.

Mainly due to the effects of dust and gas obscuration at most wavelengths, finding heavily obscured quasars (*13*) is a challenging task that has prevented the identification of larger samples, in particular, at high redshifts. Measuring their space density is even more difficult, as it requires a good knowledge of the selection function and observational biases. We have compiled observations of obscured quasars selected at various wavelengths using different techniques, described in detail in the supporting online material (SOM), including spectral fitting in x-rays (*14*) and IR selection (*15*–*17*). X-rays, especially at rest-frame energies greater than 10 keV, are not appreciably affected by obscuration. In addition, most of the absorbed energy is later reemitted at IR wavelengths. Thus, these techniques permit an estimate of the number of heavily obscured quasars at $z > 1$. In the local universe, the space density of ULIRGs (*18*), which can be used as an indicator of the total number of quasars, implies that the ratio of heavily obscured to unobscured quasars at $z = 0.1$ is ~1 (Fig. 1).

Both in the local universe and at $z \cong 1$, heavily obscured AGN are bright at mid- and far-IR wavelengths and also potentially in the submillimeter-wavelength range but are optically faint (Fig. 2). At low redshift, the ULIRG is clearly the product of a galaxy merger, whereas at high redshift a merger is suggested, but deeper data are needed to confirm this hypothesis. The rest-frame optical images of six heavily obscured quasar candidates show indications of ongoing major mergers and interactions (Fig. 3).

To interpret these observations and the evolution of these populations, we started with the standard ansatz that the gas-rich major merger of two massive galaxies produces one newly fueled quasar. This triggered quasar is originally obscured by the surrounding gas and dust (*9*), in some cases reaching Compton-thick levels (i.e., where the optical depth for Compton scattering is greater than one). After a time $\Delta t \sim 10^7$ to 10^8 years (*19*), which we estimate independently below, most of the dust and gas are removed from the central region and the quasar becomes unobscured.

To test this simple prescription, the calculated ratio of heavily obscured to unobscured sources from merger rates of massive gas-rich galaxies needs to match the observed ratio of obscured to unobscured quasars. This ratio can be calculated using the merger rate as a function of cosmic time in the context of the hierarchical cold dark matter (LCDM) structure formation paradigm. Using the assumptions described above, we estimated the ratio of obscured to unobscured sources as

$$\frac{N_{\mathrm{obsc}}}{N_{\mathrm{unobsc}}}(z) = \frac{\Delta t \frac{d^2\mathrm{Merger}}{dNdt} N_{\mathrm{gal}}(> M_{\mathrm{star}}(z)) f_{\mathrm{g}}(z)}{N_{\mathrm{unobsc}}(z)} \quad (1)$$

where N_{obsc} is the space density of heavily obscured quasars; $d^2\mathrm{Merger}/dNdt$ is the merger frequency per galaxy per unit time; N_{gal} and N_{unobsc} are the space densities of massive galaxies and unobscured quasars, respectively; and f_{g} is

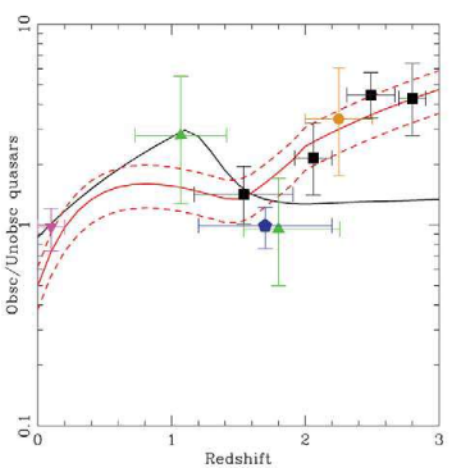

Fig. 1. The ratio of heavily obscured to unobscured quasars as a function of redshift. Measurements of the space density of obscured quasars at high redshift were obtained from x-ray [green triangles (*14*)] and mid-IR imaging [blue pentagon (*16*) and black squares (*17*)] and spectroscopy [brown circle (*15*)] selection techniques. For the $z \cong 0$ measurement, we used the luminosity function of local ULIRGs (*18*), assuming that each ULIRG is either a heavily obscured or an unobscured quasar. The solid black line shows the heavily obscured to unobscured quasar ratio expected from AGN luminosity functions derived from hard x-ray observations (*32*), and the solid red line corresponds to the ratio obtained if every gas-rich major merger of two massive galaxies generates a heavily obscured quasar, which after a time $\Delta t \cong 96$ My becomes unobscured. Dashed lines show the uncertainty in this relation, at the 90% confidence level.

[1]Institute for Astronomy, 2680 Woodlawn Drive, University of Hawaii, Honolulu, HI 96822, USA. [2]Department of Astronomy, Yale University, Post Office Box 208101, New Haven, CT 06520, USA. [3]Department of Physics, Yale University, Post Office Box 208121, New Haven, CT 06520, USA. [4]Yale Center for Astronomy and Astrophysics, Post Office Box 208121, New Haven, CT 06520, USA. [5]National Optical Astronomy Observatory, 950 North Cherry Avenue, Tucson, AZ 85719, USA.

*To whom correspondence should be addressed. E-mail: treister@ifa.hawaii.edu (E.T.); priyamvada.natarajan@yale.edu (P.N.)

the average fraction of gas-rich galaxies. The major merger frequency per galaxy in the LCDM paradigm can be parameterized as a power-law in $(1 + z)$ with a mass-dependent exponent of $\cong 1.5$ (*20*). This form is derived from model parameters constrained by observations. To estimate the space density of galaxies above a threshold stellar mass, we used the median mass measured for ULIRGs found in the Cosmic Evolution Survey (COSMOS). The median mass increases with decreasing redshift, going from $\sim 10^{11}\ M_{\odot}$ at $z \sim 2$ to $10^{11.3}\ M_{\odot}$ at $z = 0.8$ (fig. S1). We then incorporated this limiting mass into the stellar mass function computed by Marchesini *et al.* (*21*) to obtain the space density of massive galaxies as a function of redshift. Rather than directly estimate the gas content of high-redshift galaxies, which is currently observationally impossible at these redshifts, we used the average star-formation rate as a proxy for the evolution of the fraction f_g of gas-rich galaxies. The evolution of the star-formation rate can be approximated as $(1 + z)^2$ up to $z \cong 2$, remaining mostly flat at higher redshifts, on the basis of ultraviolet observations of galaxies up to $z \cong 2.5$ (*22*). Finally, the space density of unobscured quasars, $N_{\mathrm{unobsc}}(z)$, has been measured by both x-ray (*23*, *24*) and optical (*25*) surveys, and consistent results are found with these two methods. These are all the ingredients needed to compute the expected fraction of obscured to unobscured quasars, wherein Δt in Eq. (*1*) can be determined as a free parameter. The redshift dependence of each of these components is shown in fig. S2.

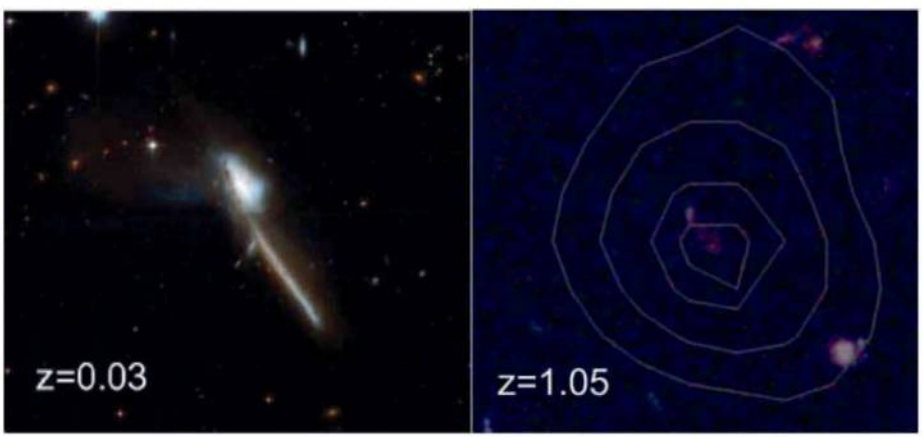

Fig. 2. Optical images of two examples of heavily obscured, luminous AGN observed with the Hubble Space Telescope (HST). Filters used are F435W (B) and F814W (I) and V,I,z in the left and right panels, respectively, and the physical size of both images is ~ 90 kpc by 90 kpc. Contours in the right panel show the Spitzer emission. (Left) The $z = 0.03$ prototype ULIRG Mrk 273; (right) a high-redshift heavily obscured quasar candidate in the GOODS-South field, with no x-ray detection. The former is part of the IRAS 1-Jy sample (*18*) and has clear indications of a major merger, whereas x-ray observations with Suzaku reveal Compton-thick obscuration levels ($N_H > 10^{24}$ cm^{-2}) and intrinsic quasar-like luminosities (*33*). The high-z source was selected as a Compton-thick AGN candidate on the basis of its high mid-IR to optical flux ratio and red optical/near-IR colors. [Left panel credit: NASA, European Space Agency (ESA), the Hubble Heritage Team (STScI/AURA)–ESA/Hubble Collaboration, and A. Evans (University of Virginia, Charlottesville, NRAO, Stony Brook University).

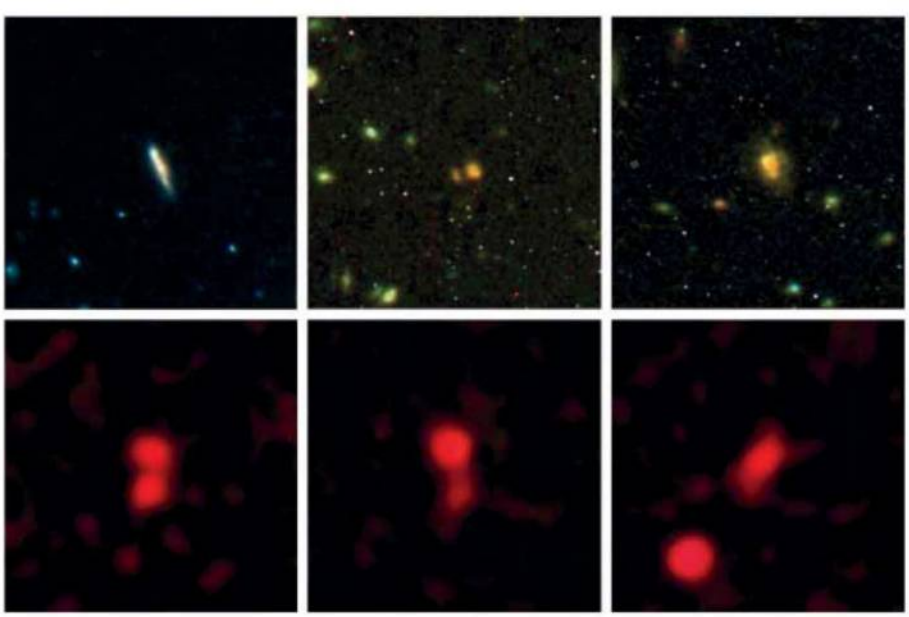

Fig. 3. Rest-frame optical images of six mid-IR–selected heavily obscured quasars at $z \sim 2$ in the Extended Chandra Deep Field-South region. Top images were obtained with the HST-WFC3 (Wide Field Camera 3) camera using the *Y*, *J*, and *H* observations of the Ultra-Deep (left) and GOODS fields. The bottom images were made by combining data in the *R*, *J*, and *K* bands obtained from ground-based telescopes, hence with a spatial resolution about 10 times as large as that of the HST images. All images are 15 arc sec by 15 arc sec.

The estimates from our simple scenario are consistent with the observations (Fig. 1), in particular considering the steep evolution in the relative number of obscured sources from $z = 1.5$ to 3. This rapid increase is not predicted or expected from existing AGN luminosity functions (Fig. 1). That is, extrapolations from the behavior of less-obscured lower-luminosity sources (with observed column densities $< 10^{23}$ cm^{-2}) do not match current observations, in particular at $z > 2$. This suggests the existence of a different channel for the triggering mechanism for quasars, compared to lower-luminosity AGN. The best-fit value of Δt we obtained is 96 ± 23 million years (My; 90% confidence level). This is very similar to the current best estimates of quasar lifetimes in their optically bright, unobscured phases [10 to 100 My (*26*)], indicating that these sources spend roughly half their life in the obscured phase.

Having determined that quasars that are fueled by the merger of massive gas-rich galaxies spend comparable amounts of time in the obscured and unobscured phases, we then estimated the implications for the mass accretion onto the nuclear supermassive black holes during these two stages. Assuming a typical accretion efficiency of $\varepsilon = 0.1$, the mass growth of the supermassive black hole due to accretion is given by

$$\Delta M_{\mathrm{BH}} = 1.6 \times 10^7 \left(\frac{L_{\mathrm{bol}}}{10^{45}\,\mathrm{erg/s}}\right)\left(\frac{T}{10^8\,\mathrm{years}}\right) M_{\odot} \qquad (2)$$

where T is the duration of the entire accretion episode that includes the obscured and unobscured phases. The typical bolometric luminosities of these sources span the range 10^{45} to 10^{47} erg/s [$\sim 10^{12}$ to $10^{14}\ L_{\odot}$ (solar luminosity)], while they have black hole masses of $M_{\mathrm{BH}} \sim 10^8$ to $10^{10}\ M_{\odot}$ (*27*, *28*). Given that the typical duration of the total (both obscured and unobscured) luminous quasar phase is $T \sim 2 \times 10^8$ years, it is possible for a quasar to build most or all of the black hole mass in a single event, which is triggered by a major merger as suggested here.

In spite of copious accretion, due to their high redshifts and strong absorption, this unexpected population of obscured quasars are not key contributors to the extragalactic x-ray background radiation. Their total contribution is estimated to be ~1 to

2% (*8*). However, they constitute a significant fraction of the supermassive black hole mass density in the universe (*29*). Adding the extra obscured accretion reported here, which lasts as long as the optically bright phase, increases our original estimate of the integrated black hole mass density at $z = 0$ by 4%, to $4.5 \times 10^5\ M_\odot\ \mathrm{Mpc}^{-3}$ (*8*). Including this additional contribution, the integrated black hole growth in the obscured quasar phase is $1.3 \times 10^5\ M_\odot\ \mathrm{Mpc}^{-3}$, or ~ 30% of the total black hole mass density at $z = 0$, in agreement with our conclusion that the obscured quasar phase can harbor a large fraction of the black hole growth (*30*). Our results are in agreement with recent estimates (*26*) that suggest an average accretion efficiency of ≤10% even accounting for heavily obscured accretion.

References and Notes

1. By quasar, we refer here to the most luminous members of the AGN family, typically $M_B < -23$, $L_X > 10^{44}$ erg/s or $L_{bol} > 10^{45}$ erg/s.
2. M. Schmidt, *Nature* **197**, 1040 (1963).
3. G. T. Richards *et al.*, *Astrophys. J.* **180** (suppl.), 67 (2009).
4. A. J. Barger *et al.*, *Astron. J.* **126**, 632 (2003).
5. N. L. Zakamska *et al.*, *Astron. J.* **126**, 2125 (2003).
6. A. Martínez-Sansigre *et al.*, *Mon. Not. R. Astron. Soc.* **370**, 1479 (2006).
7. R. Gilli, M. Salvati, G. Hasinger, *Astron. Astrophys.* **366**, 407 (2001).
8. E. Treister, C. M. Urry, S. Virani, *Astrophys. J.* **696**, 110 (2009).
9. D. B. Sanders *et al.*, *Astrophys. J.* **325**, 74 (1988).
10. D. B. Sanders, I. F. Mirabel, *Annu. Rev. Astron. Astrophys.* **34**, 749 (1996).
11. J. E. Barnes, L. E. Hernquist, *Astrophys. J.* **370**, L65 (1991).
12. R. Genzel *et al.*, *Astrophys. J.* **498**, 579 (1998).
13. By heavily obscured, we refer here to sources with neutral hydrogen column densities $N_H > 10^{23}\ \mathrm{cm}^{-2}$, enough to hide most of the soft x-rays to optical quasar signatures.
14. P. Tozzi *et al.*, *Astron. Astrophys.* **451**, 457 (2006).
15. D. M. Alexander *et al.*, *Astrophys. J.* **687**, 835 (2008).
16. F. Fiore *et al.*, *Astrophys. J.* **693**, 447 (2009).
17. E. Treister *et al.*, *Astrophys. J.* **706**, 535 (2009).
18. D.-C. Kim, D. B. Sanders, *Astrophys. J.* **119** (suppl.), 41 (1998).
19. P. F. Hopkins, L. Hernquist, T. J. Cox, D. Keres, *Astrophys. J.* **175** (suppl.), 356 (2008).
20. P. F. Hopkins *et al.*, http://arxiv.org/abs/0906.5357 (2009).
21. D. Marchesini *et al.*, *Astrophys. J.* **701**, 1765 (2009).
22. T. Dahlen *et al.*, *Astrophys. J.* **654**, 172 (2007).
23. G. Hasinger, T. Miyaji, M. Schmidt, *Astron. Astrophys.* **441**, 417 (2005).
24. A. J. Barger *et al.*, *Astron. J.* **129**, 578 (2005).
25. G. T. Richards *et al.*, *Astron. J.* **131**, 2766 (2006).
26. A. Martínez-Sansigre, A. M. Taylor, *Astrophys. J.* **692**, 964 (2009).
27. M. Dietrich, S. Mathur, D. Grupe, S. Komossa, *Astrophys. J.* **696**, 1998 (2009).
28. M. Vestergaard, P. S. Osmer, *Astrophys. J.* **699**, 800 (2009).
29. M. G. Haehnelt, P. Natarajan, M. J. Rees, *Mon. Not. R. Astron. Soc.* **300**, 817 (1998).
30. This integrated value was obtained assuming an accretion efficiency of 0.1 and is in very good agreement with observational results (*31*), even after incorporating this additional accretion.
31. A. Marconi *et al.*, *Mon. Not. R. Astron. Soc.* **351**, 169 (2004).
32. R. Della Ceca *et al.*, *Astron. Astrophys.* **487**, 119 (2008).
33. S. H. Teng *et al.*, *Astrophys. J.* **691**, 261 (2009).

34. Support for the work of E.T. and K.S. was provided by the National Aeronautics and Space Administration (NASA) through Chandra/Einstein Postdoctoral Fellowship award numbers PF8-90055 and PF9-00069, respectively, issued by the Chandra X-ray Observatory Center, which is operated by the Smithsonian Astrophysical Observatory for and on behalf of NASA under contract NAS8-03060. P.N. acknowledges the Radcliffe Institute for Advanced Study where this work was started. C.M.U. acknowledges support from NSF grant AST-0407295.

Supporting Online Material

www.sciencemag.org/cgi/content/full/science.1184246/DC1
SOM Text
Figs. S1 and S2
References

4 November 2009; accepted 17 March 2010
Published online 25 March 2010;
10.1126/science.1184246
Include this information when citing this paper.

Conversion of Sugars to Lactic Acid Derivatives Using Heterogeneous Zeotype Catalysts

Martin Spangsberg Holm,[1,2,3]* Shunmugavel Saravanamurugan,[1,2]* Esben Taarning[2,3]†

Presently, very few compounds of commercial interest are directly accessible from carbohydrates by using nonfermentive approaches. We describe here a catalytic process for the direct formation of methyl lactate from common sugars. Lewis acidic zeotypes, such as Sn-Beta, catalyze the conversion of mono- and disaccharides that are dissolved in methanol to methyl lactate at 160°C. With sucrose as the substrate, methyl lactate yield reaches 68%, and the heterogeneous catalyst can be easily recovered by filtration and reused multiple times after calcination without any substantial change in the product selectivity.

Carbohydrates represent the largest fraction of biomass, and various strategies for their efficient use as a commercial chemical feedstock are being established in the interest of supplementing, and ultimately replacing, petroleum (*1*–*4*). The thermal instability of carbohydrates is a major obstacle in this regard, and biochemical processes have proven to be more applicable than catalytic ones, in part because of their ability to operate at low temperatures. On the other hand, catalysis often presents improved process design options, resulting in higher productivity and reduced costs related to product work-up. Indeed, catalysis has proven to be scalable and able to supply numerous low-cost products from petroleum.

In contrast to the case for biochemical processes, relatively few products are directly obtainable from carbohydrates by using catalysis. Gluconic acid and sorbitol can be obtained from glucose by oxidation and hydrogenation, respectively, and acidic catalysts are currently being examined for the direct production of 5-hydroxymethylfurfural (HMF) (*5*–*7*). However, currently the production of fuels and value-added compounds from carbohydrates is dominated by fermentative processes (*8*). An important example is the fermentation of glucose to lactic acid, which is used for the production of biodegradable plastics (*9*, *10*) and solvents (*11*, *12*). Lactic acid has also been investigated as a precursor to the production of a wide range of useful compounds through catalytic transformation (*13*, *14*). However, the future role of lactic acid will largely depend on its production costs. Because the fermentation of glucose to lactic acid

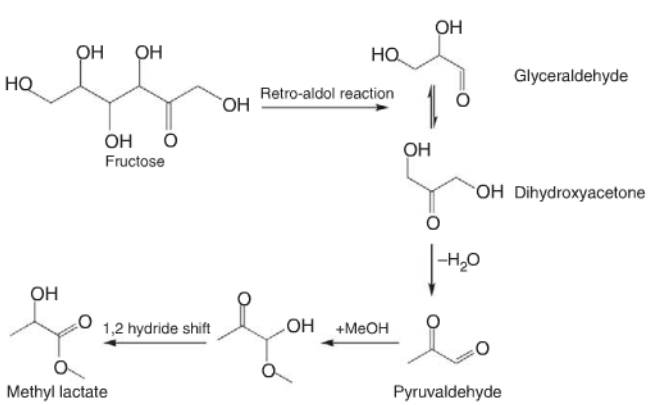

Fig. 1. Proposed reaction pathway for the conversion of fructose to methyl lactate. The reaction formally comprises a retro aldol fragmentation of fructose and isomerization-esterification of the trioses.

[1]Centre for Catalysis and Sustainable Chemistry, Department of Chemistry, Technical University of Denmark, Anker Engelundsvej 1, 2800 Kongens Lyngby, Denmark. [2]Center for Sustainable and Green Chemistry, Department of Chemistry, Technical University of Denmark, Anker Engelundsvej 1, 2800 Kongens Lyngby, Denmark. [3]Haldor Topsøe A/S, Nymøllevej 55, 2800 Kongens Lyngby, Denmark.

*These authors contributed equally to this work.
†To whom correspondence should be addressed. E-mail: esta@topsoe.dk

involves the coproduction of large amounts of salt waste, a less expensive route would be an important step toward a biomass-based chemical industry using lactic acid more widely as a feedstock. Here we show that sucrose, glucose, and fructose dissolved in methanol can be converted directly into racemic methyl lactate in yields up to 68% in a process resembling the alkaline degradation of sugars. Methyl lactate can be purified by distillation, and its one-pot formation offers an advantage over the fermentative route, wherein the esterification of lactic acid to methyl lactate is often necessary.

We recently reported that Lewis acidic zeolites and zeotypes efficiently catalyze the conversion, in methanol, of the two trioses dihydroxyacetone and glyceraldehyde to methyl lactate at moderate temperatures (*15*, *16*). Here we report that while investigating the properties of the Sn-Beta zeolite for fructose transformation, we discovered that, at elevated temperatures, fructose is transformed to methyl lactate in yields of up to 44%. We assume that this reaction proceeds via a retro aldol reaction of fructose forming two trioses (Fig. 1). These trioses are readily converted to the thermodynamically very stable methyl lactate through sequential dehydration and methanol addition, followed by a 1,2-hydride shift as reported previously (*15*–*17*). Indeed, at intermediate reaction times, small amounts of unconverted triose sugars were observed by high-performance liquid chromatography (HPLC), supporting the existence of this reaction pathway.

A retro aldol reaction is favored at high temperatures, and fructose and glucose are known to undergo fragmentation in supercritical water to form C_2 to C_4 carbohydrate products (*18*, *19*). In the presence of aqueous alkali hydroxides, the transformation of the monosaccharides to lactate salts occurs at milder conditions (100° to 260°C) (*20*–*22*). However, to obtain high lactate yields, a stoichiometric amount of base is required because of the acid-base reaction between lactic acid and hydroxide. For the Sn-Beta–catalyzed reaction in methanol, we observed methyl lactate formation from fructose at temperatures as low as 140°C. This observation suggests that the retro aldol reaction is the rate-determining step in the overall transformation of fructose, because methyl lactate is readily formed from trioses at lower temperatures (80°C) (*15*). Glucose and sucrose are less expensive and much more abundant sugars than fructose, and therefore these substrates were also investigated for the production of methyl lactate.

We have synthesized highly crystalline Beta zeolites and zeotypes with the BEA framework topology that differ in the type of metal that is incorporated into the framework according to established procedures (*23*). They can be divided into Lewis acidic (Ti-, Sn-, and Zr-Beta), Brønsted acidic (H-Al-Beta), and nonacidic (Si-Beta) classes. These materials contain well-defined metal single sites that were found to have catalytic activity in various reactions (*24*–*26*). Zeolite Beta has a three-dimensional porous system with 12-ring pores that are sufficiently large to accommodate acyclic monosaccharides (*27*). We tested these materials for the conversion of sugars at 160°C in an autoclave setup (Table 1).

In agreement with previous reports (*28*), we found that the Brønsted acidic zeolite H-Al-Beta catalyzes the dehydration of the sugars, leading to HMF derivatives and methyl levulinate from fructose and predominantly methyl-D-pyranoside from glucose and sucrose (table S1). The Lewis acidic zeolites, on the other hand, were found to induce high selectivities toward methyl lactate. Sn-Beta is the most selective, giving a methyl lactate yield of 64 to 68%, which was calculated on a carbon basis when using sucrose as the substrate. Of the three Lewis acidic zeolites, Sn-Beta has the strongest Lewis acidic sites, which could explain its higher selectivity (*15*, *29*). However, both Zr-Beta and Ti-Beta are capable of producing methyl lactate in moderate yields (31 to 44%). The nonacidic Si-Beta did not improve the yield of methyl lactate over that of the background reaction, indicating that the catalytic ability is related to the Lewis acidity of

Table 1. Conversion of sugars using different zeolite and zeotype materials. Substrate (225 mg), catalyst (160 mg), naphtalene (120 mg), and methanol (8.0 g) were stirred in an autoclave at 160°C for 20 hours. Yields are calculated on a carbon basis and given as mean values. The key experiments converting sucrose using Ti-, Zr-, and Sn-Beta were repeated five times (see table S5 for statistical information). Conversion is calculated based on the amount of unconverted hexoses. Si/M, Si/metal ratio in the synthesis gel.

Catalyst	Si/M	Substrate	Conversion	Yield of methyl lactate
H-(Al)-Beta	125	Glucose	97%	0%
H-(Al)-Beta	125	Fructose	>99%	1%
H-(Al)-Beta	125	Sucrose	99%	0%
Ti-Beta	125	Glucose	99%	31%
Ti-Beta	125	Fructose	>99%	36%
Ti-Beta	125	Sucrose	98%	44%
Zr-Beta	125	Glucose	99%	33%
Zr-Beta	125	Fructose	>99%	33%
Zr-Beta	125	Sucrose	99%	40%
Sn-Beta	125	Glucose	>99%	43%
Sn-Beta	125	Fructose	>99%	44%
Sn-Beta	125	Sucrose	>99%	64%
Si-Beta	—	Glucose	61%	5%
Si-Beta	—	Fructose	79%	9%
Si-Beta	—	Sucrose	63%	6%
No catalyst	—	Glucose	53%	5%
No catalyst	—	Fructose	67%	8%
No catalyst	—	Sucrose	54%	6%
$SnCl_4 \cdot 5H_2O$*	—	Sucrose	99%	31%
SnO_2†	—	Sucrose	81%	4%

*Equivalent molar amount of Sn as for 160-mg Sn-Beta. †160 mg of SnO_2 used.

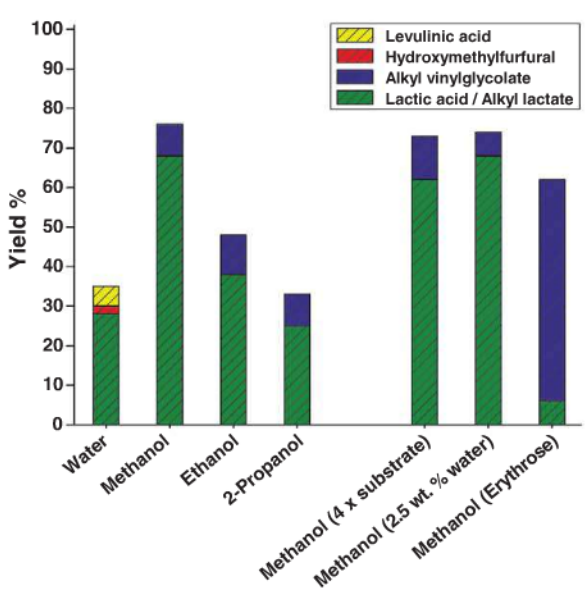

Fig. 2. Comparison of different solvents and reaction conditions for the conversion of sucrose using Sn-Beta (Si:Sn 165). Sucrose (225 mg), Sn-Beta (160 mg), and solvent (8.0 g) were stirred at 160°C for 20 hours.

the metals incorporated into the zeolite structure. Homogeneous $SnCl_4$ as well as nanocrystalline SnO_2, were also tested in the reaction. SnO_2 is inactive, whereas $SnCl_4$ shows moderate selectivity toward methyl lactate.

Glucose conversion proceeds in yields of methyl lactate comparable to those from fructose. We found that the Sn-Beta catalyst is capable of catalyzing Lobry-de Bruyn-van Ekenstein isomerization of glucose to fructose at low temperatures (100°C), which explains the similar yields obtained when using either of the hexoses. In addition, we observed that the disaccharide sucrose gives a substantially higher yield of methyl lactate as compared with fructose and glucose. This trend has also been observed for the alkaline degradation of fructose, glucose, and sucrose in water (*20*, *21*). This result is surprising, because the overall reaction pathway from sucrose to methyl lactate is thought to involve the intermediary formation of glucose and methyl fructoside by methanolysis, from which fructose is then formed via isomerization and hydrolysis, respectively (fig. S1).

Methyl lactate is not the only product formed during the reaction. The largest volatile coproduct is methyl vinylglycolate (methyl 2-hydroxy-3-butenoate), which is formed in yields ranging from 3 to 11% in all cases when using the Lewis acidic catalysts. Retro aldol reaction of glucose will produce erythrose (C_4 sugar) and glycolaldehyde (C_2). Methyl vinylglycolate formation could proceed by a reaction pathway analogous to that forming methyl lactate from trioses (fig. S1). To support this hypothesis, we heated D-erythrose to 160°C in methanol with Sn-Beta as the catalyst, and we observed methyl vinylglycolate formation in a considerably higher yield (56%) than that of methyl lactate (6%). Thus, tetroses appear to be precursors for methyl vinylglycolate (Fig. 2). Other products that were formed in small amounts from the mono- and disaccharides when using Sn-Beta are glycolaldehyde dimethylacetal (<1%), formaldehyde dimethylacetal (<1%), and methyl glycolate (<0.5%). Furthermore, we observed trace amounts of methyl 2-hydroxy butyrate and small amounts of methoxy derivatives of furfural and HMF (table S1 and fig. S2). Many of these products are similar to the saccharinic acids that are formed in the alkaline degradation of sugars, where major products are lactic acid, glycolic acid, 2,4-dihydroxybutanoic acid, as well as higher C_6 acids (*21*). In the case of Sn-Beta, we observed, using HPLC analysis, the presence of a noticeable amount of highly polar products, which could be methyl esters of the higher C_6 saccharinic acids. The combined yields of methyl lactate (68%) and methyl vinylglycolate (8%) exceed 75% for sucrose on a carbon basis when Sn-Beta (Si:Sn 165) is used as the catalyst. When the amount of sucrose and glucose is increased by a factor of four [>10 weight percent (wt %) in methanol], similar combined yields of methyl lactate and methyl vinylglycolate are obtained, and full conversion is still reached within 20 hours (Fig. 2). In this experiment, the average turnover number per Sn atom is >400 for the production of methyl lactate based on the assumed participation of all Sn atoms in the catalyst. A further increase in sucrose concentration to 20 wt % causes a drop in the yields of methyl lactate (47%) and methyl vinylglycolate (12%) in an experiment using twice the amount of Sn-Beta.

Changing the solvent from methanol to higher alcohols or water leads to the formation of the corresponding alkyl lactates and free lactic acid, respectively (Fig. 2 and see table S2 for data for glucose and fructose). Low amounts (<30%) of lactic acid are formed in water together with HMF (1 to 2%) and levulinic acid (~5%). Additionally, temperature-programmed oxidation showed that more carbon is deposited on the catalyst when water is used as the solvent (7.0 wt % of carbon per g catalyst) in place of methanol (1.3 wt %) (table S3). The change in the product composition when using water as the solvent can be explained by the auto-catalytic effect of the organic acids formed. Lactic acid and levulinic acid, being Brønsted acids, will shift the course of the reaction toward that typically seen with Brønsted acid catalysts (HMF, levulinic acid); the result is lower yields of the α-hydroxycarboxylic acid products formed in the pathway catalyzed by Lewis acids. Because small amounts of water are formed during the reaction, we examined the effect of water in methanol. Using a solvent mixture consisting of 2.5 wt % water in methanol, we obtained yields of methyl lactate similar to those obtained in pure methanol (Fig. 2). Changing the solvent to higher alcohols leads to a decrease in alkyl lactate selectivity. In ethanol, 39% of ethyl lactate is formed using sucrose as the substrate and Sn-Beta as the catalyst, whereas 25% of isopropyl lactate is formed in *i*-propyl alcohol.

Long-term stability is a very important characteristic for a heterogeneous catalyst. We therefore explored the prospects for reusing Sn-, Zr-, and Ti-Beta (Fig. 3). Each catalyst was used six times for the conversion of sucrose after calcining between each run to burn away deposited carbon. The catalysts were found to remain active with an almost unchanged selectivity even after the sixth reuse (fig. S5). After the fifth run, the zeotypes were calcined and analyzed by N_2-sorption and x-ray powder diffraction (XRPD) (fig. S6 and table S3). Analysis shows that the BEA structure is preserved and the micropore volumes for Ti-Beta and Zr-Beta remain constant; a very small volume decrease from 0.201 ml/g to 0.197 ml/g was observed for Sn-Beta. These data after >100 hours of catalyst use thus show promising stability characteristics. Further examination of the catalyst stability using a fixed bed reactor shows that Sn-Beta deactivates gradually as a function of time on stream (fig. S7). This indicates that the ability to regenerate the activity by calcination is an important feature of the catalyst. The reusability of Lewis acidic zeolites and zeotypes has also been reported in other reactions (*30*, *31*).

In contrast to the alkaline degradation, acid-catalyzed conversion of mono- and disaccharides does not consume a stoichiometric amount of base. However, the reaction pathway in the acid-catalyzed conversion is highly sensitive to the type of acid used. Whereas Brønsted acids catalyze monosaccharide dehydration reactions, leading primarily to HMF and its decomposition products, Lewis acidic zeotype catalysts lead to retro aldol reaction of the monosaccharides and subsequent transformation to α-hydroxycarboxylic acid derivatives. To achieve a high selectivity in the Lewis acid–catalyzed pathway, it is important to diminish the catalytic effect of Brønsted acids, for example, by using a solvent such as methanol in which esters, rather than free carboxylic acids, are formed.

Unlike the primary product of the Brønsted acid–catalyzed reaction, HMF, a market already exists for lactic acid and its ester derivatives. These compounds are now accessible from sucrose, glucose, and fructose, using non-noble metal–containing catalysts. However, the catalytic process results in a racemic product mixture. This plays no role for solvent or feedstock end-use, but enantiomeric purity is an important parameter in the production of biodegradable plastics.

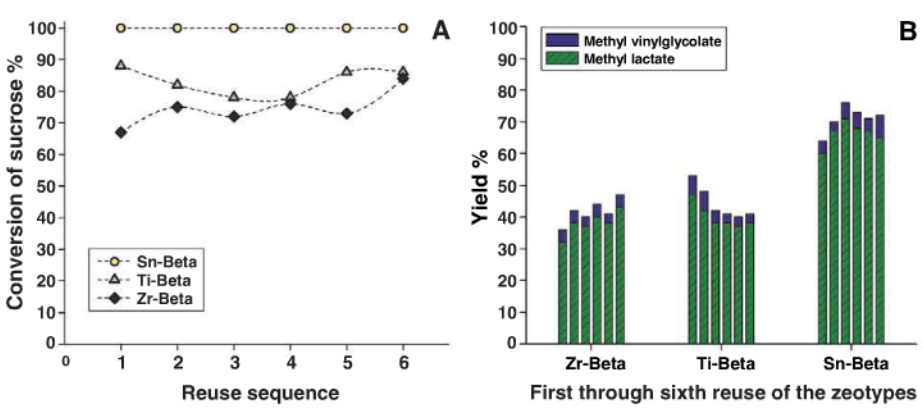

Fig. 3. Reuse of Sn-, Zr-, and Ti-Beta (Si/metal: 125) for the conversion of sucrose in methanol, with calcination of the zeotypes between each experiment. (**A**) Conversion of sucrose and (**B**) yields of methyl lactate and methyl vinylglycolate in the reuse experiments.

References and Notes

1. G. W. Huber, S. Iborra, A. Corma, *Chem. Rev.* **106**, 4044 (2006).
2. H. Danner, R. Braun, *Chem. Soc. Rev.* **28**, 395 (1999).
3. A. Corma, S. Iborra, A. Velty, *Chem. Rev.* **107**, 2411 (2007).
4. C. H. Christensen, J. Rass-Hansen, C. C. Marsden, E. Taarning, K. Egeblad, *Chem. Sus. Chem.* **1**, 283 (2008).
5. H. Zhao, J. E. Holladay, H. Brown, Z. C. Zhang, *Science* **316**, 1597 (2007).
6. Y. Román-Leshkov, J. N. Chheda, J. A. Dumesic, *Science* **312**, 1933 (2006).
7. M. Bicker, J. Hirth, H. Vogel, *Green Chem.* **5**, 280 (2003).
8. M. E. Himmel *et al.*, *Science* **315**, 804 (2007).
9. J. Lunt, *Polym. Degrad. Stabil.* **59**, 145 (1998).
10. E. T. H. Vink, K. R. Ràbago, D. A. Glassner, P. R. Gruber, *Polym. Degrad. Stabil.* **80**, 403 (2003).
11. K. L. Wasewar, A. A. Yawalkar, J. A. Moulijn, V. G. Pangarkar, *Ind. Eng. Chem. Res.* **43**, 5969 (2004).
12. R. Datta, M. Henry, *J. Chem. Technol. Biotechnol.* **81**, 1119 (2006).
13. Y. Fan, C. Zhou, X. Zhu, *Catal. Rev.* **51**, 293 (2009).
14. J. C. Serrano-Ruiz, J. A. Dumesic, *Chem. Sus. Chem* **2**, 581 (2009).
15. E. Taarning *et al.*, *Chem. Sus. Chem* **2**, 625 (2009).
16. R. M. West *et al.*, *J. Catal.* **269**, 122 (2010).
17. Y. Hayashi, Y. Sasaki, *Chem. Commun. (Camb.)* (21): 2716 (2005).
18. T. M. Aida *et al.*, *J. Supercrit. Fluid.* **42**, 110 (2007).
19. M. Sasaki, K. Goto, K. Tajima, T. Adschiri, K. Arai, *Green Chem.* **4**, 285 (2002).
20. R. Montgomery, *Ind. Eng. Chem.* **45**, 1144 (1953).
21. B. Y. Yang, R. Montgomery, *Carbohydr. Res.* **280**, 47 (1996).
22. G. Braun, U.S. patent 2,024,565 (1935).
23. Materials and methods are available as supporting material on *Science* Online.
24. J. M. Thomas, R. Raja, D. W. Lewis, *Angew. Chem. Int. Ed.* **44**, 6456 (2005).
25. M. Boronat, A. Corma, M. Renz, P. M. Viruela, *Chemistry* **12**, 7067 (2006).
26. A. Corma, *J. Catal.* **216**, 298 (2003).
27. J. Jow, G. L. Rorrer, M. C. Hawley, D. T. A. Lamport, *Biomass* **14**, 185 (1987).
28. P. Rivalier, J. Duhamet, C. Moreau, R. Durand, *Catal. Today* **24**, 165 (1995).
29. M. Renz *et al.*, *Chemistry* **8**, 4708 (2002).
30. J. C. van der Waal, E. J. Creyghton, P. J. Kunkeler, K. Tan, H. van Bekkum, *Top. Catal.* **4**, 261 (1997).
31. A. Corma, M. E. Domine, L. Nemeth, S. Valencia, *J. Am. Chem. Soc.* **124**, 3194 (2002).

32. The Catalysis for Sustainable Energy initiative is funded by the Danish Ministry of Science, Technology and Innovation. The Center for Sustainable and Green Chemistry is sponsored by the Danish National Research Foundation. Haldor Topsøe A/S holds patent application EP 090137829 related to the work described in this report. The authors thank C. Hviid Christensen (Haldor Topsøe A/S) for helpful advice.

Supporting Online Material

www.sciencemag.org/cgi/content/full/328/5978/602/DC1
Materials and Methods
Figs. S1 to S8
Tables S1 to S6
References

29 October 2009; accepted 17 March 2010
10.1126/science.1183990

Recent Hotspot Volcanism on Venus from VIRTIS Emissivity Data

Suzanne E. Smrekar,[1]* Ellen R. Stofan,[2] Nils Mueller,[3,6] Allan Treiman,[4] Linda Elkins-Tanton,[5] Joern Helbert,[6] Giuseppe Piccioni,[7] Pierre Drossart[8]

The questions of whether Venus is geologically active and how the planet has resurfaced over the past billion years have major implications for interior dynamics and climate change. Nine "hotspots"—areas analogous to Hawaii, with volcanism, broad topographic rises, and large positive gravity anomalies suggesting mantle plumes at depth—have been identified as possibly active. This study used variations in the thermal emissivity of the surface observed by the Visible and Infrared Thermal Imaging Spectrometer on the European Space Agency's Venus Express spacecraft to identify compositional differences in lava flows at three hotspots. The anomalies are interpreted as a lack of surface weathering. We estimate the flows to be younger than 2.5 million years and probably much younger, about 250,000 years or less, indicating that Venus is actively resurfacing.

Venus' resurfacing record holds important clues to its geological evolution. Venus and Earth are similar in size and in internal heat production, yet Venus is in a stagnant lid convection regime whereas Earth has vigorous plate tectonics. Venus' sparse and largely unmodified crater population has spawned a debate over whether it was resurfaced catastrophically (*1*) or gradually (*2*). These two end members have very different dynamic implications. Catastrophic resurfacing could have been caused by episodic mantle overturn (*3*) or melting in a hot mantle insulated by a stagnant lid (*4*). Gradual resurfacing is consistent with more Earth-like volcanic and interior processes (*5*). The rate and style of resurfacing have important implications for both interior evolution and climate change driven by volatile release from volcanic outgassing.

The Visible and Infrared Thermal Imaging Spectrometer (VIRTIS) on the European Space Agency's Venus Express spacecraft provided a map of thermal emission for much of the southern hemisphere of Venus' surface in the atmospheric window at 1.02 μm (*6*). Surface emissivities in the 1.02-μm band are retrieved from surface brightness by correcting for effects of instrumental stray light, viewing geometry, cloud opacity, and elevation (*7*, *8*). More accurate topographic data (*9*) allowed us to make significantly better maps of surface emissivity (*10*). Absolute surface emissivities are model-dependent (*11*) but are calculated from variations in the emitted fluxes that are up to 12% greater than the average value. These emissivity variations represent differences in material

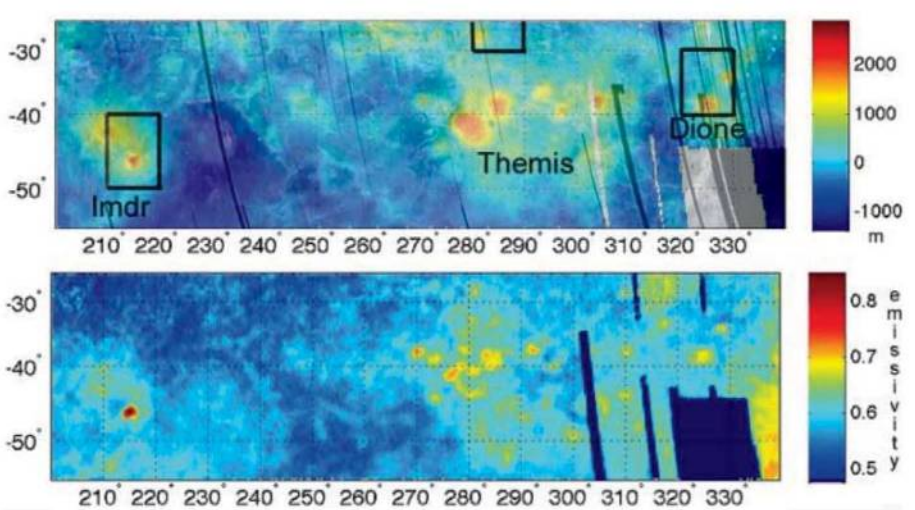

Fig. 1. (**Top**) Magellan synthetic aperture radar (SAR) image, left looking, overlain on topography. (**Bottom**) Surface emissivity derived from the VIRTIS spectrometer. Regio names are located below the topographic rises. Boxes indicate example sites shown in Fig. 2.

[1]Jet Propulsion Laboratory, Mail Stop 183-501, 4800 Oak Grove Drive, Pasadena, CA 91109, USA. [2]Proxemy Research, 20528 Farcroft Lane, Laytonsville, MD 20882, USA. [3]Institute for Planetology, Westfälische Wilhelms-Universität Münster, Wilhelm-Klemm-Strasse 10, 48149 Münster, Germany. [4]Lunar and Planetary Institute, 3600 Bay Area Boulevard, Houston, TX 77058, USA. [5]Massachusetts Institute of Technology, Earth, Atmospheric, and Planetary Sciences, Building 54-824, 77 Massachusetts Avenue, Cambridge, MA 02139, USA. [6]Institute of Planetary Research, German Aerospace Center, Rutherfordstrasse 2, D-12489 Berlin, Germany. [7]Istituto Nazionale di Astrofisica–Istituto di Astrofisica Spaziale e Fisica Cosmica (INAF-IASF), Via del Fosso del Cavaliere 100, 00133 Rome, Italy. [8]Laboratoire d'Etudes Spatiales et d'Instrumentation en Astrophysique (LESIA), Observatoire de Paris, CNRS, UPMC, Université Paris-Diderot, 5 Place Jules Janssen, 92195 Meudon, France.

*To whom correspondence should be addressed. E-mail: ssmrekar@jpl.nasa.gov

compositions in the top few micrometers of depth due to either primary compositional variations or alteration by surface weathering. VIRTIS data are averaged over 1.5 Earth years, so volcanic eruptions or flows are not likely as causes of anomalously high emissions (*7*, *8*). In general, higher emissivities imply greater abundances of ferrous silicates (*12*), although more laboratory work under Venus conditions is needed to produce a spectral library (*13*, *14*).

Here, we focus on areas of anomalously high emissivity (*7*) associated with coronae (*15*) and volcanoes at "hotspots" (Fig. 1). Hotspots on Venus were recognized, in analogy with terrestrial hotspots such as Hawaii, by their distinctive topographic rises, major volcanic centers, and gravity signatures (*16*–*18*). Of the nine recognized hotspots, only Imdr, Themis, and Dione Regiones were imaged by VIRTIS (Fig. 1). These three rises have heights that range from 0.5 to 1.6 km above the surrounding plains and rise diameters of 1400 to 2700 km. Venus' hotspots are among the most likely sites for current volcanic activity. Their thin elastic lithospheres and great apparent depths of compensation, as revealed by Magellan gravity and topography data analysis, suggest the high heat flows and broad topographic uplift of active mantle plumes (*18*–*22*).

At these hotspots, the flows that are the youngest stratigraphically (*23*–*25*) have anomalously high emissivities. All flows have digitate or sheet morphologies typical of basaltic flows. The region with the highest emissivity anomaly is at Idunn Mons, Imdr Regio's single large volcano (Fig. 2A). Two of the three large volcanoes at Dione Regio, Innini and Hathor Montes, have anomalously high emissivities (Fig. 2B). Ushas Mons does not appear to have high emissivity, although VIRTIS data are sparse in the area. However, the Ushas region has a thicker elastic lithosphere than do Innini and Hathor Montes (*22*), which is consistent with Ushas not being volcanically active, because thicker lithosphere implies lower heat flow. Themis Regio contains 13 coronae and several volcanoes (Fig. 1) with diameters greater than 100 km (the spatial resolution of the VIRTIS data), 7 of which have flows with high emissivity (*25*). Mielikki Mons at Themis Regio is representative of these flows (Fig. 2C).

Analysis of the concentration and degradation of the dark halos produced by impact craters offers some insight into relatively old and young regions. Craters with parabolic ejecta deposits, which form when fine-grained material from impacts is carried downstream by winds, are believed to be the youngest 10% of the crater population (*26*). Over time, fine-grained parabolas are removed by either weathering processes (chemical and/or aeolian) or modification by volcanism and tectonism. Regions with both a relatively low parabola crater density and larger than average numbers of geologically modified craters have been interpreted as being relatively young (*27*). Those with low parabola crater density and high total crater density are interpreted to be relatively old, with parabolas removed primarily via weathering processes. One of the high-emissivity flows in Themis Regio appears to superpose the dark parabola from an impact crater, providing further evidence for the relative youthfulness of the flows (*26*).

Although the scale of regions (5.3×10^6 km^2) assessed by (*27*) is much larger than the high-emissivity flows we examine here, their analysis is broadly consistent with the relative youth of these hotspots. Both Dione and Themis Regiones occur adjacent to one of only two regions identified as relatively young. The other area is largely outside of VIRTIS coverage. Imdr Regio is equidistant between relatively young and old areas, in an area that is of apparently average age. However, the areal extent of high-emissivity flows at Imdr Regio is smaller than at Dione Regio and much smaller than at Themis Regio (Fig. 1). We thus find some general correlation between the high-emissivity anomalies at volcanic flows and relatively young surfaces, based on dark halo degradation.

Surface observations, theoretical calculations, and laboratory experiments are consistent with weathering in the harsh Venus environment (460°C, 90 bars) producing a decrease in emissivity. Analysis of Venera 9 and 10 visible and near-infrared spectra using high-temperature

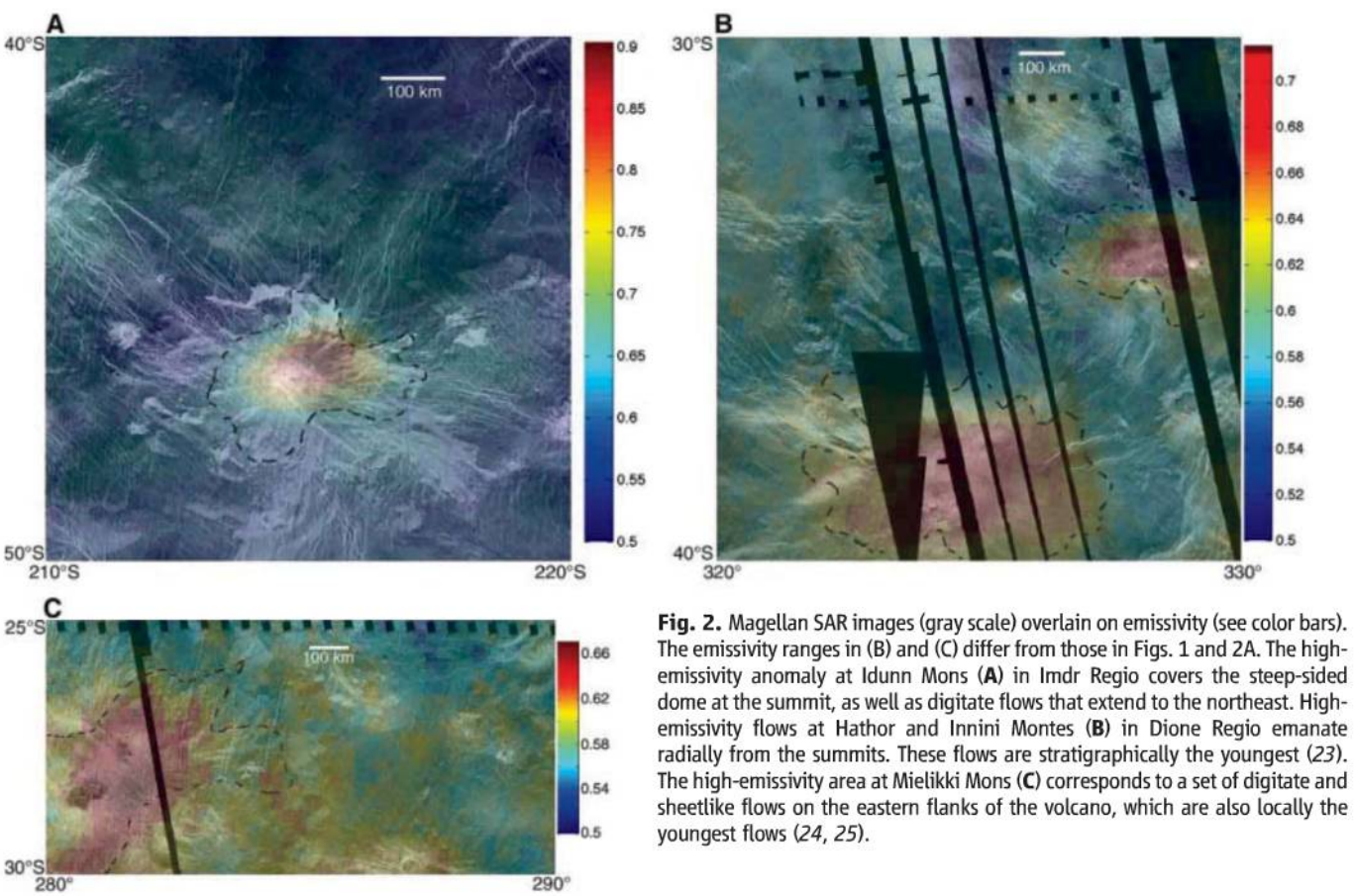

Fig. 2. Magellan SAR images (gray scale) overlain on emissivity (see color bars). The emissivity ranges in (B) and (C) differ from those in Figs. 1 and 2A. The high-emissivity anomaly at Idunn Mons (**A**) in Imdr Regio covers the steep-sided dome at the summit, as well as digitate flows that extend to the northeast. High-emissivity flows at Hathor and Innini Montes (**B**) in Dione Regio emanate radially from the summits. These flows are stratigraphically the youngest (*23*). The high-emissivity area at Mielikki Mons (**C**) corresponds to a set of digitate and sheetlike flows on the eastern flanks of the volcano, which are also locally the youngest flows (*24*, *25*).

reflectance measurements indicates the presence of ferric oxide hematite (*28*). Experiments with Venus-analog atmospheres and mineral mixtures indicate that incorporation of CO_2 or SO_2 into secondary minerals such as calcite, quartz dolomite, or anhydrite forms a crust on primary mineral grains or glasses (*29*, *30*). An iron oxide, probably hematite, was concentrated toward the top of the secondary mineral crust on a time scale of days (*30*). These secondary minerals have low emissivity at 1 μm and could mask underlying high-emissivity minerals. Because these minerals are transparent to radiation, a substantial crust micrometers thick may be required to lower emissivity. Thermodynamic calculations also predict that iron-bearing silicates, pyroxenes, and pyrite decompose in reaction with CO_2 to hematite, quartz, and other phases (*31*–*34*), all of which have lower emissivities than the initial minerals (*35*). Even if the primary compositions of these flows had unusually high concentrations of Ti, Fe, or Mg, as is found at some terrestrial hotspots (*36*, *37*), our knowledge of weathering on Venus indicates that they should weather in the same manner as more typical basalt compositions.

It is highly unlikely that the heat of active volcanism is producing the anomalies interpreted as high emissivity, because the anomalies seem to be constant with time and equivalent to less than 20 K of temperature difference (*7*, *8*). However, if any of the three areas are active, Idunn Mons in Imdr Regio is the best candidate. The emissivity anomaly at Idunn is roughly a factor of 2 greater than at the other hotspots. Although modeling of volcanic plumes shows that transporting volcanic gases to the top of the clouds is difficult (*38*), Idunn is at roughly the same latitude and upwind from the bright spot recently observed on Venus (*39*). Under ideal conditions, a volcanic plume could introduce sufficient volatiles into the atmosphere to cause brightening of the cloud-top albedo downwind of the volcano.

All plausible interpretations of the high-emissivity anomalies point to relatively recent volcanism. Our understanding of the composition of the surface, expected surface weathering products, and the emissivities of the key minerals suggest that the nominal emissivity observed over most of the southern hemisphere represents a weathered surface. If the high-emissivity anomalies are relatively unweathered basalt with an emissivity of 0.85 to 0.9 (*36*, *40*), then a 12% decrease in flux implies a weathered background emissivity of as low as 0.5 to 0.6. This value is most consistent with a fine-grained hematite.

Limited information is available about weathering rates on Venus. Results from laboratory experiments on basalts under Venus conditions predict that reaction fronts could advance several micrometers in the time frame of a year (*29*, *30*, *33*, *34*, *41*). Clearly, the experiments to date point to very rapid weathering. However, there are numerous uncertainties about the specific minerals involved, the atmospheric composition, the oxygen fugacity at the surface, and how thick a layer is needed to change the surface emissivity. Given these uncertainties, weathering experiments support the hypothesis that the flows are relatively recent but do not provide a clear age constraint.

Understanding the style and rate of resurfacing on Venus has important implications for both climate and interior dynamics. If the preexisting surface included major impact basins such as Orientale on the Moon, a minimum thickness of 1 km of volcanic flow is needed to bury the rims. Assuming a resurfacing time of 10 and 750 million years gives emplacement rates of 46 and 0.6 km^3/year, respectively (*42*). For comparison, terrestrial rates of emplacement for the mid-ocean ridge rates are ~3 km^3/year and the Columbia River Basalts are estimated at 0.16 km^3/year (*43*). The most rapid estimates for Venus are not relevant to recent flows because catastrophic resurfacing had to have ceased at least several hundred million years ago. There is indirect evidence for the equivalent of a global 1-km-thick layer of volcanism in the past 50 to 100 million years based on the amount of outgassed volatiles needed to support the current SO_2 levels in the clouds (*44*). This gives a resurfacing rate of 4.6 to 9.2 km^3/year. The equilibrium resurfacing models predict a steady resurfacing rate of 0.9 to 1 km^3/year. (*2*). Monte Carlo simulations that include a global resurfacing event suggest that only ~5% of the surface has been flooded since the resurfacing event, giving current rates as low as 0.01 km^3/year (*45*).

The cumulative area of the flows with high emissivity at Dione, Imdr, and Themis Regiones is approximately 235,000 km^2. We assume a plausible thickness range of 10 to 100 m for the flows, based on both estimates of flow thicknesses on Venus (*46*) and studies indicating that typical terrestrial basaltic flows are 20 m or less (*47*). This gives a volume of 2350 to 23,500 km^3. We take the upper bound on the age (*48*) of the flows to be 2.5 million years [catastrophic resurfacing in the past with little volcanism today (0.01 km^3/year) with the largest volume] and the lower bound to be 250,000 years (outgassing rate 10 km^3/year and the smallest volume). Assuming the equilibrium resurfacing rate of 1 km^3/year gives ages of 2500 to 25,000 years.

Several factors support the lower range of ages. Other, non-hotspot flows with high emissivity have been identified in VIRTIS data (*7*, *8*). Overall VIRTIS data cover only a third of hotspots and less than half of the regions estimated to be relatively young (*27*). Thus it is highly likely that the volume of unweathered flows is larger than our study areas by as much as an order of magnitude. The outgassing resurfacing rate (*44*) is model-dependent but does provide evidence for substantial, relatively recent volcanism. The identification of recent flows demonstrates that the scale of resurfacing events is small, on the order of 50 to several hundred kilometers. This scale is consistent with an idealized equilibrium resurfacing model and inconsistent with an idealized catastrophic resurfacing model, implying that the larger age estimates from catastrophic resurfacing rates are less likely (*2*). Finally, the limited laboratory data on weathering rates suggest even younger ages than those obtained from resurfacing models.

Venus appears to be a geologically active planet, with hotspots as important centers of heat loss, volcanism, and atmospheric H_2O and SO_2. The upper bound on the average age of these unweathered flows is at most 2.5 million years but is more likely to be hundreds to thousands or tens of thousands of years. This new evidence for geologically recent volcanism corroborates evidence from gravity and topography analysis indicating active plumes at depth. The estimated number of large mantle plumes on Venus, around nine, is similar to the number of plumes believed to come from the core/mantle boundary on Earth (*5*). The scale of the observed flows is most consistent with an equilibrium resurfacing model (*2*), which implies Earth-like interior processes rather than more exotic ones that enable catastrophic resurfacing. If the apparent concentration of volcanism at hotspots represents a change in the style of volcanism, it may indicate a transition from more secular cooling and widespread volcanism to plumes driven by cooling of the core (*49*).

References and Notes

1. G. G. Schaber *et al.*, *J. Geophys. Res.* **97**, 13,257 (1992).
2. R. J. Phillips *et al.*, *J. Geophys. Res.* **97**, 15,923 (1992).
3. E. M. Parmentier, P. C. Hess, *Geophys. Res. Lett.* **19**, 2015 (1992).
4. C. C. Reese, V. S. Solomatov, C. P. Orth, *J. Geophys. Res.* **112**, E04S04 (2007).
5. E. R. Stofan, S. E. Smrekar, in *Plates, Plumes, and Paradigms*, G. R. Foulger, J. H. Natland, D. C. Presnall, D. L. Anderson, Eds. (Special Volume 388, Geological Society of America, Denver, CO, 2005), pp. 861–885.
6. J. Lecacheux, P. Drossart, P. Laques, F. Deladerriere, F. Colas, *Planet. Space Sci.* **41**, 543 (1993).
7. N. Mueller *et al.*, *J. Geophys. Res.* **113**, E00B17 (2008).
8. J. Helbert *et al.*, *Geophys. Res. Lett.* **35**, L11201 (2008).
9. N. J. Rappaport, A. S. Konopliv, A. B. Kucinskas, P. G. Ford, *Icarus* **139**, 19 (1999).
10. We reduced the surface emissivity using the improved version of the Global Topography Data Record developed by (*9*) from updated ephemeris data. The Magellan data are referenced to the cartographic system given by (*50*) and are transformed into the system used by VIRTIS data (*51*), taking January 1991 as an approximate time of the Magellan observations. However, the best correlation of the topography implied by temperature derived from VIRTIS infrared images and Magellan altimetry is found when the Magellan coordinates are shifted another 0.15° in longitude. Estimates of Venus angular velocity [(*52*, *53*) and references therein] disagree by amounts that, over the approximately 16-year separation between Magellan and Venus Express, can accommodate this deviation.
11. To calculate emissivity values employing a two-stream approximation of radiative transfer (*12*), we assumed an atmospheric reflectivity of 0.82 and a nonabsorbing atmosphere (*54*), which is appropriate for the 1.02-μm window (*40*). We assumed that the average plains are basaltic and that weathering has lowered the emissivity. Using an average emissivity of 0.58 produced an emissivity range in this area of 0.5 to 0.91, a range consistent with expected mineralogy.
12. G. L. Hashimoto, S. Sugita, *J. Geophys. Res.* **108**, 5109 (2003).

13. J. Helbert, A. Maturilli, N. Mueller, in *Venus Geochemistry: Progress, Prospects, and New Missions* (Lunar and Planetary Institute, Houston, TX, 2009), abstr. 2010.
14. J. Helbert, A. Maturilli, *Earth Planet. Sci. Lett.* **285**, 347 (2009).
15. Coronae are circular volcano-tectonic features that are unique to Venus and have an average diameter of ~250 km (*5*). They are defined by their circular and often radial fractures and always produce some form of volcanism.
16. G. E. McGill, S. J. Steenstrup, C. Barton, P. G. Ford, *Geophys. Res. Lett.* **8**, 737 (1981).
17. R. J. Phillips, M. C. Malin, *Annu. Rev. Earth Planet. Sci.* **12**, 411 (1984).
18. E. R. Stofan, S. E. Smrekar, D. L. Bindschadler, D. Senske, *J. Geophys. Res.* **23**, 317 (1995).
19. Estimated elastic thickness values at Themis Regio are typically 10 to 20 km (*20*, *21*). The authors of (*22*) conducted a global admittance study and found values of elastic thickness of 0 to 50 km at both Dione and Themis Regiones. Their analysis also shows regions of large elastic thickness, up to 100 km, in the northern portion of Dione Regio covering Ushas Mons. Estimates of average apparent depth of compensation (ADC) for Dione and Themis Regiones are 130 km and 100 km (*21*), respectively. The elastic thickness at Imdr Regio cannot be reliably estimated due to the low resolution of the gravity field in that region (*53*). Stofan *et al.* (*18*) estimated an ADC of 260 km, which is consistent with a deep plume.
20. M. Simons, S. C. Solomon, B. H. Hager, *Geophys. J. Int.* **13**, 24 (1997).
21. S. E. Smrekar, E. R. Stofan, *Icarus* **139**, 100 (1999).
22. F. S. Anderson, S. E. Smrekar, *J. Geophys. Res. Planets* **111**, E08006 (2006).
23. S. T. Keddie, J. W. Head, *J. Geophys. Res.* **101**, 11,729 (1995).
24. E. R. Stofan, J. E. Guest, A. W. Brian, *Mapping of V-28 and V-53*, T. K. P. Gregg, K. L. Tanaka, R. S. Saunders, Eds. (U.S. Geological Society Open-File Report 2005-1271, Abstracts of the Annual Meeting of Planetary Geologic Mappers, Washington, DC, 2005), pp. 20–21.
25. E. R. Stofan, S. E. Smrekar, J. Helbert, P. Martin, N. Mueller, *Lunar Planet. Sci.* **XXXIX**, abstr. 1033 (2009).
26. B. D. Campbell *et al.*, *J. Geophys. Res.* **97**, 16,249 (1992).
27. R. J. Phillips, N. R. Izenberg, *Geophys. Res. Lett.* **22**, 1617 (1995).
28. C. M. Pieters *et al.*, *Science* **234**, 1379 (1986).
29. B. Fegley Jr., R. G. Prinn, *Nature* **337**, 55 (1989).
30. A. H. Treiman, C. C. Allen, *Lunar Planet. Sci. Conf.* **XXV**, 1415 (1994).
31. M. I. Zolotov, V. P. Volkov, in *Venus Geology, Geochemistry, Geophysics—Research Results from the USSR* (Univ. of Arizona Press, Tucson, AZ, 1992), pp. 177–199.
32. B. Fegley, A. H. Treiman, V. L. Sharpton, *Proc. Lunar Planet. Sci.* **22**, 3 (1992).
33. B. Fegley, K. Lodders, A. H. Treiman, G. Klingelhöfer, *Icarus* **115**, 159 (1995a).
34. B. Fegley *et al.*, *Icarus* **118**, 373 (1995b).
35. A. M. Baldridge, S. J. Hook, C. I. Grove, G. Rivera, *Remote Sens. Environ.* **113**, 711 (2009).
36. L. T. Elkins-Tanton *et al.*, *Contrib. Minerol. Petrol.* **153**, 191 (2007).
37. S. A. Gibson, R. N. Thompson, A. P. Dickin, *Earth Planet. Sci. Lett.* **174**, 355 (2000).
38. L. S. Glaze, *J. Geophys. Res.* **104**, 18,899 (1999).
39. *New Scientist* **23**, 52 (2009) (www.newscientist.com/article/dn17534).
40. V. S. Meadows, D. Crisp, *J. Geophys. Res.* **101**, 4595 (1996).
41. B. Fegley, *Icarus* **128**, 474 (1997).
42. E. R. Stofan, A. W. Brian, J. E. Guest, *Icarus* **173**, 312 (2005).
43. P. R. Hooper, in *Large Igneous Provinces: Continental, Oceanic and Planetary Flood Volcanism*, J. J. Mahoney, M. F. Coffin, Eds. (Monograph 100, American Geophysical Union, Washington, DC, 1997), pp. 1–28.
44. M. A. Bullock, D. H. Grinspoon, *Icarus* **150**, 19 (2001).
45. R. G. Strom, G. G. Schaber, D. D. Dawson, *J. Geophys. Res.* **99**, 10,899 (1994).
46. K. M. Roberts, J. E. Guest, J. W. Head, M. G. Lancaster, *J. Geophys. Res.* **97**, 15,991 (1992).
47. C. R. K. Kilburn, in *Encyclopedia of Volcanoes*, H. Sigurdsson, Ed. (Academic Press, San Diego, CA, 2000), pp. 291–306.
48. We have rounded these numbers in recognition that the age estimates have higher uncertainties than the volume estimates.
49. G. Choblet, E. M. Parmentier, *Phys. Earth Planet. Inter.* **173**, 290 (2009).
50. M. E. Davies *et al.*, *Celestial Mech.* **39**, 103 (1986).
51. P. K. Seidelmann *et al.*, *Celestial Mech. Dyn. Astron.* **82**, 83 (2002).
52. M. E. Davies *et al.*, *J. Geophys. Res.* **97**, 13,141 (1992).
53. A. S. Konopliv, W. S. Banerdt, W. L. Sjogren, *Icarus* **139**, 3 (1999).
54. G. L. Hashimoto, T. Imamura, *Icarus* **154**, 239 (2001).
55. This research was carried out in part at the Jet Propulsion Laboratory, California Institute of Technology, and was sponsored by the Planetary Geology and Geophysics Program and NASA. We gratefully acknowledge the work of the entire Venus Express and VIRTIS teams. We thank the European Space Agency, Agenzia Spaziale Italiana, Centre National des Etudes Spatiales, CNRS/Institut National des Sciences de l'Univers, and the other national space agencies that have supported this research. VIRTIS is led by INAF-IASF, Rome, Italy, and LESIA, Observatoire de Paris, France.

7 January 2010; accepted 25 March 2010
Published online 8 April 2010;
10.1126/science.1186785
Include this information when citing this paper.

Cryogenian Glaciation and the Onset of Carbon-Isotope Decoupling

Nicholas L. Swanson-Hysell,[1] Catherine V. Rose,[1] Claire C. Calmet,[1] Galen P. Halverson,[2]* Matthew T. Hurtgen,[3] Adam C. Maloof[1]†

Global carbon cycle perturbations throughout Earth history are frequently linked to changing paleogeography, glaciation, ocean oxygenation, and biological innovation. A pronounced carbonate carbon-isotope excursion during the Ediacaran Period (635 to 542 million years ago), accompanied by invariant or decoupled organic carbon-isotope values, has been explained with a model that relies on a large oceanic reservoir of organic carbon. We present carbonate and organic matter carbon-isotope data that demonstrate no decoupling from approximately 820 to 760 million years ago and complete decoupling between the Sturtian and Marinoan glacial events of the Cryogenian Period (approximately 720 to 635 million years ago). Growth of the organic carbon pool may be related to iron-rich and sulfate-poor deep-ocean conditions facilitated by an increase in the Fe:S ratio of the riverine flux after Sturtian glacial removal of a long-lived continental regolith.

Throughout most of the Phanerozoic Eon [542 million years ago (Ma) to present], paired records of carbonate carbon ($\delta^{13}C_{carb}$) and coeval bulk organic carbon ($\delta^{13}C_{org}$) isotopes are consistent with a model in which the organic carbon in marine sediments is derived and fractionated from contemporaneous dissolved inorganic carbon (DIC). In contrast, $\delta^{13}C_{carb}$ and $\delta^{13}C_{org}$ records from Ediacaran (635 to 542 Ma) carbonate successions (*1*–*3*) show relatively invariant $\delta^{13}C_{org}$ during large changes to $\delta^{13}C_{carb}$ across the ~580 million-year-old Shuram-Wonoka anomaly (Fig. 1 and fig. S1). This behavior has been used to develop and support a model for the Neoproterozoic (1000 to 542 Ma) carbon cycle in which invariant $\delta^{13}C_{org}$ values result from a very large oceanic reservoir of ^{13}C-depleted dissolved organic carbon (DOC) and particulate organic carbon (POC) (or, alternatively, sourced from a large sedimentary reservoir) that overwhelms the signal from primary biomass fractionated from contemporaneous DIC (*4*). We consider the large oceanic reservoir model and, as in (*2*), use the term DOC to collectively refer to organic carbon that is truly dissolved as well as suspended colloidal organic carbon and fine POC. The buildup and maintenance of a large DOC pool implies low C_{org} remineralization—perhaps associated with low oxygen and sulfate levels—but high nutrient liberation efficiency. In such an ocean, the $\delta^{13}C$ of the DIC pool is sensitive to inputs (via remineralization) from the ^{13}C-depleted DOC pool that can drive negative excursions. The end of the invariance in the $\delta^{13}C_{org}$ record in the latter stages of the Shuram-Wonoka anomaly has been interpreted as the demise of the large DOC pool (*2*, *3*).

Stratigraphically constrained coupled records of $\delta^{13}C_{carb}$–$\delta^{13}C_{org}$ at sufficient detail to test this carbon cycle model have been available only from carbonates of Ediacaran age (*2*, *3*). We present paired $\delta^{13}C_{carb}$ and $\delta^{13}C_{org}$ data from

[1]Department of Geosciences, Princeton University, Princeton, NJ 08544, USA. [2]Geology and Geophysics, University of Adelaide Mawson Laboratories, Adelaide, SA 5005, Australia. [3]Department of Earth and Planetary Sciences, Northwestern University, Evanston, IL 60208, USA.
*Present address: Department of Earth and Planetary Sciences, McGill University, Montreal, Quebec H3A 2A7, Canada.
†To whom correspondence should be addressed. E-mail: maloof@princeton.edu

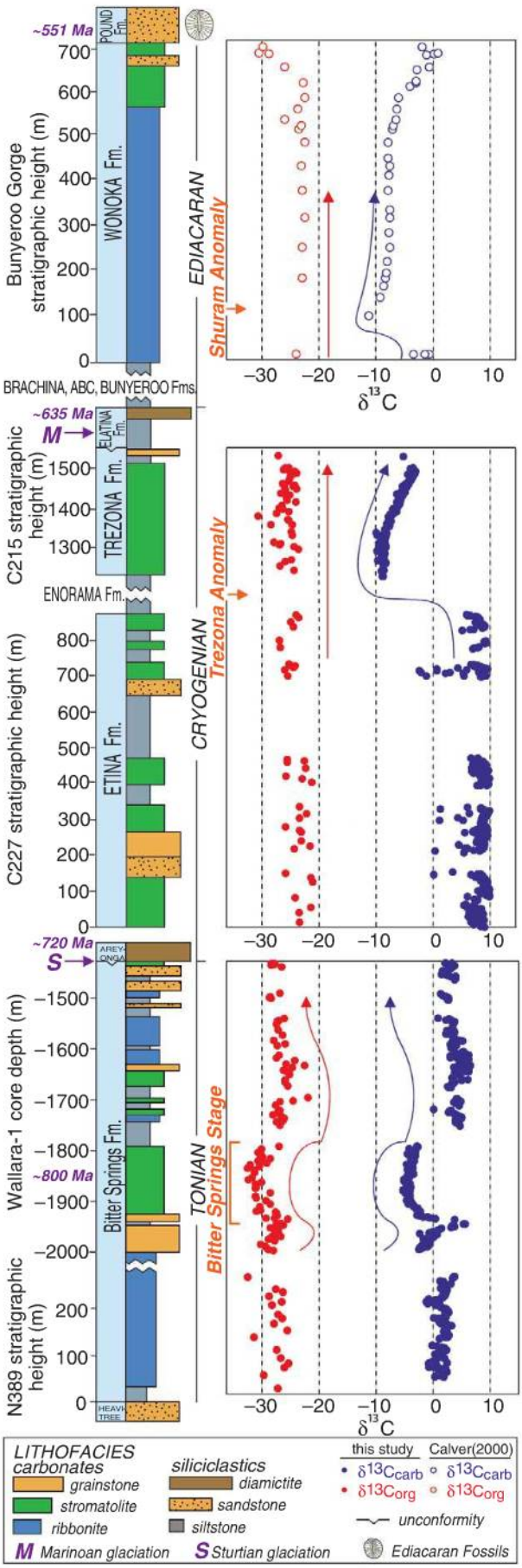

Fig. 1. Carbonate carbon isotope values and organic carbon isotope values from Neoproterozoic carbonates of Australia with simplified lithostratigraphy. The plotted lithofacies represent the lithologies that dominate each interval, with wider boxes corresponding to deposition in shallower water. N389 field-section and Wallara-1 core data are from the Bitter Springs Formation of the Amadeus Basin, deposited before the Sturtian glacial event. C227 and C215 are part of a continuous field section through the interglacial stratigraphy of the Adelaide Rift Complex. Data for the Wonoka Formation are from (*1*). The Bitter Springs, Trezona, and Shuram carbon isotope anomalies are labeled next to the carbon isotope records. The pre–Sturtian Islay anomaly is not recorded in the Bitter Springs Formation because of a disconformity at the contact with the overlying glacial sediments. The Global Boundary Stratotype Section and Point for the Cryogenian/Ediacaran Period boundary is at the contact between the glacigenic Elatina formation and the overlying Nuccaleena cap carbonate. Though it has yet to be formally defined with a stratotype section, we place the Tonian/Cryogenian boundary at the lowermost evidence for Neoproterozoic glaciation, in concurrence with the 2009 recommendation of the International Commission on Stratigraphy.

older Neoproterozoic strata: the Bitter Springs Formation of the Amadeus Basin, central Australia, that was deposited during the Tonian Period (1000 to ~720 Ma) and the Etina-Trezona Formations of the adjacent Adelaide Rift Complex deposited during the Cryogenian Period (~720 to 635 Ma) (*5*). Together with published data from the Ediacaran Wonoka Formation (*1*), also of the Adelaide Rift Complex, these records span numerous $\delta^{13}C_{carb}$ shifts throughout the Neoproterozoic Era on a single continent, enabling a test of the hypothesis that a large reservoir of DOC and corresponding invariance in $\delta^{13}C_{org}$ was a feature of the carbon cycle for the entire era.

The paired carbon isotope data from the Bitter Springs Formation demonstrate covariation across the onset of the ~800-Ma Bitter Springs stage and throughout the stage itself. At the termination of the Bitter Springs stage, $\delta^{13}C_{carb}$ values shift abruptly from –2.7 per mil (‰) to +5.3‰, whereas $\delta^{13}C_{org}$ shifts from –29.9‰ to –26.7‰ (Fig. 1). The stable isotope results are virtually identical between the 2-km-deep Wallara drill core and a surface outcrop 120 km away, indicating that the signal is basin-wide and that neither surface oxidation nor meteoric diagenesis have substantially altered the $\delta^{13}C_{carb}$–$\delta^{13}C_{org}$ record. The sympathetic shifts in $\delta^{13}C_{carb}$ and $\delta^{13}C_{org}$ across the Bitter Springs stage confirm that the stage reflects a large-scale perturbation to the isotopic composition of the DIC pool and that organic matter in the sediments is representative of coeval biomass that fixed carbon from this ^{13}C-depleted DIC (fig. S1). In stark contrast, $\delta^{13}C_{org}$ values remain invariant across the Cryogenian Trezona anomaly, in which $\delta^{13}C_{carb}$ drops by 18‰. Before the Trezona anomaly, the $\delta^{13}C_{carb}$ values of the Etina Formation plateau at ~8‰, which is similar to the values observed in Cryogenian interglacial carbonates from Namibia (*6*), Mongolia (*7*), and Scotland (*8*). After deposition of the Enorama shale, carbonates of the subtidal Trezona Formation record $\delta^{13}C_{carb}$ values of –10‰ that increase up-stratigraphy to –2‰ before the glacial sediments of the Elatina Formation. Despite these dramatic changes in $\delta^{13}C_{carb}$, $\delta^{13}C_{org}$ values remained constant at –25‰ (Fig. 1). Unlike during the Shuram-Wonoka anomaly, there was not an increase in the variability of $\delta^{13}C_{org}$ values upwards through the Trezona anomaly. The new Australian data sets do not show significant correlation between $\delta^{13}C_{org}$ and total organic carbon, a proxy that is sometimes used as evidence for alteration of the $\delta^{13}C_{org}$ signal (fig. S3). Taken together, the new data constrain the buildup of a large DOC pool to after the Bitter Springs stage of the mid-to-late Tonian but before the onset of the end-Cryogenian glaciation.

This timing for the growth of the DOC pool and the onset of non-steady-state dynamics is consistent with very low sulfate levels in the Cryogenian oceans (*9*) and a return to ferruginous conditions in the deep ocean during early

Cryogenian glaciation (*10*, *11*). In such an ocean, decreased rates of aerobic respiration and bacterial sulfate reduction would slow organic carbon remineralization and extend the residence time of DOC. Preferential remineralization of organic P over C, as occurs with increasing depth in the modern ocean (*12*), could increase the C:P ratio of DOC with the liberated phosphate, helping to sustain the productivity necessary to accumulate a large DOC pool. Furthermore, anoxic bottom-water conditions would favor burial of high C:P organic matter because of decreased burial of P bound to Fe oxyhydroxides (*13*), further maintaining nutrient supply and sustaining the primary productivity required to explain elevated Cryogenian $\delta^{13}C_{carb}$ values (*14*).

The return to ferruginous ocean conditions and the buildup of DOC can be explained as a consequence of global glaciation. The development of a thick continental regolith of unconsolidated, chemically leached debris and soil during the 1.5 billion years between the ~2.2-billion-year-old Paleoproterozoic Makganyene glaciation of South Africa (*15*) and the ~720-Ma early Cryogenian pan-glacial event (*16*) would have suppressed the Fe:S ratio of continental runoff. After reaching a depth of ~0.5 m, the thickness of regolith is inversely proportional to the weatherability of the top of bedrock (Fig. 2B) (*17*, *18*). Although the average concentrations of Fe oxides are similar between sedimentary rocks and the rest of the upper continental crust, the average concentration of S is eight times greater in sedimentary lithologies (*19*). Thus, the development of a thick regolith on continental interiors in the absence of glacial erosion and the preferential weathering of S-rich sedimentary and ophiolitic rocks on continental margins, where tectonic uplift could facilitate physical removal of regolith, would have limited relative Fe input to the ocean. This mechanism for maintaining high relative S delivery helps to explain evidence for widespread euxinic conditions through the Mesoproterozoic [1.6 to 1.0 billion years ago (*20*, *21*)].

The association of banded-iron formation (BIF) with Sturtian-age glacial deposits demonstrates that during the glaciation, Fe supply from hydrothermal and continental-weathering sources exceeded sulfide availability (*9*). This Fe input removed available oxidants, resulting in anoxia, low sulfate levels, and BIF deposition. Although the presence of BIF associated with the glaciation indicates transient ferruginous conditions, the maintenance of iron-rich deep oceans (*10*, *11*) requires that a high relative flux of Fe continued in the post-glacial period. Ubiquitous continental ice sheets during the Sturtian glaciation would have scoured continental interiors, removing the thick mantle of regolith. The relatively thick Sturtian glacial deposits may represent physical evidence of redeposited regolith that was eroded by dynamic early Cryogenian ice sheets, whereas the relatively thin Marinoan glacial deposits may reflect the activity of stable late Cryogenian ice sheets frozen to scoured bedrock—similar to the Pleistocene evolution of the Canadian Shield and Laurentide ice sheet (*22*). When ice sheets retreated during the high CO_2 escape from the early Cryogenian glaciation, the vigorous weathering of freshly exposed continental crust would result in a higher proportional delivery of Fe to S into the ocean than during the preceding 1.5 billion years. This postulated increase in the relative delivery of material derived from continental interiors as compared with continental margins is supported by a steady increase in the $^{87}Sr/^{86}Sr$ composition of the ocean after the Sturtian ice age (*23*). Because the DOC reservoir does not build up until after the Sturtian glaciation in this model, it predicts that $\delta^{13}C_{org}$ will vary across the immediately pre-Sturtian Islay negative $\delta^{13}C_{carb}$ anomaly (*8*).

The sudden post-Sturtian increase in weatherability could have led to lower equilibrium atmospheric CO_2 during the Cryogenian without changes to volcanic CO_2 input (Fig. 2C). Changes in CO_2 are connected to the evolving sensitivity of silicate weathering rates to CO_2 [weatherability (k_w)] and the varying fraction of total carbon burial that occurs as organic carbon (f_{org}) (*14*). High steady-state values of $\delta^{13}C_{carb}$ during the late Tonian have been used to argue that a high f_{org} helped lower CO_2 before glaciation (*14*). The prevalence of continental landmass at low latitude that facilitated high f_{org} may have increased k_w because of the abundance of silicate rocks associated with Grenville-age orogenic belts in tropical weathering regimes. Landscape disequilibrium associated with Bitter Springs–stage rapid true-polar wander (*24*) and increased delivery of moisture to continental interiors during the opening of incipient ocean basins as Rodinia rifted apart (*25*) would have further increased k_w. Together, these late Tonian changes would have reduced CO_2 enough to initiate Sturtian glaciation. However, it was the Sturtian glaciers themselves that scoured the continents, removing the long-lived Proterozoic regolith, greatly increasing continental weatherability, and setting up a new climatic regime with lower CO_2, a ferruginous ocean with high $\delta^{13}C_{carb}$, and a large DOC pool.

Although the close association of the Trezona anomaly below Marinoan glacial deposits has been interpreted as evidence for a causal relationship between the two (*14*), the glacioeustatic sea level fall related to Marinoan glaciation did not occur until after recovery from the most negative $\delta^{13}C_{carb}$ values. In some sections, Trezona Formation $\delta^{13}C_{carb}$ values recover to ~0‰ and are followed by more than 100 m of shallowing-upward peritidal sandstones before the first glacial deposits, further attenuating the connection between the Trezona anomaly and glaciation. If the increase in k_w and sustained high f_{org} of the Cryogenian led to global cooling and oxygen release, the Trezona anomaly could reflect oxygenation of the deep ocean and partial remineralization of the large ^{13}C-depleted DOC pool, as has been suggested for the Shuram-Wonoka anomaly. Organic carbon remineralization represents a negative climate feedback, releasing CO_2 and preventing glaciation—which is consistent with the lack of glacioeustatic change during the Trezona anomaly itself. The $\delta^{13}C_{carb}$ recovery and eventual Marinoan glaciation oc-

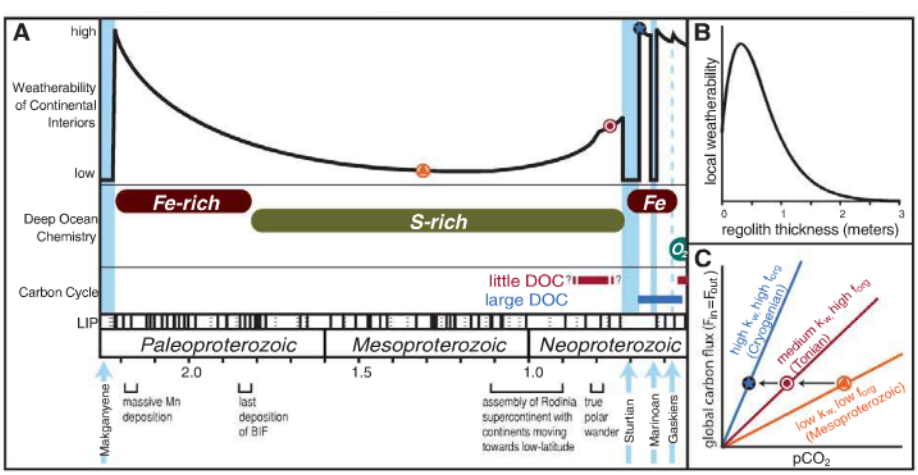

Fig. 2. (**A**) Summary illustration relating Proterozoic deep-ocean chemistry [modified from (*26*)], small versus large DOC carbon cycle, and the weatherability of continental interiors. Before the first Neoproterozoic glaciation, there was no unusual concentration of large igneous province events [shown as compiled by (*27*), with solid and dashed lines indicating <20- and >20-Ma uncertainty, respectively]. Because local weatherability is a function of regolith thickness [(**B**), modified from (*18*)], regolith development on continental interiors through the nonglacial Mesoproterozoic (*28*) would lead to the depicted decrease in regional weatherability in (A). The relationship shown schematically in (**C**) is $F_{in} = (k_w \times M_{CO_2})/(1 - f_{org})$, where k_w is the slope of the weathering-CO_2 feedback and is partly a function of the regional weatherability depicted in (B). An increase in k_w and in the relative burial of C as organic matter can result in a decrease in CO_2, as shown for the Mesoproterozoic → Tonian → Cryogenian, without changes in volcanic An increase input.

curred when the large DOC pool had been reduced in size enough to no longer represent a negative feedback to global climatic cooling.

References and Notes

1. C. R. Calver, *Precambrian Res.* **100**, 121 (2000).
2. D. A. Fike, J. P. Grotzinger, L. M. Pratt, R. E. Summons, *Nature* **444**, 744 (2006).
3. K. A. McFadden *et al.*, *Proc. Natl. Acad. Sci. U.S.A.* **105**, 3197 (2008).
4. D. H. Rothman, J. M. Hayes, R. E. Summons, *Proc. Natl. Acad. Sci. U.S.A.* **100**, 8124 (2003).
5. Data tables and methods are available as supporting material on *Science* Online.
6. G. P. Halverson, P. F. Hoffman, D. P. Schrag, A. C. Maloof, A. H. N. Rice, *Geol. Soc. Am. Bull.* **117**, 1181 (2005).
7. F. A. Macdonald, D. S. Jones, D. P. Schrag, *Geology* **37**, 123 (2009).
8. A. R. Prave, A. E. Fallick, C. W. Thomas, C. M. Graham, *J. Geol. Soc. London* **166**, 845 (2009).
9. M. T. Hurtgen, M. A. Arthur, N. Suits, A. J. Kaufman, *Earth Planet. Sci. Lett.* **203**, 413 (2002).
10. D. E. Canfield *et al.*, *Science* **321**, 949 (2008).
11. C. Li *et al.*, *Science* **328**, 80 (2010).
12. P. Sannigrahi, E. D. Ingall, R. Benner, *Geochim. Cosmochim. Acta* **70**, 5868 (2006).
13. P. Van Cappellen, E. D. Ingall, *Paleoceanography* **9**, 677 (1994).
14. D. P. Schrag, R. A. Berner, P. F. Hoffman, G. P. Halverson, *Geochem. Geophys. Geosyst.* **10**, 1029/2001GC000219 (2002).
15. R. E. Kopp, J. L. Kirschvink, I. A. Hilburn, C. Z. Nash, *Proc. Natl. Acad. Sci. U.S.A.* **102**, 11131 (2005).
16. F. A. Macdonald *et al.*, *Science* **327**, 1241 (2010).
17. F. Ahnert, Ed., *Geomorphological Models: Theoretical and Empirical Aspects* (Catena, Reiskirchen, Germany, 1987), pp. 31–50.
18. E. J. Gabet, S. M. Mudd, *Geology* **37**, 151 (2009).
19. K. H. Wedepohl, *Geochim. Cosmochim. Acta* **59**, 1217 (1995).
20. D. E. Canfield, *Nature* **396**, 450 (1998).
21. T. W. Lyons, A. D. Anbar, S. Severmann, C. Scott, B. C. Gill, *Annu. Rev. Earth Planet. Sci.* **37**, 507 (2009).
22. P. U. Clark, D. Pollard, *Paleoceanography* **13**, 1 (1998).
23. G. P. Halverson, F. O. Dudas, A. C. Maloof, S. A. Bowring, *Palaeogeogr. Palaeoclimatol. Palaeoecol.* **256**, 103 (2007).
24. A. C. Maloof *et al.*, *Geol. Soc. Am. Bull.* **118**, 1099 (2006).
25. Y. Goddéris *et al.*, *C. R. Geosci.* **339**, 212 (2007).
26. D. T. Johnston, F. Wolfe-Simon, A. Pearson, A. H. Knoll, *Proc. Natl. Acad. Sci. U.S.A.* **106**, 16925 (2009).
27. R. E. Ernst, K. L. Buchan, *Spec. Pap. Geol. Soc. Am.* **352**, 483 (2001).
28. L. C. Kah, R. Riding, *Geology* **35**, 799 (2007).

29. We thank K. Bovee, R. Levin, W. Jacobsen, L. Wingate, and L. Godfrey for assistance with sample preparation and analysis and D. Rothman, L. Kah, R. Kopp, N. Cassar, J. Higgins, J. Husson, and D. Sigman for comments and discussions. This work was supported by NSF grants EAR-0514657 and EAR-084294 to A.C.M., EAR-0720045 to M.T.H., an American Association of Petroleum Geologists Grant to C.V.R., and an NSF East Asia and Pacific Summer Institute fellowship to N.L.S.-H.

Supporting Online Material

www.sciencemag.org/cgi/content/full/328/5978/608/DC1
Materials and Methods
Figs. S1 to S4
Table S1
References

10 November 2009; accepted 11 March 2010
10.1126/science.1184508

Asian Monsoon Transport of Pollution to the Stratosphere

William J. Randel,[1]* Mijeong Park,[1] Louisa Emmons,[1] Doug Kinnison,[1] Peter Bernath,[2,3] Kaley A. Walker,[4,3] Chris Boone,[3] Hugh Pumphrey[5]

Transport of air from the troposphere to the stratosphere occurs primarily in the tropics, associated with the ascending branch of the Brewer-Dobson circulation. Here, we identify the transport of air masses from the surface, through the Asian monsoon, and deep into the stratosphere, using satellite observations of hydrogen cyanide (HCN), a tropospheric pollutant produced in biomass burning. A key factor in this identification is that HCN has a strong sink from contact with the ocean; much of the air in the tropical upper troposphere is relatively depleted in HCN, and hence, broad tropical upwelling cannot be the main source for the stratosphere. The monsoon circulation provides an effective pathway for pollution from Asia, India, and Indonesia to enter the global stratosphere.

The Asian summer monsoon circulation contains a strong anticyclonic vortex in the upper troposphere and lower stratosphere (UTLS), spanning Asia to the Middle East. The anticyclone is a region of persistent enhanced pollution in the upper troposphere during boreal summer, linked to rapid vertical transport of surface air from Asia, India, and Indonesia in deep convection, and confinement by the strong anticyclonic circulation (*1*–*6*). A mean upward circulation on the eastern side of the anticyclone extends the transport into the lower stratosphere, as evidenced by satellite observations of water vapor (*7*) and ozone (*8*), plus carbon monoxide and other pollution tracers (*1*, *4*, *5*). Model calculations have suggested that transport from the monsoon region could contribute substantially to the budget of stratospheric water vapor (*8*, *9*), but this effect has not been isolated from broader-scale tropical upwelling in observational data.

Hydrogen cyanide (HCN) is produced primarily as a result of biomass and biofuel burning and is often used as a tracer of pollution originating from fires (*10*–*12*). In the free atmosphere,

[1]National Center for Atmospheric Research, Boulder, CO, USA. [2]Department of Chemistry, University of York, Heslington, UK. [3]Department of Chemistry, University of Waterloo, Waterloo, Ontario, Canada. [4]Department of Physics, University of Toronto, Toronto, Ontario, Canada. [5]School of GeoSciences, University of Edinburgh, Edinburgh, UK.

*To whom correspondence should be addressed. E-mail: randel@ucar.edu

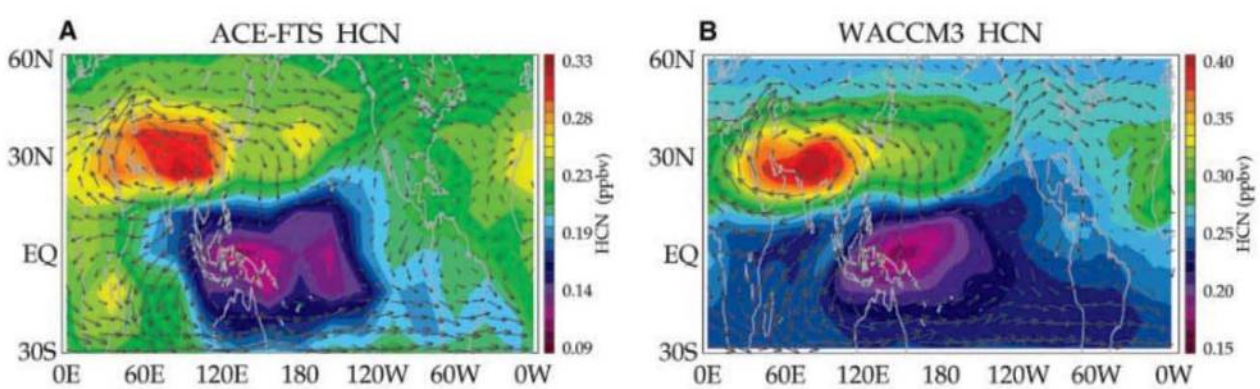

Fig. 1. Time average mixing ratio [parts per billion by volume (ppbv)] of HCN near 13.5 km during boreal summer (June to August) derived from (**A**) ACE-FTS observations and (**B**) WACCM chemical transport model calculations. Arrows in both panels denote winds at this level derived from meteorological analysis, showing that the HCN maximum is linked with the upper tropospheric Asian monsoon anticyclone.

HCN has a long photochemical lifetime of more than 4 years (*12*, *13*), but it has a strong sink resulting from contact with the ocean surface (*11*, *12*). In the tropics, this behavior results in relatively low values of HCN in the troposphere apart from seasons with local biomass burning (*10*, *14*). Global satellite observations of HCN in the upper troposphere from the Atmospheric Chemistry Experiment Fourier Transform Spectrometer (ACE-FTS) satellite instrument (*15*–*17*) (Fig. 1A) reveal the signature of air depleted in HCN over the tropical oceans, together with enhanced values isolated within the Asian monsoon anticyclone during boreal summer (June to August). The tropical minimum for HCN is a distinctive signature that is very different from most other tropospheric pollution tracers, such as carbon monoxide (*18*). The overall structure of HCN is accurately simulated by a three-dimensional (3D) chemical transport model (Fig. 1B) incorporating HCN sources from wildfires and biofuel combustion, plus an imposed sink from contact with the ocean surface (*19*). The realistic structure in this simulation suggests a reasonable understanding of the processes leading to the observed global-scale HCN behavior, especially the role of the oceanic regions in depleting HCN, and the Asian monsoon circulation in transporting HCN from the surface to the upper troposphere.

The relative minimum in HCN over the tropical Pacific ocean is a feature that is observed throughout the year (fig. S1). In addition to the maximum associated with the Asian monsoon during boreal summer, seasonally varying sources of HCN include burning over Indonesia and Africa during boreal spring (March to May), and burning over Africa and South America during austral spring (September to November), with these emissions transported to the upper troposphere by deep convection. However, the upper tropospheric circulation associated with the Asian summer monsoon is more coherent and vigorous than the monsoonal circulations in these other regions and seasons, with a vertical extent that reaches across the tropopause into the lower stratosphere. A longitudinally averaged cross section of the satellite measurements during boreal summer (Fig. 2) shows high HCN values throughout the extratropical Northern Hemisphere, extending across the tropopause into the lower stratosphere; the pronounced cross-tropopause maximum near 30° N is associated with the monsoon anticyclone shown in Fig. 1. The high HCN values in the stratosphere extend to low latitudes and vertically over the equator and are transported into the middle stratosphere in the upward Brewer-Dobson circulation within the so-called tropical pipe (*20*). The enhanced summer HCN values are observed to persist in the Northern Hemisphere lower stratosphere through the following seasons (fig. S2).

Further evidence of the Asian monsoon-stratosphere coupling comes from examining interannual variations of HCN in the satellite record. Measurements of HCN from the Aura Microwave Limb Sounder (MLS) satellite instrument (*21*) complement the ACE-FTS observations, providing continuous space-time coverage for ~7-km-thick layers covering the lower to middle stratosphere (but not below the tropopause). Time series of the MLS data in the lower stratosphere (~16 to 23 km) from late 2004 to the end of 2009 (Fig. 3) show HCN maxima in the Northern Hemisphere subtropics during each boreal summer (~June to October); this is a clear fingerprint of the Asian monsoon influence (consistent with the ACE-FTS observations in Fig. 2 and fig. S2). In this short time record, the HCN maxima extend most strongly to near-equatorial latitudes during 2005 and 2007, and less so in the other years. Previous analyses (*22*) have demonstrated that these 2005 and 2007 equatorial HCN maxima propagate coherently upward into the stratosphere with the tropical Brewer-Dobson circulation; this so-called tape-recorder effect is evident in other stratospheric trace constituents (e.g., H_2O) that have seasonal or interannual anomalies originating near the tropical tropopause (*23*). Figure 3 demonstrates that these stratospheric anomalies are linked to enhanced boreal summer (Asian monsoon) maxima during 2005 and 2007. Figure 3 also shows isolated HCN maxima in the Southern Hemisphere

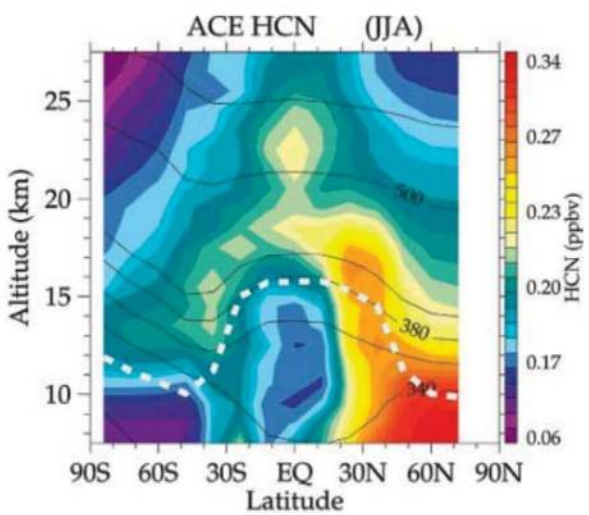

Fig. 2. Time and zonal average mixing ratio (ppbv) of HCN during boreal summer (June to August) derived from ACE-FTS satellite measurements. The white dashed line denotes the tropopause, and black lines denote isentropic levels.

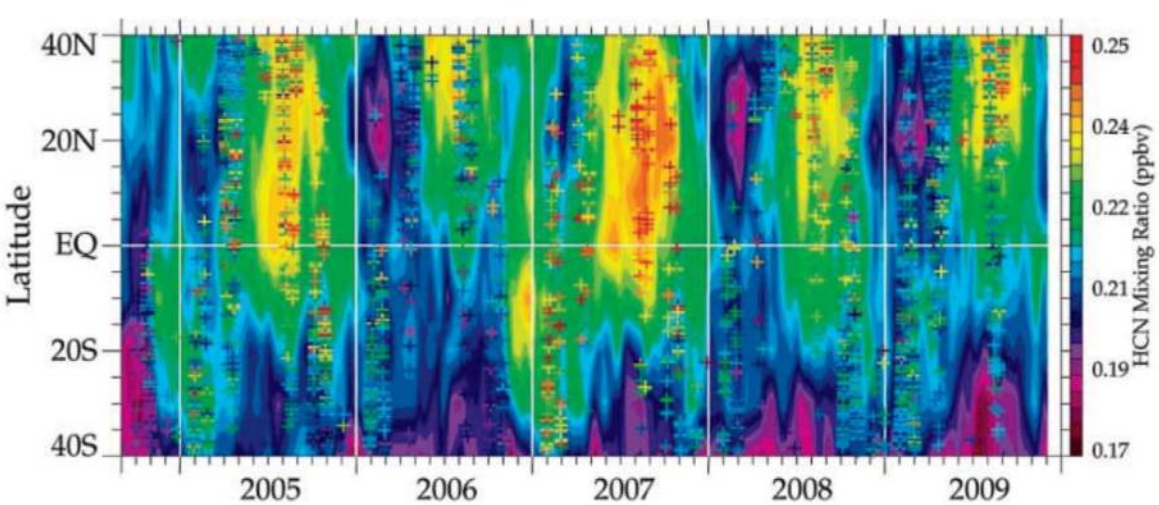

Fig. 3. Color contours show latitude-time variations of HCN mixing ratio (ppbv) for the lower stratosphere layer, 16 to 23 km, measured by the Aura MLS satellite during September 2004 to November 2009. These MLS data are zonal mean values averaged over individual week periods, as described in (*22*). Colored crosses indicate HCN for the 16- to 23-km layer derived from the ACE satellite measurements, with each cross indicating an individual profile measurement. Comparison of the MLS and ACE-FTS data are shown in fig. S3.

subtropics (~0° to 20°S) during late 2004 and late 2006, which result from enhanced austral spring burning over Indonesia during these years (*24*). However, direct transport to the stratosphere from these episodes appears smaller than the boreal summer sources linked to the Asian monsoon.

The exact causes of the enhanced tropical lower stratospheric HCN during 2005 and 2007 seen in Fig. 3 are difficult to determine from the limited sampling of the satellite observations. We have searched for systematic changes in transport or circulation of the Asian monsoon anticyclone during these years [or links to the stratospheric quasibiennial oscillation (QBO)], but we do not find obvious links to the enhanced HCN anomalies. Rather, it is likely that these patterns reflect variations in tropospheric sources, subsequently transported through the monsoon circulation; we note that the detailed attribution of such tropospheric sources is difficult based on the sparsely sampled ACE-FTS measurements. Recent model simulations of global HCN variability (*25*) suggest enhanced sources linked to the Indonesian fires in late 2004 and 2006, and the persistence into the following years and entrainment into the Asian monsoon circulation is reasonable given the long HCN photochemical lifetime in the free atmosphere.

These HCN observations demonstrate a large discernible chemical influence on the stratosphere from the Asian monsoon circulation. This pathway complements the large-scale troposphere-to-stratosphere transport that occurs in the deep tropics throughout the year (*26*), and there are likely distinct source regions for air within each pathway. Upwelling over the deep tropics primarily transports air with recent contact with the ocean surface and less concentrated anthropogenic influences. In contrast, transport in the monsoon region connects surface air with enhanced pollution (biomass and biofuel burning, plus urban and industrial emissions) to the lower stratosphere. Model calculations (*6*) suggest that surface emissions over a broad region covering India to eastern Asia are entrained into the monsoon circulation and transported to the lower stratosphere. This air will have enhanced black and organic carbon, sulfur dioxide (SO_2), reactive nitrogen species (NOx), and possibly short-lived halogen compounds from Asian industrial emissions, which have the potential to influence stratospheric ozone chemistry, aerosol behavior, and associated radiative balances. For example, a recent increase in background stratospheric aerosol concentrations has been observed, possibly linked to growth in SO_2 emissions over China since 2002 (*27*), and the monsoon is an effective pathway for such transport. The monsoon influence on the stratosphere is expected to become increasingly important given the ongoing growth of Asian emissions (*28*), with large continued increases over the next decades expected for SO_2 and NOx. Furthermore, potential changes in the strength and variability of the Asian monsoon circulation in an evolving climate [linked to increased convection and rainfall (*29*)] could modify this transport pathway, with potential influence on composition and climate of the stratosphere.

References and Notes

1. Q. Li *et al.*, *Geophys. Res. Lett.* **32**, L14826 (2005).
2. W. J. Randel, M. Park, *J. Geophys. Res.* **111**, (D12), D12314 (2006).
3. R. Fu *et al.*, *Proc. Natl. Acad. Sci. U.S.A.* **103**, 5664 (2006).
4. M. Park, W. J. Randel, A. Gettelman, S. Massie, J. Jiang, *J. Geophys. Res.* **112**, D16309 (2007).
5. M. Park *et al.*, *Atmos. Chem. Phys.* **8**, 757 (2008).
6. M. Park, W. J. Randel, L. K. Emmons, N. J. Livesey, *J. Geophys. Res.* **114**, D08303 (2009).
7. K. H. Rosenlof, A. F. Tuck, K. K. Kelly, J. M. Russell III, M. P. McCormick, *J. Geophys. Res.* **102**, (D11), 13,213 (1997).
8. A. Gettelman, D. E. Kinnison, T. J. Dunkerton, G. P. Brasseur, *J. Geophys. Res.* **109**, (D22), D22101 (2004).
9. R. N. Bannister, A. O'Neill, A. R. Gregory, K. M. Nissen, *Q. J. R. Meteorol. Soc.* **130**, 1531 (2004).
10. C. P. Rinsland *et al.*, *J. Geophys. Res.* **104**, (D15), 18,667 (1999).
11. H. B. Singh *et al.*, *J. Geophys. Res.* **108**, (D20), 8795 (2003).
12. Q. B. Li *et al.*, *J. Geophys. Res.* **108**, (D21), 8827 (2003).
13. A. Kleinböhl *et al.*, *Geophys. Res. Lett.* **33**, L11806 (2006).
14. A. Lupu *et al.*, *Atmos. Chem. Phys.* **9**, 4301 (2009).
15. P. F. Bernath *et al.*, *Geophys. Res. Lett.* **32**, L15S01 (2005).
16. The ACE-FTS is a solar occultation instrument that provides limited space-time sampling, and the climatological HCN patterns in Figs. 1 and 2, and figs. S1 and S2, are derived by combining data from all years during 2004 to 2009.
17. C. D. Boone *et al.*, *Appl. Opt.* **44**, 7218 (2005).
18. D. P. Edwards *et al.*, *J. Geophys. Res.* **109**, (D24), D24202 (2004).
19. Figure 1B shows results from the National Center for Atmospheric Research 3D Whole Atmosphere Community Climate Model (WACCM). This version of WACCM is relaxed to observed meteorological fields from the Goddard Modeling and Assimilation Office (GMAO) GEOS5.1 data assimilation system. HCN has been added to the standard chemical mechanism with a chemical loss by reactions with OH [with a corresponding lifetime of 4.3 years (*13*)] and with $O(^1D)$. The model also includes wet deposition through washout (which is weak because HCN is insoluble) and parameterized dry deposition over open-ocean [with a corresponding lifetime of 3 months (*12*)]. HCN emissions were determined by scaling CO emissions (using 0.012 HCN/CO molar ratio) for biomass burning and anthropogenic biofuel combustion.
20. R. A. A. Plumb, *J. Geophys. Res.* **101**, (D2), 3957 (1996).
21. H. C. Pumphrey, C. J. Jimenez, J. W. Waters, *Geophys. Res. Lett.* **33**, L08804 (2006).
22. H. C. Pumphrey, C. Boone, K. A. Walker, P. Bernath, N. J. Livesey, *Geophys. Res. Lett.* **35**, L05801 (2008).
23. P. W. Mote *et al.*, *J. Geophys. Res.* **101**, (D2), 3989 (1996).
24. J. A. Logan *et al.*, *Geophys. Res. Lett.* **35**, L03816 (2008).
25. Q. Li, P. I. Palmer, H. C. Pumphrey, P. Bernath, E. Mahieu, *Atmos. Chem. Phys.* **9**, 8531 (2009).
26. S. Fueglistaler, H. Wernli, T. Peter, *J. Geophys. Res.* **109**, (D3), D03108 (2004).
27. D. Hofmann, J. Barnes, M. O'Neill, M. Trudeau, R. Neely, *Geophys. Res. Lett.* **36**, L15808 (2009).
28. T. Ohara *et al.*, *Atmos. Chem. Phys.* **7**, 4419 (2007).
29. H. Ueda, A. Iwai, K. Kuwako, M. E. Hori, *Geophys. Res. Lett.* **33**, L06703 (2006).

30. The ACE mission is funded primarily by the Canadian Space Agency. Some funding was also provided by the UK Natural Environment Research Council (NERC). The U.S. National Center for Atmospheric Research is sponsored by the National Science Foundation. We also acknowledge support from the U.S. National Aeronautics and Space Administration.

Supporting Online Material

www.sciencemag.org/cgi/content/full/science.1182274/DC1
SOM Text
Figs. S1 to S3

21 September 2009; accepted 3 March 2010
Published online 25 March 2010;
10.1126/science.1182274
Include this information when citing this paper.

Lab Experiments for the Study of Social-Ecological Systems

Marco A. Janssen,[1]* Robert Holahan,[2] Allen Lee,[1] Elinor Ostrom[1,2]

Governance of social-ecological systems is a major policy problem of the contemporary era. Field studies of fisheries, forests, and pastoral and water resources have identified many variables that influence the outcomes of governance efforts. We introduce an experimental environment that involves spatial and temporal resource dynamics in order to capture these two critical variables identified in field research. Previous behavioral experiments of commons dilemmas have found that people are willing to engage in costly punishment, frequently generating increases in gross benefits, contrary to game-theoretical predictions based on a static pay-off function. Results in our experimental environment find that costly punishment is again used but lacks a gross positive effect on resource harvesting unless combined with communication. These findings illustrate the importance of careful generalization from the laboratory to the world of policy.

Designing and conducting laboratory experiments in the social sciences enables the unpacking of complex problems to examine the effects of different components on outcomes and to replicate results with diverse participants (*1*). In this report, we discuss an experimental research program on the study of social-ecological systems, especially the governance of common-pool resources (CPRs). CPRs are resource systems where the harvesting of resource units by one user subtracts units from a pool potentially available to others. Examples in the field include forests, pastures, fisheries, and water systems.

The widely accepted economics textbook model of CPRs (*2*, *3*) is a simple, static production function that is used to conclude that the users of a

CPR would drastically overharvest or exhaust it. In his often-cited article, Hardin (*4*) concluded that overharvesting of a CPR was inevitable unless an external authority imposed rules on the helpless users. Hardin's judgment has been widely accepted because of its consistency with predictions from resource economics (*3*) and noncooperative game theory (*5*) and with well-publicized examples of resource collapses (*6*, *7*).

Extensive field research has challenged the prediction that it is impossible for users to self-organize (*8*). Many users have crafted their own institutions to overcome the temptations to overharvest, but others have not. Successful efforts reflect the struggle involved to overcome the incentives to overharvest and the costs of self-organization (*9*).

In light of substantial fieldwork on CPRs and growing use of experimental methods related to a variety of social dilemma games, researchers initiated the first CPR experiments in the late 1980s to test the simple model that was accepted as representing the core dilemma faced by harvesters (*10*). The initial CPR experiments focused on testing the accepted economic model of resource harvesting. We present an experimental environment that goes beyond traditional dilemma experiments to include spatial and temporal dynamics as used in laboratory experiments of complex systems (*11*–*13*) but not yet of CPR dilemmas.

When participants in the initial CPR experiments made independent and anonymous decisions, they substantially overharvested as predicted (*10*). Keeping the underlying mathematical structure representing the costs and benefits of harvesting constant, scholars slowly added variables identified as present in successful and unsuccessful field sites to the experimental settings and found that several made a substantial difference. Allowing participants to engage in face-to-face communication, called "cheap talk" by game theorists, in a CPR experiment where contribution levels were still made anonymously made a very substantial difference (*10*), as it had in many other dilemma situations (*14*).

Further, enabling participants to pay a fee in order to fine another participant also improved gross benefits in CPR experiments (*10*), as well as in some public-good experiments (*15*, *16*). In multiple CPR and public-good experiments, however, the costs of punishment outweighed the benefits of increased cooperation (*10*, *17*–*19*). In the CPR experiments, net benefits became positive when a further experimental enhancement was made—allowing the participants to communicate among themselves and to decide whether or not to adopt a sanctioning system and how much the fines and fees should be (*10*, *20*, *21*). In public-good experiments, increasing the number of rounds also led to net benefits (*22*), as well as combining communication with punishment (*19*, *23*).

The experiments reported herein take an important step toward approximating more closely the decisions users face in field settings, where the decision to harvest usually involves spatial and temporal dynamics instead of simple decisions regarding how much to harvest in an unchanging ecology (*24*–*26*). In a fishery, for example, the fish move rapidly from one location to another. Fishers have to figure out where and how many fish to collect without knowing for sure the specific benefits and costs of each harvesting decision (*3*, *26*).

In previous resource dilemma experiments, participants made decisions individually on a round-by-round basis. Each round typically required one decision. In field settings, decision-making does not have this orderly fashion. The study of dynamic decision-making includes decisions made in context and over time (*11*). Computerized microworlds are used to study dynamic decision-making such as fighting forest fires or leading an organization (*12*). We used methods of dynamic decision-making in order to perform controlled experiments that examine the relevant complexity of social-ecological systems.

Our experimental environment is built as follows (*27*). In each experiment, a group of five participants harvests tokens from a shared renewable resource on a 29-by-29 computer-simulated grid of cells (Fig. 1A). The resource's renewal rate is density dependent (Fig. 1B) to reflect simple ecological dynamics. The participants collect tokens in real time by pressing the arrow keys (left, right, up, and down) to move their avatars around the screen and pressing the space bar to collect a token from the cell on which the avatar is located. Each token is worth 2 cents. Participants make multiple decisions within each 4-min decision period. When participants behave like short-term, entirely self-interested actors, the resource will rapidly be exhausted, the group will collect only a few more than the initial number of 210 tokens, and the participants will face an empty screen for the remaining time in the decision period. On the other hand, if participants restrain themselves and deliberately think about where and when to harvest, the group earnings can increase to 665 tokens in a 4-min decision period [the average expected maximum is derived in the supporting

[1]Arizona State University, Post Office Box 872402, Tempe, AZ 85287–2402, USA. [2]Indiana University, 513 North Park Avenue, Bloomington, IN 47408–3895, USA.

*To whom correspondence should be addressed. E-mail: Marco.Janssen@asu.edu

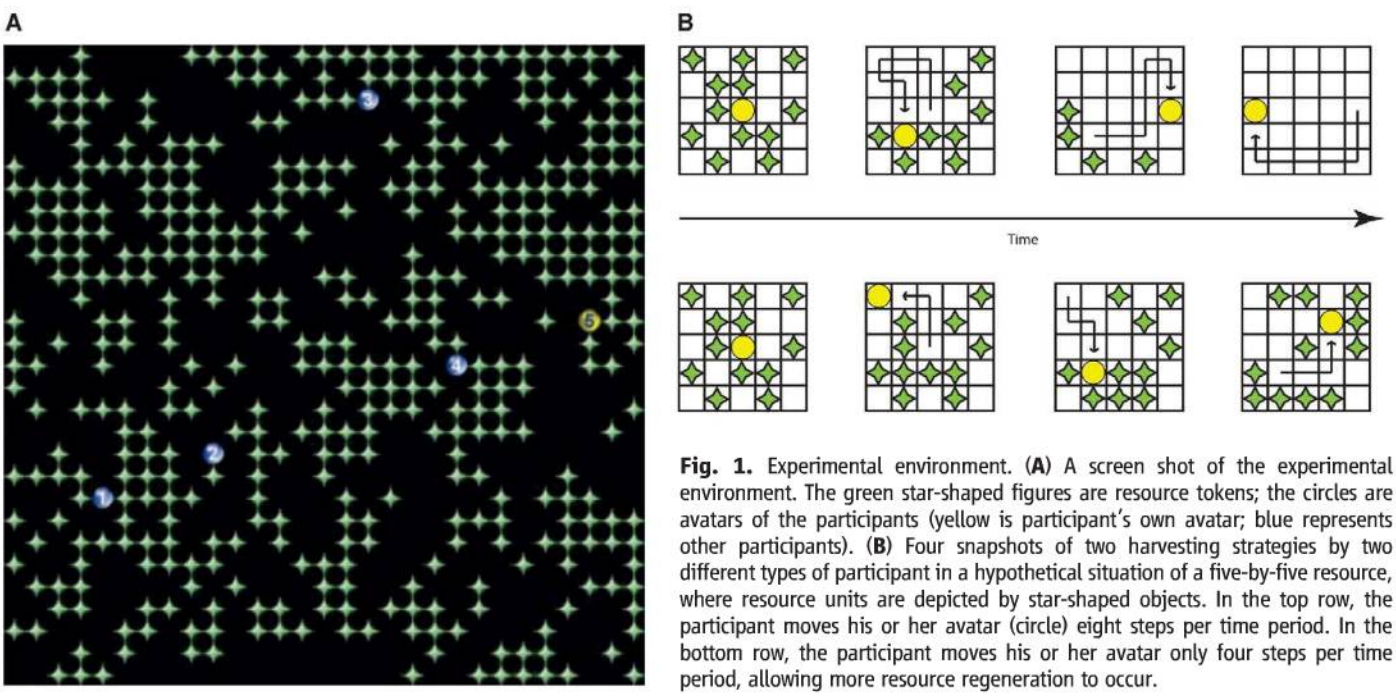

Fig. 1. Experimental environment. (**A**) A screen shot of the experimental environment. The green star-shaped figures are resource tokens; the circles are avatars of the participants (yellow is participant's own avatar; blue represents other participants). (**B**) Four snapshots of two harvesting strategies by two different types of participant in a hypothetical situation of a five-by-five resource, where resource units are depicted by star-shaped objects. In the top row, the participant moves his or her avatar (circle) eight steps per time period. In the bottom row, the participant moves his or her avatar only four steps per time period, allowing more resource regeneration to occur.

online material (SOM)]. In the optimal strategy, the group maintains a 50% density of tokens for most of the decision period and then rapidly harvests the remaining tokens at the end of the decision period. In periods where punishment is allowed, participants can subtract two tokens from another participant at the cost of one of their own tokens. Written communication, when implemented, takes place via text messages in a "chat room" before a decision period.

We conducted a series of experiments to test the impact of communication and punishment. The findings that participants use costly punishment, contrary to theoretical predictions, has stimulated a large number of CPR and public-good experiments during the past decade to test the generality of the earlier findings (*16*). In previous experiments, all participants first made an investment decision and then were given a special decision moment when they could decide to punish one of the other participants. In the current experimental environment, all decisions are real time (within the 4-min period).When the period includes costly punishment, participants can pay to punish whenever they see reason to as long as they have funds in their account and tokens remain on the screen to be harvested.

To test the effect of costly punishment versus communication, we performed a series of experiments using six different treatments. Each treatment consisted of three consecutive 4-min periods of costly punishment (P), communication (C), or a combination of both (CP) and three consecutive 4-min periods when neither communication nor punishment (NCP) is allowed. All treatments thus consisted of six decision periods, each lasting 4 min. Half the treatments started with NCP and the others finished with NCP. Each treatment was run five or six times. In total, 165 persons participated in 33 groups.

When participants started with three periods of NCP, the resource was consistently depleted within about 90 s, confirming that without communication or punishment, the "tragedy of the commons" prediction of Hardin is supported (Fig. 2). In this treatment, we found that the depletion of the resource occurred even faster in periods 2 and 3 than it did in period 1.

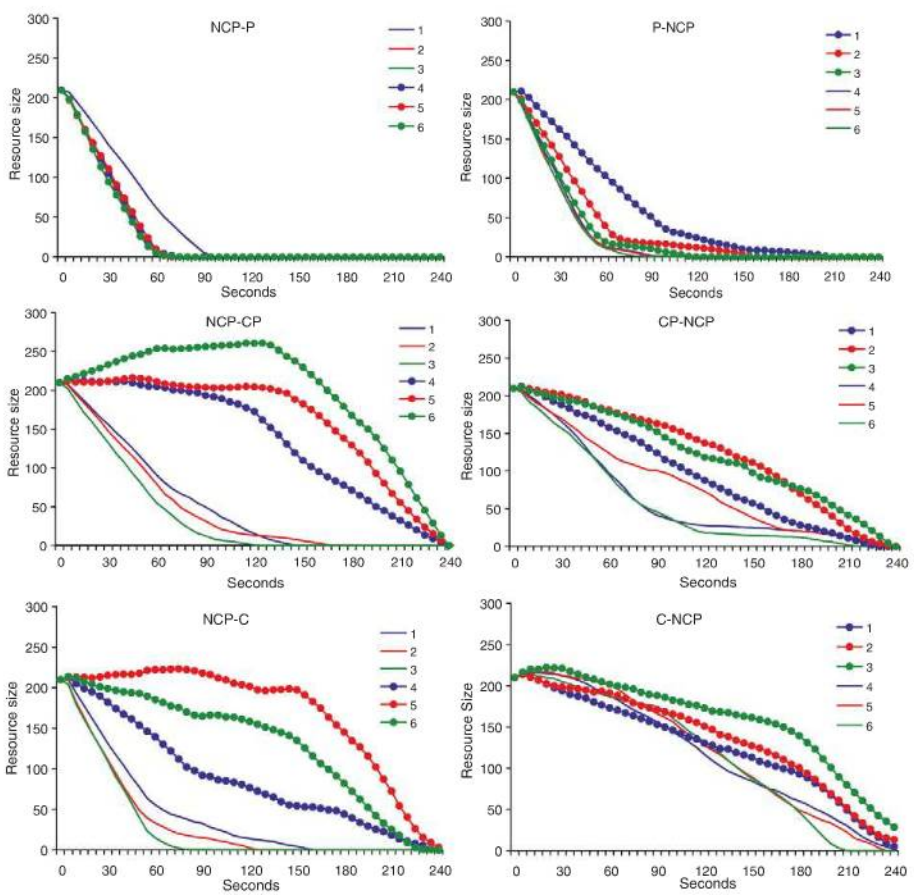

Fig. 2. Resource availability at given times. The diagrams show the average remaining level of the resource for the five or six groups of each treatment. Each diagram shows a treatment condition, and each line represents a particular period. The treatment is a combination of two sets of three periods of a specific condition. The names for these conditions are noted in the upper left of each display: NCP for neither communication nor costly punishment, C for communication, P for costly punishment, CP for communication and costly punishment. A treatment A-B refers to condition A for the first three periods and B for the last three periods. The colors and shapes referring to data of each period are noted in the upper right.

Periods with communication lead on average to a slower harvesting rate and more resource regeneration. Thus, earnings in periods 4 to 6 of C were significantly higher than in periods 1 to 3 of NCP. The strategies discussed by the participants in the C periods focused on the timing and location of harvesting. A common strategy worked out during the communication phase was to refrain from any harvesting for a set length of time, thereby allowing the resource to regenerate (see examples in SOM). When participants started with C periods, the amount of earnings did not drop significantly when participants were no longer able to communicate after period 3 (Fig. 3).

When P was introduced in period 4 after the first three periods were NCP, significant reductions in gross earnings occurred (Fig. 3), with an average of three punishment events per period. When participants started with CP periods and ended with NCP periods, significant reductions in the gross levels of tokens collected from the resource also occurred in the last three periods. Reduction in earnings in the last NCP periods were not found, however, when C is used in the first three periods. A puzzling finding is why communication with punishment does not lead to as long-lasting cooperative behavior as communication without punishment. Additional analysis (see SOM) shows that when participants used punishment in CP periods, we observed a reduction of the earnings in the last three NCP periods. This did not happen when participants did not use punishment in CP periods. It appears that the use of punishment erodes any cooperative agreements that were made, which are then less likely to persist when punishment and communication are not available anymore.

Punishment was not used by the participants in half of the periods when it was allowed. On average, there were 2.03 punishment events if communication was possible before the periods and 3.09 punishment events if communication was not allowed before the periods. In experiments with and without communication, a participant who was punished punished back 9 and 13% of the time, respectively. This appears to be a form of retaliation. Public-good studies that allow counterpunishment also found low levels of punishment and cooperation (*28*, *29*).

In the postexperiment survey, participants indicated that an important reason for the reluctance to punish others when communication was not allowed was their fear of retaliation (table S6). This reason was not mentioned for the treatments in which participants can communicate. If participants can communicate, the main reason they gave for punishing others, when they did, was for not following the agreements. Going too fast or having too many tokens were given as other reasons for punishment when participants cannot communicate, which is confirmed by the analysis of punishment events. In addition to using costly punishment, participants will scold others whom they consider to be free riders if communication is enabled (see examples in the SOM).

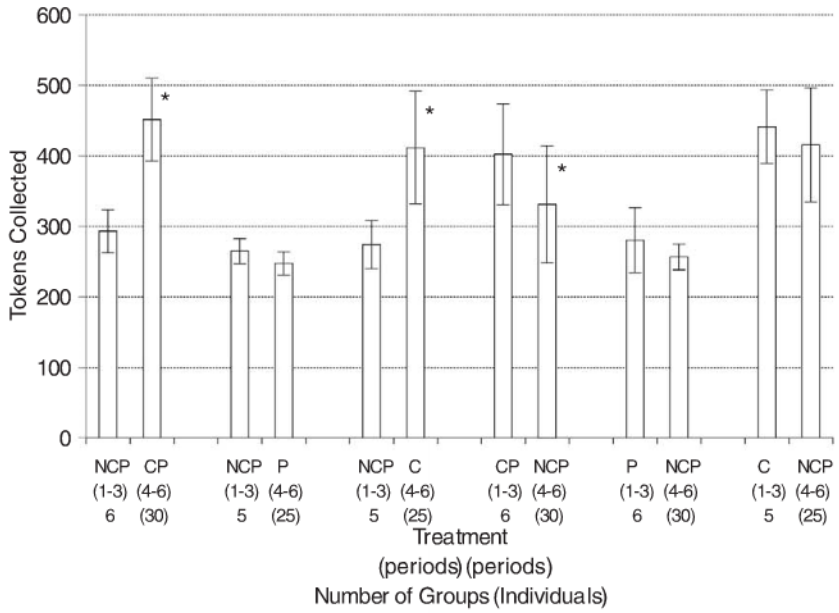

Fig. 3. Average net number of tokens collected by groups per period. The tokens lost due to punishment are subtracted from the total tokens harvested. Six different treatments are distinguished with combinations of neither communication nor costly punishment (NCP), communication (C), costly punishment (P), or communication and costly punishment (CP). Asterisks (*) refer to statistically significant differences between the first three and last three periods ($P < 0.01$) using a pairwise, two-tailed Mann-Whitney test.

Table 1. Punishment, communication, and harvesting levels. A multilevel mixed-effects linear regression is performed with the gross number of tokens that groups collected for each period. The independent variables are a set of dummy variables: whether participants could communicate and/or punish during the period and whether participants could have communicated and/or punished during the first three periods. Learning is tested by the effect of experiencing the same condition during multiple periods by including a dummy variable that indicates whether it is the first, second, or third time in this condition. LearnNCP is zero when it is not in the NCP condition, 1 for the first time in a NCP condition, 2 for the second time, and 3 for the third time. LearnCP, LearnC, and LearnP are defined in the same way.

Independent variables	Dependent variable: tokens harvested by group (SE)
Constant	298.147** (13.494)
Communication in current period (0 = no, 1 = yes)	92.130** (23.157)
Punishment in current period (0 = no, 1 = yes)	3.862 (22.475)
Communication and punishment in current period (0 = no, 1 = yes)	13.015 (26.944)
Communication in first three periods (0 = no, 1 = yes)	121.260** (16.744)
Punishment in first three periods (0 = no, 1 = yes)	−31.554* (15.786)
Communication and punishment in first three periods	−17.230 (26.476)
LearnNCP	−9.576* (4.818)
LearnCP	4.314 (3.505)
LearnC	17.111* (8.649)
LearnP	−13.127 (8.255)
−Log likelihood	1038.726
Number of decision periods	198
Variance contributions	
Group	38.567 (5.709)
Individual	39.138 (2.164)
χ^2	66.55 ($P < 0.001$)

*$P < 0.05$, **$P < 0.01$

A statistical analysis in Table 1 summarizes our findings. Communication leads to a significant increase in the number of tokens groups collected. In each C period, the number of tokens collected increases. When communication is not allowed in subsequent periods, previous communication still has a positive effect on the level of cooperation. The number of tokens collected remains significantly higher than without any communication.

Why does costly punishment (without communication) in a dynamic spatial environment lack a positive effect on resource use? In a modestly complex dynamic and spatial environment where participants can punish back but cannot discuss why they are punished, receiving a sanction does not carry a clear message. Does the sanction relate to the amount harvested, the location, the spatial pattern of harvesting, the speed in which the avatar moves over the screen, etc.? Communication can answer these questions and becomes an important attribute of the experiment for raising payoffs. When communication is possible, punished participants correct their harvesting rate by slowing down. On the other hand, punished participants in periods without communication do not behave differently from other participants (table S6).

What makes communication effective and able to affect decisions even after it is no longer feasible? Why is costly punishment ineffective in the short run with negative effects in the long run? Although the effectiveness of communication for small groups has been known for a long time, scholars propose diverse motivations (*30*). Communication can affect the understanding participants have of the resource system (*31*), change the expectations of others' behavior (*32*), coordinate strategies (*31*), or create the feeling of peer pressure (*31*, *32*) or a "group feeling" (*31*). When groups in the field are dependent on the resources, can meet from time to time to discuss the problems they face, and can make their own agreements, they are more likely to self-organize to govern the commons (*24*).

We have presented an experimental environment that begins to capture the spatial and temporal complexity of field settings. Our experiments confirm that participants will use costly punishment. The use of punishment without communication, however, does not increase gross payoffs. When communication is allowed, the performance of the group increases significantly. The performance is not sustained when punishment is used and communication is no longer possible. These results stress the importance of communication in commons dilemmas. This new experimental environment will enable scholars to test the generalizability of these results for different contexts such as mobile versus stationary resource units, visibility of resource extraction activities, and predictability of resource dynamics (*24*).

In order to translate findings from experimental research to policy analysis for social-ecological systems, it is important to understand the structures of both the social systems and the resource systems. Field studies have established the im-

portance of including this complexity, and we have demonstrated how experimental research can begin to introduce more of the spatial and temporal processes found in many social-ecological systems.

References and Notes

1. A. Falk, J. J. Heckman, *Science* **326**, 535 (2009).
2. H. S. Gordon, *J. Polit. Econ.* **62**, 124 (1954).
3. C. W. Clark, *The Worldwide Crisis in Fisheries* (Cambridge Univ. Press, Cambridge, 2006).
4. G. Hardin, *Science* **162**, 1243 (1968).
5. P. S. Dasgupta, G. M. Heal, *Economic Theory and Exhaustible Resources* (Cambridge Univ. Press, Cambridge, 1979).
6. J. Radovich, in *Resource Management and Environmental Uncertainty*, M. Glantz, J. D. Thompson, Eds. (Wiley, New York, 1981), pp. 107–136.
7. R. A. Myers, J. A. Hutchings, N. J. Barrowman, *Ecol. Appl.* **7**, 91 (1997).
8. National Research Council, *The Drama of the Commons* (National Academies Press, Washington, DC, 2002).
9. T. Dietz, E. Ostrom, P. C. Stern, *Science* **302**, 1907 (2003).
10. E. Ostrom, J. M. Walker, R. Gardner, *Am. Polit. Sci. Rev.* **86**, 404 (1992).
11. B. Brehmer, *Acta Psychol. (Amst.)* **81**, 211 (1992).
12. D. Dörner, *The Logic of Failure* (Perseus Books, Reading, MA, 1996).
13. R. L. Goldstone, M. E. Roberts, T. M. Gureckis, *Curr. Dir. Psychol. Sci.* **17**, 10 (2008).
14. D. Sally, *Rationality Soc.* **7**, 416 (1995).
15. E. Fehr, S. Gächter, *Am. Econ. Rev.* **90**, 980 (2000).
16. S. Gächter, B. Herrmann, *Philos. Trans. R. Soc. London Ser. B* **364**, 791 (2009).
17. B. Herrmann, C. Thöni, S. Gächter, *Science* **319**, 1362 (2008).
18. M. R. Sefton, R. Shupp, J. Walker, *Econ. Inq.* **45**, 671 (2007).
19. O. Bochet, T. Page, L. Putterman, *J. Econ. Behav. Organ.* **60**, 11 (2006).
20. Ö. Gürerk, B. Irlenbusch, B. Rockenbach, *Science* **312**, 108 (2006).
21. M. Casari, L. Luini, *J. Econ. Behav. Organ.* **71**, 273 (2009).
22. S. Gächter, E. Renner, M. Sefton, *Science* **322**, 1510 (2008).
23. O. Bochet, L. Putterman, *Eur. Econ. Rev.* **53**, 309 (2009).
24. E. Ostrom, *Science* **325**, 419 (2009).
25. E. Schlager, W. Blomquist, S. Y. Tang, *Land Econ.* **70**, 294 (1994).
26. J. A. Wilson, J. M. Acheson, M. Metcalfe, P. Kleban, *Mar. Policy* **18**, 291 (1994).
27. Materials and methods, experimental design and protocol, and additional analysis are available as supporting material on *Science* Online.
28. L. Denant-Boemont, D. Masclet, C. N. Noussair, *Econ. Theory* **33**, 145 (2007).
29. N. Nikiforakis, *J. Public Econ.* **92**, 91 (2008).
30. N. R. Buchan, E. J. Johnson, R. T. A. Croson, *J. Econ. Behav. Organ.* **60**, 373 (2006).
31. G. Bornstein, in *Social Dilemmas*, W. Leibrand, D. Messick, H. Wilke, Eds. (Pergamon Press, Oxford, UK, 1992), pp. 247–263.
32. D. M. Messick, M. B. Brewer, in *Review of Personality and Social Psychology*, L. Wheeler, P. Shaver, Eds. (Sage, Beverly Hills, CA, 1983), pp. 11–44.

33. This research was funded by the U.S. NSF (grants BCS 0625354 and SES 0748632). We thank R. Goldstone, R. Tobias, J. Walker, and the Workshop's Experimental Reading Group for helpful comments and the Interdisciplinary Experimental Laboratory at Indiana University for providing use of its facility.

Supporting Online Material

www.sciencemag.org/cgi/content/full/328/5978/613/DC1
Materials and Methods
Figs. S1 to S10
Tables S1 to S7

19 October 2009; accepted 22 March 2010
10.1126/science.1183532

Coordinated Punishment of Defectors Sustains Cooperation and Can Proliferate When Rare

Robert Boyd,[1,2]* Herbert Gintis,[2,3,4]* Samuel Bowles[2,5]*

Because mutually beneficial cooperation may unravel unless most members of a group contribute, people often gang up on free-riders, punishing them when this is cost-effective in sustaining cooperation. In contrast, current models of the evolution of cooperation assume that punishment is uncoordinated and unconditional. These models have difficulty explaining the evolutionary emergence of punishment because rare unconditional punishers bear substantial costs and hence are eliminated. Moreover, in human behavioral experiments in which punishment is uncoordinated, the sum of costs to punishers and their targets often exceeds the benefits of the increased cooperation that results from the punishment of free-riders. As a result, cooperation sustained by punishment may actually reduce the average payoffs of group members in comparison with groups in which punishment of free-riders is not an option. Here, we present a model of coordinated punishment that is calibrated for ancestral human conditions and captures a further aspect of reality missing from both models and experiments: The total cost of punishing a free-rider declines as the number of punishers increases. We show that punishment can proliferate when rare, and when it does, it enhances group-average payoffs.

Humans are a uniquely cooperative species. In even the simplest societies, people cooperate in large groups of genealogically distant individuals (*1*–*3*). In the laboratory, subjects routinely cooperate in situations in which selfish agents would free-ride on the cooperation of others (*4*, *5*). Recent theoretical studies provide an evolutionary explanation for such cooperative behavior: Punishment reduces gain to free-riding, so groups with more punishers can sustain more cooperation (*6*–*9*). Punishment is costly, but unlike unconditional altruism its costs are greatly reduced when punishers are common because punishment then occurs at very low frequency, is effective, and its costs can be shared. As a result, a modest advantage of groups in which cooperation is sustained by the presence of punishers is sufficient to compensate them for the cost of punishment.

There are two important problems with this explanation of human cooperation. First, punishment can reduce the average payoffs of group members because the costs of punishment may exceed the gains from cooperation (*5*). This problem is exacerbated when punishers target cooperative group members, as sometimes occurs in experiments (*10*–*12*). Second, the initial emergence of punishment remains a puzzle. In order to survive, punishers must engage in enough punishment of defectors so that the induced cooperation more than offsets the cost of punishing. Rare punishers do not have the benefit of outnumbering their targets, so the cost of punishing a free-rider is substantial. Moreover, they usually bear this cost alone rather than sharing it with other punishers (*13*–*16*).

These problems are an artifact of the unrealistic way that punishment is implemented in existing models and in most experiments. In these models, punishment is an unconditional and uncoordinated individual action automatically triggered by defection. Similarly and with few exceptions (*17*), in experiments individuals cannot coordinate their punishment. In contrast, ethnographic evidence indicates that punishment is coordinated by means of gossip and other communication among punishers, is contingent on the expected effectiveness of punishment in inducing cooperation, and is not undertaken unless it is judged as legitimate by most group members (*18*–*20*). When it occurs, punishment is usually collective and conveys a message of peer condemnation. Consistent with the anthropological evidence, in behavioral experiments with communication or with the option of coordinating behavior punishment is often highly effective in raising group average payoffs (*21*).

We analyzed a model of the evolution of punishment that incorporates two empirically based features absent from previous work. First, punishment is coordinated among group members so that it is contingent on the number of others predisposed to participate in the punishment. This means that when individuals willing to punish are rare, they demur and so bear only the cost of signaling their willingness to punish. They thus avoid the cost of punishing when it

[1]Department of Anthropology, University of California, Los Angeles, CA 90064, USA. [2]Behavioral Sciences Program, Santa Fe Institute, 1399 Hyde Park Road, Santa Fe, NM 87501, USA. [3]Department of Economics, Central European University, Nádor utca 9, 1051 Budapest, Hungary. [4]Collegium Budapest, Szentharomsag utca 2, 1014 Budapest, Hungary. [5]Department of Economics, University of Siena, Piazza San Francesco 7, Siena 53100, Italy.

*To whom correspondence should be addressed. E-mail: rboyd@anthro.ucla.edu (R.B.); hgintis@comcast.net (H.G.); samuel.bowles@gmail.com (S.B.)

does not pay. Second, consistent with the "strength in numbers" and "divide and rule" maxims punishment is characterized by increasing returns to scale, so the total cost of punishing a single free-rider declines as the number of punishers increases. Adding these two features resolves the problems with previous models. Our model shows that for levels of relatedness consistent with recent genetic data from hunter-gather populations (*22*), punishment can proliferate when rare, and when it is common it increases group-average fitness.

In our model, a large population of individuals interact repeatedly in groups of size n. Groups are randomly formed, so there is no genetic assortment. Later, we will introduce an empirically plausible degree of genetic assortment. The model is fully described in (*23*). After the formation of a group, there is an initial period of an interaction that has three stages. First is a signaling stage, in which individuals can signal their intent to punish defectors. The cost of signaling, q, is high enough so that it does not pay to signal and then fail to punish. There follows a cooperation stage, during which individuals can choose to cooperate or defect. Cooperation costs the cooperator c and benefits each member of the group b/n ($b > c > b/n$). Lastly, there is a punishment stage in which punishers can coordinate to inflict a cost p on the target at an expected cost to each punisher of k/n_p^a, where n_p is the number of punishers. Given that a greatly outnumbered target is unlikely to inflict costs on any of the punishers, it is plausible that $a > 1$: There are increasing returns to scale, so the punishers' total cost of a punishment episode decreases as the number of punishers increases. During subsequent periods, there are only cooperation and punishment stages. The interaction continues to another period with probability $(1 - 1/T)$, so T is the expected number of periods until the group disbands and new groups are drawn from the population.

Population structures like this one, in which groups do not persist but are created anew for each interaction by drawing individuals from a larger population (*24*–*26*), are useful because they provide an analytically tractable approximation to more realistic structures. In the first interaction of such models, individuals have no common history (as they would if we modeled persistent groups) and hence cannot know anything about strategies of other group members. To address this information problem, we introduced a first "information gathering" period in which individuals know nothing about their group mates. This extreme assumption exaggerates the costs of signaling and establishing whether a quorum for punishment exists, but it captures an important fact: Even in the more realistic setting of persistent groups, individuals change, die, or leave the group and are replaced by migrants or offspring. This means that actors must deal with situations in which the past behavior of some group members is unknown, which is analogous to the first period in the present model. We believe that the present model represents a worst case for the evolution of punishment because it maximizes the level of uncertainty about the strategies of others.

Individuals have one of two heritable strategies: "punisher" and "nonpunisher." Cooperation and free-riding are not inherited strategies. Rather, they are choices that individuals make in light of the incentives provided by the prospect of punishment. During the first interaction, punishers signal that they are willing to punish. Next, if at least τ ($0 \le \tau \le n - 1$) other group members signal, punishers cooperate with probability $1 - e$ and defect with probability e and then punish any individual who did not cooperate. We refer to punishers with a threshold of τ as "τ-punishers." If fewer than τ other individuals signaled during the first stage, punishers defect and do not punish. Nonpunishers do not signal, defect, and do not punish, and as a result are punished if there are at least $\tau + 1$ punishers in the group. During subsequent periods, both types cooperate with probability $1 - e$ and defect with probability e if defectors were punished the last time a defection occurred. Punishers punish defectors if at least τ other individuals punished the last time a defection occurred. The cost of being punished to the target, p, is greater than the net cost of cooperating, $c - b/n$, so on average cooperation is the payoff maximizing action if punishment is anticipated. A fraction e individuals nonetheless defects, either due to error or because cooperation is more costly for some individuals and so it does pay for them to cooperate, even if they expect to be punished. Nonpunishers are a plausible ancestral state for the evolution of punishment. They do not cooperate or punish, nor do they respond to unverified threats. However, once they have been punished they cooperate in subsequent periods in order to avoid more punishment.

It has been argued that punishment can evolve only when it is linked to cooperation (*27*).

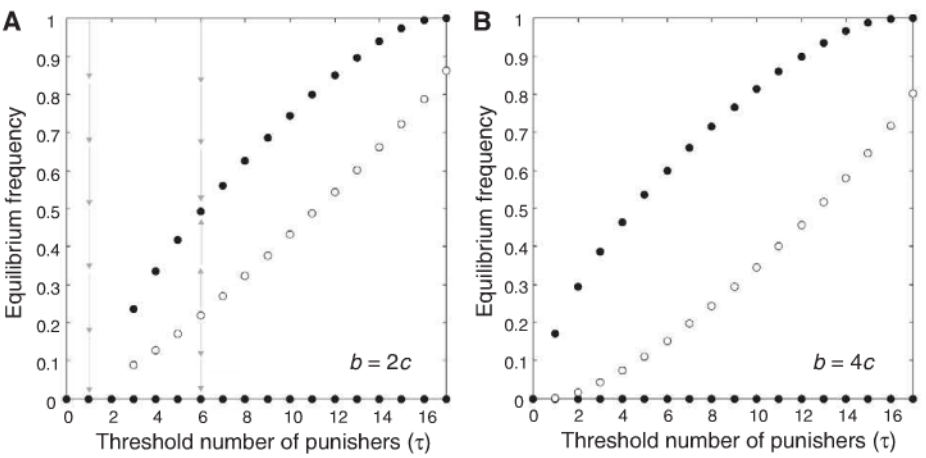

Fig. 1. Equilibrium frequencies of punishers with a threshold frequency of τ when group members are unrelated for two values of b. For each value of τ, the solid circles give locally stable equilibrium frequencies of the punishing type, and the open circles give interior unstable equilibrium frequencies. (**A**) $b = 2c$. For $\tau < 3$, the only stable equilibrium is a population without punishers. For larger thresholds, there are two stable equilibrium frequencies, zero and a stable interior equilibrium at which punishers and nonpunishers coexist. The arrows indicate the effect of natural selection at points above and below the solid and open circles. In these cases, the unstable equilibria mark the frequency that punishers must achieve before they are favored by selection. (**B**) $b = 4c$. Now, there are two equilibria for all values $\tau > 0$. Benchmark parameters are $c = 0.01$, $q = k = p = 1.5c$, $r = 0$, $a = 2$, $e = 0.1$, $n = 18$, and $T = 25$. The parameter r is the genetic relatedness among group members.

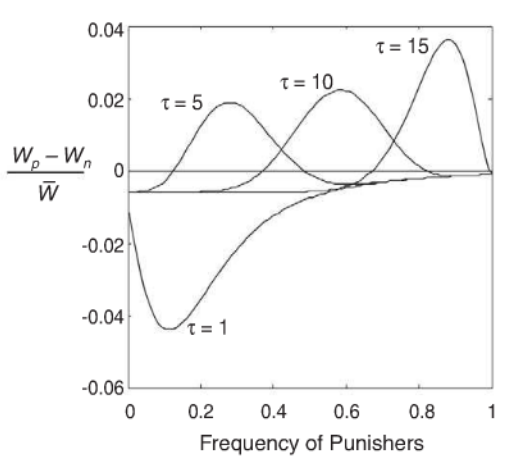

Fig. 2. The difference in fitness of punishers (W_p) and nonpunishers (W_n) as a function of the frequency of punishers. When this difference is positive, punishers increase in frequency, and when it is negative punishers decrease in frequency. Equilibria occur when this difference is zero (evolutionarily stable when the function intersects the horizontal axis from above and unstable otherwise). When $\tau = 1$, punishment at the threshold does not pay for any frequency of punishers, and thus increasing the frequency of punishers from zero decreases their relative fitness. For larger values of τ, punishment at the threshold does pay, and thus increasing the frequency of punishers increases their fitness. This leads to a stable polymorphic equilibrium at which punishers and nonpunishers coexist. $b = 2c$; other parameters are as in Fig. 1A.

After the first period, punishers and nonpunishers cooperate under exactly the same conditions: the presence of sufficiently many punishers in the group so that free-riding does not pay, so that the linkage between cooperation and punishment is very weak. In (*23*), we show that even this weak linkage is not necessary for the evolution of punishment.

After the social interaction just described, individuals reproduce at a rate that is proportional to their payoff as compared with the population-average payoff leading to the equations (*23*) that describe how natural selection changes the frequencies of the two types through time.

In the absence of genetic assortment, there are two long-run evolutionary outcomes (Fig. 1). First, a population of all nonpunishers is evolutionarily stable as long as solitary punishers do not punish ($\tau > 0$). When punishers are rare in the population, they will most often be alone in a group. Thus, they pay the cost of signaling but do not reap the benefits of cooperation, and as a result will have lower fitness than nonpunishers. Punishers who are willing to punish alone ($\tau = 0$) cannot invade a population of all nonpunishers unless the benefits from cooperation are so large that a single punisher can recoup the costs of signaling and punishing everyone else in the group. Here, we assume that this "Lone Ranger" condition is not satisfied so that only punishment by two or more punishers pays.

Mixtures of punishers and nonpunishers can also be evolutionarily stable. Punishers have an advantage over nonpunishers only in groups in which there are exactly $\tau + 1$ punishers because in such "threshold groups," each punisher is necessary to sustain punishment and therefore cooperation. In groups with fewer than $\tau + 1$ punishers, punishers pay the cost of signaling, but because they do not punish they (like all group members) enjoy no cooperative benefits. In groups with more than the critical number of punishers, a punisher who switched to nonpunishing would enjoy the same payoff from cooperation as other group members without paying the costs of signaling and punishment. This means that selection cannot favor τ-punishers unless they are in groups in which there are exactly $\tau + 1$ punishers and the benefits from cooperation are enough to compensate punishers for the costs of signaling and punishment. Moreover, the advantage enjoyed by punishers in these critical groups must be large enough to offset the payoff disadvantages suffered by punishers in groups with fewer or more than the critical numbers of punishers.

The existence of a stable mixture of punishers and nonpunishers depends on the value of the punishment threshold, τ. When the threshold is too low, punishment does not pay even at the threshold, and nonpunishment is the only evolutionarily stable strategy. At higher thresholds, punishment does pay in threshold groups, and this means that punishment may be favored if such groups are sufficiently common. Thus, as the frequency of punishers in the metapopulation increases from zero, the fraction of groups with the threshold number of punishers increases, and so does the expected fitness of punishers (Fig. 2). Once the fraction of threshold groups is high enough, the punishers' advantage in these groups offsets their disadvantage in all other groups. Then, natural selection will increase the frequency of punishers. This marks the unstable equilibria (open circles) shown in Fig. 1 and the leftmost zero intercept on the horizontal axis for each of the functions in Fig. 2.

Further increases in the metapopulation frequency of punishers eventually decrease the fraction of threshold groups. When, as a result, the fitness of punishers and nonpunishers is equalized, there is a stable polymorphic equilibrium (Fig. 1, solid circles, and Fig. 2, rightmost horizontal-axis intersection). As τ increases, the frequency of punishers at the polymorphic equilibrium also increases, but the minimum initial frequency of punishers required for selection to move a population to this equilibrium also increases, making it less accessible if punishers are initially rare.

At the stable polymorphic equilibrium, punishment is not altruistic: The punisher that switched to nonpunisher would experience no change in payoff. When groups are formed at random, averaged over all groups, the long-run benefits of punishment exactly compensate for the costs. However, it is mutually beneficial to the group (Fig. 3) in that populations with the equilibrium frequency of punishers have higher average fitness than populations without punishers. We show below that modest amounts of positive assortment in the formation of groups allow for the evolution of altruistic punishment.

The results presented so far depend critically on two parameters: the extent of economies of scale in punishment, a, and the cost punishers have to pay to signal their willingness to punish, q. Considering the first, were we to assume $a = 1$ (constant returns to scale) the total cost of punishing defectors would be independent of the number of punishers, and much higher frequencies of punishment would be required before punishment would become evolutionarily stable (*23*). This supports the intuition that increasing returns is crucial, and therefore the notion of coordinated punishment is important.

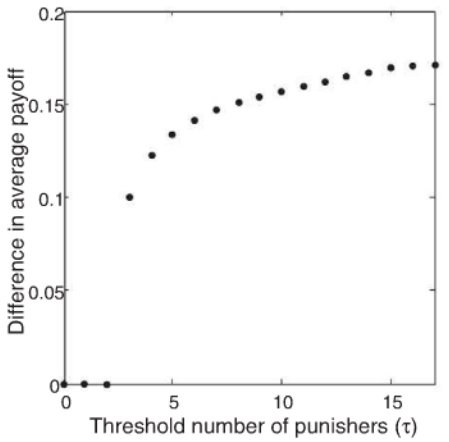

Fig. 3. The difference in average fitness between the polymorphic equilibrium at which punishers are present and the monomorphic nonpunishing equilibrium. Whenever the polymorphic equilibrium exists, it has higher average fitness, but near maximum benefit differences occur for relatively low thresholds. Benchmark parameters are as in Fig. 1A.

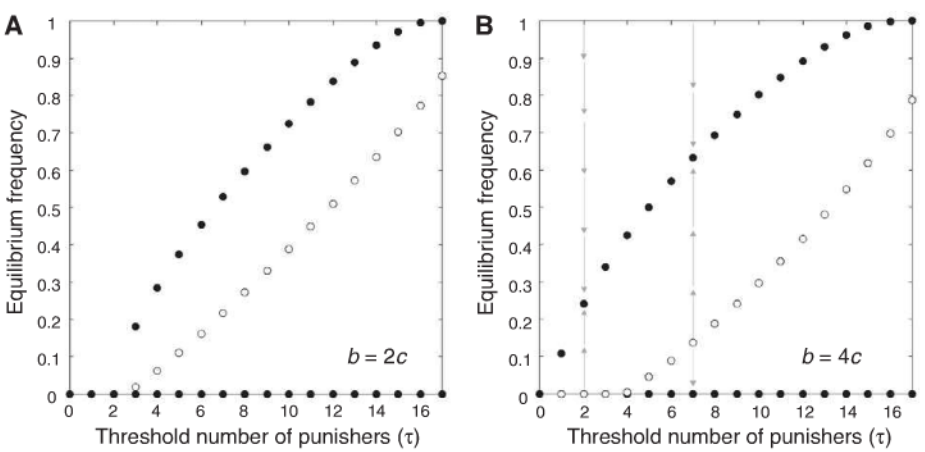

Fig. 4. Equilibrium frequencies of punishers with a threshold frequency of τ with modest assortment ($r = 0.07$) and two values of b. As in Fig. 1, for each value of τ the solid circles give locally stable equilibrium frequencies of the punishing type, and the open circles give unstable equilibrium frequencies. **(A)** $b = 2c$. As in the case with no assortment, for large enough values of τ there are two equilibria, but punishers cannot invade and increase when rare. **(B)** $b = 4c$. Now for $0 < \tau \leq 3$, rare punishers invade a population of nonpunishers, and the only stable equilibrium is a mixture of punishers and nonpunishers in which cooperation is sustained in most groups. For larger thresholds, there are two stable equilibrium frequencies, zero and a mixed strategy at which punishers and nonpunishers coexist. In these cases, the unstable equilibria (open circles) mark the frequency that punishers must achieve before they are favored by selection. Benchmark parameters are as in Fig. 1A, except $r = 0.07$.

To determine the minimum cost of signaling, q, necessary to ensure that the signal is honest, we introduced a third strategy: "liar," who may benefit by "turning on" the punishment process without paying the costs. During the first period, liars signal that they are punishers, incurring the signaling cost, and then cooperate so as to avoid punishment during the first period. However, they do not punish, and therefore avoid the associated costs. In subsequent periods, liars count the number of other group members that signaled in the first period and cooperate if the number of such signalers is greater than $\tau + 1$. Because liars never punish, after the first period they behave like nonpunishers and so receive the nonpunisher payoff. At equilibrium, punishers and nonpunishers have the same fitness, and thus liars can invade if their expected payoff during the first period is greater than the expected payoff of nonpunishers during the first period. This leads to a minimum cost of signaling, given in (*23*). The value of q used in our calculations satisfies this condition for all results presented here.

Although punishment is evolutionarily stable in this model, so is nonpunishment. A complete account of the evolution of cooperation must explain how punishing strategies can increase when rare. In their classic work on pairwise reciprocity, Axelrod and Hamilton (*24*) showed that a small amount of nonrandom assortment, such as interaction between weakly related group members, destabilizes noncooperative equilibria but not cooperative equilibria. This principle holds in a wide range of pairwise cooperative interactions, but not in larger groups (*13*–*15*).

To explore the effects of genetic assortment, we dropped our assumption that groups are formed at random and assumed that the relatedness within groups is $r > 0$, so that individuals are more likely to interact with individuals similar to themselves than expected by chance. Figure 4 shows the equilibrium behavior assuming that $r = 0.07$, which is a rough estimate of the average relatedness within human foraging groups (*22*). For low thresholds ($\tau \leq 3$), the only stable equilibrium is a mixture of punishers and nonpunishers, which means that punishers invade when rare. And because of the population structure (between-group genetic differences), punishment may also be altruistic at the polymorphic equilibrium.

This result persists when groups are much larger ($n = 72$) and for lower levels of relatedness if the benefit-cost ratio is somewhat higher (*23*). However, modest assortment does not allow punishment strategies with higher thresholds to invade populations of punishers with lower thresholds, so there is no evolutionary process in this model that would ratchet up the threshold levels. Thus, consistent with ethnographic observation the model predicts that only some individuals will engage in punishment. However, even when $\tau = 3$—meaning that a minimum of four out of 18 individuals punish—groups achieve about two thirds of the maximum gains from cooperation attainable with higher thresholds (Fig. 3).

Unlike many models of the evolution of punishment, this one does not suffer from a "second-order free-rider" problem in which individuals who cooperate but do not punish out-compete the punishers. To see why, consider a new strategy: "contingent cooperators," who cooperate during the first period if there are $\tau + 1$ signaling individuals but do not punish. Contingent cooperators avoid punishment during the first period and otherwise behave like nonpunishers, and thus have higher fitness than nonpunishers. As a result, they invade the polymorphic punisher-nonpunisher equilibrium, replacing the nonpunishers. However, because they still respond to punishment, and punishment still benefits punishers, the population evolves to a stable equilibrium at which punishers and contingent cooperators coexist and that cannot be invaded by other second-order free-riding types. The frequency of punishers at this new equilibrium is approximately the same as in the original punisher-nonpunisher equilibrium (*23*).

In our model, the initial proliferation of punishment occurs under plausible levels of group genetic differences and results in persistent and high levels of cooperation. This result depends on the contingent nature of punishment and the existence of increasing returns to punishment. It differs from the model of Hauert *et al.* (*28*), in which the population cycles between periods of cooperation, defection, and opting-out of the interaction entirely, the latter strategy invading the all-defect phase of the cycle and subsequently being invaded by cooperators. Although their model applies to some forms of cooperation, the present model is a more realistic representation of the nature and dynamics of human cooperation (*29*, *30*).

References and Notes

1. C. Boehm, *Hierarchy in the Forest: The Evolution of Egalitarian Behavior* (Harvard Univ. Press, Cambridge, MA, 2000).
2. P. Wiessner, *Evol. Hum. Behav.* **23**, 407 (2002).
3. H. Kaplan, K. Hill, *Curr. Anthropol.* **26**, 223 (1985).
4. E. Fehr, U. Fischbacher, *Nature* **425**, 785 (2003).
5. E. Fehr, S. Gachter, *Am. Econ. Rev.* **90**, 980 (2000).
6. R. Boyd, H. Gintis, S. Bowles, P. J. Richerson, *Proc. Natl. Acad. Sci. U.S.A.* **100**, 3531 (2003).
7. R. Andrés Guzmán, C. Rodríguez-Sickert, R. Rowthorn, *Evol. Hum. Behav.* **28**, 112 (2007).
8. K. Sigmund, *Trends Ecol. Evol.* **22**, 593 (2007).
9. J. Henrich, R. Boyd, *J. Theor. Biol.* **208**, 79 (2001).
10. O. Bochet, T. Page, L. Putterman, *J. Econ. Behav. Organ.* **60**, 11 (2006).
11. B. Herrmann, C. Thöni, S. Gächter, *Science* **319**, 1362 (2008).
12. M. Cinyabuguma, T. Page, L. Putterman, *Exp. Econ.* **9**, 265 (2006).
13. R. Boyd, P. J. Richerson, *J. Theor. Biol.* **132**, 337 (1988).
14. K. Panchanathan, R. Boyd, *Nature* **224**, 115 (2003).
15. R. Boyd, P. J. Richerson, *Ethol. Sociobiol.* **13**, 171 (1992).
16. A. Gardner, S. West, *Am. Nat.* **164**, 753 (2004).
17. E. Ostrom, J. Walker, R. Gardner, *Am. Polit. Sci. Rev.* **86**, 404 (1992).
18. P. Wiessner, *Hum. Nat.* **16**, 115 (2005).
19. C. Boehm, *Curr. Anthropol.* **34**, 227 (1993).
20. N. Q. Mahdi, *Ethol. Sociobiol.* **7**, 295 (1986).
21. A. Ertan, T. Page, L. Putterman, *Eur. Econ. Rev.* **53**, 495 (2009).
22. S. Bowles, *Science* **314**, 1569 (2006).
23. Materials and methods are available as supporting material on *Science* Online.
24. R. Axelrod, W. D. Hamilton, *Science* **211**, 1390 (1981).
25. M. A. Nowak, K. Sigmund, *J. Theor. Biol.* **194**, 561 (1998).
26. G. S. Van Doorn, G. M. Hengeveld, F. J. Weissing, *Behaviour* **140**, 1333 (2003).
27. L. Lehmann, F. Rousset, D. Roze, L. Keller, *Am. Nat.* **170**, 21 (2007).
28. C. Hauert, A. Traulsen, H. Brandt, M. A. Nowak, K. Sigmund, *Science* **316**, 1905 (2007).
29. R. Boyd, S. Mathew, *Science* **316**, 1858 (2007).
30. S. Mathew, R. Boyd, *Proc. Biol. Sci.* **276**, 1167 (2009).

31. We thank the Behavioral Sciences Program of the Santa Fe Institute, the U.S. National Science Foundation, the European Science Foundation, and the University of Siena for research support. The authors declare no competing interests.

Supporting Online Material

www.sciencemag.org/cgi/content/full/328/5978/617/DC1
Materials and Methods
Figs. S1 to S7
References

22 October 2009; accepted 23 March 2010
10.1126/science.1183665

Maternal Control of Haplodiploid Sex Determination in the Wasp *Nasonia*

Eveline C. Verhulst, Leo W. Beukeboom, Louis van de Zande*

All insects in the order Hymenoptera have haplodiploid sex determination, in which males emerge from haploid unfertilized eggs and females are diploid. Sex determination in the honeybee *Apis mellifera* is controlled by the *complementary sex determination* (*csd*) locus, but the mechanisms controlling sex determination in other Hymenoptera without *csd* are unknown. We identified the sex-determination system of the parasitic wasp *Nasonia*, which has no *csd* locus. Instead, maternal input of *Nasonia vitripennis transformer* (*Nvtra*) messenger RNA, in combination with specific zygotic *Nvtra* transcription, in which *Nvtra* autoregulates female-specific splicing, is essential for female development. Our data indicate that males develop as a result of maternal imprinting that prevents zygotic transcription of the maternally derived *Nvtra* allele in unfertilized eggs. Upon fertilization, zygotic *Nvtra* transcription is initiated, which autoregulates the female-specific transcript, leading to female development.

Mechanisms for sex determination are remarkably variable. In many insect species, a primary signal initiates one of two alternative routes of regulatory gene cascades (*1*). This cascade leads to sex-specific differential splicing of the gene *doublesex* (*dsx*) and the pro-

duction of either male- or female-specific DSX proteins (*2*–*11*). The splicing factor transformer (TRA) (*12*–*15*), termed feminizer (FEM) in *Apis mellifera* (*16*), mediates the primary sex-determining signal in females by regulating the female-specific splicing of *dsx* pre-mRNA. In males, no functional TRA/FEM protein is present because of sex-specific splicing of *tra/fem* pre-mRNA, leading to default male-specific splicing of *dsx* primary transcripts.

In diploid insects, sex is mostly signaled by components of sex chromosomes (for example, XY and ZW). In Hymenoptera, however, sex is usually regulated by the ploidy of the embryo (*17*, *18*): Males are haploid, developing from unfertilized eggs, whereas diploid females develop from fertilized eggs. In the honeybee *A. mellifera*, the *complementary sex determiner* (*csd*) gene (which exhibits homology to *tra/fem*) (*19*, *20*) initiates the female sex-determining route when the animal is heterozygous at this locus, whereas homozygosity or hemizygosity leads to maleness. A *csd* mechanism of sex determination can easily be determined because it results in predictable proportions of homozygous diploids that develop into males (*21*). Because a number of Hymenoptera, including *Nasonia*, do not produce diploid males upon inbreeding (*22*), it was surmised that another mechanism controls haplodiploid sex determination in these species.

We screened the *Nasonia* genome (*22*) for motifs matching the *Drosophila tra* and *Apis csd* genes, which resulted in the identification of a single gene (*16*, *22*) composed of nine exons and containing two Arg/Ser-domains (SR-domains), of which one is located entirely in exon one and the second spans exons four to seven. In exons seven and eight, a proline-rich (Pro) domain is present. Reverse-transcriptase polymerase chain reaction (RT-PCR) showed that female-specific splicing retains only the first part of exon two and yields a single transcript encoding a full-length protein, containing both SR domains and the Pro-rich domain. In male *Nasonia*, either the complete exon two or different 3′ parts of exon two can be retained by cryptic 3′ splice-site recognition to yield three different transcripts, all of which encode truncated proteins containing only the first SR domain (*22*). This gene was named *Nasonia vitripennis transformer* (*Nvtra*). *Nvtra* expression was knocked down by injecting double-stranded RNA (dsRNA) against a non–sex-specific part of *Nvtra* in 1- to 2-day-old female pupae (*23*) carrying the recessive eye color mutation STDR (st^{DR}/st^{DR}). After emergence, neither phenotypic nor behavioral changes were observed as compared with control uninjected females. *Nvtra* dsRNA-injected females were capable of mating and ovipositing and were fully fertile. The levels of *Nvtra* mRNA 5 days after dsRNA injection, when the females were in the late pupal stage, showed a 2.8-fold decrease in *Nvtra* expression [$t(16) = 3.86$, $P = 0.0007$, Fig. 1A] relative to uninjected controls.

In control females, only the female-specific *Nvtra* splice form was present. However, *Nvtra* dsRNA-injected females had a decreased amount of female-specific splice form and produced all three male-specific *Nvtra* splice forms (Fig. 1B). Apparently, repression of *Nvtra* also disrupted female-specific splicing of *Nvtra* pre-mRNA itself. For control females, *N. vitripennis doublesex* (*Nvdsx*) female-specific splicing along with very low quantities of a male-specific *Nvdsx* splice form (*11*) were observed. In *Nvtra* dsRNA-injected females, the expression of the predominant female splice form of *Nvdsx* decreased, whereas expression of the male-specific splice form increased (Fig. 1B). This indicates that, in *Nasonia*, an active NvTRA is necessary for female-specific splicing of *Nvdsx* mRNA. The presence of both male- and female-specific splice forms of *Nvtra* and *Nvdsx* was observed to be correlated with the degree of femaleness in haploid *Nasonia* gynandromorphs (*11*, *22*, *24*), indicating that these genes function in sex-specific phenotype establishment. The fact that a similar *Nvtra* and *Nvdsx* transcript composition in dsRNA-injected females nevertheless leads to complete morphological and functional females indicates either that the essential period of this *Nvtra*/*Nvdsx*-mediated phenotypic establishment is before the pupal stage or that the lower level of female-specific *Nvtra* is still sufficient to elicit female development.

To monitor the relative levels of *Nvtra* and *Nvdsx* during early and late embryonic development, we sampled embryos over time and determined the ratio of *Nvtra* and *Nvdsx* transcripts. In 0- to 1-hour-old embryos, an eightfold excess of *Nvtra* over *Nvdsx* was observed [$t(18) = 3.62$, $P = 0.0020$, table S1]. Because no appreciable zygotic gene expression occurs at this early stage (*25*), this relatively high level of *Nvtra* mRNA must be provided to the egg during oogenesis as a maternal factor and should be the female-specific splice variant only. RT-PCR confirmed this expectation, by showing only female-specific transcripts of *Nvtra* in 0- to 5-hour-old embryos from fertilized and unfertilized eggs (Fig. 2A).

As expected, virgin *Nvtra* dsRNA-injected STDR females produced only st^{DR} males (fig. S1). When injected STDR females were mated to wild-type (st^{+}) males, they still produced only male offspring of which 44% had the st^{DR} red-eye phenotype (representing unfertilized eggs) and 56% had wild-type eyes and must therefore be diploid (st^{DR}/st^{+}) (Table 1). Both haploid and diploid adult males had only the male-specific splice forms of both *Nvtra* and *Nvdsx* (Fig. 1B). Because neither intersex nor female offspring were observed, *Nvtra* dsRNA-injected females exhibit a complete sex reversal in their offspring. Flow cytometry confirmed the diploidy of the st^{DR}/st^{+} males (fig. S2). We mated a subset of these diploid st^{DR}/st^{+} males to STDR females.

Evolutionary Genetics, Centre for Ecological and Evolutionary Studies, University of Groningen, Netherlands.

*To whom correspondence should be addressed. E-mail: louis.van.de.zande@rug.nl

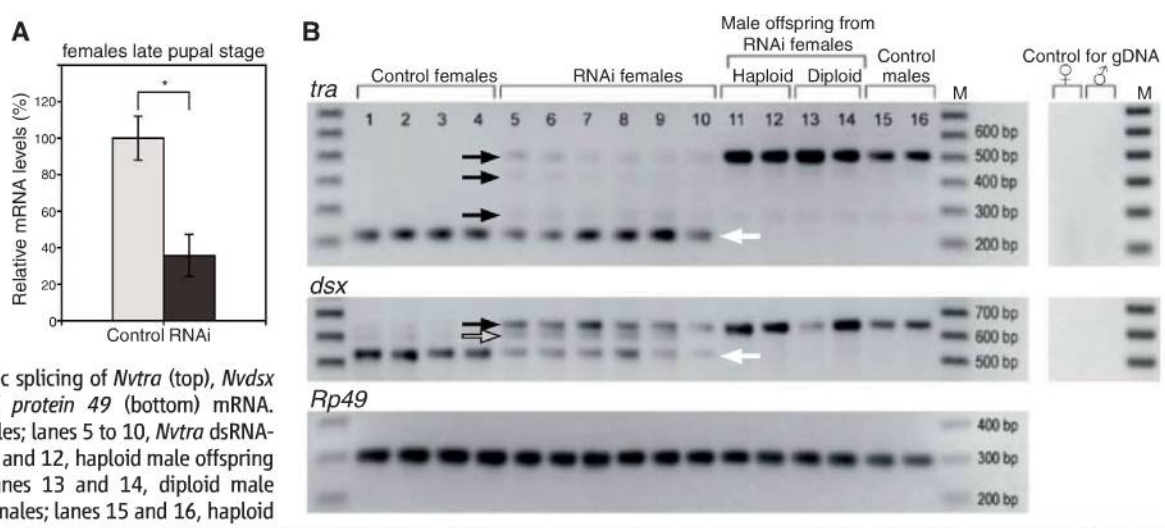

Fig. 1. Sex-specific differential splicing of *Nvtra* and the functional relationship of *Nvtra* and *Nvdsx*. (**A**) Relative levels of *Nvtra* mRNA after RNAi in control (light gray bar) and *Nvtra* dsRNA-injected (black bar) females in the late pupal stage. Error bars represent SE. *$P < 0.001$. (**B**) RT-PCR analysis of sex-specific splicing of *Nvtra* (top), *Nvdsx* (middle), and *Ribosomal protein 49* (bottom) mRNA. Lanes 1 to 4, control females; lanes 5 to 10, *Nvtra* dsRNA-injected females; lanes 11 and 12, haploid male offspring from injected females; lanes 13 and 14, diploid male offspring from injected females; lanes 15 and 16, haploid male offspring from control females. M is a 100-bp molecular size marker. Black arrows indicate male-specific splice forms, gray arrow indicates an unknown splice form, and white arrows indicate female-specific splice forms. A control for amplification from residual genomic DNA is present in the rightmost panel.

The female offspring of this cross all had wild-type eyes. Because male gametogenesis does not involve reduction division, we assume that these males had transmitted their complete diploid genome to generate triploid $st^{DR}/st^{DR}/st^{+}$ daughters, as reported earlier for diploid males from a triploid strain (*26*).

To assess whether *Nvtra* dsRNA-injected mothers provided lower amounts of *Nvtra* to the eggs, we measured the relative levels of *Nvtra* in the offspring of *Nvtra* dsRNA-injected and uninjected females. We found that very early embryos (0 to 3 hours old), in which zygotic gene expression has not yet started (*25*), resulting from both virgin and mated *Nvtra* dsRNA-injected females, had decreased levels of *Nvtra* mRNA to about 20% of that of early embryos from control noninjected females [$t(35) = -3.92$, $P = 0.0002$, Fig. 2B].

Our results suggest that a threshold level of maternally provided female-specific *Nvtra* mRNA is essential for female development of the fertilized egg, because knockdown of *Nvtra* in mothers leads to the production of diploid male offspring. They also indicate that female-specific *Nvtra* splicing depends on an autoregulatory loop. First, knockdown of *Nvtra* in the mother leads to the disruption of the female-specific splicing of both *Nvtra* and *Nvdsx* in these mothers. Second, the diploid male offspring from *Nvtra* dsRNA-injected mothers had only male-specific spliced *Nvtra* transcripts, indicating the dependence of a functional NvTRA protein for female-specific splicing. Third, the high sensitivity of the diploid embryos from the injected mothers to the lowered levels of female-specific *Nvtra* resulting in a full sex reversal indicates that sufficient NvTRA is needed for female-specific splicing. Fourth, eight putative TRA/TRA2 binding motifs (U/G)GAAGAU(U/A) in the *tra/fem*-regulated *dsx* and *fruitless* (*fru*) genes of *N. vitripennis* and *A. mellifera* (*27*) are located in the male-specific exon *2m1* (*22*) and in the intronic region between exons two and three of the *Nvtra* gene. Based upon similar arguments, *tra* autoregulatory loops have been proposed for the dipterans *Ceratitis capitata, Bactrocera oleae*, *Lucilia cuprina* and *A. mellifera* (*14*, *20*, *28*, *29*). We conclude that *Nvtra* is part of the *Nasonia* sex-determining cascade and is responsible for the sex-specific splicing of *Nvdsx*. In addition, sufficient levels of female-specific *Nvtra* transcripts are necessary to maintain the female-specific splicing pattern of *Nvtra* itself.

In diploid houseflies (*Musca domestica*), which lack haplodiploidy, the dominant male-determining M factor represses the sex-determining F factor, resulting in male development (*30*). In the absence of M, F, which is an ortholog of the *Ceratitis tra* gene (*13*), is activated, leading to female development. In *M. domestica*, the M factor can be located on the Y chromosome and/or on one of the autosomes. In other Diptera, such as *Ceratitis* and *Lucilia*, the M factor leads to male development by blocking the transcription or translation of female *tra* or by interfering with *tra* splicing (*13*, *29*). Only males can provide the M factor for the next generation. Therefore, M factors are incompatible with haplodiploid sex determination, where only unfertilized eggs develop into males. This implies that in *Nasonia*, a different mechanism is responsible for the development of males in the presence of maternally provided *Nvtra* mRNA or protein. Thus, we conclude that maternal *Nvtra* mRNA is most likely provided to all eggs as a means to start the female-specific autoregulatory loop.

Because fertilization per se had been ruled out as a sex-determining factor in *Nasonia* before (*31*), and because unfertilized eggs will develop as males, we asked whether the presence of a paternal genome together with a maternal genome explains why only fertilized eggs develop as females. Quantitative PCR (qPCR) showed that in 1- to 3-hour-old embryos from both fertilized and unfertilized eggs, the maternally provided *Nvtra* mRNA input gradually decayed (Fig. 3A). In embryos from unfertilized eggs, a low level of *Nvtra* mRNA was maintained throughout the 23 hours of embryonic development (Fig. 3A). In sharp contrast, a 15-times-higher expression of *Nvtra* in embryos from fertilized eggs was observed 7 hours after egg laying [$t(8) = 4.18$, $P = 0.0031$, Fig. 3A], which cannot be explained by the presence of two versus one *Nvtra* alleles in these embryos and calls for a regulatory explanation. After this peak expression, a significantly higher level ($F_{15,63} = 5.25$, $P < 0.0001$) of *Nvtra* mRNA was maintained as compared with embryos from unfertilized eggs (Fig. 3A). We used a Russian strain of *N. vitripennis* that harbors a deletion of 18 base pairs (bp) in the first exon of the *Nvtra* gene, which apparently does not affect the function of the gene, to monitor the paternal genome for the onset of zygotic *Nvtra* production. RT-PCR of *Nvtra* transcripts in these samples showed that in offspring from fertilized (diploid) eggs, zygotic *Nvtra* mRNA is transcribed from the paternal genome 5 hours after egg laying (Fig. 3B) and confirmed our assumption that, in early (0 to 3 hours) *Nasonia* embryos, no zygotic *Nvtra* transcription takes place. A reciprocal cross yielded identical results. Unfortunately, because of the repetitive nature of the indel and its flanking region, we were unable to design primers to perform qPCR to quantify the relative contributions of the paternal and maternal *Nvtra* alleles, respectively.

Because 1- to 5-hour-old embryos from fertilized and unfertilized eggs contained only female-specific *Nvtra* mRNA (Figs. 2A and 3C), we hypothesize that the absence of sufficient zygotic *Nvtra* expression to initiate the autoregulatory loop results in default male-specific splicing (Fig. 3C). However, in embryos from fertilized eggs, the female-specific splicing of *Nvtra* is maintained (Fig. 3C) because of the availability of zygotic *Nvtra* mRNA. The low levels of the male-specific splice forms observed in these pooled embryo samples most likely result from the unfertilized eggs laid by the mated STDR females (a typical brood contains 20% males). One explanation could be that only the paternal allele of *Nvtra* is transcribed in the early embryo, thus allowing the loop of autoregulatory splicing to take place. Alternatively, a trans factor necessary for the

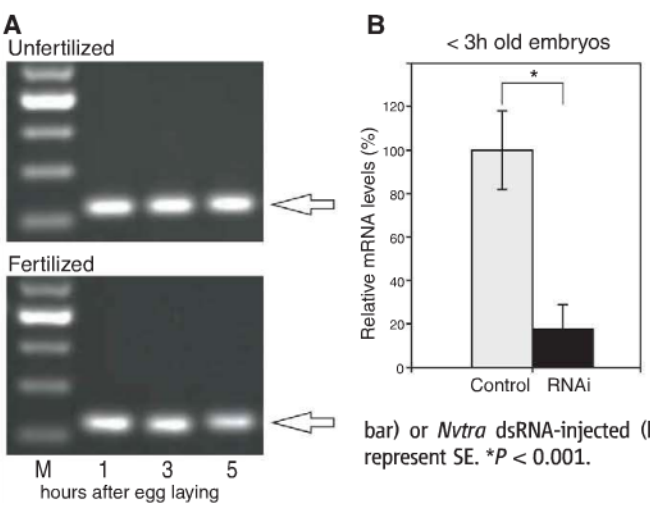

Fig. 2. Maternal input in early embryos. (**A**) Maternal input of female-specific *Nvtra* mRNA in early embryos from unfertilized (top) and fertilized (bottom) eggs shown 1, 3, and 5 hours after egg laying. Open arrows indicate female-specific *Nvtra* splice forms of 228 bp. M is a 100-bp size marker. (**B**) Relative *Nvtra* mRNA levels in equally mixed embryos from mated and unmated control (gray bar) or *Nvtra* dsRNA-injected (black bar) females. Error bars represent SE. *$P < 0.001$.

Table 1. *Nvtra* dsRNA-injected females and their offspring numbers. Number of *Nvtra* dsRNA-injected females [P: parental females (RNAi)] that produced offspring [P: parental females (fertile)] as virgin or as mated to AsymC males and the offspring they produced (F_1: haploid males; F_1: diploid females; and F_1: diploid males).

	P: ♀ (RNAi)	P: ♀ (fertile)	F_1: haploid ♂	F_1: diploid ♀	F_1: diploid ♂
Virgin	60	17	418	0	0
Mated	60	26	295	0	379

timely onset of zygotic *Nvtra* transcription may be silenced in the maternal genome set of the embryo.

Our data show that maternal provision of *Nvtra* to all embryos, followed by sufficient early zygotic *Nvtra* expression, which occurs only in fertilized eggs, is necessary for female development in *Nasonia*. RNA interference (RNAi) treatment decreased the maternal provision of *Nvtra* to the eggs, which alone would be sufficient for the production of diploid males. It is possible that the resulting small interfering RNAs (siRNAs) were also transmitted to the eggs, resulting in a decrease in zygotic *Nvtra* transcript expression in addition to a decrease in maternal *Nvtra* input. Either way, the simplest explanation for the mechanism behind *Nasonia* sex determination appears to be maternal input of *Nvtra* mRNA combined with a form of maternal imprinting (*31*).

Several insects have maternal input of *tra* mRNA followed by an autoregulatory loop for the continuous production of female-specific *tra* (*13*, *20*, *29*). However, in *Nasonia*, male development does not result from disruption of the *Nvtra* autoregulatory loop by paternal repression (for example, an M factor) or a nonfunctioning CSD, but is most likely caused by maternal silencing of the *tra* gene. The presence of a paternal genome leads to zygotic expression of *Nvtra*, but maternally provided *Nvtra* mRNA is required to initiate female-specific splicing. Hence, in *Nasonia*, females regulate the sex of the offspring by providing a feminizing effect by maternal input of *Nvtra*, while at the same time preventing zygotic expression of *Nvtra* in haploid offspring. Pane *et al.* (*13*) suggested that the sensitivity of the *tra* autoregulation is evolutionarily important for the recruitment of upstream regulators. Indeed, in *A. mellifera*, *csd* originated as a duplication of *fem* (=*tra*) (*16*). The gregarious lifestyle of *Nasonia* implies potential high levels of inbreeding, so the evolution of a *csd* sex-determining mode is under constraint. Instead, a maternal imprinting event seems to be an upstream regulator, rendering the system dependent on zygotic expression. This is analogous to the observed evolutionary modulation of the maternal provision versus zygotic transcription of patterning determinants by Rosenberg *et al.* (*32*). The interplay of maternal and zygotic provision of sensitive sex-determination regulatory factors may facilitate the recurrent appearance of thelytokous reproduction in haplodiploid insects.

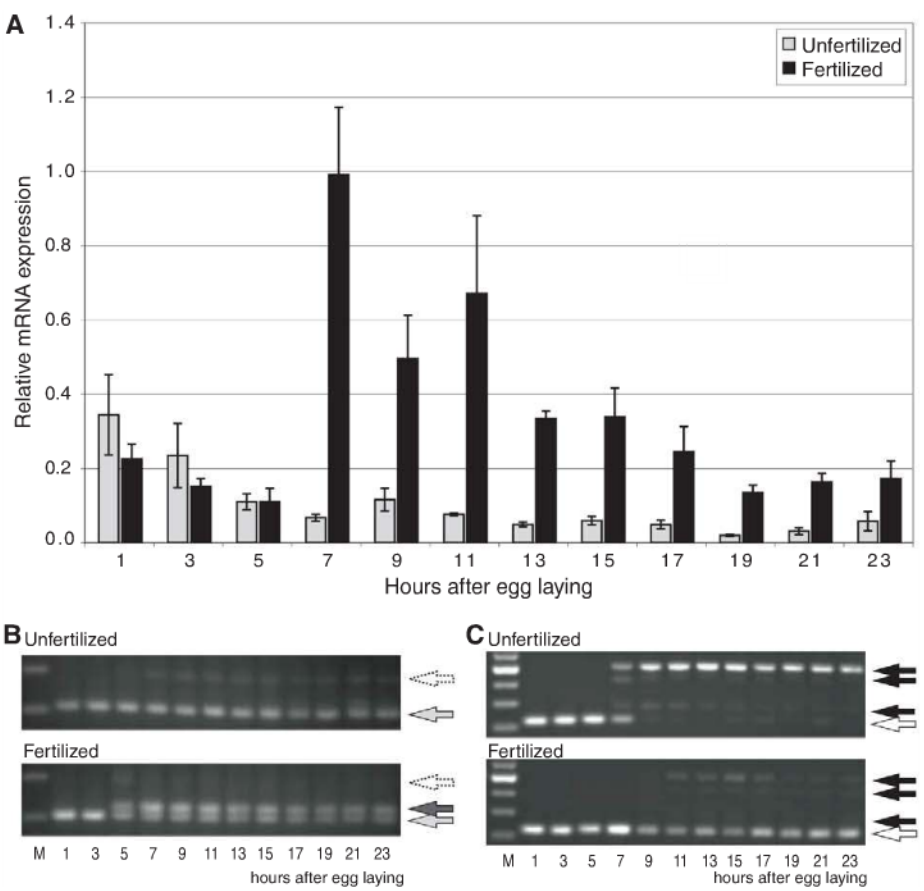

Fig. 3. Expression and splicing of *Nvtra* during embryonic development. (**A**) Relative *Nvtra* mRNA levels in embryos from unfertilized (gray bars) and fertilized (black bars) eggs at different developmental times, indicated as hours after egg laying. Error bars represent SE. (**B**) *Nvtra* mRNA originating as maternal input (light gray arrows) or transcribed from the paternal genome (dark gray arrows) in embryos from unfertilized (top) and fertilized (bottom) eggs. Open dotted arrow indicates amplification resulting from residual genomic DNA. M is a 100-bp size marker. (**C**) Temporal pattern of sex-specific splicing of *Nvtra* mRNA in embryos from unfertilized (top) and fertilized (bottom) eggs. Black arrows indicate male-specific splice forms. White arrows indicate female-specific splice form.

References and Notes

1. A. S. Wilkins, *Bioessays* **17**, 71 (1995).
2. K. C. Burtis, B. S. Baker, *Cell* **56**, 997 (1989).
3. G. Saccone *et al.*, in *Proceedings: Enhancement of the Sterile Insect Technique through Genetic Transformation using Nuclear Techniques* (International Atomic Energy Agency/Food and Agriculture Organization, Vienna, 1996), pp. 16–32.
4. D. C. A. Shearman, M. Frommer, *Insect Mol. Biol.* **7**, 355 (1998).
5. S. Kuhn, V. Sievert, W. Traut, *Genome* **43**, 1011 (2000).
6. M. Hediger *et al.*, *Dev. Genes Evol.* **214**, 29 (2004).
7. D. Lagos, M. F. Ruiz, L. Sánchez, K. Komitopoulou, *Gene* **348**, 111 (2005).
8. M. F. Ruiz *et al.*, *Genetics* **171**, 849 (2005).
9. C. Scali, F. Catteruccia, Q. Li, A. Crisanti, *J. Exp. Biol.* **208**, 3701 (2005).
10. S. Cho, Z. Y. Huang, J. Zhang, *Genetics* **177**, 1733 (2007).
11. D. C. Oliveira *et al.*, *Insect Mol. Biol.* **18**, 315 (2009).
12. J. M. Belote, M. McKeown, R. T. Boggs, R. Ohkawa, B. A. Sosnowski, *Dev. Genet.* **10**, 143 (1989).
13. A. Pane, M. Salvemini, P. Delli Bovi, C. Polito, G. Saccone, *Development* **129**, 3715 (2002).
14. D. Lagos, M. Koukidou, C. Savakis, K. Komitopoulou, *Insect Mol. Biol.* **16**, 221 (2007).
15. M. F. Ruiz *et al.*, *PLoS ONE* **2**, e1239 (2007).
16. M. Hasselmann *et al.*, *Nature* **454**, 519 (2008).
17. G. E. Heimpel, J. G. de Boer, *Annu. Rev. Entomol.* **53**, 209 (2008).
18. L. Sánchez, *Int. J. Dev. Biol.* **52**, 837 (2008).
19. M. Beye, M. Hasselmann, M. K. Fondrk, R. E. Page Jr., S. W. Omholt, *Cell* **114**, 419 (2003).
20. T. Gempe *et al.*, *PLoS Biol.* **7**, e1000222 (2009).
21. E. van Wilgenburg, G. Driessen, L. W. Beukeboom, *Front. Zool.* **3**, 1 (2006).
22. J. H. Werren *et al.*, *Science* **327**, 343 (2010).
23. J. A. Lynch, C. Desplan, *Nat. Protoc.* **1**, 486 (2006).
24. L. W. Beukeboom *et al.*, *Science* **315**, 206 (2007).
25. M. A. Pultz *et al.*, *Development* **132**, 3705 (2005).
26. L. W. Beukeboom, A. Kamping, *Genetics* **172**, 981 (2006).
27. R. C. Bertossa, L. van de Zande, L. W. Beukeboom, *Mol. Biol. Evol.* **26**, 1557 (2009).
28. A. Pane, A. De Simone, G. Saccone, C. Polito, *Genetics* **171**, 615 (2005).
29. C. Concha, M. J. Scott, *Genetics* **182**, 785 (2009).
30. A. Dübendorfer, M. Hediger, G. Burghardt, D. Bopp, *Int. J. Dev. Biol.* **46**, 75 (2002).
31. L. W. Beukeboom, A. Kamping, L. van de Zande, *Semin. Cell Dev. Biol.* **18**, 371 (2007).
32. M. I. Rosenberg, J. A. Lynch, C. Desplan, *Biochim. Biophys. Acta. Gene Regul. Mech.* **1789**, 333 (2009).

33. The authors thank the Werren lab (University of Rochester, United States), D. Bopp, M. H. Linskens, A. Rensink, and A. Kamping for technical assistance and discussions and four anonymous reviewers for helpful suggestions. This work was partly funded by Pioneer grant ALW 833.02.003 from the Netherlands Organization for Scientific Research (NWO).

Supporting Online Material

www.sciencemag.org/cgi/content/full/328/5978/620/DC1
Materials and Methods
Figs. S1 and S2
Tables S1 and S2
References

10 December 2009; accepted 16 March 2010
10.1126/science.1185805

Lateral Transfer of Genes from Fungi Underlies Carotenoid Production in Aphids

Nancy A. Moran[1]* and Tyler Jarvik[2]

Carotenoids are colored compounds produced by plants, fungi, and microorganisms and are required in the diet of most animals for oxidation control or light detection. Pea aphids display a red-green color polymorphism, which influences their susceptibility to natural enemies, and the carotenoid torulene occurs only in red individuals. Unexpectedly, we found that the aphid genome itself encodes multiple enzymes for carotenoid biosynthesis. Phylogenetic analyses show that these aphid genes are derived from fungal genes, which have been integrated into the genome and duplicated. Red individuals have a 30-kilobase region, encoding a single carotenoid desaturase that is absent from green individuals. A mutation causing an amino acid replacement in this desaturase results in loss of torulene and of red body color. Thus, aphids are animals that make their own carotenoids.

Carotenoids are a distinctive, widespread class of molecules with diverse metabolic and ecological roles in organisms (*1*). Variants of these colored compounds are synthesized with the same small set of homologous enzymes, of which copies are distributed in many species of Bacteria, Archaea, Fungi, and plants. Animals require carotenoids for several functions, ranging from ornamentation to antioxidants and immune system modulators to precursors for visual pigments [e.g., (*1*–*4*)]. But animals obtain these compounds from food, and so far, no animal has been reported to make its own carotenoids. Here we report the presence and expression of carotenoid biosynthetic genes in aphids (Insecta: Hemiptera). Further, we show that they underlie production of carotenoids and color, including a genetic color polymorphism affecting interactions with natural enemies (*5*). Phylogenetic analyses imply the ancestral transfer of these genes from a fungus to an ancestor of numerous modern aphid species.

Carotenoids have been reported from several species of aphids, and carotenoid content has been shown to differ between color morphs in two color polymorphic species, *Macrosiphum liriodendron* and *Sitobion avenae* (*6*–*10*). Green forms contain α-, β-, and γ-carotene (all yellow or yellow-orange compounds), whereas red (or brownish) forms of the same species also contain lycopene or torulene (red compounds) (*6*, *7*, *10*).

The pea aphid, *Acyrthosiphon pisum*, displays a red-green color polymorphism (Fig. 1, A and B) in which color is stable within all-female parthenogenetic clones (although environmental factors can cause temporary variation within each type). The color polymorphism appears to be maintained by frequency-dependent selection imposed by natural enemies that search for prey using different visual cues, which results in differential susceptibility of the red and green individuals (*5*, *11*).

Carotenoid assays of *A. pisum* samples from our laboratory colonies (*12*) revealed that green clones contain mostly γ-carotene, β-carotene, and α-carotene, whereas red clones contain these compounds plus torulene and dehydro-γ,ψ-carotene (a carotenoid similar to torulene) (Fig. 1D). These two compounds, completely absent from green clones (Fig. 1D), can be derived from γ-carotene through a desaturation step (fig. S1) (*13*, *14*). They are vermilion (bright red), the color of the water-insoluble pigments extracted from red *A. pisum*, whereas the other carotenoids are pale to bright yellow, the color of the water-insoluble pigments extracted from green *A. pisum*.

Because animals are generally considered to lack the enzymatic machinery required for carotenoid biosynthesis, one explanation for the presence of carotenoids in aphids is that they are sequestered from the diet. However, carotenoids, as lipid-soluble compounds, are not expected to occur in significant quantities in phloem sap; furthermore, the carotenoid profiles of aphids differ dramatically from those in their host plants (*8*). An alternative explanation, proposed by several authors, is that aphids acquire carotenoids from their bacterial endosymbionts (*7*, *9*, *10*). However, genome sequencing has revealed that neither the primary symbiont *Buchnera aphidicola* (*15*) nor two facultative symbionts (*16*, *17*) have any genes with homology to carotenoid biosynthetic genes. Furthermore, facultative endosymbionts can be eliminated from clones or transferred between clones without affecting color (*18*, *19*). Finally, such endosymbionts are inherited maternally, whereas, in both *A. pisum* and the peach-potato aphid, *Myzus persicae*, red-green color shows Mendelian inheritance, with red dominant to green in both species (*20*–*22*). We verified this pattern of inheritance in our laboratory lines of *A. pisum* (table S1). Thus, these colors are dependent on genes encoded in the aphid genome. In principle, such genes could affect the ability to sequester or display carotenoids rather than encoding enzymes of carotenoid biosynthesis directly.

The recent release of the genome sequence of *A. pisum* (*23*) allowed us to search for carotenoid

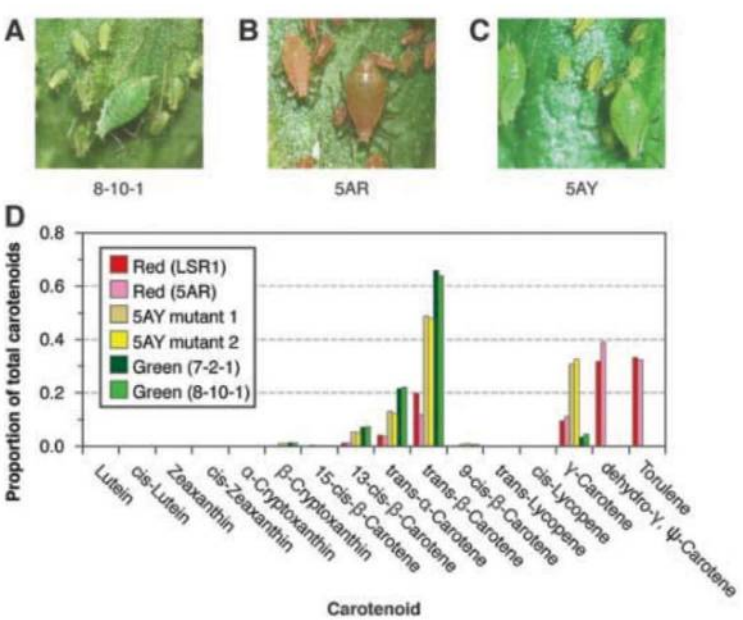

Fig. 1. Coloration and carotenoids in the pea aphid. Typical green (**A**) and red (**B**) aphid clones, (**C**) 5AY, a green mutant clone arising from the red clone 5A. (**D**) Profiles of carotenoids in red (5A, LSR1), mutant red→green (5AY, two samples), and green (8-10-1, 7-2-1) pea aphid clones. Torulene and a related red compound are restricted to red clones; the mutant 5AY clone lacks these and displays an elevation in their predicted precursor, γ-carotene.

[1]Department of Ecology and Evolutionary Biology, 1041 East Lowell Street, University of Arizona, Tucson, AZ 85721, USA. [2]Department of Chemistry and Biochemistry, University of Arizona, Tucson, AZ 85721, USA.

*To whom correspondence should be addressed. E-mail: nancy.moran@yale.edu

biosynthetic genes. Searches against a database of RefSeq proteins inferred from the genome, using as queries sequences of carotenoid biosynthetic enzymes from bacteria and plants, revealed close homology with four carotenoid desaturase homologs and three proteins consisting of fused carotenoid cyclase–carotenoid synthase enzymes (Table 1). Searching the GenBank protein database using the inferred aphid proteins as queries revealed the closest sequence homology to carotenoid biosynthetic genes of several fungi, but no detectable homology to enzymes encoded by any other available animal genome. In phylogenetic analyses for both the carotenoid cyclase–carotenoid synthase proteins and for the carotenoid desaturase proteins, the aphid copies form a highly supported clade that is nested within a fungal clade with strong support (Fig. 2, A and B). Furthermore, the relation to fungal enzymes is strongly supported by the similarity of the gene arrangement between *A. pisum* and certain fungi. Although bacteria and plants also contain homologs of these genes, only fungi display a fusion of carotenoid cyclase and carotenoid synthase (*24*–*26*). Furthermore, in *A. pisum*, all three carotenoid synthase–carotenoid cyclase and three of the four carotenoid desaturase genes are paired with divergent orientation of transcription in aphid genome scaffolds; this arrangement is otherwise only described from certain fungi (fig. S2) (*25*, *26*).

Contamination of the DNA sample used for the aphid genome project with fungal DNA was ruled out as an explanation for the presence of these genes. In the *A. pisum* genome project, all of the carotenoid biosynthetic genes occur on large scaffolds that contain other genes with closest homology to other insects or repetitive elements characteristic of the aphid genome. Coding regions of carotenoid genes show typical depth of coverage and are joined to aphid-specific sequences on individual clone inserts. Furthermore, expression of all seven *A. pisum* genes was supported by expressed sequence tag (EST) data collected from aphids grown in several laboratories (Table 1). Polymerase chain reaction (PCR) experiments confirmed the presence and expression of these genes in all tested samples of *A. pisum,* both from field collections and from laboratory colonies. The only exception was one carotenoid desaturase locus, which was absent from green clones of pea aphids, as explained further below.

Taken together, this evidence supports the transfer of these genes from a fungus to an aphid ancestor as a single event, followed by duplication within the aphid genome. Such transfer preserved the gene arrangement observed in certain fungi, in which the entire region, encompassing divergently transcribed carotenoid desaturase and carotenoid synthase–carotenoid cyclase loci, comprises only about 5 kilobases (kb) (*25*, *26*). The aphid copies have much larger introns and larger intergenic spacers (Table 1 and fig. S2), which reflect typical gene structure in the aphid genome (*23*). The gene arrangement differs from that in studied species of Ascomycetes (*27*), which reinforces our phylogenetic evidence that the donor was not in this group. Potentially, the ancestral gene donor was a fungal pathogen or symbiont of aphids, or of an aphid host plant.

In both the carotenoid cyclase and carotenoid desaturase trees, *A. pisum* sequences and EST sequences from *Myzus persicae* form clades together, which implies that the transfer preceded their shared ancestor, at the base of the aphid clade corresponding to the aphid tribe Macrosiphini.

We used the red-green genetic polymorphism and a spontaneously arising laboratory mutant (Fig. 1, A to C) to determine whether a difference in one of these loci underlies observed differences between *A. pisum* clones in color and in carotenoid content. First, we sequenced the full-length genomic DNA containing these genes for two green clones (8-10-1 and SCC13), two red clones (5A and LSR1), and two samples of a mutant yellow-green clone that arose from clone 5A but lacked red color (clone 5AY). Most genes gave highly similar products for all lines, with a low level of allelic divergence, which indicated heterozygosity of about 0.13%, generally consistent with previous studies of sequence variation in *A. pisum* populations (*28*). However, both green lines failed to amplify for any primer pairs designed in the region of one of the four copies of carotenoid desaturase (XP_001943938, corresponding to a portion of Scaffold NW_001918682, Table 1), whereas both red lines gave products and sequences that were identical (LSR1) or near identical (5A) to the sequence from the genome project. (LSR1 was used in the genome project.) Furthermore, both sequenced red lines showed no heterozygosity in this region in contrast to all other regions, which showed clear evidence of heterozygosity. After manual assembly of traces from the genome project and from our own sequencing, we reconstructed a 30-kb scaffold for this region, which we resequenced for LSR1 (fig. S3).

These observations suggest that the red lines are heterozygous and that the red allele contains over 30 kb missing in the green allele. Genetic crosses confirm that both of these red lines were heterozygous for color, giving rise to a mixture of red and green progeny when crossed with green lines (table S1). In PCR screens of 60 F_1 lines from the largest such cross, all red progeny yielded amplicons of the expected length, whereas no green

Table 1. Genes in the *A. pisum* genome with closest homology to carotenoid biosynthetic enzymes, including scaffold of origin and matching EST sequences. Similar color indicates that the gene is on the same scaffold. The 3′ end of scaffold NW_001925130 overlaps with the 5′ end of NW_001923501 for 5400 base pairs, and PCR demonstrated continuity of these scaffolds. Pink row is the gene corresponding to *tor*^{R} and conferring red color (see text). Protein length, amino acids; ESTs are those present in GenBank, mostly from clone LSR1.

	Protein		mRNA		ESTs		Scaffold		Gene		
Enzyme type	Accession	Length (aa)	Accession	Length (bp)	(*n*)	LOC_ID/ ACYPI_ID	Accessions	Length (bp)	Start	End	Length (bp)
Carotenoid synthase/ cyclase	XP_001943170	608	XM_001943135	1,981	4	LOC100161104/ ACYPI002354	NW_001938125/ SCAFFOLD9039	96,434	60,929	75,839	14,910
Carotenoid synthase/ cyclase	XP_001950787	588	XM_001950729	2,223	9	LOC100159332/ ACYPI000715	NW_001925130/ SCAFFOLD17863	49,317	1,564	8,266	6,702
Carotenoid synthase/ cyclase	XP_001950868	589	XM_001950833	1,770	8	LOC100164140/ ACYPI005179	NW_001925130/ SCAFFOLD17863	49,317	36,365	42,379	6,014
Carotenoid desaturase	XP_001943225	373	XM_001943190	1,247	3	LOC100159050/ ACYPI000460	NW_001938125/ SCAFFOLD9039	96,434	76,368	93,106	16738
Carotenoid desaturase	XP_001950764	528	XM_001950729	2,718	7	LOC100161380/ ACYPI002604	NW_001925130/ SCAFFOLD17863	49,317	19,665	22,451	2,786
Carotenoid desaturase	XP_001946689	526	XM_001946654	2,693	25	LOC100169110/ ACYPI009757	NW_001923501/ SCAFFOLD16397	29,128	8,574	16,388	7,814
Carotenoid desaturase	XP_001943938	510	XM_001943903	2,410	57	LOC100169245/ ACYPI009883	NW_001918682/ SCAFFOLD12059	31,283	1,415	8,641	7,226

progeny yielded amplicons for sequences within this region. To determine whether the correlation of this genomic region with color extended across green and red clones generally, we surveyed several green and red *A. pisum* clones from North American locations. This region was present in every red aphid sample and absent from all green aphid samples (fig. S4).

We designated this locus *tor* (for torulene production), with alleles tor^R and tor^G. The structure of tor^G was not determined but is inferred to consist of a large deletion relative to tor^R. Males derived from a heterozygous clone (5A) all have tor^R, which indicates that it occurs on an autosome and not the X chromosome, for which males are haploid.

The mutant line 5AY has stable yellow-green color (Fig. 1C) and has a carotenoid content similar to green clones except that γ-carotene is elevated relative to β- and α-carotene (Fig. 1D). In contrast to the red parental line (5A), 5AY also resembles green clones in completely lacking torulene and dehydro-γ,ψ-carotene (Fig. 1D). Genomic sequences corresponding to coding regions for all seven carotenoid biosynthetic genes were obtained for 5AY. All sequences were identical to those of 5A for a total of 60 kilobase pairs of sequence, except for a single base difference within the tor^R allele. This mutation was derived in the 5AY lineage in the laboratory. This G→A substitution was predicted to cause a single–amino acid replacement (glutamic acid→lysine at position 32). This replacement affects the substrate-binding site of the carotenoid desaturase and results in a change from a negatively charged to a positively charged residue at a site that is conserved across members of this family from bacteria, plants, and fungi (fig. S5). This mutation therefore appears to be a radical change in the *tor* locus that results in a failure to make torulene and dehydro-γ,ψ-carotene and the ensuing accumulation of the predicted substrate, γ-carotene.

Experiments in bacteria and fungi show that distinct carotenoid profiles can result from small changes in enzyme amino acid sequence or expression (*14*, *24*). Thus, following a single transfer of carotenoid biosynthetic genes from a fungus to aphids, gene duplications, sequence diversification, and shifts in expression of copies could have resulted in a variety of carotenoids that contribute to aphid colors and affect color polymorphisms in several species (*6*, *7*, *10*, *20*). In *A. pisum*, the red-green polymorphism has been shown to affect susceptibility to natural enemies (*5*, *11*, *29*), and aphid carotenoids may confer other benefits not yet investigated.

Recent studies in animals have revealed several cases of DNA acquisition from bacterial sources (*30*, *31*), including some cases involving functional genes (*32*–*34*). A comprehensive search of the *A. pisum* genome for bacterium-derived genes revealed a total of only 12 apparently functional transferred genes, derived from a smaller number of acquisition events followed by duplication (*33*). However, that search did not use a strategy designed to identify genes derived from fungi or other eukaryotes, so the carotenoid biosynthetic genes were not detected. We searched the *A. pisum* genome for additional genes derived from fungi but detected only the seven loci homologous with genes for carotenoid biosynthesis (Table 1).

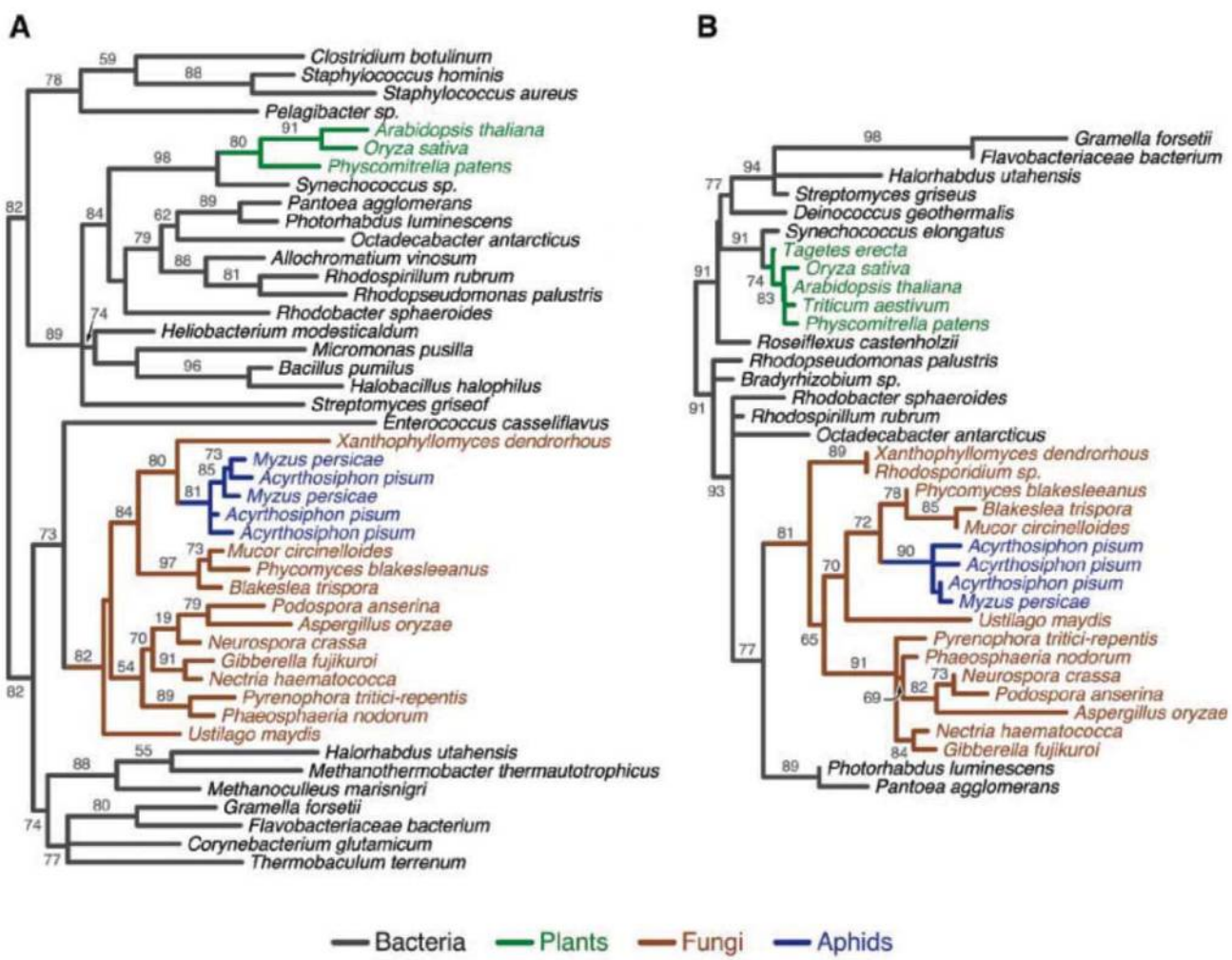

Fig. 2. Phylogenetic relations of inferred carotenoid biosynthetic enzymes from the pea aphid genome. (**A**) Carotenoid desaturases and (**B**) carotenoid cyclase–carotenoid synthases. Sequences are from aphids, bacteria, plants, and fungi; no homologs were detectable in other sequenced animal genomes. Bootstrap support greater than 50% is indicated on branches.

Our case is unusual in that the genes originate from a fungus and have a known ecological role in the recipient. In view of the widespread dependence of animals on carotenoids, it is perhaps curious that acquisition of genes underlying carotenoid biosynthesis has not been more frequent. Whereas the phylogenies for these genes suggest several events of horizontal gene transfer among divergent bacterial lineages (Fig. 2), the trees support only a single acquisition by plants (from their plastid symbionts) and a single origin within Fungi (Fig. 2). Likewise, the transfer documented here, from a fungus to an aphid ancestor, is, so far, the only acquisition of carotenoid biosynthetic machinery known in animals.

References and Notes

1. T. W. Goodwin, *Annu. Rev. Nutr.* **6**, 273 (1986).
2. P. D. Fraser, P. M. Bramley, *Prog. Lipid Res.* **43**, 228 (2004).
3. M. Rothschild, in *Coevolution of Animals and Plants*, L. E. Gilbert, P. H. Raven, Eds. (Univ. of Texas Press, Austin, 1975), pp. 20–47.
4. A. V. Badyaev, *Evol. Biol.* **34**, 61 (2007).
5. J. E. Losey, A. R. Ives, J. Harmon, F. Ballantyne, C. Brown, *Nature* **388**, 269 (1997).
6. A. G. Andrewes *et al.*, *Acta Chem. Scand.* **25**, 3878 (1971).
7. K. S. Brown, *Chem. Soc. Rev.* **4**, 263 (1975).
8. B. Czeczuga, *Zool. Pol.* **25**, 27 (1976).
9. E. J. Houk, *J. Insect Physiol.* **20**, 471 (1974).
10. R. L. Jenkins, H. D. Loxdale, C. P. Brookes, A. F. G. Dixon, *Physiol. Entomol.* **24**, 171 (1999).
11. J. P. Harmon, J. E. Losey, A. R. Ives, *Oecology* **115**, 287 (1998).
12. Materials and methods are available as supporting material on *Science* Online.
13. J. C. Verdoes *et al.*, *Appl. Environ. Microbiol.* **69**, 3728 (2003).
14. D. Umeno, A. V. Tobias, F. H. Arnold, *Microbiol. Mol. Biol. Rev.* **69**, 51 (2005).
15. S. Shigenobu, H. Watanabe, M. Hattori, Y. Sakaki, H. Ishikawa, *Nature* **407**, 81 (2000).
16. P. H. Degnan, Y. Yu, N. Sisneros, R. A. Wing, N. A. Moran, *Proc. Natl. Acad. Sci. U.S.A.* **106**, 9063 (2009).
17. P. H. Degnan *et al.*, *Environ. Microbiol.*, published online 16 October 2009 (www3.interscience.wiley.com/cgi-bin/fulltext/122652702/HTMLSTART.
18. K. M. Oliver, J. A. Russell, N. A. Moran, M. S. Hunter, *Proc. Natl. Acad. Sci. U.S.A.* **100**, 1803 (2003).
19. K. M. Oliver, N. A. Moran, M. S. Hunter, *Proc. Natl. Acad. Sci. U.S.A.* **102**, 12795 (2005).
20. F. P. Müller, *Archiv Freunde Naturgesch. Mecklenburg* **7**, 228 (1961).
21. F. P. Müller, *Z. Pflanzenkr.* **69**, 129 (1962).
22. H. Takada, *Appl. Entomol. Zool. (Jpn.)* **16**, 242 (1981).
23. International Aphid Genomics Consortium, *PLoS Biol.* **8**, e1000313 (2010).
24. J. C. Verdoes, K. P. Krubasik, G. Sandmann, A. J. van Ooyen, *Mol. Gen. Genet.* **262**, 452 (1999).
25. N. Arrach, R. Fernández-Martín, E. Cerdá-Olmedo, J. Avalos, *Proc. Natl. Acad. Sci. U.S.A.* **98**, 1687 (2001).
26. M. Rodríguez-Sáiz *et al.*, *Appl. Environ. Microbiol.* **70**, 5589 (2004).
27. P. Linnemannstöns, M. M. Prado, R. Fernández-Martín, B. Tudzynski, J. Avalos, *Mol. Gen. Genet.* **267**, 593 (2002).
28. J. A. Brisson, S. V. Nuzhdin, D. L. Stern, *BMC Genet.* **10**, 22 (2009).
29. R. Libbrecht, D. M. Gwynn, M. D. E. Fellowes, *J. Insect Behav.* **20**, 25 (2007).
30. N. Kondo, N. Nikoh, N. Ijichi, M. Shimada, T. Fukatsu, *Proc. Natl. Acad. Sci. U.S.A.* **99**, 14280 (2002).
31. J. C. Hotopp *et al.*, *Science* **317**, 1753 (2007).
32. N. Nikoh, A. Nakabachi, *BMC Biol.* **7**, 12 (2009).
33. N. Nikoh *et al.*, *PLoS Genet.* **6**, e1000827 (2010).
34. M. E. Rumpho *et al.*, *Proc. Natl. Acad. Sci. U.S.A.* **105**, 17867 (2008).

35. We are indebted to K. Vogel for samples of aphids, including crosses he performed for other experiments. We thank N. Craft and staff at Craft Technologies for high-performance liquid chromatography analyses of aphid samples, K. Hammond for care of pea aphid colonies, K. Hammond and H. Dunbar for noticing the mutant 5AY female, J. Russell and S. Via for aphid clones, B. Nankivell for preparation of figures and of the manuscript, H. Ochman for comments on the paper, members of the Ochman-Moran laboratory for comments on the project, and A. Badyaev for discussions of carotenoids in animals. This project was funded by NSF 0626716 to N.M. GenBank accession for the DNA sequence is GU456379.

Supporting Online Material

www.sciencemag.org/cgi/content/full/328/5978/624/DC1
Materials and Methods
Figs. S1 to S5
Tables S1 to S4
References

15 January 2010; accepted 1 March 2010
10.1126/science.1187113

D-Amino Acids Trigger Biofilm Disassembly

Ilana Kolodkin-Gal,[1] Diego Romero,[2] Shugeng Cao,[3] Jon Clardy,[3] Roberto Kolter,[2] Richard Losick[1]*

Bacteria form communities known as biofilms, which disassemble over time. In our studies outlined here, we found that, before biofilm disassembly, *Bacillus subtilis* produced a factor that prevented biofilm formation and could break down existing biofilms. The factor was shown to be a mixture of D-leucine, D-methionine, D-tyrosine, and D-tryptophan that could act at nanomolar concentrations. D-Amino acid treatment caused the release of amyloid fibers that linked cells in the biofilm together. Mutants able to form biofilms in the presence of D-Amino acids contained alterations in a protein (YqxM) required for the formation and anchoring of the fibers to the cell. D-Amino acids also prevented biofilm formation by *Staphylococcus aureus* and *Pseudomonas aeruginosa*. D-amino acids are produced by many bacteria and, thus, may be a widespread signal for biofilm disassembly.

Most bacteria form multicellular communities known as biofilms in which cells are protected from environmental insults (*1*, *2*). However, as biofilms age, nutrients become limiting, waste products accumulate, and it is advantageous for the biofilm-associated bacteria to return to a planktonic existence (*2*). Thus, biofilms have a finite lifetime, characterized by eventual disassembly. *Bacillus subtilis* forms communities on semi-solid surfaces and thick pellicles at the air/liquid interface of standing cultures (*1*, *3*–*5*). Cells in the biofilms are held together by an extracellular matrix consisting of exopolysaccharide and amyloid fibers composed of the protein TasA (*5*–*7*). The exopolysaccharide is produced by the *epsA-O* operon, and the TasA protein is encoded by the *yqxM-sipW-tasA* operon (*8*). After 3 days of incubation in a biofilm-inducing medium, *B. subtilis* formed thick pellicles at the air/liquid interface of standing cultures (Fig. 1A). Upon incubation for an additional 3 to 5 days, however, the pellicles lost their integrity (Fig. 1B). To investigate whether mature biofilms produce a factor that triggers biofilm disassembly, we asked whether a conditioned medium would prevent pellicle formation when added to a fresh medium (*9*). Medium from an 8-day-old culture was applied to a C18 column (Sep Pak, Waters, Milford, MA), and concentrated eluate from the column was added to a freshly inoculated culture. The eluate was sufficient to prevent pellicle formation (Fig. 1C). Concentrated eluate from a 3-day-old culture had little effect on pellicle formation (Fig. 1D). Further purification of the factor was achieved by eluting the cartridge stepwise with methanol. Elution with 40% methanol resulted in a fraction that was active in inhibiting pellicle formation (Fig. 1E), but had little effect on cell growth (fig. S1). The activity was resistant to heating at 100°C for 2 hours and proteinase K treatment (Fig. 1F).

Bacteria produce D-amino acids in stationary phase (*10*). We asked whether the biofilm-inhibiting factor was composed of one or more D-amino acids. Indeed, D-tyrosine, D-leucine, D-tryptophan, and D-methionine were active in inhibiting biofilm formation in a liquid medium, as well as on a solid medium (Fig. 1, G and H, and figs. S2 and S3). In contrast, the corresponding L-isomers and D-isomers of other amino acids (such as D-alanine and D-phenylalanine) were inert in our biofilm-inhibition assay. Next, we determined the minimum concentration needed to prevent biofilm formation. Individual D-amino acids varied in their activity, with D-tyrosine being more effective (3 μM) than D-methionine

[1]Department of Molecular and Cellular Biology, Harvard University, Cambridge, MA 02138, USA. [2]Department of Microbiology and Molecular Genetics, Harvard Medical School, Boston, MA 02115, USA. [3]Department of Biological Chemistry and Molecular Pharmacology, Harvard Medical School, Boston, MA 02115, USA.

*To whom correspondence should be addressed. E-mail: losick@mcb.harvard.edu

(2 mM), D-tryptophan (5 mM), or D-leucine (8.5 mM). A mixture of all four D-amino acids was particularly potent, with a minimum inhibitory concentration of ~10 nM. Thus, D-amino acids can act synergistically. Not only did the D-amino acids prevent biofilm formation, but they also disrupted existing biofilms. The addition of D-tyrosine or a mixture of the four D-amino acids (but not the corresponding L-amino acids) caused pellicle breakdown (Fig. 2A).

D-Amino acids are generated by racemases (*11*). Genetic evidence consistent with the idea that the biofilm-inhibiting factor is D-amino acids came from mutants of *ylmE* and *racX*, genes whose predicted products exhibit sequence similarity to known racemases. Strains mutant for *ylmE* or *racX* alone showed a modest delay in pellicle disassembly (fig. S4). However, pellicles formed by cells doubly mutant for the putative racemases were substantially delayed in disassembly (fig. S4). Conversely, cells engineered to overexpress *ylmE* were blocked in biofilm formation (fig. S5). Also, conditioned medium from the double mutant was ineffective at inhibiting biofilm formation, in contrast to conditioned medium from the wild type (Fig. 2B). Next, we asked whether D-amino acids are produced in sufficient abundance to account for disassembly of mature biofilms. Accordingly, we carried out liquid chromatography–mass spectrometry, followed by the identification of the D-amino acids using derivatization with Nα-(2,4-dinitro-5-fluorophenyl)-L-alaninamide (L-FDAA) on conditioned medium collected at early and late times after pellicle formation. D-tyrosine (6 μM), D-leucine (23 μM), and D-methionine (5 μM) were present at concentrations at or above those needed to inhibit biofilm formation by day 6, but only at concentrations of <10 nM at day 3. In contrast, the *ylmE racX* double mutant was blocked in D-tyrosine production and impaired in D-leucine production at day 6 (table S1).

How do D-amino acids disassemble biofilms? D-amino acids did not inhibit growth (fig. S6), nor did they inhibit the expression of the matrix operons *epsA-O* and *yqxM-sipW-tasA* (fig. S7). D-amino acids are incorporated into the peptide side chains of peptidoglycan in place of the terminal D-alanine (*10*). Using ^{14}C– D-tyrosine, we confirmed that D-tyrosine (but not ^{14}C–L-proline) was incorporated into the cell wall (fig. S8), with incorporation beginning at day 3 (fig. S9). Finally, in keeping with the idea that D-amino acids act via their incorporation into the wall, the effects of D-tyrosine and other D-amino acids were prevented by D-alanine (Fig. 1, K and L, and fig. S2).

We hypothesized that TasA fibers are anchored to the cell wall and that the incorporation of biofilm-disassembling D-amino acids into the cell wall might disengage the fibers from their anchor. To investigate this possibility, we examined the localization of a functional fusion of TasA with the fluorescent reporter mCherry. Treatment with D-tyrosine had little effect on the accumulation of TasA-mCherry (fig. S10). In contrast, when the cells were washed by centrifugation, re-suspended, and then examined by fluorescence microscopy, untreated cells, which were often in clumps, were intensely decorated with TasA-mCherry (Fig. 3A). In contrast, D-tyrosine–treated cells, which were largely unclumped, showed only low levels of fluorescence (17-fold lower; table S2). Similar results were obtained with D-leucine and with the D-amino acid mixture. We also carried out electron microscopy (EM) with gold-labeled antibodies to TasA (anti-TasA) to visualize unmodified TasA. TasA fibers were anchored to the cells of untreated pellicles (Fig. 3B, images 1 and 2). In contrast, cells treated with D-tyrosine consisted of

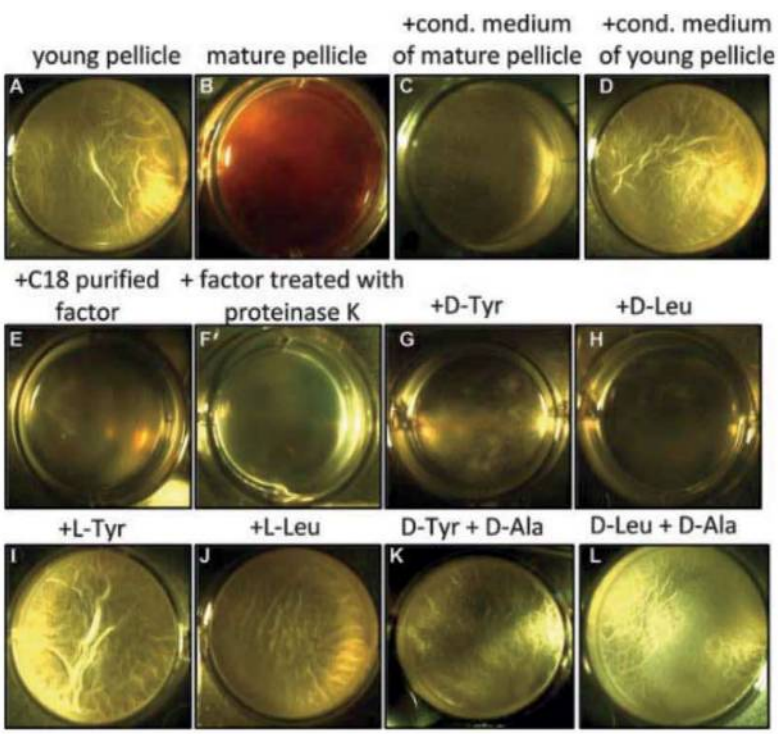

Fig. 1. Conditioned medium blocks pellicle formation. *B. subtilis* strain NCIB3610 was grown at 22°C in 12-well plates in a liquid biofilm-inducing medium for 3 days (**A**) or 8 days (**B**). (**C** and **D**) Cells grown for 3 days in a medium with added dried and resuspended methanol eluate (1:100 v/v) from a C18 column (Sep Pak) that had been loaded with conditioned (cond.) medium from a 6- to 8-day-old culture (C) or a 3-day-old culture (D). The final concentration of concentrated factor added to the wells represented a 1:4 dilution on a volume basis of the original conditioned medium. (**E**) The factor was further purified on the C18 column by stepwise elution with methanol. The result of adding 3 μl of the 40% methanol eluate is shown. (**F**) Before addition to fresh medium, the 40% methanol eluate was incubated with proteinase K beads. (**G** to **L**) Wells containing MSgg medium supplemented with D-tyrosine (3 μM), D-leucine (8.5 mM), L-tyrosine (7 mM), L-leucine (8.5 mM), D-tyrosine (3 μM), and D-alanine (10 mM) or with D-leucine (8.5 mM) and D-alanine (10 mM) were inoculated with strain NCIB3610 and incubated for 3 days. The diameter of all wells was 22.1 mm.

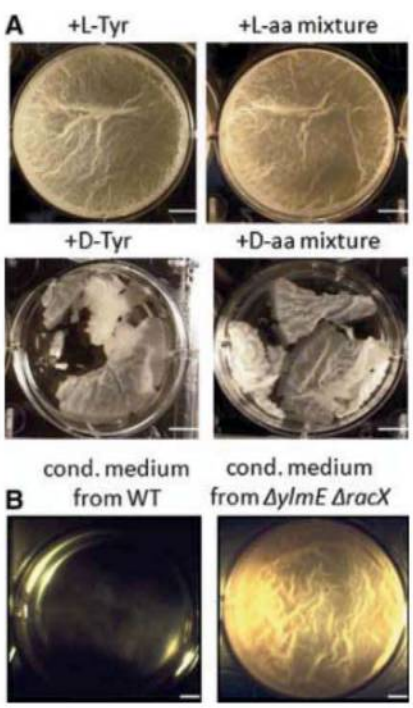

Fig. 2. D-amino acids break down pellicles, and inhibition of pellicle formation by conditioned medium depends on racemase genes . (**A**) Three-day-old cultures with added (as a 10 μl drop to the surface of the pellicles to achieve the indicated final concentration) L-tyrosine (7 mM), a mixture of L-amino acids (5 mM each), D-tyrosine (3 μM), or a mixture of D-amino acids (2.5 nM each). (**B**) Effect of concentrated C18 column (Sep Pak) eluate from a conditioned medium from an 8-day-old culture from the wild type or from a strain (IKG55) doubly mutant for *ylmE* and *racX*. Scale bars, 7 mm.

a mixture of cells that were largely undecorated with TasA fibers and free TasA fibers or aggregates of fibers that were not anchored to cells (Fig. 3B, images 3 to 6).

Next, we isolated D-amino acid–resistant mutants (Fig. 4A). Wrinkled papillae appeared spontaneously on the flat colonies formed during growth on a solid medium containing D-tyrosine (Fig. 4A) or D-leucine (fig. S2). When purified, these spontaneous mutants gave rise to wrinkled colonies and pellicles in the presence of individual D-amino acids. We isolated several such mutants and found that they contained mutations in the 3′ region of *yqxM* (table S3). Two mutations that conferred resistance to D-tyrosine were examined in detail: (i) *yqxM2* was an insertion of G:C at base pair 728 and (ii) *yqxM6* was a deletion of A:T at base pair 569 (Fig. 4B). The presence of *yqxM2* and *yqxM6* restored clumping and cell decoration by TasA-mCherry to cells treated with D-tyrosine (Fig. 3A and fig. S12; see above text). Because YqxM is required for the association of TasA with cells (*6*), the discovery that the biofilm-inhibiting effect of D-amino acids could be overcome by mutants of YqxM reinforces the view that the effect of D-amino acid incorporation into the cell wall is to impair the anchoring of the TasA fibers to the cell. A domain near the C terminus of YqxM could trigger the release of TasA in response to the presence of D-amino acids in the cell wall.

Finally, we wondered whether D-amino acids would inhibit biofilm formation by other bacteria. The pathogens *Staphylococcus aureus* and *Pseudomonas aeruginosa* form biofilms on plastic surfaces (*12*), which can be detected by washing away unbound cells and staining the bound cells with crystal violet. D-tyrosine and the D-amino acid mixture were effective in preventing biofilm formation (fig. S13), whereas L-tyrosine and L-amino acids had no effect. Furthermore, the effect of D-amino acids was prevented by the presence of D-alanine (fig. S13), suggesting that D-amino acids acted to block biofilm formation by replacement of D-alanine in the peptide side chain. Given that many bacteria produce D-amino acids, these amino acids may provide a general strategy for biofilm disassembly. If so, then D-amino acids might prove widely useful in medical and industrial applications for the prevention or eradication of biofilms.

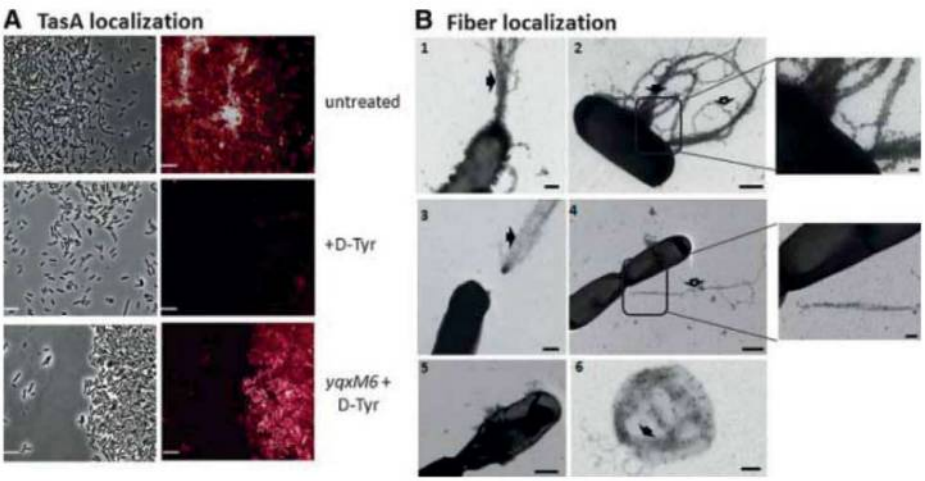

Fig. 3. D-tyrosine causes the release of TasA fibers. (**A**) Cell association of TasA-mCherry by fluorescence microscopy. Wild-type cells and *yqxM6* (IKG51) mutant cells containing the *tasA-mCherry* fusion were grown to stationary phase (optical density at 600 nm = 1.5) with shaking in a biofilm-inducing medium in the presence (+D-Tyr) or absence (untreated) of D-tyrosine (6 μM), as indicated. The cells were then washed in phosphate-buffered saline and visualized by fluorescence microscopy. Scale bars, 4 μm. (**B**) Cell association of TasA fibers by EM. 24-hour-old cultures were incubated without (images 1 and 2) or with (images 3 to 6) D-tyrosine (0.1 mM) for an additional 12 hours. TasA fibers were stained by immunogold labeling with anti-TasA antibodies and visualized by transmission electron microscopy. Solid black arrows indicate fiber bundles; open arrows indicate individual fibers. Scale bars in the enlargements of images 2 and 4 and in image 6, 100 nm; all other scale bars, 500 nm. Images 1 and 2 show fiber bundles attached to cells; images 3, 4, and 6 show individual fibers and bundles detached from cells; and images 3 to 5 show cells with little or no fiber material. For further details, see the supporting online material (*9*).

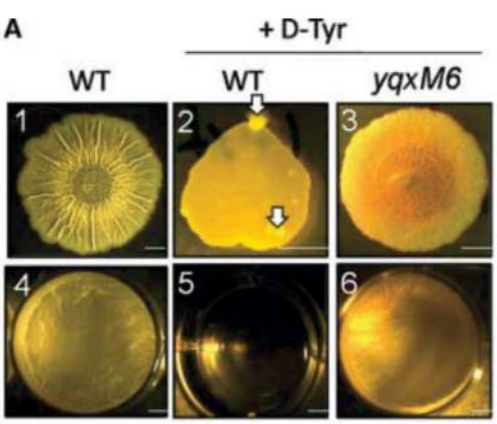

Fig. 4. Biofilm formation by YqxM mutants resistant to D-tyrosine. (**A**) Wild-type or *yqxM6* (IKG51) mutant cells grown on a solid (images 1 to 3) or liquid (images 4 to 6) biofilm-inducing medium. Cells were grown in the absence (1 and 4) or presence (2, 3, 5, and 6) of D-tyrosine (3 μM). Arrows in image 2 indicate papillae of spontaneous resistances mutants. Scale bars, 3 mm. (**B**) C-terminal amino acid sequences for wild-type YqxM and the indicated frame-shift mutants (altered sequences in blue).

B C-terminus YqxM wild-type and mutant sequences

181 192 227 253
EPMRLAKCDEKP // AVTKEKETQSDQKESGEEDKSNEADQ-COOH **WT**

181 192 227
EPMRLAKCDEKP // AVTKEKETQSDQKESGRG-COOH **YqxM2**

181
EPMRLANAMKNRQSLKKKQSRTSKRRMKQHKKIYRKKQ-COOH **YqxM6**

References and Notes

1. D. López, H. Vlamakis, R. Kolter, *FEMS Microbiol. Rev.* **33**, 152 (2009).
2. E. Karatan, P. Watnick, *Microbiol. Mol. Biol. Rev.* **73**, 310 (2009).
3. C. Aguilar, H. Vlamakis, R. Losick, R. Kolter, *Curr. Opin. Microbiol.* **10**, 638 (2007).
4. H. Vlamakis, C. Aguilar, R. Losick, R. Kolter, *Genes Dev.* **22**, 945 (2008).
5. S. S. Branda, J. E. González-Pastor, S. Ben-Yehuda, R. Losick, R. Kolter, *Proc. Natl. Acad. Sci. U.S.A.* **98**, 11621 (2001).
6. S. S. Branda, F. Chu, D. B. Kearns, R. Losick, R. Kolter, *Mol. Microbiol.* **59**, 1229 (2006).
7. D. Romero, C. Aguilar, R. Losick, R. Kolter, *Proc. Natl. Acad. Sci. U.S.A.* **107**, 2230 (2010).
8. F. Chu, D. B. Kearns, S. S. Branda, R. Kolter, R. Losick, *Mol. Microbiol.* **59**, 1216 (2006).
9. Materials and methods are available as supporting material on *Science* Online.
10. H. Lam *et al.*, *Science* **325**, 1552 (2009).
11. T. Yoshimura, N. Esak, *J. Biosci. Bioeng.* **96**, 103 (2003).
12. M. Otto, *Curr. Top. Microbiol. Immunol.* **322**, 207 (2008).

13. We thank T. Norman for the analysis of table S2. I.K.-G. and D.R. are postdoctoral fellows of the Human Frontier Science Program and Fulbright/Ministerio de Educación y Ciencia (Spain), respectively. This work was funded by NIH grants to R.K. (GM58213), J.C. (GM086258 and CA24487), and R.L. (GM18546), as well as grants from BASF to R.K. and R.L. Additionally, we have filed a patent application on the use of D-amino acids for biofilm disassembly.

Supporting Online Material

www.sciencemag.org/cgi/content/full/328/5978/627/DC1
Materials and Methods
Figs. S1 to S13
Tables S1 to S3
References

22 February 2010; accepted 18 March 2010
10.1126/science.1188628

Light-Induced Structural Changes in a Photosynthetic Reaction Center Caught by Laue Diffraction

Annemarie B. Wöhri,[1]* Gergely Katona,[2] Linda C. Johansson,[2] Emelie Fritz,[2] Erik Malmerberg,[2] Magnus Andersson,[1] Jonathan Vincent,[3] Mattias Eklund,[3] Marco Cammarata,[4] Michael Wulff,[4]† Jan Davidsson,[3] Gerrit Groenhof,[5] Richard Neutze[2]‡

Photosynthetic reaction centers convert the energy content of light into a transmembrane potential difference and so provide the major pathway for energy input into the biosphere. We applied time-resolved Laue diffraction to study light-induced conformational changes in the photosynthetic reaction center complex of *Blastochloris viridis*. The side chain of TyrL162, which lies adjacent to the special pair of bacteriochlorophyll molecules that are photooxidized in the primary light conversion event of photosynthesis, was observed to move 1.3 angstroms closer to the special pair after photoactivation. Free energy calculations suggest that this movement results from the deprotonation of this conserved tyrosine residue and provides a mechanism for stabilizing the primary charge separation reactions of photosynthesis.

All photosynthetic reaction centers share a conserved functional core and are believed to have evolved from a single common ancestor. In the reaction center of the purple bacterium *Blastochloris viridis* (RC_{vir}) (*1*), transmembrane subunits H, L, and M support four bacteriochlorophylls, two bacteriopheophytins, a bound menaquinone (Q_A), a mobile ubiquinone (Q_B), and a single nonheme iron, creating an electron transfer chain that spans the membrane (Fig. 1A). Photoexcitation of a strongly interacting pair of bacteriochlorophyll molecules, the "special pair" (P), promotes the movement of an electron to the primary and secondary quinone acceptors, Q_A and Q_B, respectively (black arrows, Fig. 1A). After the reduction of P^+ from the tetraheme cytochrome c subunit (red arrows, Fig. 1A), the absorption of a second photon by the special pair triggers a second electron transfer to Q_B^-, which is protonated from the cytoplasm and released as ubiquinol (QH_2) into the membrane. Coupled cyclic electron transfer reactions involving the integral membrane cytochrome bc_1 complex and soluble cytochrome c_2 ensure that

[1]Department of Chemical and Biological Engineering, Chalmers University of Technology, Box 462, SE-40530 Göteborg, Sweden. [2]Department of Chemistry, Biochemistry and Biophysics, University of Gothenburg, Box 462, SE-40530 Göteborg, Sweden. [3]Department of Photochemistry and Molecular Science, Uppsala University, Box 523, SE-75120 Uppsala, Sweden. [4]European Synchrotron Radiation Facility, BP 220, Grenoble Cedex 38043, France. [5]Computational Biomolecular Chemistry Group, Department of Theoretical and Computational Biophysics, Max Planck Institute for Biophysical Chemistry, Am Fassberg 11, D-37077 Göttingen, Germany.

*Present address: AstraZeneca Research and Development, Cell, Protein, and Structural Sciences, SE 43183 Mölndal, Sweden.

†Present address: SLAC National Accelerator Laboratory, 2575 Sand Hill Road, Menlo Park, CA 94025, USA.

‡To whom correspondence should be addressed. E-mail: Richard.Neutze@chem.gu.se

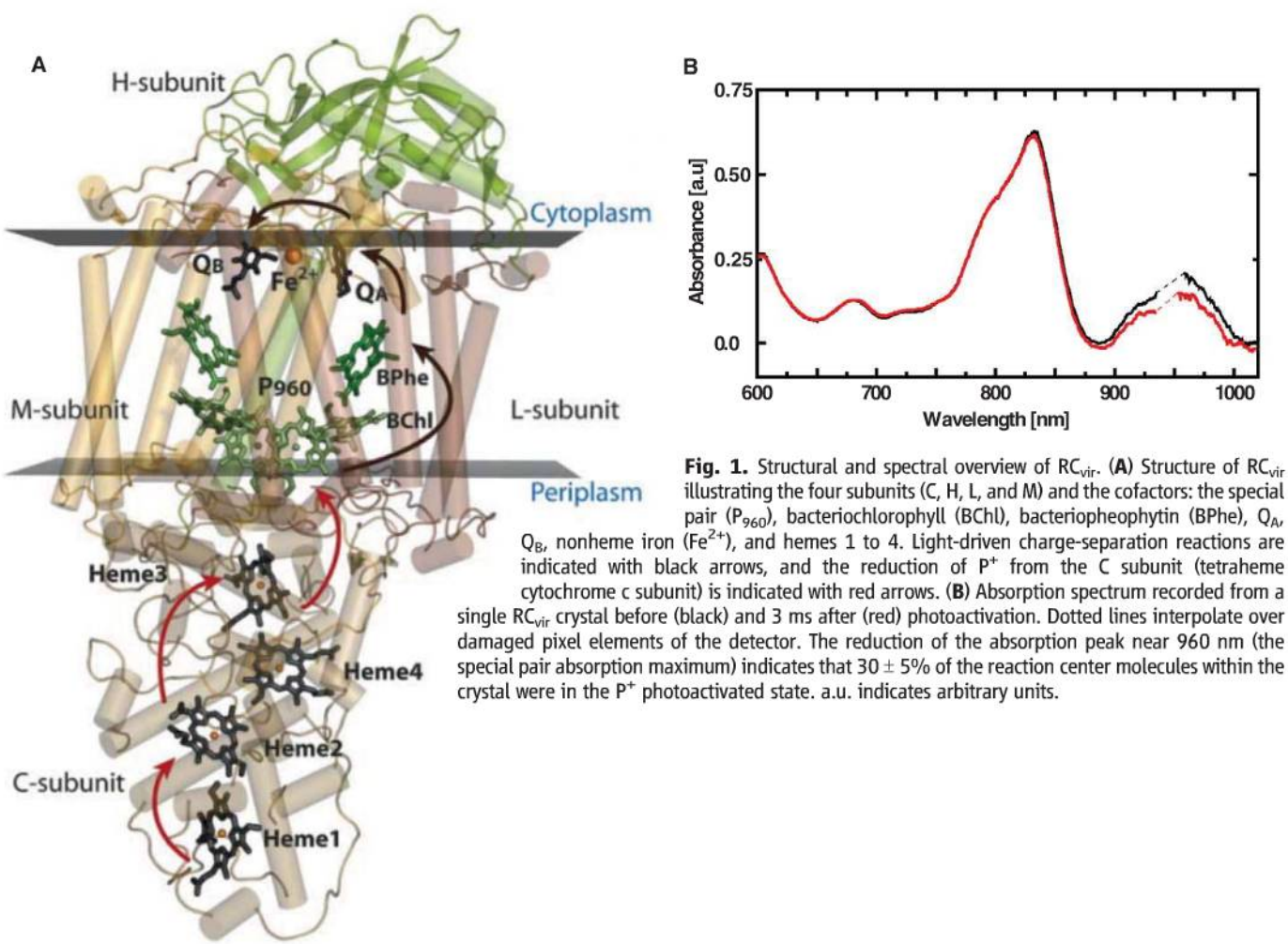

Fig. 1. Structural and spectral overview of RC_{vir}. (**A**) Structure of RC_{vir} illustrating the four subunits (C, H, L, and M) and the cofactors: the special pair (P_{960}), bacteriochlorophyll (BChl), bacteriopheophytin (BPhe), Q_A, Q_B, nonheme iron (Fe^{2+}), and hemes 1 to 4. Light-driven charge-separation reactions are indicated with black arrows, and the reduction of P^+ from the C subunit (tetraheme cytochrome c subunit) is indicated with red arrows. (**B**) Absorption spectrum recorded from a single RC_{vir} crystal before (black) and 3 ms after (red) photoactivation. Dotted lines interpolate over damaged pixel elements of the detector. The reduction of the absorption peak near 960 nm (the special pair absorption maximum) indicates that 30 ± 5% of the reaction center molecules within the crystal were in the P^+ photoactivated state. a.u. indicates arbitrary units.

the tetraheme cytochrome c subunit is reduced from the periplasm (fig. S1). As a consequence, two protons are pumped for every photon absorbed, and the resulting transmembrane potential difference is primarily harvested by adenosine triphosphate (ATP) synthase to regenerate ATP.

Protein conformational changes are believed to participate in the function and regulation of photosynthetic reaction centers. X-ray diffraction studies of crystals of the *Rhodobacter sphaeroides* reaction center (RC_{sph}) illuminated at room temperature before rapid freezing implicated a substantial movement of Q_B upon its reduction to semiquinone (*2*). A concerted movement of the H subunit was also observed in crystals of the same reaction center after prolonged illumination with bright light (*3*). Time-resolved Laue diffraction provides a direct approach for observing protein conformational changes in real time at room temperature. This method has captured light-induced electron density changes in myoglobin: carbon monoxide complexes (*4*, *5*) and photoactive yellow protein (*6*, *7*), although similar studies of a photosynthetic reaction center did not reveal any structural changes (*8*).

In this work, we used time-resolved Laue diffraction (*9*) to probe light-driven conformational changes occurring at room temperature in RC_{vir} crystals grown from a lipidic-sponge phase matrix (*10*). Time-resolved single-crystal microspectrophotometry (*9*) established that the photooxidized P^+ state persisted with 30 ± 5% occupancy 3 ms after exposure to green light (Fig. 1B), and these crystals diffracted to 2.5 Å resolution when exposed to a single polychromatic x-ray pulse train of 86-μs duration (fig. S2). Table S1 summarizes the Laue diffraction data and refinement statistics processed to 2.95 Å resolution for both the resting state (laser off, F_{dark}) and 3 ms after photoactivation (laser on, F_{light}), and fig. S3 illustrates the $2F_{obs} - F_{calc}$ electron density map. An overview of the experimental $F_{light} - F_{dark}$ difference Fourier electron density map is shown in Fig. 2A. As with an earlier Laue diffraction study on RC_{vir} (*8*), no significant difference density features arise to suggest a movement of ubiquinone within the Q_B pocket, perhaps because of variable Q_B occupancy in this crystal form (*10*).

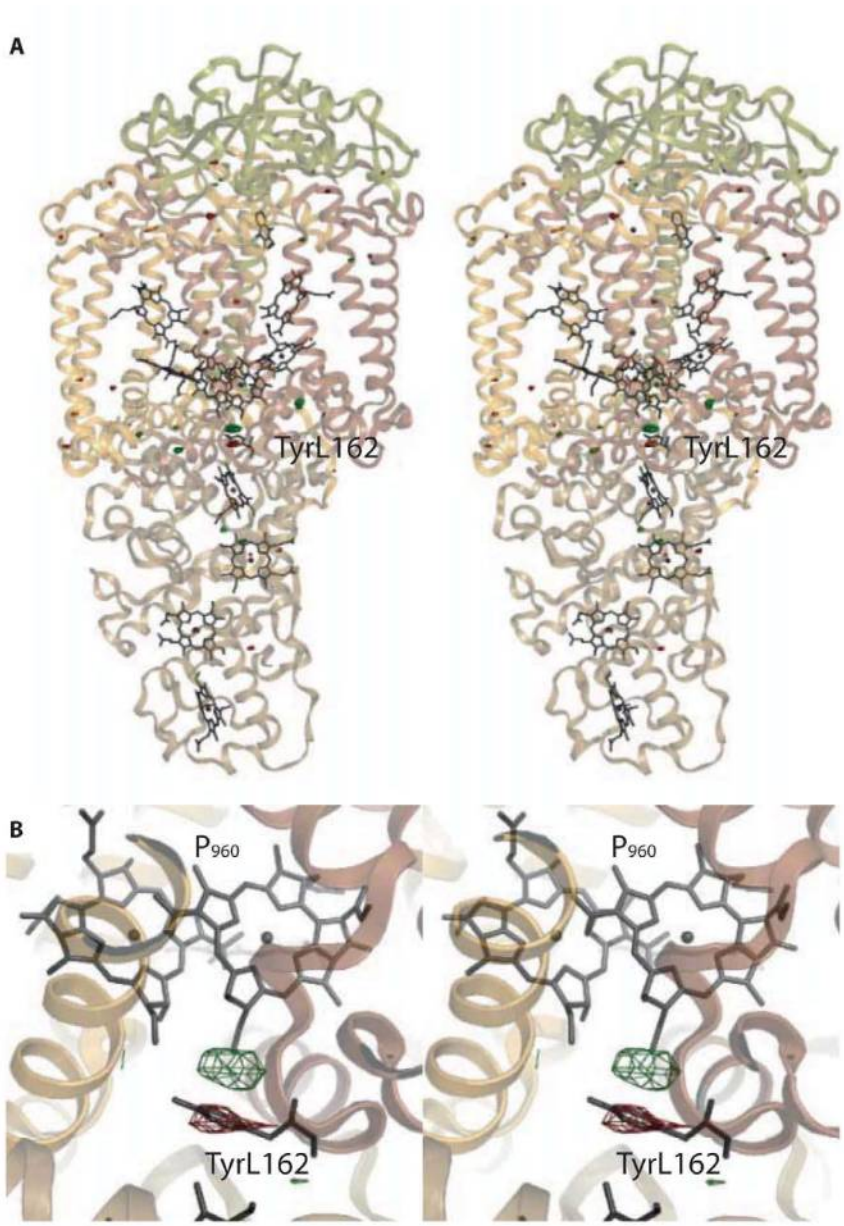

Fig. 2. Experimentally observed electron density changes in RC_{vir}. (**A**) Long-distance stereo overview of the $F_{light} - F_{dark}$ difference Fourier electron density map recorded 3 ms after laser photoactivation (green mesh, positive density; red mesh, negative density; contoured at 4.0 σ). (**B**) Close-up stereoview of the difference Fourier map near the special pair. Complementary positive and negative electron density changes (contoured at 4.0 σ) indicate the movement of TyrL162 toward P^+.

Both the strongest positive (green) and negative (red) difference electron density peaks (table S2) are associated with the side chain of Tyr^{162} of the L subunit (TyrL162) (Fig. 2B). Paired negative and positive difference density features are the fingerprint of conformational change and reveal that the side chain of TyrL162 reorients toward P^+ in the photoactivated state. These features are also the most reproducible difference density peaks observed in maps recovered from three independent crystals (table S2 and fig. S4A), and they persisted after diffraction data from all three crystals were merged (table S2 and fig. S4B). Theoretical difference Fourier maps calculated to 2.95 Å resolution from the photoactivated and resting-state models reproduced these difference density features (fig. S5), and the crystallographic occupancy was 35 ± 5% for the new conformation, consistent with spectroscopic characterization of the P^+ state (Fig. 1B).

TyrL162 is strictly conserved in purple bacterial reaction centers (*11*, *12*) and lies between the special pair of bacteriochlorophylls and the highest potential heme c_{559} (heme 3, Fig. 1A) of the cytochrome c subunit. Its side chain hydroxyl group forms a H-bond interaction with a water molecule (Wat501), which in turn is coordinated by two other water molecules and the hydroxyl group of SerM188 (Fig. 3A). Structural refinement of the photoactivated state (table S1) established that the hydroxyl oxygen of TyrL162 undergoes a 1.3 Å movement toward P^+ (Fig. 3B), effectively bringing it into steric contact with the L-branch bacteriochlorophyll of P (fig. S6). This conformational change also creates new H-bond interactions of TyrL162 with the hydroxyl group of ThrM185 and Wat10 (Fig. 3B). A possible movement of Wat501 that would preserve its H bond to TyrL162 could not be refined because of spatial overlap with the resting-state model.

Photooxidation of the special pair changes the electrostatic environment of TyrL162, and this must drive its movement toward the transient

positive charge, which implies that TyrL162 is negatively charged in the photoactivated state. Conversely, it is energetically unfavorable to bury an isolated charge within the low dielectric environment of a cellular membrane, such that the photooxidized special pair could be stabilized by the creation of a nearby phenolate anion. The transient formation of H-bond interactions by TyrL162 with ThrM185 and Wat10 (Fig. 3B) would also stabilize its deprotonated form. Molecular dynamics trajectories demonstrate that the deprotonated form of TyrL162 adopts a conformation 1.1 Å closer (on average) to the photooxidized special pair than when it is protonated (Fig. 3, C and D) and 1.3 Å closer than that adopted without photoactivation, consistent with our structural findings. We thus conclude that the photooxidation of P to P^+ changes the chemical environment of TyrL162 such that its deprotonated form becomes favored. Fourier transform infrared spectroscopy studies of electrochemically oxidized reaction centers have observed a difference signal at 1532 cm^{-1} for RC_{vir} (1526 cm^{-1} for RC_{sph}) that was interpreted as arising from conformational or hydrogen bond changes of a tyrosine residue located near the special pair (*13*). Although this feature might also be taken to indicate TyrL162 deprotonation, its unique assignment is challenging because the prosthetic groups also contribute a strong difference signal in this region (*14*).

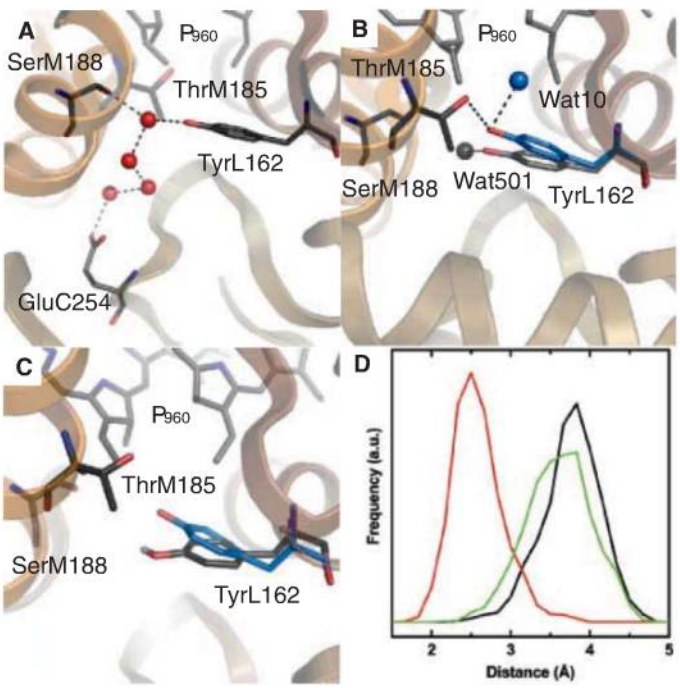

Fig. 3. Modeled light-induced structural changes in RC_{vir} and their dependence on the protonation state of TyrL162. (**A**) Resting-state conformation of TyrL162. A chain of water molecules (red spheres) stretches from TyrL162 toward the protein's surface via SerM188 and GluC254. (**B**) Refined movement of TyrL162 (blue) overlaid on its resting-state conformation (gray). In the photoactivated conformation, TyrL162 forms H-bond interactions with ThrM185 and Wat10. (**C**) Snapshots from molecular dynamics trajectories showing a reorientation of TyrL162 toward P^+ observed when TyrL162 is deprotonated (blue) but not when protonated (gray). (**D**) Histogram plot showing the frequency with which a given minimum distance from the TyrL162 side chain to the photooxidized special pair occurs when TyrL162 is protonated (green) or deprotonated (red) and for the nonilluminated state (black). Histograms were extracted from the final 30 ns (after 10-ns equilibration) of molecular dynamics trajectories.

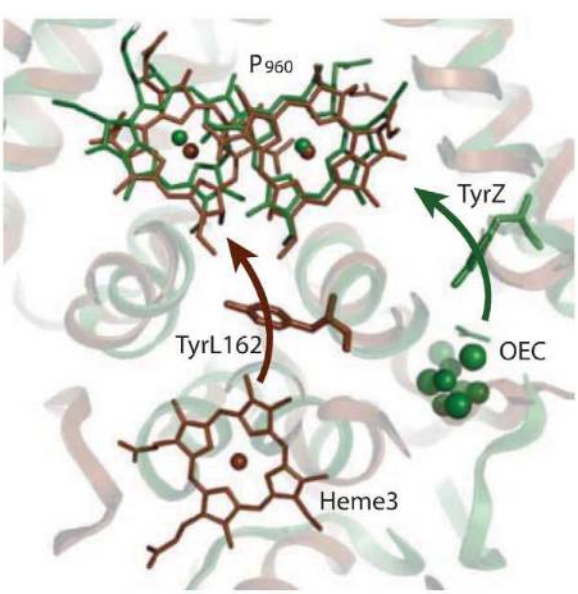

Fig. 4. Structural overlay of photosystem II (green, PDB entry 1S5L) and RC_{vir} (brown) near the special pair. TyrL162 lies between the high-potential heme of the cytochrome c subunit (heme 3) and the special pair of RC_{vir} (brown, P_{960}), whereas Tyr_Z lies between the oxygen-evolving center (OEC) and the special pair of photosystem II (green). Arrows indicate the movement of electrons as the photooxidized special pair is reduced.

The free energy required for the transfer of the hydroxyl proton of TyrL162 to the carboxylate moiety of GluC254 (Fig. 3A) was also calculated from molecular dynamics trajectories of both the resting ($P:Q_A$) and the photoactivated ($P^+:Q_A^-$) states with the tetraheme cytochrome c subunit both fully oxidized and fully reduced. From these trajectories, we observe that the energy requirements for proton transfer were lowered upon photoactivation by the same amount independent of whether the cytochrome subunit was oxidized or reduced [46 ± 3 kJ mol^{-1} and 47 ± 6 kJ mol^{-1}, respectively (fig. S7)]. These values correspond to a relative change of 8 ± 1 pK_a units (where K_a is the acid dissociation constant) such that, should the resting-state pK_a values of TyrL162 and GluC254 be close to their reference values of 9.8 and 4.3, respectively (*15*), spontaneous proton transfer would occur. Moreover, the water-mediated hydrogen bond network that connects these two groups (Fig. 3A and fig. S8) also provides an efficient channel for conducting a proton into the bulk (pH = 8.1) via the solvent-exposed GluC254, such that TyrL152 could spontaneously deprotonate even if its resting pK_a value was significantly elevated. In this manner, the excess positive charge on P^+ induces a proton transfer from TyrL162 in a direction opposite to that of the electron transfer, illustrating how coupled electron-proton transfer reactions arise in photosynthetic energy conversion. This principle could be translated into future synthetic systems for artificial photosynthesis (*16*, *17*).

Spectroscopic studies of TyrL162 mutants of RC_{sph} have established that this aromatic residue strongly influences the binding affinity of the soluble cytochrome c_2 to photooxidized RC_{sph} (*18*, *19*), and this effect correlates with the kinetics of electron transfer to the special pair (*19*). For RC_{vir}, which has a permanently bound tetraheme cytochrome c subunit, the mutation of TyrL162 has considerably less effect on the rate of electron transfer from heme c_{559} to P^+ (*11*), and the specific differences could be explained in terms of a super exchange mechanism with the residue at L162 mediating the electron transfer (*20*). This electron transfer reaction, however, is drastically inhibited below 215 K in the wild-type RC_{vir}, and both the extent of inhibition and its temperature dependence are strongly perturbed by mutation of TyrL162 (*12*). This remarkable temperature sensitivity has been interpreted in terms of a loss of mobility of TyrL162 at low temperature (*21*, *22*) or resulting from the suppression of unspecified structural reorganizations associated with the oxidation of heme c_{559} (*12*). Our observation that TyrL162 changes conformation in response to photooxidation of P^+ adds credence to suggestions that the specific orienta-

tion (*21*) and protonation state (*22*) of TyrL162 may be important for the mechanism of electron transfer, and the transient creation of a negatively charged tyrosyl group between heme c_{559} and P^+ could stabilize the oxidized form of the cytochrome subunit (*12*).

From the temperature dependence of the $P^+:Q_A^- \rightarrow P:Q_A$ charge recombination reaction, it was proposed that structural changes occurring in response to electron transfer decrease the free energy gap between P^+ and Q_A^- of RC_{sph} by about 12 kJ mol^{-1} (*23*). Similar measurements of the pH dependence of the RC_{vir} charge recombination reaction showed the $P^+:Q_A^-$ state to be stabilized by a chemical group with an approximate pK_a of 9 (*24*). Prolonged exposure to bright light is also known to reversibly stabilize the $P^+:Q_A^-$ state of RC_{sph}, slowing the charge recombination reaction by up to three orders of magnitude (*3*, *25*, *26*). Light-induced deprotonation and conformational switching of TyrL162 could contribute to all three stabilization effects, because the creation of a phenolate anion in immediate proximity to the special pair effectively neutralizes the energetic penalty associated with the buried positive charge on P^+.

Electron paramagnetic resonance spectroscopy studies of RC_{sph} mutants that increase the midpoint potential of the special pair have shown that TyrL162 can form a (deprotonated) tyrosyl radical in response to charge separation (*27*), confirming that TyrL162 can be deprotonated by photooxidation of the special pair. Photooxidation of photosystem II also creates a tyrosyl radical ($Tyr_Z^{\bullet}$) (*28*, *29*), which oxidizes the manganese cluster and leads to the synthesis of molecular oxygen from water. Crystal structures of photosystem II (*30*) reveal that Tyr_Z lies between the oxygen-evolving center and the special pair in a position functionally analogous to that occupied by TyrL162 of RC_{vir} (Fig. 4). Our findings suggest that the deprotonation and coupled conformational switching of TyrL162 may have aided the spontaneous formation of tyrosine radicals in an ancient reaction center, thereby creating the chemical potential to extract electrons from clusters of manganese atoms (*31*) and ultimately oxidize water to oxygen.

References and Notes

1. J. Deisenhofer, O. Epp, K. Miki, R. Huber, H. Michel, *Nature* **318**, 618 (1985).
2. M. H. Stowell *et al.*, *Science* **276**, 812 (1997).
3. G. Katona *et al.*, *Nat. Struct. Mol. Biol.* **12**, 630 (2005).
4. V. Srajer *et al.*, *Science* **274**, 1726 (1996).
5. F. Schotte *et al.*, *Science* **300**, 1944 (2003).
6. U. K. Genick *et al.*, *Science* **275**, 1471 (1997).
7. B. Perman *et al.*, *Science* **279**, 1946 (1998).
8. R. H. Baxter *et al.*, *Proc. Natl. Acad. Sci. U.S.A.* **101**, 5982 (2004).
9. Materials and methods are available as supporting material on *Science* Online.
10. A. B. Wöhri *et al.*, *Biochemistry* **48**, 9831 (2009).
11. B. Dohse *et al.*, *Biochemistry* **34**, 11335 (1995).
12. J. M. Ortega, B. Dohse, D. Oesterhelt, P. Mathis, *Biophys. J.* **74**, 1135 (1998).
13. M. Leonhard, W. Mäntele, *Biochemistry* **32**, 4532 (1993).
14. S. Buchanan, H. Michel, K. Gerwert, *Biochemistry* **31**, 1314 (1992).
15. R. L. Thurlkill, G. R. Grimsley, J. M. Scholtz, C. N. Pace, *Protein Sci.* **15**, 1214 (2006).
16. N. S. Lewis, D. G. Nocera, *Proc. Natl. Acad. Sci. U.S.A.* **103**, 15729 (2006).
17. L. Hammarström, S. Styring, *Philos. Trans. R. Soc. London Ser. B* **363**, 1283 (2008).
18. J. Wachtveitl, J. W. Farchaus, P. Mathis, D. Oesterhelt, *Biochemistry* **32**, 10894 (1993).
19. X. M. Gong, M. L. Paddock, M. Y. Okamura, *Biochemistry* **42**, 14492 (2003).
20. Y. Ohtsuka, K. Ohkawa, H. Nakatsuji, *J. Comput. Chem.* **22**, 521 (2001).
21. B. Cartling, *J. Chem. Phys.* **95**, 317 (1991).
22. B. Cartling, *Chem. Phys. Lett.* **196**, 128 (1992).
23. B. H. McMahon, J. D. Müller, C. A. Wraight, G. U. Nienhaus, *Biophys. J.* **74**, 2567 (1998).
24. P. Sebban, C. A. Wraight, *Biochim. Biophys. Acta* **974**, 54 (1989).
25. F. van Mourik, M. Reus, A. R. Holzwarth, *Biochim. Biophys. Acta* **1504**, 311 (2001).
26. U. Andréasson, L. E. Andréasson, *Photosynth. Res.* **75**, 223 (2003).
27. A. J. Narváez, R. LoBrutto, J. P. Allen, J. C. Williams, *Biochemistry* **43**, 14379 (2004).
28. B. A. Barry, G. T. Babcock, *Proc. Natl. Acad. Sci. U.S.A.* **84**, 7099 (1987).
29. R. J. Debus, B. A. Barry, I. Sithole, G. T. Babcock, L. McIntosh, *Biochemistry* **27**, 9071 (1988).
30. K. N. Ferreira, T. M. Iverson, K. Maghlaoui, J. Barber, S. Iwata, *Science* **303**, 1831 (2004); published online 5 February 2004 (10.1126/science.1093087).
31. J. F. Allen, W. Martin, *Nature* **445**, 610 (2007).

32. Refined crystallographic coordinates and structure factor amplitudes are deposited within the Protein Data Bank (PDB) with codes 2x5u (dark state) and 2x5v (photoactivated state). We thank L. Hammarström for valuable discussions and acknowledge financial support from the Swedish Science Research Council (Vetenskapsrådet), European Commission [Research Training Network (RTN) "Fast light-actuated structural changes" (FLASH), and Integrated Project, the European Membrane Protein Consortium (EMEP)], European Molecular Biology Organization (EMBO), Human Frontier Science Program (HFSP), and the University of Gothenburg Quantitative Biology Platform.

Supporting Online Material

www.sciencemag.org/cgi/content/full/328/5978/630/DC1
Materials and Methods
Figs. S1 to S10
Tables S1 to S3
Scheme S1
References

21 December 2009; accepted 17 March 2010
10.1126/science.1186159

The Genome of the Western Clawed Frog *Xenopus tropicalis*

Uffe Hellsten,[1*] Richard M. Harland,[2] Michael J. Gilchrist,[3] David Hendrix,[2] Jerzy Jurka,[4] Vladimir Kapitonov,[4] Ivan Ovcharenko,[5] Nicholas H. Putnam,[6] Shengqiang Shu,[1] Leila Taher,[5] Ira L. Blitz,[7] Bruce Blumberg,[7] Darwin S. Dichmann,[2] Inna Dubchak,[1] Enrique Amaya,[8] John C. Detter,[9] Russell Fletcher,[2] Daniela S. Gerhard,[10] David Goodstein,[1] Tina Graves,[11] Igor V. Grigoriev,[1] Jane Grimwood,[1,12] Takeshi Kawashima,[2,13] Erika Lindquist,[1] Susan M. Lucas,[1] Paul E. Mead,[14] Therese Mitros,[2] Hajime Ogino,[15] Yuko Ohta,[16] Alexander V. Poliakov,[1] Nicolas Pollet,[17] Jacques Robert,[18] Asaf Salamov,[1] Amy K. Sater,[19] Jeremy Schmutz,[1,12] Astrid Terry,[1] Peter D. Vize,[20] Wesley C. Warren,[11] Dan Wells,[19] Andrea Wills,[2] Richard K. Wilson,[11] Lyle B. Zimmerman,[21] Aaron M. Zorn,[22] Robert Grainger,[23] Timothy Grammer,[2] Mustafa K. Khokha,[24] Paul M. Richardson,[1] Daniel S. Rokhsar[1,2]

The western clawed frog *Xenopus tropicalis* is an important model for vertebrate development that combines experimental advantages of the African clawed frog *Xenopus laevis* with more tractable genetics. Here we present a draft genome sequence assembly of *X. tropicalis*. This genome encodes more than 20,000 protein-coding genes, including orthologs of at least 1700 human disease genes. Over 1 million expressed sequence tags validated the annotation. More than one-third of the genome consists of transposable elements, with unusually prevalent DNA transposons. Like that of other tetrapods, the genome of *X. tropicalis* contains gene deserts enriched for conserved noncoding elements. The genome exhibits substantial shared synteny with human and chicken over major parts of large chromosomes, broken by lineage-specific chromosome fusions and fissions, mainly in the mammalian lineage.

African clawed frogs (the genus *Xenopus*, meaning "strange foot") comprise more than 20 species of frogs native to Sub-Saharan Africa. The species *Xenopus laevis* was first introduced to the United States in the 1940s where a low-cost pregnancy test took advantage of the responsiveness of frogs to human chorionic gonadotropin (*1*). Since the frogs were easy to raise and had other desirable properties such as large eggs, external development, easily manipulated embryos, and transparent tadpoles, *X. laevis* gradually developed into one of the most productive model systems for vertebrate experimental embryology (*2*).

However, *X. laevis* has a large paleotetraploid genome with an estimated size of 3.1 billion bases (Gbp) on 18 chromosomes and a generation time of 1 to 2 years. In contrast, the much smaller diploid western clawed frog, *X. tropicalis*, has a small genome, about 1.7 Gbp on 10 chromosomes (*3*), matures in only 4 months, and requires less space than its larger cousin. It is thus

readily adopted as an alternative experimental subject for developmental and cell biology (Fig. 1).

As a group, amphibians are phylogenetically well positioned for comparisons to other vertebrates, having diverged from the amniote lineage (mammals, birds, reptiles) some 360 million years ago. The comparison with mammalian and bird genomes also provides an opportunity to examine the dynamics of tetrapod chromosomal evolution.

The *X. tropicalis* draft genome sequence described here was produced from ~7.6-fold redundant random shotgun sampling of genomic DNA from a seventh-generation inbred Nigerian female. The assembly (*4*) (tables S1 to S3 and accession number AAMC00000000) spans about 1.51 Gbp of scaffolds, with half of the assembled sequence contained in 272 scaffolds ranging in size from 1.56 to 7.82 Mb. Of known genes, 97.6% are present in the assembly, attesting to its near completeness in genic regions (*4*). Nearly 2 million *Xenopus* expressed sequence tags (ESTs) from diverse developmental stages and adult tissues complement the genome and enable studies of alternative splicing and identification of developmental stage- and tissue-specific genes (*4*).

More than one-third of the frog genome consists of transposable elements (TEs) (table S7), higher than the 9% TE density in the chicken genome (*5*) but comparable to the 40 to 50% density in mammalian genomes (*6*, *7*). Many families of frog TEs are more than 25% divergent from their consensus sequence, so like mammalian and bird TEs they have persisted for as long as 20 to 200 million years (*5*, *6*). This contrasts with the faster turnover observed in insects, nematodes, fungi, and plants (*6*, *8*, *9*). Recently active TEs (1 to 5 million years ago) are more common in frogs than in mammals or birds, and their prevalence is comparable to that in fish, insects, nematodes, and plants. Among these is an unusually high diversity of very young families of L1 non-LTR (long terminal repeat) retrotransposons, Penelope, and DIRS retrotransposons. In contrast to those of other vertebrates, most recognizable frog TEs (72%) are DNA transposons, rather than the retrotransposons that dominate other genomes (*5*–*8*, *10*). Among these families (*11*, *12*), we identified *Kolobok* as a previously uncharacterized superfamily of DNA transposons. The genome also contains LTR retrotransposons of all major superfamilies, with higher diversity than in all other studied eukaryotes (table S8). Although most are ubiquitous, *Copia*, *BEL*, and *Gypsy* elements are not found in birds and mammals, suggesting that this subset became immobile after divergence from the amphibian lineage.

Using homology-based gene prediction methods and deep *Xenopus* EST and cDNA resources, we estimated that the *X. tropicalis* genome contains 20,000 to 21,000 protein-coding genes. These include orthologs of 79% of identified human disease genes (*4*). The genome contains 1850 tandem expanded gene families with between 2 and 160 copies, accounting for nearly 24% of protein-coding loci. The largest expansion comprises tetrapod-specific olfactory receptors (class II) occupying the first 1.7 Mb on scaffold_24. Other large expansions include protocadherins, bitter-taste receptors, and vomeronasal (pheromone) receptors (table S9).

The *X. tropicalis* genome displays long stretches of gene colinearity with human and chicken (Fig. 2). Of the 272 largest scaffolds (totaling half the assembly), 267 show such colinearity (*4*). Sixty percent of all gene models on these scaffolds can be directly associated with a human and/or chicken ortholog by conserved synteny. Patches of strict conserved colinearity are interrupted by large-scale inversions within the same linkage groups, and more rarely by chromosome breakage and fusion events, similar to the findings reported for the human and chicken genome (Fig. 2) (*5*) and in agreement with persistent conservation of linkage groups across chordates (*13*).

We uniquely placed 1696 markers from the existing genetic map of *X. tropicalis* (http://tropmap.biology.uh.edu/map.html) onto a total of 691 scaffolds constituting more than 764 Mb of genomic sequence (*4*, *14*). To identify lineage-specific fusion- and breakage-events within the mammals and sauropsids, we analyzed blocks of conserved synteny between frog, human, and chicken. These blocks were detected with genomic probes comprising three-way orthologs between these tetrapods. Of these probes, 5642 define conserved linkage blocks containing at least 15 genes and at least 2 Mb of sequence (*4*, *14*). The tetrapod ancestry of human and chicken chromosome 1 is outlined in Fig. 2. Notably, a core of more than 150 Mb of sequence spanning the centromere of human chromosome 1 [chicken chromosome 8, frog linkage group (LG) VII] has remained largely intact during ~360 million years of evolution since the tetrapod ancestor (Fig. 2A). Detailed shared synteny is interrupted by large-scale inversions, but gene order is frequently conserved over stretches of tens of megabases. Human chromosome 1 is seen to have grown by three lineage-specific

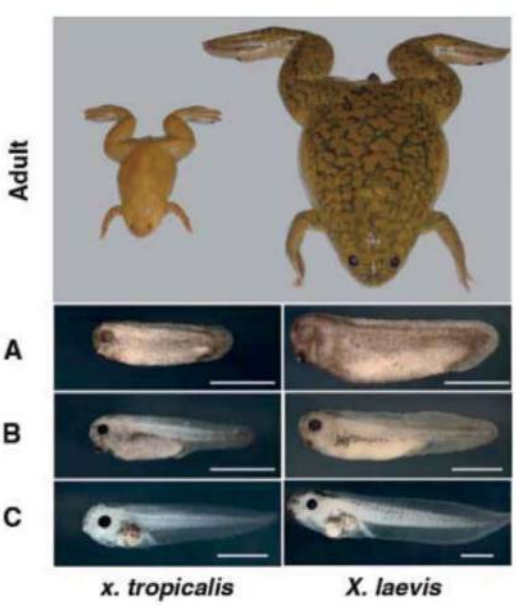

Fig. 1. Comparison of adults and tadpoles of *X. tropicalis* and *X. laevis*. Adult body length is 5 and 10 cm, respectively. (**A**) Tailbud, (**B**) swimming tadpole, and (**C**) feeding tadpole. Bar, 1 mm.

[1]Department of Energy Joint Genome Institute, Walnut Creek, CA 94598, USA. [2]Center for Integrative Genomics, University of California Berkeley, Berkeley, CA 94720, USA. [3]Division of Systems Biology, MRC National Institute for Medical Research, The Ridgeway, London NW7 1AA, UK. [4]Genetic Information Research Institute, Mountain View, CA 94043, USA. [5]National Center for Biotechnology Information, National Library of Medicine, National Institutes of Health, Bethesda, MD 20894, USA. [6]Department of Ecology and Evolutionary Biology, Rice University, Houston, TX 77005, USA. [7]Department of Developmental and Cell Biology, 4410 Natural Sciences Building 2, University of California Irvine, Irvine, CA 92697–2300, USA. [8]The Healing Foundation Centre, University of Manchester, Oxford Road, Manchester M13 9PT, UK. [9]DOE Joint Genome Institute, Los Alamos National Laboratory, Los Alamos, NM 87545, USA. [10]Office of Cancer Genomics, National Cancer Institute, NIH, DHHS Bethesda, MD 20892, USA. [11]Genome Sequencing Center, Washington University School of Medicine, St. Louis, MO 63108, USA. [12]Joint Genome Institute HudsonAlpha Institute for Biotechnology, 601 Genome Way, Huntsville, AL 35806, USA. [13]Okinawa Institute of Science and Technology, 12-22, Suzaki, Uruma, Okinawa 904-2234, Japan. [14]Department of Pathology, St. Jude Children's Research Hospital, 262 Danny Thomas Place, D4047C, Mailstop 342, Memphis, TN 38105, USA. [15]Nara Institute of Science and Technology, 8916-5 Takayama, Ikoma, Nara, Japan. [16]Department of Microbiology and Immunology, University of Maryland School of Medicine, Baltimore, MD 21201, USA. [17]Programme d'Epigénomique, CNRS, Genopole, Université d'Evry Val d'Essonne, F-91058 Evry, France. [18]Department of Microbiology and Immunology, Box 672, University of Rochester, Medical Center, Rochester, NY 14642, USA. [19]Department of Biology and Biochemistry, University of Houston, Houston, TX 77204–5001, USA. [20]Department of Biological Sciences, University of Calgary, 2500 University Drive NW, Calgary, Alberta T2N 1N4, Canada. [21]MRC National Institute for Medical Research, London NW7 1AA, UK. [22]Division of Developmental Biology, Cincinnati Children's Hospital Medical Center, Cincinnati, OH 45229, USA. [23]Department of Biology, Gilmer Hall, Post Office Box 400328, Charlottesville, VA 22904–4328, USA. [24]Department of Pediatrics and Genetics, Yale University School of Medicine, Post Office Box 208064, New Haven, CT 06520–8064, USA.

*To whom correspondence should be addressed. E-mail: uhellsten@lbl.gov

mammalian fusions. In contrast, there are several mammalian-specific breakpoints (Fig. 2B). The genomic material on the entire q arm of chicken shows linkage conservation to frog LG VI, whereas the human counterparts are scattered over regions of chromosomes 2, 3, 11, 13, 21, and X. The p arm indicates two mammalian breaks, suggesting that regions of chromosomes 7, 12, and 22 were once part of the same chromosome.

By extending this analysis to all human and chicken chromosomes, we identified 22 human fusion and 21 fission events, versus only four fusions and one break in chicken. Clearly, the mammalian lineage has undergone considerably more rearrangement than that of the sauropsids, although the total chromosome count appears to have remained fairly constant. The segments analyzed here are distributed on 23 human and 22 chicken chromosomes, consistent with a derivation from 24 or 25 ancestral amniote chromosomes. The chicken microchromosomes are unresolved by this analysis, however, preventing determination of the exact ancestral chromosome number. Both the vertebrate and eumetazoan ancestors have been suggested to have had about a dozen large chromosomes (*13*, *15*). The current analysis indicates that the amniote ancestor had twice as many, suggesting substantial chromosome breakage on the amniotic stem.

The extensive conserved synteny among tetrapods allows us to provisionally place frog scaffolds without genetic markers onto the linkage map. These are shown in Fig. 2 as black bars within the blocks of conserved linkage with frog. A total of 170 large scaffolds containing about 200 Mb of sequence were assigned a linkage group in this manner. Such in silico inferred linkages will ultimately need to be verified experimentally, but have already proven useful in the positional identification and cloning of the gene responsible for the *muzak* mutation, which affects heart function (*16*).

The *X. tropicalis* genome exhibits extensive sequence conservation with other vertebrates, with the amphibian sequence filling a phylogenetic gap. Recognizable noncoding sequence conservation diminishes steadily with increasing evolutionary distance (fig. S6). Frog genes adjacent to conserved noncoding sequences (CNS) are enriched or depleted in several gene ontology categories, including sensory perception of smell, response to stimulus, and regulation of transcription, among others (table S16).

Gene deserts (defined as the top 3% of the longest intergenic regions) cover 17% of the genome and vary between 201 kbp and 1.2 Mbp. The 683 gene deserts contain almost 25% of CNSs. In mammalian genomes, these gene deserts have been found to harbor cis-regulatory elements (*17*).

The power of genome comparison and high-throughput transgenesis in *Xenopus* is illustrated in fig. S7, where several mammalian-*Xenopus* CNSs at the *Six3* locus were assayed for enhancers regulating its eye- and forebrain-specific expression. The analysis suggests that frog-mammal comparisons may be more suitable than fish-mammal comparisons for identifying conserved cis-regulatory elements (see, e.g., CNS5 in fig. S7).

Developmental pathways controlling early vertebrate axis specification were first implicated by work in *Xenopus* (*2*), but some interesting amphibian modifications can be found. For example, a *Wnt* ligand required for dorsal development, named *Wnt11b* in *X. tropicalis*, has been lost from mammals, but is found in the chick and zebrafish (as *silberblick*) (*18*). Despite its retention in these vertebrates, there is no evidence to support a maternal role in axis formation similar to that in *Xenopus*. Similarly, a *tbx16* homolog, *vegT*, is retained in frog, fish, and chick, but is uniquely used in *Xenopus* for the establishment of the endoderm and mesoderm (*19*).

X. tropicalis also shows multiplications of genes deployed at the blastula and gastrula stages. For example, mammals have a single *nodal* gene, whereas *X. tropicalis* has more than six. Synteny relationships reveal that *nodal4* on scaffold 204 is orthologous to the single human *nodal*, whereas a cluster of more than six *nodals* on scaffold 34 is orthologous to the chicken *nodal*. Further analysis suggests that these two *nodal* loci arose in one of the whole-genome duplications at the base of vertebrate evolution and that the birds and mammals subsequently lost different *nodal* genes, whereas the lizard *Anolis carolinensis* has retained both copies (*4*).

The theme of duplication is reiterated by several transcription factors that act during gastrulation (*4*). The transcriptional activator *siamois*, expressed in the organizer, is triplicated locally in the genome; so far this gene is unique to the frog. The *ventx* genes are expressed at the same time, but opposite the organizer, and are present in six linked copies.

Conservation of the vertebrate immune system is highlighted by mammalian and *Xenopus* genome comparisons (*20*, *21*). Although orthology is usually obvious, synteny has been an important tool to identify diverged genes. For example, a diverged *CD8 beta* retains proximity to *CD8 alpha*, and *CD4* neighbors *Lag3* and *B* protein. Similarly, an interleukin-2/interleukin-21–like sequence was identified in a syntenic region between the *tenr* and *centrin4* genes. The immunoglobulin repertoire provides further links between vertebrate immune systems. The *IgW* immunoglobulin was thought to be unique to shark/lungfish, but an orthologous *IgD* isotype in frog provides a connection between the fish and amniote gene families (*22*, *23*).

Unique antimicrobial peptides play an important role in skin secretions that are absent in birds, reptiles, and mammals. Antimicrobial peptides (caerulein, levitide, magainin, PGLa/PYLa, PGQ, xenopsin), neuromuscular toxins (e.g., xenoxins),

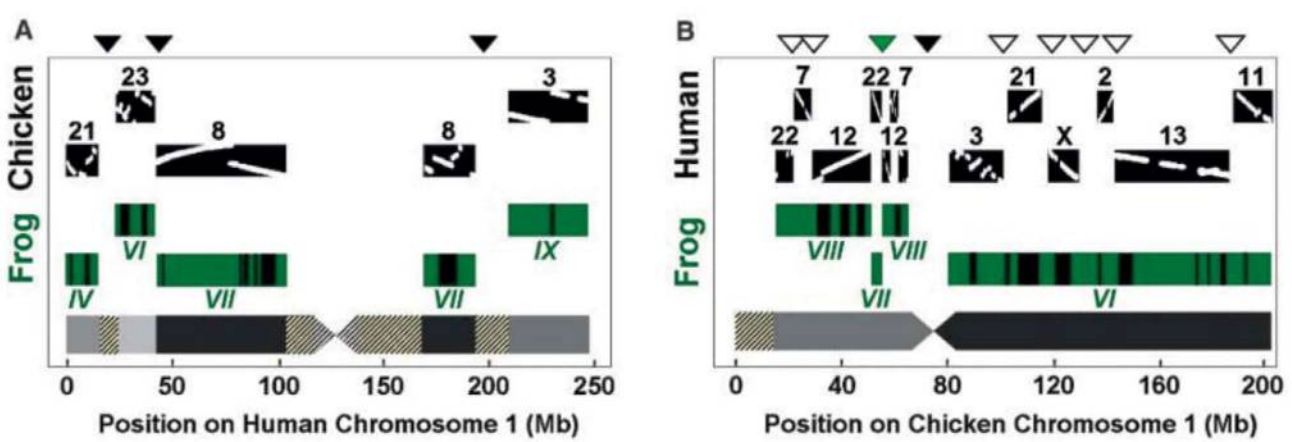

Fig. 2. Blocks of conserved tetrapod linkage for human (**A**) and chicken (**B**) chromosome 1 reveal fusions (solid black triangles) and break points (unfilled triangles) in amniotes. A total of three human fusions (A), seven human breaks (B), and one chicken fusion (B) are observed. The green triangle in (B) indicates the position of an apparent frog-specific break or ancestral amniote fusion. Gray areas indicate origin in different ancestral chromosomes. Shaded areas show larger regions with insufficient three-way synteny information. Detailed comparison of gene order in human and chicken reveals multiple large-scale inversions (dot plots on the black blocks). The green frog blocks consist of multiple scaffolds, 55 in (A) and 97 in (B). Bars on the frog blocks show the location of scaffolds that do not contain markers from the linkage map, but have been predicted to associate with the linkage group by conserved synteny.

and neuropeptides (e.g., thyrotropin-releasing hormone) (*24*) are secreted by granular glands, and the first group represents an important defense against pathogens (*25*). Antimicrobial peptides are clustered in at least seven transcription units >350 kbp on scaffold 811, with no intervening genes.

X. tropicalis occupies a key phylogenetic position among previously sequenced vertebrate genomes, namely amniotes and teleost fish. Given the utility of the frog as a genetic and developmental biology system and the large and increasing amounts of cDNA sequence from the pseudo-tetraploid *X. laevis*, the *X. tropicalis* reference sequence is well poised to advance our understanding of genome and proteome evolution in general, and vertebrate evolution in particular.

References and Notes

1. L. Hogben, C. Gordon, *J. Exp. Biol.* **7**, 286 (1930).
2. D. D. Brown, *J. Biol. Chem.* **279**, 45291 (2004).
3. J. Tymowska, *Cytogenet. Cell Genet.* **12**, 297 (1973).
4. Supporting material is available on *Science* Online.
5. International Chicken Genome Sequencing Consortium, *Nature* **432**, 695 (2004).
6. International Human Genome Sequencing Consortium, *Nature* **409**, 860 (2001).
7. Mouse Genome Sequencing Consortium, *Nature* **420**, 520 (2002).
8. V. V. Kapitonov, J. Jurka, *Genetica* **107**, 27 (1999).
9. V. V. Kapitonov, J. Jurka, *Proc. Natl. Acad. Sci. U.S.A.* **100**, 6569 (2003).
10. International Rice Genome Sequencing Project, *Nature* **436**, 793 (2005).
11. N. L. Craig, R. Craigie, M. Gellert, A. M. Lambowitz, Eds., *Mobile DNA II* (American Society for Microbiology, Washington, DC, 2002).
12. V. V. Kapitonov, J. Jurka, *DNA Cell Biol.* **23**, 311 (2004).
13. N. H. Putnam *et al.*, *Science* **317**, 86 (2007).
14. Dataset S1 is available on *Science* Online.
15. I. G. Woods *et al.*, *Genome Res.* **15**, 1307 (2005).
16. A. Abu-Daya, A. K. Sater, D. E. Wells, T. J. Mohun, L. B. Zimmerman, *Dev. Biol.* **336**, 20 (2009).
17. M. A. Nobrega, I. Ovcharenko, V. Afzal, E. M. Rubin, *Science* **302**, 413 (2003).
18. R. J. Garriock, A. S. Warkman, S. M. Meadows, S. D'Agostino, P. A. Krieg, *Dev. Dyn.* **236**, 1249 (2007).
19. M. Kofron *et al.*, *Development* **126**, 5759 (1999).
20. L. Du Pasquier, J. Schwager, M. F. Flajnik, *Annu. Rev. Immunol.* **7**, 251 (1989).
21. J. Robert, Y. Ohta, *Dev. Dyn.* **238**, 1249 (2009).
22. Y. Ohta, M. Flajnik, *Proc. Natl. Acad. Sci. U.S.A.* **103**, 10723 (2006).
23. Y. Zhao *et al.*, *Proc. Natl. Acad. Sci. U.S.A.* **103**, 12087 (2006).
24. G. Kreil, in *The Biology of Xenopus*, R. C. Tinsley, H. R. Kobels, Eds. (The Zoological Society of London, Oxford, 1996), pp. 263–277.
25. L. A. Rollins-Smith, *Integr. Comp. Biol.* **45**, 137 (2005).

26. This work was performed under the auspices of the U.S. Department of Energy's Office of Science, Biological and Environmental Research Program, and by the University of California, Lawrence Berkeley National Laboratory, under contract DE-AC02-05CH11231, Lawrence Livermore National Laboratory under contract DE-AC52-07NA27344, and Los Alamos National Laboratory under contract DE-AC02-06NA25396. This research was supported in part by the Intramural Research Program of the NIH, National Library of Medicine, and by a grant to R.K.W. from the National Human Genome Research Institute (NHGRI U01 HG02155) with supplemental funds provided by the National Institute of Child Health and Human Development. We thank R. Gibbs and S. Scherer of the Human Genome Sequencing Center, Baylor College of Medicine, for their contributions to identification and mapping of simple sequence length polymorphisms.

Supporting Online Material

www.sciencemag.org/cgi/content/full/328/5978/633/DC1
Materials and Methods
SOM Text
Figs. S1 to S9
Tables S1 to S17
References
Dataset S1

22 October 2009; accepted 16 February 2010
10.1126/science.1183670

Analysis of Genetic Inheritance in a Family Quartet by Whole-Genome Sequencing

Jared C. Roach,[1]* Gustavo Glusman,[1]* Arian F. A. Smit,[1]* Chad D. Huff,[1,2]* Robert Hubley,[1] Paul T. Shannon,[1] Lee Rowen,[1] Krishna P. Pant,[3] Nathan Goodman,[1] Michael Bamshad,[4] Jay Shendure,[5] Radoje Drmanac,[3] Lynn B. Jorde,[2] Leroy Hood,[1]† David J. Galas[1]†

We analyzed the whole-genome sequences of a family of four, consisting of two siblings and their parents. Family-based sequencing allowed us to delineate recombination sites precisely, identify 70% of the sequencing errors (resulting in >99.999% accuracy), and identify very rare single-nucleotide polymorphisms. We also directly estimated a human intergeneration mutation rate of ~1.1×10^{-8} per position per haploid genome. Both offspring in this family have two recessive disorders: Miller syndrome, for which the gene was concurrently identified, and primary ciliary dyskinesia, for which causative genes have been previously identified. Family-based genome analysis enabled us to narrow the candidate genes for both of these Mendelian disorders to only four. Our results demonstrate the value of complete genome sequencing in families.

Whole-genome sequences from four members of a family represent a qualitatively different type of genetic data than whole-genome sequences from individual or sets of unrelated genomes. They enable inheritance analyses that detect errors and permit the identification of precise locations of recombination events. This leads in turn to near-complete knowledge of inheritance states through the precise determination of the parental chromosomal origins of sequence blocks in offspring. Confident predictions of inheritance states and haplotypes power analyses that include the identification of genomic features with nonclassical inheritance patterns, such as hemizygous deletions or copy number variants (CNVs). Identification of inheritance patterns in the pedigree permits the detection of ~70% of sequencing errors and sharply reduces the search space for disease-causing variants. These analyses would be far less powerful in studies that had fewer markers (such as standard genotype or exome data sets) or that had sequences from fewer family members.

DNA from each family member was extracted from peripheral blood cells and sequenced at CGI (Mountain View, California) with a nanoarray-based short-read sequencing-by-ligation technology (*1*), including an adaptation of the pairwise end-sequencing strategy (*2*). Reads were mapped to the National Center for Biotechnology Information (NCBI) reference genome (fig. S1 and tables S1 and S2). Polymorphic markers used for this analysis were single-nucleotide polymorphisms (SNPs) with at least two variants among the four genotypes of the family, averaging 802 base pairs (bp) between markers. We observed 4,471,510 positions at which at least one family member had an allele that varied from the reference genome. This corresponds to a Watterson's theta (θ_W) of 9.5×10^{-4} per site for the two parents and the reference sequence (*3*), given the fraction of the genome successfully genotyped in each parent (fig. S1). This is a close match to the estimate of $\theta_W = 9.3 \times 10^{-4}$ that we obtained by combining two previously published European genomes and the reference sequence (*4*). Of the 4.5 million variant positions, 3,665,772 were variable within the family; the rest were homozygous and identical in all four members. Comparisons to known SNPs show that 323,255 of these 3.7 million SNPs are novel.

For each meiosis in a pedigree, each base position in a resulting gamete will have inherited one of two parental alleles. The number of inheritance patterns of the segregation of alleles in

[1]Institute for Systems Biology, Seattle, WA 98103, USA. [2]Department of Human Genetics, Eccles Institute of Human Genetics, University of Utah, Salt Lake City, UT 84109, USA. [3]Complete Genomics, Inc. (CGI), Mountain View, CA 94043, USA. [4]Department of Pediatrics, University of Washington, Seattle, WA 98195, USA. [5]Department of Genome Sciences, University of Washington, Seattle, WA 98195, USA.

*These authors contributed equally to this work.
†To whom correspondence should be addressed. E-mail: dgalas@systemsbiology.org (D.J.G.); lhood@systemsbiology.org (L.H.)

gametes is therefore 2^n, where n is the number of meioses in a pedigree. In a nuclear family of four, the Mendelian inheritance patterns can be grouped into four inheritance states for each variant position, with children receiving (i) the same allele from both the mother and the father (identical), (ii) the same allele from the mother but opposites from the father (haploidentical maternal), (iii) the same allele from the father, but opposites from the mother (haploidentical paternal), or (iv) opposites from both parents (nonidentical) (fig. S2). Adjacent variant base pairs in alignments of the family genomes have the same inheritance state unless a recombination has occurred between these bases in one of the meioses. This delineates inheritance blocks.

Many algorithms can identify the boundaries of blocks, and theory-driven implementations are in wide use (*5*–*7*). For our complete genome sequence data, we developed an algorithm to identify all states, including non-Mendelian states. One non-Mendelian state will occur in regions where highly similar sequences are inadvertently compressed computationally (for example, during sequence assembly of CNVs). In such a "compression block," many positions will appear to be heterozygous in all individuals, regardless of the inheritance patterns of the positions contributing to the compression. Other non-Mendelian patterns are seen in regions prone to errors in sequence calling or assembly or that have inherited hemizygous deletions. For both of these patterns, many positions will be observed as Mendelian inheritance errors (MIEs). Our algorithm identified six states: one for each of the four Mendelian inheritance states, one for a compression state, and one for a MIE-prone state (*4*). We identified 1.5% of the genome in this pedigree as 409 compression blocks and 1.7% as 126 error-prone blocks. Because these blocks are a source of false positives for recombination predictions, SNPs, and disease candidate alleles, their identification is important (Fig. 1). The power to precisely determine inheritance-state boundaries is striking in families of at least four and would be reduced had we sequenced fewer individuals (Fig. 2). Meiotic gene conversions could in principle be recognized in the same way as inheritance blocks; they would be indistinguishable from a short region flanked by meiotic recombinations in the same meiosis. We found that the great majority of candidate gene-conversion regions were caused by reads mismapped to repetitive DNA, such as CNVs or satellites, and did not conclusively identify gene-conversion regions.

Recombination in maternal meioses is thought to occur 1.7 times more frequently than in paternal meioses (*8*). We inferred 98 crossovers in maternal and 57 in paternal meioses (count includes both offspring), which is consistent with this estimate. The median resolution of the 155 crossover sites was 2.6 kb, with a few sites localized within a 30-bp window (Fig. 1). Crossover sites were significantly correlated with hotspots of recombination as inferred from HapMap data, in which a hotspot is defined as a region with ≥10 centimorgan (cM)/Mb; 92 of the 155 recombinations took place in a hotspot.

By identifying inconsistencies across the 22% of the genomes of the two children in "identical" blocks, for which they are effectively twins, we computed an error rate of 1.0×10^{-5}. We also determined error rate through other methods, including resequencing, which gave similar estimates, ranging from 8.1×10^{-6} to 1.1×10^{-5} (*4*). Furthermore, ~70% of the errors in a four-person pedigree can be detected as apparent MIEs and inconsistencies in inheritance state blocks, so the effective base-pair error rate in the context of a pedigree is $\sim 3 \times 10^{-6}$.

Analysis of the mutation rate, including germline and early embryonic somatic mutations, requires highly accurate sequence data. Even with such data, however, most apparent aberrations in allele inheritance will be due to errors in the data and not to mutation. Our data had thousands of such false-positive candidates for each true de novo mutation. Our initial data encompassed 2.3 billion bases and contained 49,720 candidate MIEs that were consistent with the presence of a single-nucleotide mutation. After excluding sites in MIE-prone and compression states as well as sites that were unsuitable for probe design, 33,937 potential mutations among 1.83 billion bases remained. We resequenced each of these candidates and applied a stringent base-calling algorithm to confirm 28 candidates as de novo mutations. In a final confirmation step, we verified all 28 mutations with mass spectrometry (table S3) (*4*), corresponding to a mutation rate of 3.8×10^{-9} per position per generation per haploid genome.

Because the raw estimate of 3.8×10^{-9} does not account for the true mutations that were not conclusively identified through resequencing, we estimated a false-negative rate by applying the base-calling algorithm to 5 Mb of independent resequencing data, divided into 25 randomly selected regions of the genome. A comparison of the resequencing data with the complete genome sequence for the same regions provided a de novo mutation false negative rate of 0.662 [95% confidence interval (CI) 0.644 to 0.680]. Adjusting for the false-negative rate produced an unbiased mutation rate estimate of 1.1×10^{-8} per position per haploid genome, corresponding to approximately 70 new mutations in each diploid human genome (95% CI of 6.8×10^{-9} to 1.7×10^{-8}) (*4*). In great apes, CpG sites are

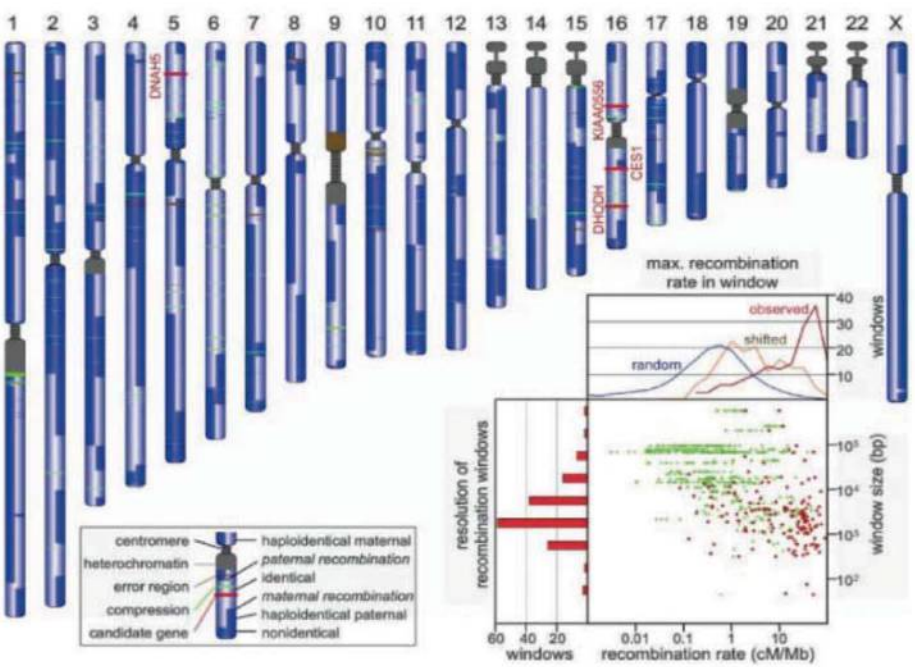

Fig. 1. The landscape of recombination. Each chromosome in this schematic karyotype is used to represent information abstracted from the four corresponding chromosomes of the two children in the pedigree. It is vertically split to indicate the inheritance state from the father (left half) and mother (right half), as shown in the key. The three compound heterozygous (*DHODH*, *DNAH5*, and *KIAA0556*) and one recessive (*CES1*) candidate gene, depicted by red bands, lie in "identical" blocks. (Inset) Scatterplot of HapMap recombination rates (in centimorgans per megabase) within the predicted crossover regions. The maximum value of centimorgans per megabase found in each window is shown in red. The left histogram shows the size distribution of recombination windows ($\log_{10}$ value of -0.58 ± 0.92). The top graph shows the centimorgans per megabase distribution for the observed maximal values (red), for similarly sized windows shifted by 6 kb (orange), and for similarly sized windows randomly chosen from the entire genome (blue). A shift of 6 kb from the observed locations eliminates the correlation with hotspots. Of 155 recombination windows, 92 contained a HapMap site with >10 cM/Mb. Only five randomly picked windows are expected to contain such high recombination rates.

reported to mutate at a rate 11 times higher than other sites (*9*). We observed five CpG mutations, closely matching this estimate. Of the remaining 23 mutations, seven were transversions and 16 were transitions. This yields a transition-to-transversion ratio of 2.3 (table S3), which is once again similar to a previous estimate of 2.2 for non-CpG sites (*10*).

Although both the observed transition-to-transversion ratio and the proportion of CpG mutations in our data match predictions, our estimated human mutation rate is lower than previous estimates, the most widely cited of which is 2.5×10^{-8} per generation (*10*) based on three parameters: a human-chimpanzee nucleotide divergence per site (K_1) of 0.013, a species divergence time of 5 million years ago, and an ancestral effective population size of 10,000. More recent estimates indicate a nucleotide divergence of 0.012 (*9*), species divergence time between 6 and 7 million years ago (*11*–*15*), and ancestral effective population size between 40,000 and 148,000 (*16*–*19*). With these parameter ranges and a generation length of 15 to 25 years, the mutation rate estimate is between 7.6×10^{-9} and 2.2×10^{-8} per generation, which is consistent with our intergenerational estimate of 1.1×10^{-8}. Our estimate is within 1 SD of an earlier estimate of 1.7×10^{-8} (SD of 9×10^{-9}) based on 20 disease-causing loci (*20*). The rate we report is for autosomes and should be substantially lower than that of the Y chromosome because in the male germ line, more cell divisions occur per generation. Although our rate differs approximately as expected from the recently reported estimate of 3.0×10^{-8} (95% CI, 8.9×10^{-9} to 7.0×10^{-8}) for the Y chromosome, this difference is not significant (*21*).

Genomic inheritance analysis facilitates the identification of alleles that cause genetic disorders. Because genome sequences from a family of four provide near-exact determination of inheritance-state boundaries, the number of false-positive disease-gene candidates is greatly reduced as compared with those of analyses lacking the context of a pedigree or complete genome sequence (Fig. 3 and tables S3 and S4). Two disorders in this family—Miller syndrome and primary ciliary dyskinesia, which affect both offspring but neither parent—provided an opportunity to test this application. A parsimonious explanation is that each phenotype arises from defects in a single gene or a site regulating a single gene. The inheritance mode is undetermined, but a recessive mode is more consistent with observed data. We therefore examined each candidate variant by testing each of three inheritance modes: dominant, simple recessive, or compound heterozygote (a subcategory of recessive).

The two recessive modes require that both offspring have identical dysfunctional variants for which the parents are heterozygous and which may come either from the same position (simple recessive) or occur at distinct positions within the same gene (compound heterozygote). Genes that are consistent with these two recessive modes must lie in "identical" inheritance blocks because both offspring are affected, limiting the search space to the 22% of the genome in these blocks. Because the phenotypes are rare, they are likely to be encoded by rare variants, which further limits the possibilities. Only two missense SNPs in the *CES1* gene matched the simple recessive mode (table S4), whereas three genes fit the compound heterozygote mode: *DHODH*, *DNAH5*, and *KIAA0556* (Fig. 1). A small number of possibly detrimental variants outside exons also matched the simple recessive mode: two in highly conserved regions, one in an intronic sequence near a splice site, five in non–protein-coding transcripts, and one in an untranslated region (UTR). Concurrent with this study, the core exomes of the two affected offspring were sequenced along with those of two unrelated individuals with Miller syndrome (*22*). Compared with that study of only affected individuals, our analysis of just two affected

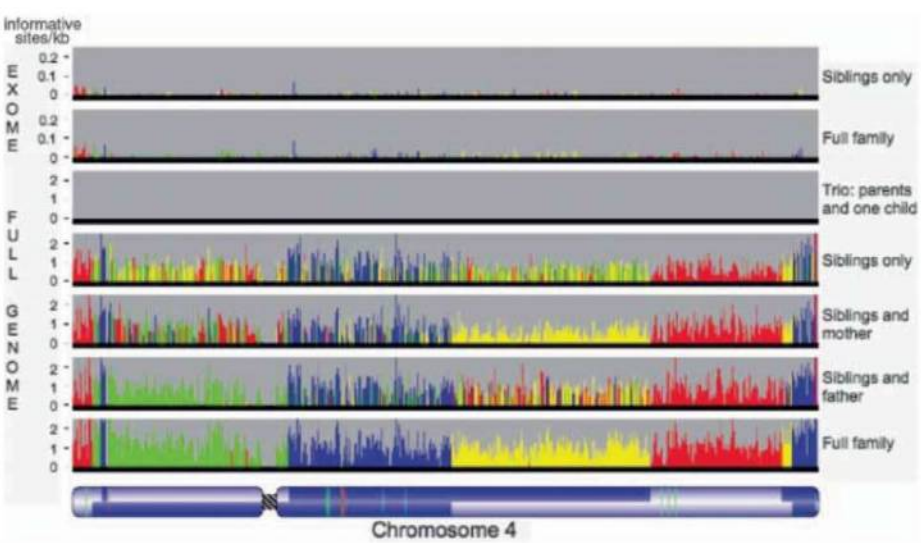

Fig. 2. Power of four. Shown are inheritance states for a single chromosome in six scenarios representing restrictions of the data set to the exome (for two siblings only or for the full family) or to subsets of the family (parents and one child, two siblings, or siblings and one parent), as compared with analysis with full data from all four family members. The most supported state for each bin is shown as a color; the height of each histogram bar is proportional to the number of informative markers supporting that state. The father has two regions of homozygosity (bottom, thin red lines) on the short arm of the chromosome, where it is not possible to distinguish the haploidentical maternal from identical states (fig. S2A, panel b). These regions are undetected when the mother's genotypes are missing because all marker positions in the region are uninformative (second from bottom). A pedigree of two parents and one child has only one inheritance state and so provides no information on recombination. Red, identical; blue, nonidentical; green, haploidentical maternal; yellow, haploidentical paternal. Chromosome structure is annotated as in Fig. 1.

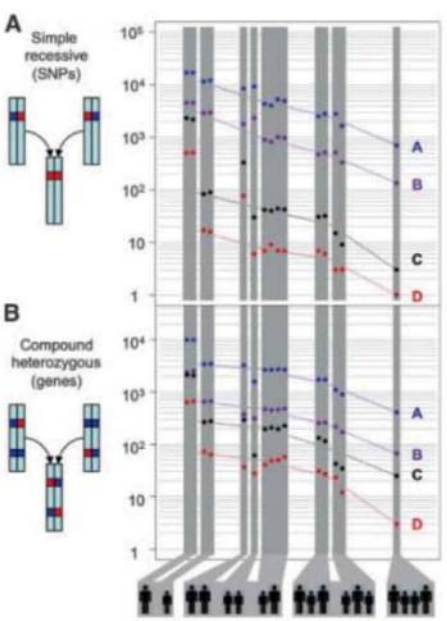

Fig. 3. The power of family genome inheritance analysis. The number of false-positive candidates drops exponentially as the number of family members increases. (**A**) Number of candidate SNPs that are consistent with a simple recessive inheritance mode. (**B**) Number of candidate genes that are consistent with a compound heterozygous model. The different groupings of parents (large silhouettes) and children (small silhouettes) are depicted below. Dashed lines join the average values of each grouping. For this figure, "probably detrimental" includes missense, nonsense, splice defect, and non-initiation; "possibly detrimental" also includes UTR, noncoding, and splice region. A block of SNPs so that all SNPs in the block are within 5 kb of another SNP in the block is counted only once because together these are likely to encode at most one phenotype. "A," all probably detrimental SNPs; "B," all possibly detrimental SNPs; "C," rare possibly detrimental SNPs; "D," rare probably detrimental SNPs.

offspring and their unaffected parents reduced the number of gene candidates in the core exome from nine to four; had we not sequenced the parents, we would have had 34 rather than four candidates (Fig. 3 and table S5). The exome study supported *DHODH* as the primary gene for Miller syndrome. *DNAH5* had been previously identified as a cause of primary ciliary dyskinesia, and so is probably the cause in these offspring as well (*23*).

Family genome analysis can clearly be effective for finding candidate genes that encode Mendelian traits because sequence accuracy is enhanced. In addition, delineation of recombination sites identifies inherited chromosome segments precisely and reduces the chromosomal search space for candidate genes (in this case to 22% of the genome). The ability to identify large effects of very rare alleles in small pedigrees can complement the power of genome-wide association studies in identifying weak effects of common alleles in large populations. An unknown fraction of important phenotypes in humans are encoded by nonexonic variants identified only by means of whole-genome sequencing. When the cost of recruiting additional families is expensive relative to sequencing costs, sequencing genomes of families will be an economical strategy for the identification of many disease-causing genes. Constraining searches to very rare variants can provide considerable power, as recently demonstrated for Freeman-Sheldon syndrome and congenital chloride diarrhea (*24*, *25*). De novo mutations can be assayed, either as we have reported here or through family sequencing of more than two generations. As our knowledge of gene function increases, we will be able to use the power of family genome analysis rapidly to identify disease-gene candidates. These data, along with relevant environmental and medical information, will characterize the integrated medical records of the future.

References and Notes

1. R. Drmanac *et al.*, *Science* **327**, 78 (2010).
2. J. C. Roach, C. Boysen, K. Wang, L. Hood, *Genomics* **26**, 345 (1995).
3. G. A. Watterson, *Theor. Popul. Biol.* **7**, 256 (1975).
4. Materials and methods are available as supporting material on *Science* Online.
5. K. P. Donnelly, *Theor. Popul. Biol.* **23**, 34 (1983).
6. L. Kruglyak, M. J. Daly, M. P. Reeve-Daly, E. S. Lander, *Am. J. Hum. Genet.* **58**, 1347 (1996).
7. G. R. Abecasis, S. S. Cherny, W. O. Cookson, L. R. Cardon, *Nat. Genet.* **30**, 97 (2002).
8. P. M. Petkov, K. W. Broman, J. P. Szatkiewicz, K. Paigen, *Trends Genet.* **23**, 539 (2007).
9. Chimpanzee Sequencing and Analysis Consortium, *Nature* **437**, 69 (2005).
10. M. W. Nachman, S. L. Crowell, *Genetics* **156**, 297 (2000).
11. Y. Haile-Selassie, *Nature* **412**, 178 (2001).
12. Y. Haile-Selassie, B. Asfaw, T. D. White, *Am. J. Phys. Anthropol.* **123**, 1 (2004).
13. Y. Haile-Selassie, G. Suwa, T. D. White, *Science* **303**, 1503 (2004).
14. A. L. Deino, L. Tauxe, M. Monaghan, A. Hill, *J. Hum. Evol.* **42**, 117 (2002).
15. M. Brunet *et al.*, *Nature* **418**, 145 (2002).
16. F. C. Chen, W. H. Li, *Am. J. Hum. Genet.* **68**, 444 (2001).
17. R. Burgess, Z. Yang, *Mol. Biol. Evol.* **25**, 1979 (2008).
18. N. Takahata, *Jpn. J. Genet.* **68**, 539 (1993).
19. J. D. Wall, *Genetics* **163**, 395 (2003).
20. A. S. Kondrashov, *Hum. Mutat.* **21**, 12 (2003).
21. Y. Xue *et al.*, *Curr. Biol.* **19**, 1453 (2009).
22. S. B. Ng *et al.*, *Nat. Genet.* **42**, 30 (2010).
23. H. Olbrich *et al.*, *Nat. Genet.* **30**, 143 (2002).
24. S. B. Ng *et al.*, *Nature* **461**, 272 (2009).
25. M. Choi *et al.*, *Proc. Natl. Acad. Sci. U.S.A.* **106**, 190961 (2009).

26. This study was supported by the University of Luxembourg–Institute for Systems Biology Program and by these NIH grants: Center for Systems Biology GM076547 (L.H. and L.R.), RO1GM081083 (A.F.S. and G.G.), R01HL094976 and RZ1HG004749 (J.S.), RC2HG005608 (M.D. and J.S.), and R01HD048895 (M.B.). H. Tabor assisted with ethical review. J. Xing performed the principal components analysis. H. Mefford performed CNV analysis. A. Bigham and K. Buckingham evaluated candidate genes in unrelated individuals. D. Ballinger, A. Sparks, A. Halpern, and G. Nilsen assisted with sequencing and analysis. R. Bressler, S. Dee, and D. Mauldin assisted with bioinformatics. S. Ng and R. Qiu performed the capture array. S. Bloom obtained the resequencing data on the Illumina Genome Analyzer. M. Janer and S. Li performed Sequenom analysis. D. Cox commented on an early version of the manuscript. R. Durbin and D. Altshuler granted permission for our use of 1000 genomes SNP data. CGI employees (R.D. and K.P.) have stock options in the company. J.S. has consulted for CGI. L.H. is a scientific advisor to CGI and holds stock in the company. The dbGAP accessions can be found at www.ncbi.nlm.nih.gov/projects/gap/cgibin/study.cgi?study_id=phs000244.v1.p1 (accession phs000244.v1.p1).

Supporting Online Material

www.sciencemag.org/cgi/content/full/science.1186802/DC1
Materials and Methods
Figs. S1 to S5
Tables S1 to S5
References

7 January 2010; accepted 5 March 2010
Published online 11 March 2010;
10.1126/science.1186802
Include this information when citing this paper.

NEW PRODUCTS

BENCHTOP BATH

The FTS Multi-Cool is a mechanically refrigerated benchtop bath that eliminates the need for costly consumables such as liquid nitrogen and dry ice. Compact and completely self-contained, the Multi-Cool provides up to 8 liters of working fluid volume at temperatures between –80°C and +100°C. The low temperature bath features precise control to within ±0.1°C.

SP Industries
For info: 800-824-0400 | www.ftssystems.com/multicoolbath.htm

CALCIUM MOBILIZATION ASSAY

The FluoForte Calcium Assay Kit for monitoring calcium mobilization in live cells across a broad spectrum of biological targets contains the brightest and most sensitive fluorescent Ca^{2+} indicator on the market, according to the manufacturer. Featuring a large assay window, the FluoForte reagent can measure calcium changes in challenging cell lines and with difficult receptors, generating a strong green fluorescent signal. This homogeneous assay is suitable for analyzing both G protein-coupled receptor and calcium ion channel targets. The easy-to-use protocol does not require a wash step or the addition of a quencher dye that could potentially modify pharmacological parameters. The FluoForte dye can be loaded at 37°C or room temperature, which makes it amenable to high throughput screening applications.

Enzo Life Sciences
For info: 800-942-0430 | www.enzolifesciences.com

HISTOLOGICAL EXAMINATIONS

The Leica SCN400 Slide Scanner offers an alternative to the microscope for the examination of histological samples in pathology, research, and teaching. The custom-tailored lens is designed for high-resolution scans to ensure that the resolution and color fidelity of the image on the screen are just as good as those of the microscope image. The system's Dynamic Focus feature keeps the sample in focus for the full duration of the scan, so even difficult samples can be digitized easily. The Leica SCN400 can load and scan up to four specimens at a time. A scanning rate of 100 seconds per 15-mm-by-15-mm area at 20x magnification means sample throughput is high. The matching Leica SL801 autoloader can scan up to 384 samples at the same time, overnight if required, offering new options for automated operation.

Leica
For info: +49(0)6441-29-2550 | www.leica-microsystems.com

CO-IMMUNOPRECIPITATION KIT

The Pierce Co-Immunoprecipitation Kit is for the isolation of native protein complexes from a lysate or complex mixture using purified antibodies immobilized onto an agarose support. The kit makes use of an amine-reactive resin for the direct coupling of 10–50 micrograms of antibody. Traditional co-immunoprecipitation methods that rely on protein A or protein G result in co-elution of the antibody's heavy and light chains, which may migrate with relevant bands, masking important results. The resin chemistry also enables immobilization independent of antibody isotype or species. The kit includes optimized buffers for protein binding and recovery, reagents to perform control experiments, and efficient spin columns and collection tubes that shorten the protocol and minimize handling.

Thermo Fisher Scientific
For info: 815-968-0747 | www.thermo.com/pierce

HYDROGEL KIT

The Extracel-SS Hydrogel Kit is an extracellular matrix designed to quickly and safely retrieve cells from encapsulation within the gel. The kit makes use of a fall-apart cross-linker that allows for dissolution of the hydrogel using a small amount of reducing agent. The gel is reconstituted by simply adding water to the three vials and mixing them together with desired cells. Gelation occurs in about 30 minutes.

Glycosan BioSystems
For info: 801-583-8212 | www.glycosan.com/extracel_ss.html

SEQUENCING COMPUTING

IlluminaCompute is an integrated computing solution for Illumina's Genome Analyzer sequencing platform. The system brings together Illumina's powerful sequencing software with high-performance blade servers from Dell and modular storage capacity from Isilon Systems to create a flexible and scalable system for human-scale genomic data analysis. The new system conserves information technology resources by providing centralized high-performance computational and storage infrastructure in place of the support required for individual, decentralized analysis servers. IlluminaCompute is a unique blending of hardware, informatics software, and high-availability storage that is tuned specifically for a high throughput sequence analysis workflow.

Illumina
For info: 800-809-4566 | www.illumina.com

Electronically submit your new product description or product literature information! Go to **www.sciencemag.org/products/newproducts.dtl** for more information.

Newly offered instrumentation, apparatus, and laboratory materials of interest to researchers in all disciplines in academic, industrial, and governmental organizations are featured in this space. Emphasis is given to purpose, chief characteristics, and availabilty of products and materials. Endorsement by *Science* or AAAS of any products or materials mentioned is not implied. Additional information may be obtained from the manufacturer or supplier.

Multiply The Power of Science

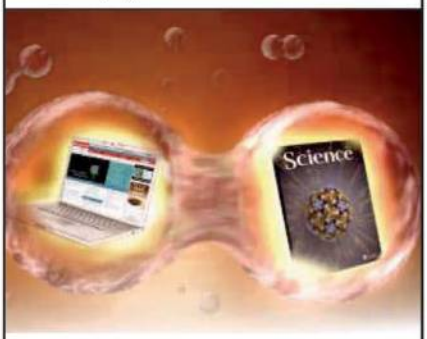

Science Careers Classified Advertising

For full advertising details, go to ScienceCareers.org and click For Employers, or call one of our representatives.

Tracy Holmes
Worldwide Associate Director
Science Careers
Phone: +44 (0) 1223 326525

UNITED STATES & CANADA

E-mail: advertise@sciencecareers.org
Fax: 202-289-6742

Tina Burks
East Coast/Midwest/Canada
Phone: 202-326-6577

Nicholas Hintibidze
West Coast/South Central
Phone: 202-326-6533

Online Job Posting Questions
Phone: 202-326-6577

EUROPE & REST OF WORLD

E-mail: ads@science-int.co.uk
Fax: +44 (0) 1223 326532

Alex Palmer
Phone: +44 (0) 1223 326527

Dan Pennington
Phone: +44 (0) 1223 326517

Susanne Kharraz Tavakol
Phone: +44 (0) 1223 326529

Lisa Patterson
Phone: +44 (0) 1223 326528

JAPAN

ASCA Corporation
Jie Chin
Phone: +81-3-6802-4616
Fax: +81-3-6802-4615
E-mail: careerads@sciencemag.jp

To subscribe to *Science*:
In US call 866 434-2227
In the rest of the world call +1 202 326-6417

All ads submitted for publication must comply with applicable US and non-US laws. *Science* reserves the right to refuse any advertisement at its sole discretion for any reason, including without limitation for offensive language or inappropriate content, and all advertising is subject to publisher approval. *Science* encourages our readers to alert us to any ads that they feel may be discriminatory or offensive.

Science Careers
From the journal *Science* AAAS

Science Careers is the forum that answers questions.

Visit our ENHANCED WEBSITE!

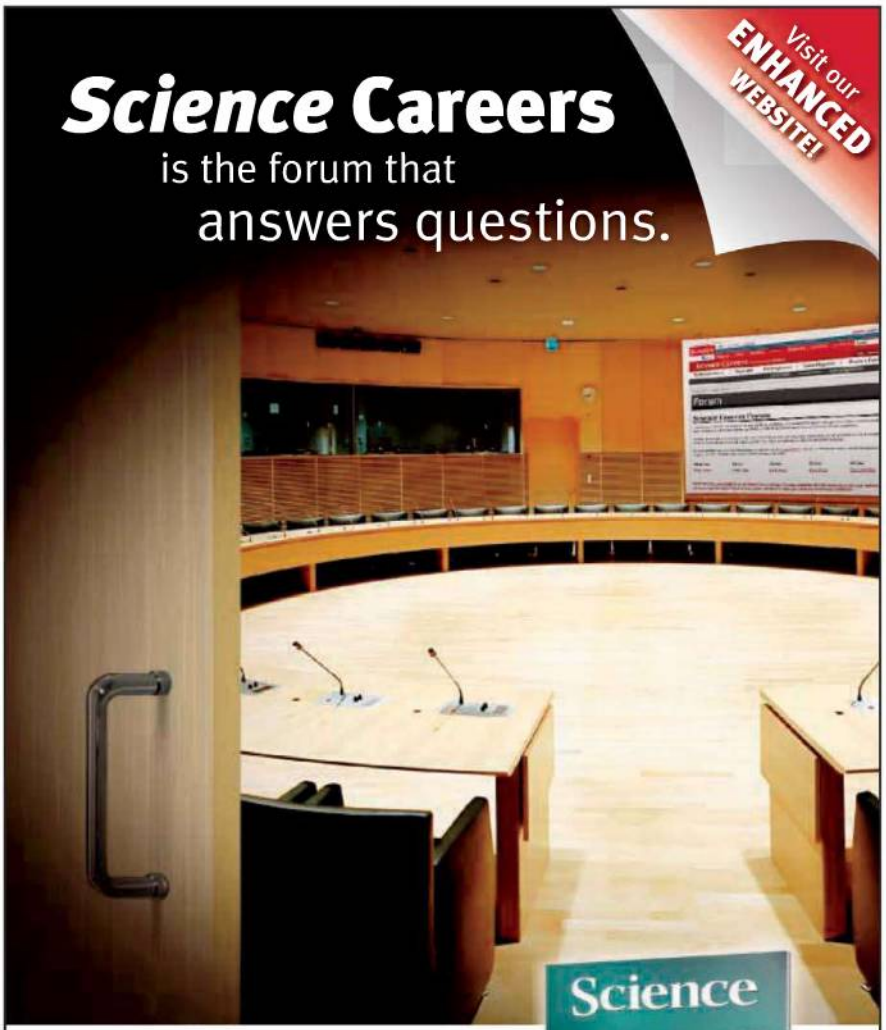

Your Future Awaits.

Science Careers is dedicated to opening new doors and answering questions on career topics that matter to you. We're the go-to career site for connecting with top employers, industry experts, and your peers. We're the source for the latest and most relevant career information across the globe.

With community feedback and a professional atmosphere, our careers forum allows you to connect with colleagues and associates to get the advice and guidance you seek.

Science Careers Forum:

- » Relevant Career Topics
- » Advice and Answers
- » Community, Connections, and More!

Visit the forum and get your questions answered today!

Science Careers
From the journal *Science* AAAS
ScienceCareers.org

vetmeduni vienna

Messerli-Stiftung

Vacancy announcements

Based on the agreement between the Messerli Foundation for the Promotion of Research in the Field of Ethics and Animals and the University of Veterinary Medicine, Vienna, the University of Vienna and the Medical University of Vienna, the following professorial positions are announced in connection with the establishment of the "Messerli Institute for Man-Animal Interactions":

1. **"Ethics in Man-Animal Interactions"**
   Position: A professor responsible for research and education in the field of **"Ethics in Man-Animal Interactions"** at the University of Veterinary Medicine, Vienna and the University of Vienna.
   RESPONSIBILITIES: The successful candidate should work on ethical questions related to the handling of animals, paying close attention to scientific and legal issues.

2. **"Research and Documentation of the Legal Provisions governing Man-Animal Interactions"**
   Position: A professor responsible for research and education in the field of **"Research and Documentation of the Legal Provisions governing Man-Animal Interactions"** at the University of Veterinary Medicine, Vienna and the University of Vienna.
   RESPONSIBILITIES: The successful candidate should document and undertake scientific work on legal questions relating to Interactions between man and animals, with a focus on animal welfare and veterinary laws, including issues such as animal experimentation and the laws relating to animal transport as well as those stemming from civil and criminal law such as shooting and fishing rights.

3. **"Scientific Basis for Animal Welfare and Man-Animal Interactions"**
   Position: A professor responsible for research and education in the field of **"Scientific Basis for Animal Welfare and Man-Animal Interactions"** at the University of Veterinary Medicine, Vienna and the Medical University of Vienna.
   RESPONSIBILITIES: The successful candidate should address scientific issues in connection with animals' ability to perceive (via the senses) as well as the regulation and processing by the central nervous system and/or cognition.

4. **"Comparative Medicine"**
   Position: A professor responsible for research and education in the field of **"Comparative Medicine"** at the University of Veterinary Medicine, Vienna and the Medical University of Vienna.
   RESPONSIBILITIES: The successful candidate should work on the comparative aspects of human and veterinary medicine, developing and undertaking comparative research projects (e.g. in cancer research) in collaboration with the Medical University of Vienna and the University of Veterinary Medicine, Vienna. He or she should also emphasize research on the "three Rs" in collaboration with the field of "Laboratory Animal Studies" at the participating universities.

REQUIRED QUALIFICATIONS:

a) extensive teaching experience
b) proven success in scientific research as demonstrated by publications in relevant journals
c) evidence of integration in the international scientific community
d) proven ability to attract third-party funding
e) suitability for a managerial position – good communication and organizational skills
f) ability to work in a team
g) management experience

The University of Veterinary Medicine, Vienna, the University of Vienna and the Medical University of Vienna are striving to increase the proportion of female scientists, especially in higher positions. Applications from qualified female scientists are thus particularly welcomed. Women of equivalent qualification will be given precedence over male applicants. Candidates must be prepared to submit to an assessment procedure.

Applications should be submitted in writing together with the normal supporting documents (cv, list of publications, summary of research and teaching activities to date, presentation of previous experience in organization, management and leadership) by **1 June 2010** to: **Büro des Senates der Veterinärmedizinischen Universität Wien, Veterinärplatz 1, A-1210 Wien, Austria**.

universität wien

MEDIZINISCHE UNIVERSITÄT WIEN

Institute of Medical Biology
A*STAR

VACANCIES

The Institute of Medical Biology (IMB), a Singapore government-funded research institute under the Agency for Science, Technology and Research (A*STAR), was formed in 2007 to promote translational research into the mechanisms underlying human disease. Today, our research activities extend across stem cells and differentiation, cancer, epithelial biology and genetic diseases. Situated in a lively international community in state-of-the-art facilities on the iconic Biopolis campus, IMB's scientists are gaining new understanding of disease processes that will lead to the development of novel therapeutic strategies for improved quality of life. More information on IMB can be found at our website at **http://www.imb.a-star.edu.sg**.

1. PRINCIPAL INVESTIGATOR POSITIONS

We are looking to appoint 2-3 additional Principal Investigator-led research teams. Appointed PIs will be internationally established scientists with proven track record in research excellence, or more junior group leaders with a very strong CV, and will be working in an area that augments or complements the research strengths of the Institute (for example, epithelial stem cells). The research teams are supported by the institute's core funding budget.

2. MICROSCOPISTS

(i) *IMB Microscopy Unit Manager:* IMB is currently seeking a well-qualified microscopist to oversee our state-of-the-art IMB Microscopy Unit (IMU). The successful candidate is expected to have understanding of, and familiarity with, basic and advanced high resolution fluorescence microscopes and preferably also electron microscopy, and must have excellent communication and management skills.
(ii) We are also seeking an *electron microscopy officer* with practical expertise in preparation of material for EM work and operation of transmission and scanning EMs, to work with several different user groups.

3. POSTDOCTORAL SCIENTISTS

We are also seeking enthusiastic and gifted postdoctoral scientists (with PhD) and/or clinician scientists (MD or PhD) for a number of positions within IMB laboratories. Candidates must have a passionate enthusiasm for research, have strong background in molecular/ cell/ medical biology, and be self-motivated and energetic workers. Evidence of good publications, technical independence in molecular and cell biology techniques, and an ability to take the initiative would also be an advantage, to gain the most out of this highly collaborative and international research environment.

In all cases, remuneration will depend on qualifications and experience. To apply, please submit your application via **http://www.imb.a-star.edu.sg/Vacancies/tabid/242/Default.aspx** by **21 May 2010** (only online applications will be considered). Applications should be accompanied with a detailed CV, research outline, names of referees and contact details. We regret that only shortlisted candidates will be notified. For enquiries, please contact **hr@imb.a-star.edu.sg**.

Institute of Medical Biology, A*STAR
8A Biomedical Grove,
#06-06 Immunos,
Singapore 138648
Tel (65) 64070150
Fax: (65) 64642049
Website: www.imb.a-star.edu.sg

FACULTY POSITIONS
Biomedical Research and Basic Medical Science Education

VTC | Virginia Tech Carilion School of Medicine and Research Institute

The Virginia Tech Carilion School of Medicine and Research Institute is a unique, public-private partnership between a cutting-edge research university, Virginia Tech, and a major healthcare system, Carilion Clinic. The partnership leverages Virginia Tech's world-class strength in basic sciences, bioinformatics, and engineering with Carilion Clinic's highly experienced medical staff and rich history in medical education. A new 153,000-square-foot building will house the Research Institute and School of Medicine. The facility is located in Roanoke, Virginia within an emerging biomedical complex and in close proximity to Carilion Roanoke Memorial Hospital. Please see www.vtc.vt.edu for more information on this exciting new venture. Recruitment is underway for faculty positions for both the Research Institute and School of Medicine.

INSTRUCTIONAL FACULTY POSITIONS in Basic Medical Sciences

The Virginia Tech Carilion School of Medicine (VTCSOM) exemplifies a new way forward in medical education, educating physician thought leaders through inquiry, research and discovery. The charter class of 42 students matriculates August 2, 2010. Up to six additional faculty positions are being recruited in the basic medical sciences, including biochemistry, physiology, immunology, microbiology/virology, and pharmacology. Positions are 12 month, non-tenure track, 3-year fixed term, renewable appointments with primary responsibility to the VTCSOM instructional programs in Roanoke, with some contribution to Virginia Tech. The VTCSOM curriculum is based on a Patient-Centered Learning model. Faculty members at all ranks with a strong commitment to the mission of the new medical school are invited to apply. A Ph.D. or equivalent in one of the identified basic medical sciences disciplines is required. Apply to posting number 0100167, at **http://www.hr.vt.edu/employment/**.

Review of applications will begin May 15 and continue until filled. Inquires may be addressed to **Dr. Richard C. Vari**, VTCSOM Associate Dean for Medical Education, (540) 581-0125, **rcvari@carilionclinic.org**.

FACULTY POSITIONS in Biomedical Sciences Research

The newly established Virginia Tech Carilion Research Institute (VTCRI) announces openings for faculty positions at all levels. Applications are welcome from scientists who utilize contemporary experimental and/or computational approaches to investigate biological function in humans or model organisms in health and/or disease throughout the lifespan. Successful candidates should have a Ph.D., and/or MD, or DVM, postdoctoral experience and a record of outstanding research accomplishment. Candidates with strong records of research productivity who utilize molecular, genetic, biophysical, cell biological, imaging, computational and/or behavioral approaches to study cardiovascular, endocrine, immune or nervous system function in health and/or disease including cancer are encouraged to apply. A competitive allowance for laboratory start up and operations support will be provided. Apply to posting number 0100198, **http://www.hr.vt.edu/employment/**.

Inquiries may be addressed to **Dr. Michael Friedlander**, VTCRI Executive Director, **friedlan@vt.edu**. Applications will be reviewed and appointments made on a rolling basis.

Virginia Tech and its partner entities have a strong commitment to the principle of diversity and, in that spirit, seek a broad spectrum of candidates including women, minorities, and people with disabilities.

The University of Oklahoma
HEALTH SCIENCES CENTER

CHAIR
Department of Microbiology and Immunology
University of Oklahoma College of Medicine

The University of Oklahoma College of Medicine invites applications and nominations for the position of Chair of the Department of Microbiology and Immunology.

The Department of Microbiology and Immunology is a vigorous department of 13 faculty members with a strong record of NIH funding. The research interests of the department include bacterial and viral pathogenesis, humoral and cellular immunity, the role of the MHC complex in autoimmune diseases and genomics. Departmental faculty members contribute to the MD, PhD and DDS degree programs The Department has a vigorous graduate program. Applicants must have a PhD or MD or equivalent degree and must show strong evidence of academic leadership and peer recognition as an accomplished researcher and educator. The successful candidate is expected to have a strong research program as demonstrated by continuous NIH funding. In addition, the candidate would have demonstrated a strong commitment to professional and graduate education and the ability to recruit and develop outstanding faculty.

The Health Sciences Center has targeted growth in four broad areas: infectious diseases, cancer, diabetes, and neuroscience/vision. The incoming Chair will have the opportunity to recruit into those programs as well. The position provides open faculty lines and appropriate laboratory space. *The successful applicant may be eligible to receive one of several Endowed Professorships.*

The College of Medicine is located within the University of Oklahoma Health Sciences Center (OUHSC), a 325-acre comprehensive academic health center, recently noted for having one of the best academic institution work environments in the country by *The Scientist* (Nov, 2009). OUHSC is situated in the capital city of Oklahoma City, an area experiencing economic growth and undergoing extensive revitalization. Oklahoma City is one of the most affordable and attractive major metropolitan areas in which to live. Combine Oklahoma City residents' increased spending power with renowned festivals, national sporting events, treasure-filled museums, a variety of districts highlighting arts and entertainment, and a mild climate with year-round sunshine, and Oklahoma City offers something for everyone.

Review of applications will begin in May 2010 and continue until the position is filled. Candidates should send a letter, both electronically and postal, describing their research interests, administrative and educational philosophies and long-term goals, a curriculum vitae and the names, addresses (postal and email) and phone of at least three professional references to:

Mrs. Paula Slaughter
Attn: Microbiology Chair Search Committee
College of Medicine, University of Oklahoma Health Sciences Center
PO Box 26901, BMSB 553, Oklahoma City, OK 73126-0901
Phone: 405-271-5533; E-mail: paula-slaughter@ouhsc.edu

The University of Oklahoma Health Sciences Center is an Equal Opportunity/ Affirmative Action Employer.

THE HORMEL INSTITUTE
UNIVERSITY OF MINNESOTA
THREE (3) ASSISTANT PROFESSOR/ASSOCIATE PROFESSOR/ PROFESSOR/ENDOWED PROFESSOR POSITIONS

The Hormel Institute, a biomedical research center of the University of Minnesota, was established in 1942 and has a long reputation in producing world class medical research. The Institute's research success has resulted in a major expansion of its research facilities and includes a new state of the art laboratory building and complete renovation of existing research facilities. The Hormel Institute offers its research scientists complete access to state of the art equipment that includes a FACS cell sorter; confocal microscopy; flow cytometry; protein crystallography robotics and diffraction system; and the Blue Gene/L, the world's fastest supercomputer. In conjunction with the building expansion will be the addition of three (3) new faculty positions. We are seeking applications for faculty appointments at the level of Assistant Professor, Associate Professor, Professor, and/or Endowed Professor.

Qualifications: Candidates must demonstrate the ability to establish an independent, extramurally funded program of cancer-related research that will complement ongoing programs. Preference will be given to applicants with a strong background in areas to include molecular/cell biology, protein crystallography, biological computation/informatics, stem cell, or cancer biology and a successful research record in one of the following areas: signal transduction, gene expression, functional genomics, molecular carcinogenesis, chemoprevention or other areas of cancer research. A Ph.D. (or equivalent) degree and 2 to 3 years of postdoctoral experience are required for Assistant Professor, external funding is preferred. The ability to acquire extramural funding is required for appointment of Associate Professor or Professor. For endowed professorships, the applicant should be an internationally renowned researcher with substantial external funding. Please apply online at the UMN website **http://www1.umn.edu/ohr/employment/index.html** and refer to **Requisition Number 154060 (Professor)**, **Number 154740 (Associate Professor)**, or **Number 154741 (Assistant Professor)**. In addition, please submit a curriculum vitae, a research plan, and the names of three references to **Dr. Zigang Dong**, **ambode@hi.umn.edu**.

The University of Minnesota shall provide equal access to and opportunity in its programs, facilities, and employment without regard to race, color, creed, religion, national origin, gender, age, marital status, disability, public assistance status, veteran status, sexual orientation, gender identity, or gender expression.

ASSOCIATE DEAN FOR RESEARCH AND GRADUATE STUDIES
College of Pharmacy

The College of Pharmacy is seeking an Associate Dean for Research and Graduate Studies to represent and serve as an advocate for the research mission and post-graduate education within the College, the University and with external stakeholders. The successful candidate should have the skills to develop research priorities, respond to new research opportunities, and support research career development.

Requirements include an earned doctorate (Pharm.D, Ph.D. or equivalent) and experience leading an active, externally funded research program. Preferred qualifications include a broad vision of interdisciplinary research and of the future of research in the College of Pharmacy, a record of committed leadership, and excellent interpersonal skills including the ability to bring diverse viewpoints to consensus decisions.

See **www.pharmacy.umn.edu./jobs** for full position description and application instructions.

UNIVERSITY OF MINNESOTA
College of Pharmacy
Driven to Discover℠

The University of Minnesota is an equal opportunity educator and employer.

A*STAR INVESTIGATORSHIPS

A prestigious award to recognise young scientific talent

Singapore's Agency for Science, Technology & Research (A*STAR) invites applications for A*STAR Investigatorships

A*STAR Investigatorships aim to support and promote early independent career development of the next generation of world leaders in scientific research. Applicants should have obtained their PhD not more than 48 months prior to the application date, and should have already demonstrated a strong ability and creativity in research. Applicants with MD-PhD should be in their last year of, or have completed their clinical specialty training at the time of application.

The award provides for an **independent** position for a duration of 3+3 years, with a review at the end of the 2nd year and a possibility of "fast-track" promotion. Tenable at one of A*STAR's prestigious biomedical research institutes, A*STAR Investigators may select a mentor from A*STAR but will conduct and publish their research independently.

A*STAR Investigatorship will receive attractive remuneration, support for set-up costs, research funding, research staff and access to state-of-the-art scientific equipment and facilities including the Biopolis Shared Facilities andthe Biological Resource Centre. Each **A*STAR Investigatorship** laboratory will be funded with up to US$500K p.a.

Candidates with research interest in these areas are strongly encouraged to apply:

- Bioengineering & Nanotechnology
- Bioimaging
- Bioprocessing & Biotechnology
- Chemical Synthesis
- Computational Biology & Bioinformatics
- Genomics & Proteomics
- Immunology
- Medical Biology & Clinical Sciences
- Molecular & Cell Biology
- Stem Cells

The **A*STAR Investigatorships Selection Panel**

- **Professor Tadataka Yamada**
  President, Global Health Program, Bill and Melinda Gates Foundation
- **Professor Sir David Lane**
  Chief Scientist, A*STAR
- **Professor Edward Holmes**
  Executive Deputy Chairman, Translational and Clinical Sciences, Biomedical Research Council, A*STAR; Executive Chairman, National Medical Research Council, Singapore
- **Professor Alex Matter**
  Chief Executive Officer, Experimental Therapeutics Centre (ETC), A*STAR
- **Professor Paul Matsudaira**
  Professor of Biological Sciences and Head, Department of Biological Sciences, National University of Singapore

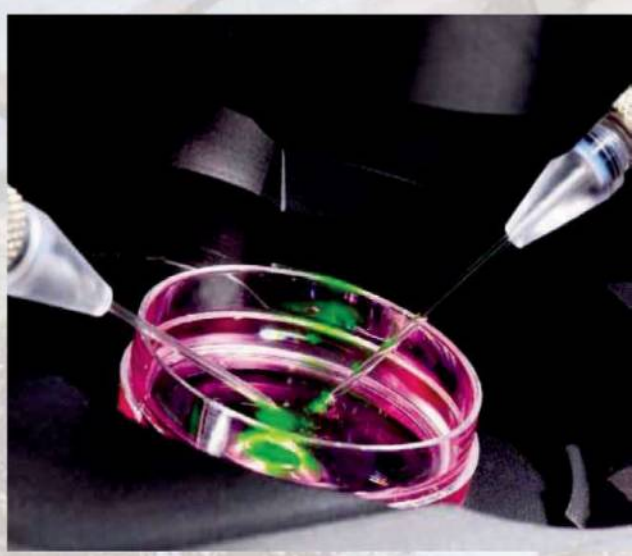

Up to 10 shortlisted candidates will be invited to Singapore for interviews and a review based on a scientific presentation, expected to be held in October 2010.

Closing date: 31 July 2010
**Applications would be accepted throughout the year.*

Application Materials
The following materials should be filled up and submitted by mail, or email to the contacts as shown below.

- Application form
- Curriculum vitae
- 5-page research proposal
- At least 3 referral letters

A*STAR Investigatorships 2010
Agency for Science, Technology & Research,
20 Biopolis Way, #08-01 Centros
Singapore 138668
Email: A-STAR_ADMIN_BMRC@a-star.edu.sg

http://www.a-star.edu.sg/AwardsScholarships/Investigatorships/AIBiomedicalSciences/tabid/335/Default.aspx

Agency for Science, Technology and Research
SINGAPORE

Translational Neuroscience
The University of Texas at Austin, and the Dell Pediatric Research Institute

University of Texas at Austin in conjunction with the Dell Pediatric Research Institute invites applications for **tenured and tenure-track faculty positions at the assistant, associate, and full professor levels. Up to six positions are being made available for individuals or research teams with research programs focused on mechanisms of neuroscience-based diseases**. We are particularly interested in candidates with MD, PhD, or combined MD/PhD degrees who use genetic and molecular approaches to investigate neurological and/or psychiatric disorders. Ample opportunities are available for candidates with clinical interests through the Seton Family of Hospitals and the UT Southwestern sponsored clinical training programs in Austin. Successful candidates will join an expanding and vibrant basic and clinical neuroscience community at the University of Texas at Austin and will be expected to develop and maintain active, translational research programs. Academic appointments will be made in the appropriate academic unit within the College of Natural Sciences, College of Liberal Arts, College of Pharmacy, or School of Engineering. The positions will include competitive salary and start-up packages and have laboratories in the new Dell Pediatric Research Institute Building adjacent to the Dell Children's Medical Center.

Austin is located in the Texas hill country and is widely recognized as one of America's most beautiful and livable cities (see: **www.austintexas.org/home/**). Please send curriculum vitae, summary of research interests, and names of three references to:

Mary Ann Rankin, Dean or **Daniel Johnston, Director**
College of Natural Sciences **Institute for Neuroscience**

Institute for Neuroscience
The University of Texas at Austin
1 University Station, C7000
Austin, TX 78712

The University of Texas at Austin is an Equal Opportunity Employer. Qualified women and minorities are encouraged to apply; a background check will be conducted on applicants selected.

IDA

The Institute for Defense Analyses Center for Computing Sciences is looking for outstanding Ph.D. level scientists, mathematicians and engineers to address problems in high-performance computing, cryptography and network security. IDA/CCS is an independent research center sponsored by the National Security Agency. IDA/CCS scientists and engineers work on difficult scientific problems, problems vital to the nation's security. Stable funding provides for a vibrant research environment and an atmosphere of intellectual inquiry free of administrative burdens.

Research at IDA/CCS emphasizes computer science, computer architecture, electrical engineering, information theory and all branches of mathematics. Because CCS research staff work on complex topics often engaging multidisciplinary teams, candidates should demonstrate depth in a particular field as well as a broad understanding of computational science and technology.

Developing imaginative computational solutions employing novel digital technology is one of several long-term themes of work at CCS. The Center is equipped with a very large variety of hardware and software. The latest developments in high-end computing are heavily used and projects routinely challenge the capability of the most advanced architectures.

IDA/CCS offers a competitive salary, an excellent benefits package and a superior professional working environment. IDA/CCS is located in a modern research park in the Maryland suburbs of Washington, DC. U.S. citizenship and a DoD TS//SI clearance are required. CCS will sponsor this clearance for those selected. Please send responses or inquiries to: **Dawn Porter Administrative Manager IDA Center for Computing Sciences 17100 Science Drive Bowie, MD 20715-4300; dawn@super.org; (301) 805-7528**.

The Institute for Defense Analyses is proud to be an Equal Opportunity Employer.

Johns Hopkins University
School of Medicine
Director
Chemoprotection Center

The Johns Hopkins University School of Medicine seeks applicants to direct a new academic Chemoprotection Center (CpC) dedicated to developing strategies for reducing the risk of cancer and other chronic diseases. The CpC will be one of the Centers in the recently founded Institute for Basic Biomedical Sciences which was designed to facilitate more interdisciplinary approaches to solving basic biomedical problems. In addition to the Director, the CpC is projected to house 3-5 additional faculty members. Generous support and new space is available.

The Research in the CpC will build on many years of chemoprotection research at Johns Hopkins. The program crosses conventional departmental and disciplinary boundaries. It is devised to span a wide range of approaches from basic synthetic and analytical chemistry to elucidation of molecular mechanisms, evaluation of new chemoprotective agents in cell and animal systems, and translation of results into the clinic. Dietary approaches based on identification of bioactive natural products are a prominent feature of the existing program. Scientific exploration of plants for chemoprotective phytochemicals have been a significant effort.

Candidates for this position will hold M.D. and/or Ph.D. degrees, and will be appointed to senior academic ranks. Candidates should have a strong record of scientific accomplishment, and demonstrated interests in developing broad and imaginative, interdisciplinary approaches to disease prevention.

Academic appointments will be in basic science departments and, if appropriate, also in clinical departments. Consideration of applicants will begin **June 1, 2010** and will continue until the position is filled.

Philip A. Cole M.D., Ph.D. • Stephen V. Desiderio M.D., Ph.D. • Paul Talalay M.D.

Please submit a Curriculum Vitae and a statement of research interests and plans to: **RuthDillinger@gmail.com** Or mail to: **Ruth Dillinger, Johns Hopkins University School of Medicine, 725 North Wolfe Street, WBSB 406, Baltimore, MD 21205 USA**.

The Johns Hopkins University is an Equal Opportunity/Affirmative Action Employer committed to the advancement of individuals without regard to ethnicity, gender, religion, age, disability, or other protected status.

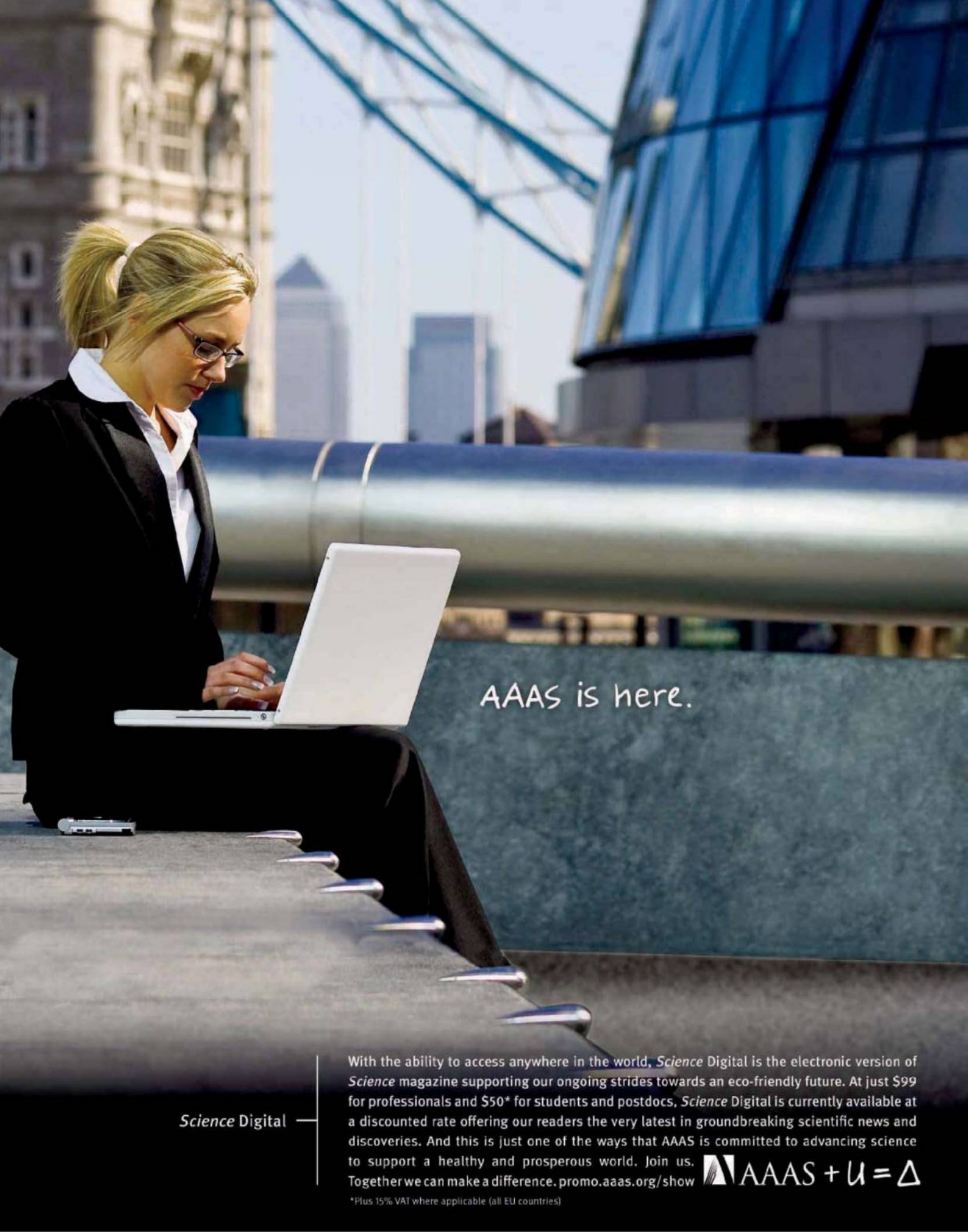

Science Digital

With the ability to access anywhere in the world, *Science* Digital is the electronic version of *Science* magazine supporting our ongoing strides towards an eco-friendly future. At just $99 for professionals and $50* for students and postdocs, *Science* Digital is currently available at a discounted rate offering our readers the very latest in groundbreaking scientific news and discoveries. And this is just one of the ways that AAAS is committed to advancing science to support a healthy and prosperous world. Join us. Together we can make a difference. promo.aaas.org/show

AAAS + U = Δ

*Plus 15% VAT where applicable (all EU countries)

Cancer Science Institute of Singapore

Faculty and Post-Doctoral Fellow Recruitment

CSI Singapore, National University of Singapore, is a state-of-the-art research center with a multifaceted and coordinated approach to cancer research, extending from basic cancer studies all the way to experimental therapeutics. The focus of the institute is on cancers endemic to Asian populations such as gastric, liver, lung, leukemia and breast cancers. The institute houses a full spectrum of research and clinical translational facilities. This major center is led by a team of world-class scientists with significant government funding from Singapore's National Research Foundation and Ministry of Education.

We are seeking individuals with exceptional scientific credentials to join a vibrant, dynamic team at CSI Singapore.

Principal Investigators

Qualified candidates at Professor, Associate Professor and Assistant Professor levels should be at the cutting edge of their field with an established record of excellence in cancer research. Candidates should have the capability and experience of leading high-level, innovative research programs resulting in international quality publications. Successful candidates can look forward to stable funding for up to 5 years commensurate with their abilities, ample laboratory space and resources, a competitive salary package and a dynamic working environment. Candidates with research emphasis in gastric, liver and lung cancers will be strongly considered.

Post-Doctoral Fellows

Post-Doctoral Fellow candidates should be highly motivated, creative individuals with an outstanding PhD degree in a related discipline. Successful candidates can look forward to working with top cancer researchers in an internationally represented environment.

Interested candidates should send their CV and the names of three referees to:
Professor Daniel G. Tenen
Director, Cancer Science Institute of Singapore (CSI Singapore), NUS
Email: csi_careers@nus.edu.sg

Please indicate the position you are applying for in the subject title.

Visit our website at www.csi.nus.edu.sg

Department of Biochemistry and Molecular Biology Faculty Positions

The Department of Biochemistry and Molecular Biology at the University of Maryland School of Medicine, chaired by **Richard L. Eckert, Ph.D.**, is undergoing a major expansion (**http://medschool.umaryland.edu/biochemistry/**). Highly qualified individuals will be considered at the **Assistant, Associate** and **Full Professor** levels. The department has significant strengths in muscle biology, cell signaling, cancer biology, structural biology and imaging, and a highly successful graduate training program. The expansion will include positions in epithelial biology, signal transduction, cell biology and biochemistry and stem cells with a focus on investigators utilizing biochemical, cellular and animal model approaches to understand protein and cell function in normal, diseased and cancerous tissue. Successful candidates are expected to establish and maintain active research programs, and participate in department teaching and service opportunities. The Medical School and the Department are highly ranked with respect to NIH funding. The Department provides excellent laboratory facilities, competitive salaries and startup packages, and access to numerous core facilities.

Applicants should hold a Ph.D. or M.D., have substantial research experience, and a strong desire to participate in an interactive, multidisciplinary research environment. Interested applicants are invited to submit a letter of interest and curriculum vitae by e-mail and have three letters of reference sent by e-mail to **biochemjobs@som.umaryland.edu**.

The University of Maryland, Baltimore is an Equal Opportunity, Affirmative Action Employer.

Tenure-Track Reseach Scientist Genetics

The Marshfield Clinic Research Foundation (MCRF) invites applicants for 2 open-rank tenure-track Research Scientists in the Center for Human Genetics. Scientists with innovative approaches to the genetics of complex diseases are especially encouraged to apply for appointment in 2010. MCRF has a history of important medical discoveries in the field of genetics.

MCRF has extensive population-based resources, including the Personalized Medicine Research Project. This project has DNA, plasma, and serum samples for 20,000 adults from a defined geographical area; access to their electronic medical records; information on environment and life-style; and the consent of subjects to be re-contacted. The appointed individuals will be expected to establish independent and collaborative research programs and contribute to the Wisconsin Genomics Initiative, and the University of Wisconsin Institute for Clinical and Translational Research, a joint undertaking of UW-Madison and MCRF.

To ensure consideration, complete applications should be received by Tuesday, June 1, 2010, although applications will be accepted until the positions are filled. Interested applicants should send their resume to:

Marshfield Clinic®
Research Foundation

Marshfield Clinic, Attn: Rhonda Thompson
1000 N. Oak Avenue, Marshfield, WI 54449
Phone: (715) 389-3049

Marshfield Clinic is an Affirmative Action/Equal Opportunity Employer that values diversity. Minorities, females, individuals with disabilities and veterans are encouraged to apply.

POSITIONS OPEN

Yale

POSTDOCTORAL RESEARCH ASSOCIATE
Molecular Biology/Gene Knockdown Technology
Yale Medical School

Position available at Yale Medical School for Ph.D. or M.D. **MOLECULAR BIOLOGIST,** with experience and publications in gene knockdown technology, to join multidisciplinary group studying nervous system injury with emphasis on neuropathic pain. Experience with in vivo as well as in vitro gene knockdown is desirable. Superb opportunity to work in a highly collaborative environment with cell and molecular biologists, electrophysiologists, pharmacologists, and others. Send statement of interest, curriculum vitae, and three letters of reference to: **Stephen G. Waxman, M.D., Ph.D., Director, Neuroscience and Regeneration Research Center, VA Connecticut (127A), 950 Campbell Avenue, West Haven, CT 06516. E-mail: stephen.waxman@yale.edu**. *Women and members of underrepresented minority groups are encouraged to apply. Affirmative Action/Equal Opportunity Employer.*

Columbia University's Department of Medicine, Division of Nephrology, invites applications for clinical faculty positions at the level of **ASSISTANT PROFESSOR OF CLINICAL MEDICINE.** The position requires inpatient care, clinical research, and teaching of students, residents, and fellows. Candidates should demonstrate experience in an academic nephrology setting, including inpatient consultation, hemodialysis, and peritoneal dialysis. Additionally, candidates may present demonstrated experience in the areas of transplantation, glomerular disease, or critical care medicine. Candidates must hold an M.D. or equivalent medical professional degree and be Board certified in internal medicine and Board certified or eligible in nephrology and must be eligible to practice in the state of New York. Applicants should apply online at **website: https://academicjobs.columbia.edu/applicants/Central?quickFind=52946**.

Columbia University is an Equal Opportunity/Affirmative Action Employer.

The Department of Environmental Toxicology and The Institute of Environmental and Human Health (TIEHH), Texas Tech University, have up to four positions available for Ph.D. students who are interested in research that lies at the interface of environmental, ecological, and human health sciences. These competitive **ASSISTANTSHIPS** offer generous support along with a tuition allowance, with the specific area of research to be determined based on applicant and faculty interest. Interested students are encouraged to peruse the TIEHH **website: http://www.tiehh.ttu.edu** to find information regarding ongoing research areas. In addition, information regarding the application process can be found at **website: http://www.tiehh.ttu.edu/application_process.html**.

POSTDOCTORAL POSITION
in microfluidics

A Postdoctoral position is immediately available in the laboratory of **Daniel Attinger** at Columbia University. Our research focus is on multiphase microfluidics. The postdoctoral scientist will lead and perform experimental research on microfluidic bioreactors and evaporative self-assembly of nanoparticles. She/he should have strong analytical skills in fluid mechanics and transport phenomena as well as strong experimental skills in microfabrication. The position is for one year, with competitive salary and benefits. Full description and application information are available on our laboratory **website: http://www.me.columbia.edu/lmtp/.**

POSITIONS OPEN

Northeastern University

SENIOR LABORATORY TECHNICIAN

The Laboratory for Adult Stem Cell Biology and Central Nervous System Regeneration in the Department of Biology, Northeastern University, is dedicated to elucidating fundamental mechanisms that mediate the development of adult-born neurons in the central nervous system, and to exploring the role of such cells for neuronal regeneration after brain and spinal cord injury. To help fulfill this mission, we seek a Senior Laboratory Technician who will assume major responsibility in the daily operation of the Laboratory. Under the direction of the Principal Investigator, who also serves as Chair of the Department of Biology, **Professor G.K.H. Zupanc,** the incumbent will participate in conducting experiments, recording and analyzing data, and organizing results in a form suitable for publication.

Applicants should have a B.A./B.S. in biology, neuroscience, or related area and at least five years of work experience in a biological laboratory, or an M.S. degree with at least three years of similar experience. Previous familiarity with immunohistochemistry, cell culture techniques, biochemical assays, microscopy, and/or image analysis would be an additional asset. Motivation to learn new techniques as well as excellent communication and interpersonal skills are essential.

For more information, see **website: http://www.biology.neu.edu/faculty03/Zupanc.html**. To apply for the position, electronically send your curriculum vitae to **e-mail: biojobs@neu.edu**.

Northeastern University is an Equal Opportunity, Affirmative Action Educational Institution and Employer, Title IX University. Northeastern University particularly welcomes applications from minorities, women, and persons with disabilities. Northeastern University is an E-Verify Employer.

POSTDOCTORAL FELLOWS
PROTEIN SCIENCE
Mechanism and Antagonism of HIV-1 Host Cell Entry

Postdoctoral positions available to investigate structure-based antagonism of HIV-1 envelope function in cell entry. Candidates sought with expertise/interest in one or more of the following specific areas: (1) Biophysical mechanisms of protein interactions. (2) Recombinant protein engineering. (3) Peptide and peptidomimetic synthesis. Resumes and three support letters to: **Prof. Irwin Chaiken, Department of Biochemistry and Molecular Biology, Drexel University College of Medicine.**

E-mail: ichaiken@drexelmed.edu
Website: http://www.drexelmed.edu/chaikengroup

POSITIONS OPEN

Yale University School of Medicine Department of Pediatrics, Division of Pediatric Respiratory Medicine, is currently searching for a junior investigator/scientist (**ASSISTANT PROFESSOR**) with expertise in CFTR protein biology, gene transfer, and stem cell biology to interface and collaborate with a large group of investigators and clinician-scientists interested in cystic fibrosis. Successful candidates will have established or emerging research programs in cystic fibrosis and the immune response. Interested persons should send curriculum vitae, brief statement of research interests, and three letters of recommendation exclusively to the following address: **Marie Egan, M.D., Yale Department of Pediatrics, P.O. Box 208064, New Haven, CT 06520-8064. Or e-mail: marie.egan@yale.edu**. The deadline is May 31, 2010. *Yale University is an Equal Opportunity, Affirmative Action Employer. Women and minorities are encouraged to apply.*

CAL POLY

FULL-TIME LECTURER POSITIONS IN BOTANY, ANATOMY/PHYSIOLOGY, AND MICROBIOLOGY. The Biological Sciences Department at California Polytechnic State University, San Luis Obispo, is seeking full-time lecturers to begin September 2010. For details, qualifications, and application instructions (online faculty application required), visit **website: http://www.calpolyjobs.org** and refer to **Requisition #102076.** Review begins June 7, 2010. *Equal Employment Opportunity.*

CALL FOR ABSTRACTS & SCHOLARSHIP/GLOBAL HEALTH TRAVEL AWARD APPLICATIONS

This October, Keystone Symposia will host the first Global Health Series meeting of its 2010–2011 season. The meeting is generously supported by a three-year grant from the Bill & Melinda Gates Foundation.

Immunological Mechanisms of Vaccination

Sheraton Seattle Hotel, Seattle, Washington, USA
October 27–November 1, 2010

Scientific Organizers:

Bali Pulendran, Rino Rappuoli and Bruce A. Beutler

Keynote Speakers:

Dr. Tadataka Yamada, Bill & Melinda Gates Foundation
Dr. Anthony S. Fauci, National Institutes of Health

Meeting Session Topics:

- Innate Sensing of Pathogens and Vaccines
- Understanding T and B Cell Memory to Vaccines
- Systems Biological Approaches to Vaccination and Infections
- Novel Approaches to Understanding Host-Microbe Interactions
- Translating Immunity to Vaccines
- Immunity and Vaccines Against Pandemics and Emerging Pathogens
- Immunology of Adjuvants

The meeting will provide an outstanding opportunity to learn about the latest research results from experts in the field, present one's own research, and interact with potential new collaborators. Scholarships are available for students and postdoctoral fellows, and Global Health Travel Awards are available to eligible candidates from developing countries.

Global Health Travel Award Application Deadline: ***June 1, 2010*** */ Scholarship & Abstract Deadline:* ***June 28, 2010*** */ Late-Breaking Abstract Deadline:* ***July 30, 2010*** */ Early Registration Deadline:* ***August 27, 2010***

KEYSTONE SYMPOSIA™
on Molecular and Cellular Biology
Accelerating Life Science Discovery

www.keystonesymposia.org/10S1 • 1.800.253.0685 • 1.970.262.1230

CONFIRMED SPEAKERS: Alan Aderem • Rafi Ahmed • Norman Baylor • Bruce A. Beutler • Robert L. Coffman • Joe D. Cohen • Shane Crotty • Ennio De Gregorio • Peter C. Doherty • Anthony S. Fauci • Kate A. Fitzgerald • Ronald N. Germain • Stephen L. Hoffman • Stefan H.E. Kaufmann • Philippa C. Marrack • M. Juliana McElrath • Dana Philpott • Bali Pulendran • Firdausi Qadri • Lalita Ramakrishnan • Rino Rappuoli • Steven Reed • Supachai Rerks-Ngarm • Maria Rescigno • Robert A. Seder • Rafick-Pierre Sekaly • Ralph M. Steinman • Kanta Subbarao • Tadataka Yamada

Bioreality.

You aren't imagining things.
Knockout rats are finally here.

SAGE™ LABS
Sigma Advanced Genetic Engineering

Sigma Life Science introduces SAGE™ Labs (Sigma Advanced Genetic Engineering), an initiative dedicated to unlocking new possibilities for *in vivo* gene targeting. Using Sigma's exclusive CompoZr® ZFN gene editing technology, we focus on the development and characterization of unique, next-generation rodent research models to support your scientific objectives, leaving you free to focus on your next brilliant discovery.

sageresearchmodels.com